

INFORMATION TO USERS

This manuscript has been reproduced from the microfilm master. UMI films the text directly from the original or copy submitted. Thus, some thesis and dissertation copies are in typewriter face, while others may be from any type of computer printer.

The quality of this reproduction is dependent upon the quality of the copy submitted. Broken or indistinct print, colored or poor quality illustrations and photographs, print bleedthrough, substandard margins, and improper alignment can adversely affect reproduction.

In the unlikely event that the author did not send UMI a complete manuscript and there are missing pages, these will be noted. Also, if unauthorized copyright material had to be removed, a note will indicate the deletion.

Oversize materials (e.g., maps, drawings, charts) are reproduced by sectioning the original, beginning at the upper left-hand corner and continuing from left to right in equal sections with small overlaps.

Photographs included in the original manuscript have been reproduced xerographically in this copy. Higher quality 6" x 9" black and white photographic prints are available for any photographs or illustrations appearing in this copy for an additional charge. Contact UMI directly to order.

**Bell & Howell Information and Learning
300 North Zeeb Road, Ann Arbor, MI 48106-1346 USA
800-521-0600**

UMI[®]

A STUDY OF THE OCEAN SOURCE OF CARBON DISULPHIDE

by

Huixiang Xie

**Submitted in partial fulfillment of the requirements
for the degree of Doctor of Philosophy**

at

**Dalhousie University
Halifax, Nova Scotia
November, 1998**

© Copyright by Huixiang Xie, 1998



National Library
of Canada

Acquisitions and
Bibliographic Services

395 Wellington Street
Ottawa ON K1A 0N4
Canada

Bibliothèque nationale
du Canada

Acquisitions et
services bibliographiques

395, rue Wellington
Ottawa ON K1A 0N4
Canada

Your file Votre référence

Our file Notre référence

The author has granted a non-exclusive licence allowing the National Library of Canada to reproduce, loan, distribute or sell copies of this thesis in microform, paper or electronic formats.

The author retains ownership of the copyright in this thesis. Neither the thesis nor substantial extracts from it may be printed or otherwise reproduced without the author's permission.

L'auteur a accordé une licence non exclusive permettant à la Bibliothèque nationale du Canada de reproduire, prêter, distribuer ou vendre des copies de cette thèse sous la forme de microfiche/film, de reproduction sur papier ou sur format électronique.

L'auteur conserve la propriété du droit d'auteur qui protège cette thèse. Ni la thèse ni des extraits substantiels de celle-ci ne doivent être imprimés ou autrement reproduits sans son autorisation.

0-612-49301-6

Canada

DALHOUSIE UNIVERSITY

FACULTY OF GRADUATE STUDIES

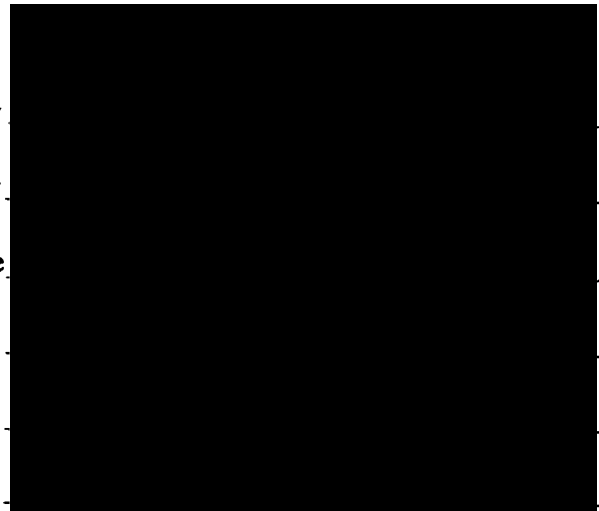
The undersigned hereby certify that they have read and recommend to the Faculty of Graduate Studies for acceptance a thesis entitled "A Study of the Ocean Source of Carbon Disulphide"

by Huixiang Xie

in partial fulfillment of the requirements for the degree of Doctor of Philosophy.

Dated: November 9, 1998

External Examiner
Research Supervisor
Examining Committee



DALHOUSIE UNIVERSITY

DATE: November 19, 1998

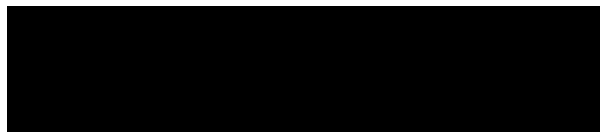
AUTHOR: Huixiang Xie

TITLE: A Study of the Ocean Source of Carbon Disulphide

DEPARTMENT OR SCHOOL: Oceanography

DEGREE: Ph.D. CONVOCATION: Spring YEAR: 1999

Permission is herewith granted to Dalhousie University to circulate and to have copied for non-commercial purposes, at its discretion, the above title upon the request of individuals or institutions.



Signature of Author

The author reserves other publication rights, and neither the thesis nor extensive extracts from it may be printed or otherwise reproduced without the author's written permission.

The author attests that permission has been obtained for the use of any copyrighted material appearing in this thesis (other than brief excerpts requiring only proper acknowledgement in scholarly writing), and that all such use is clearly acknowledged.

To Lu and David

Table of Contents

	Page
List of Figures and Tables	ix
Abstract	xiv
List of Abbreviations and Symbols Used	xv
Acknowledgments	xix
Chapter 1 Introduction	1
1.1 Sources of natural sulphur gases in the atmosphere	1
1.2 DMS and tropospheric sulphate aerosols	1
1.3 OCS and stratospheric aerosols	8
1.4 Atmospheric CS₂	10
1.5 Sources and sinks of atmospheric CS₂	13
1.5.1 Anthropogenic sources	13
1.5.2 Emission from land	13
1.5.3 Emission from oceans	15
1.5.4 Sinks	16
1.6 Potential sources of oceanic CS₂	17
1.6.1 Marine sediments	17
1.6.2 Marine phytoplankton	18
1.6.3 Photochemical production	20
1.7 Conclusions	23
Chapter 2 Methods	26
2.1 Water Sampling	26
2.1.1 Sampling locations	26
2.1.2 Sample collection	26
2.1.3 Sample transfer	32
2.1.4 Sample storage	32

	Page
2.2 Analysis of carbon disulphide	34
2.2.1 Introduction	34
2.2.2 Purge and trap preconcentration	35
2.2.3 Oxygen-doped GC/ECD	38
2.2.4 GC/MS	43
2.2.5 Carbon disulphide standards	44
2.3 Photochemical Studies	47
2.3.1 Irradiation vessels and sample transfer	47
2.3.2 Full-spectrum irradiation	48
2.3.3 Wavelength-dependent irradiation	50
2.3.4 Quantification of Light Intensity	50
2.3.5 Measurement of optical absorbance	60
2.4 Laboratory culture experiments	63
2.4.1 Cultures	63
2.4.2 Culture apparatus	63
2.4.3 Inoculation	66
2.4.4 Culture sampling	67
2.4.5 Gas sampling	67
2.5 Water temperature, salinity, wind speed, and chlorophyll-<i>a</i>	68
Chapter 3 Carbon Disulphide Distributions in the Oceans	70
3.1 Carbon disulphide in surface water	70
3.1.1 Concentrations	70
3.1.2 Carbon disulphide and sea surface temperature	72
3.1.3 Carbon disulphide and salinity	76
3.1.4 Carbon disulphide and chlorophyll- <i>a</i>	79
3.1.5 Discussion	79

	Page
3.2 Vertical distribution	86
3.2.1 Elevated surface concentration	86
3.2.2 Subsurface maxima	89
3.3 Summary	99
Chapter 4 Ocean-Atmosphere Exchange of Carbon Disulphide	101
4.1 Introduction	101
4.2 Henry's law constant for CS₂	102
4.3 The exchange velocity	103
4.4 Flux calculation	109
4.5 Extrapolation to the global oceans	118
4.6 Summary	124
Chapter 5 Carbon Disulphide Production in Phytoplankton Cultures	126
5.1 Introduction	126
5.2 Results	126
5.2.1 Growth of the cultures	126
5.2.2 CS₂ production in the cultures	133
5.3 Discussion	135
5.3.1 Possible pathways for CS₂ production in the cultures	135
5.3.2 Loss of CS₂ in the cultures	143
5.3.3 Extrapolation to the real oceans	144
5.4 Summary	145
Chapter 6 Photochemical Production of CS₂ in Marine Waters	147
6.1 Introduction	147
6.2 CDOM absorptivity	149
6.3 Irradiation time	152
6.4 Full-spectrum irradiation	155

	Page
6.5 Wavelength-dependent irradiation	157
6.5.1 Photo-production rate vs. wavelength	157
6.5.2 Quantum-yield spectra	160
6.5.2.1 Introduction	160
6.5.2.2 Results	165
6.6 Estimation of CS₂ photo-production in the world oceans	174
6.7 Identification of CS₂ precursors	181
6.8 Effect of OH radicals on CS₂ photo-production	187
6.9 Comparison between photo-production of CS₂ and OCS	188
6.10 Summary	194
Chapter 7 Conclusions and Directions for Future Studies	195
7.1 Conclusions	195
7.2 Future studies	198
Bibliography	205

List of Figures and Tables

- Figure 1.1 The chemical and physical transformations of biogenic sulphur in the atmospheric cycle.
- Figure 2.1 Cruise tracks and station positions of CSS *Hudson*, RRS *Challenger*, and NOAA *Discoverer*.
- Figure 2.2 Test of sample storage effect.
- Figure 2.3 Purge-trap preconcentration interfaced with oxygen-doped GC/ECD or GC/MS.
- Figure 2.4 Chromatograms from (A) offshore water in Labrador Sea and (B) coastal water in the Northwest Arm of Halifax, Nova Scotia, Canada.
- Figure 2.5 Typical calibration curve of the oxygen-doped GC/ECD.
- Figure 2.6 Schematic diagram for preparation of CS₂ gas standard.
- Figure 2.7 Schematic representation of the cross section of the irradiation system.
- Figure 2.8 Transmittance curves of six cutoff light filters and the resulting quasi-monochromatic transmittance bands.
- Figure 2.9 Quantum yield and fraction of light absorbed from 250 to 600 nm for a 0.006 M ferrioxalate actinometer over a 1-cm pathlength.
- Figure 2.10 Fe(II) concentration as a function of irradiation time during full spectral exposures.
- Figure 2.11 Output spectrum of the solar simulator.
- Figure 2.12 Differential spectral irradiance between the successive cutoff light filters.
- Figure 3.1 Distributions of surface water concentration of CS₂ and SST.
- Figure 3.2 Distributions of surface water concentration of CS₂ and salinity.
- Figure 3.3 Distributions of surface water concentration of CS₂ and salinity

along a transect from Galway Bay, Ireland to the open North Atlantic.

- Figure 3.4 Distributions of surface water concentrations of CS₂ and Chl-*a*.
- Figure 3.5 Representative profiles obtained in the Northeast Atlantic.
- Figure 3.6 Vertical profiles obtained in waters off the coast of Nova Scotia.
- Figure 3.7 Representative profiles obtained in the Pacific Ocean.
- Figure 3.8 Modelled photo-production rate of CS₂ as a function of depth.
- Figure 4.1 Henry's law constant for CS₂ in aqueous solution as a function of temperature.
- Figure 4.2 Exchange velocity as a function of wind speed.
- Figure 4.3 Schmidt number for CS₂ as function of temperature.
- Figure 4.4 Comparison between spot wind speed and climatological wind speed for (a) *Hudson* cruise, (b) *Discoverer* cruise, and (c) *Challenger* cruise.
- Figure 4.5 Exchange velocity and sea-to-air flux of CS₂ obtained for the *Hudson* cruise.
- Figure 4.6 Exchange velocity and sea-to-air flux of CS₂ obtained for the *Discoverer* cruise.
- Figure 4.7 Exchange velocity and sea-to-air flux of CS₂ obtained for the *Challenger* cruise.
- Figure 4.8 Sea-to-air flux of CS₂ vs. sea surface temperature for the open ocean data.
- Figure 5.1 Total CS₂, cell number and Chl-*a* as a function of time for the cultures in which CS₂ is produced.
- Figure 5.4 Quantum-yield spectrum of CS₂ photo-production and irradiance spectrum of the fluorescent tubes.

- Figure 5.5 Photochemical CS₂ formation in the filtrate of *P. purpureum* and the culture medium (from the control vessel) that were irradiated with simulated solar radiation.
- Figure 5.6 Absorption spectra of the filtrates from the cultures of *Nitzschia frustula* and *Chlamydomonas plethora*.
- Figure 6.1 Preliminary tests on photochemical formation of CS₂ in seawater.
- Figure 6.2 Absorptivity at 350 nm as a function of salinity for surface water samples collected during the *Challenger* cruise.
- Figure 6.3 (a) Average absorption spectrum for surface water samples. (b) Spectral slope for surface water samples as a function of salinity.
- Figure 6.4 Vertical profiles of absorption, temperature and Chl-*a*.
- Figure 6.5 Time series of CS₂ photo-production in a surface sample at station C27 with the solar simulator in the WDI mode.
- Figure 6.6 Vertical profiles of CS₂ before and after irradiation.
- Figure 6.7 Comparison between vertical distributions of photo-production rate of CS₂ and absorptivity at 350 nm.
- Figure 6.8 Photo-production rate of CS₂ vs. absorptivity at 350 nm.
- Figure 6.9 Photo-production rate of CS₂ as a function of cutoff wavelength.
- Figure 6.10 Average quantum-yield spectrum of carbon disulphide derived from the differential irradiance data.
- Figure 6.11 Comparison between the average quantum-yield spectra of CS₂ derived from the Rundel method and that from the differential irradiance method.
- Figure 6.12 Comparison between the mean photo-production rates calculated from the measured values and those calculated using the quantum yield data derived from the Rundel method.

- Figure 6.13** Spectral absorption coefficients for CDOM, seawater, phytoplankton, and suspended mineral (including detritus).
- Figure 6.14** Modelled photo-production spectra of CS₂ at 50°N.
- Figure 6.15** Modelled wavelength-integrated photo-production of CS₂ as a function of latitude and its seasonal variability.
- Figure 6.16** Enhancement of CS₂ and OCS photo-production caused by addition of CYS or CYST to water samples.
- Figure 6.17** Effects of MET on photo-production of CS₂ and OCS.
- Figure 6.18** Effect of changing cysteine concentration on photo-production of CS₂.
- Figure 6.19** Effect of nitrite on the photo-production of CS₂ and OCS.
- Figure 6.20** Examples showing similarity in the vertical distributions of CS₂ and OCS photo-production rates obtained during the *Challenger* cruise.
- Figure 6.21** CS₂ and OCS distributions in surface water along a transect during the *Challenger* cruise.
- Figure 6.22** Comparison between the average apparent quantum-yield spectrum of CS₂ derived from the Rundel method and that of OCS from Weiss et al. [1995b].
- Table 1.1** Flux estimates of natural sulphur gases.
- Table 1.2** Summary of measurements of atmospheric CS₂.
- Table 1.3** Estimates of sources and sinks for tropospheric CS₂ and OCS.
- Table 2.1** Description of the RSS *Challenger* cruise showing sampling time, locations and methods, and irradiation mode for studies on photo-production of CS₂.
- Table 2.2** Precision and recovery of standard additions to seawater samples measured by the oxygen-doped GC/ECD.

- Table 2.3** **Rate of Fe(II) change before and after correction for non-uniform distribution of incident light in the solar simulator.**
- Table 2.4** **Cultures and species examined.**
- Table 3.1** **CS₂ concentrations in surface waters.**
- Table 3.2** **Estimates of potential photo-production rates, chemical destruction rates at the depth of the subsurface CS₂ maximum, and the loss rates due to eddy diffusion just above the maximum.**
- Table 4.1** **Dimensionless Henry's law constant for CS₂ from Elliott [1989].**
- Table 4.2** **Flux estimates of CS₂ in the investigated oceans.**
- Table 4.3** **Flux estimates of CS₂ in the global oceans using method one.**
- Table 4.4** **Flux estimates of CS₂ in the global oceans using method two.**
- Table 5.1** **Maximum carbon disulphide production rates normalised to Chl-*a* and other related information.**
- Table 5.2** **Carbon disulphide change, the potential photo-production and chemical destruction over the durations of the culture experiments.**
- Table 6.1** **Photo-production rate of CS₂ as a function of cutoff wavelength.**
- Table 6.2** **Carbon disulphide quantum-yield data derived from the differential irradiance method.**
- Table 6.3** **Predicted photo-production rates of CS₂ in the samples that were used to determined the quantum yields.**
- Table 6.4** **Parameters for the least-squares fit of equation 6.3 in the text.**
- Table 6.5** **Estimates of CS₂ photo-production in the world ocean under cloud-free condition.**

Abstract

The environmental importance of atmospheric carbon disulphide (CS_2) is recognised by its potential role as a major precursor of carbonyl sulphide (OCS). Oxidation of CS_2 could also contribute to the formation of sulphur dioxide in the mid or high troposphere. The ocean is believed to emit CS_2 to air, but large uncertainty may exist in the assessments of sea-to-air fluxes of this compound partly due to the meager database we currently have for CS_2 in the ocean. In addition, little is known about how CS_2 is produced in marine waters. This work is intended to re-assess the flux estimates, and to identify and evaluate the potential sources for oceanic CS_2 .

Two analytical methods were developed for measuring CS_2 in marine waters: oxygen-doped GC/ECD and GC/MS. Both methods used a purge-and-trap system for preconcentration. CS_2 was measured in both the surface and subsurface waters during three cruises: two in the North Atlantic and one in the Pacific Ocean. Surface water concentrations averaged 13 pM S (picomoles of sulphur per litre) in the open ocean and 30 pM S in coastal waters. All the investigated waters were supersaturated in CS_2 relative to the atmosphere. The estimated sea-to-air flux is 0.18 (0.13-0.24) Tg CS_2 yr⁻¹. Two distinct types of vertical profiles were observed: one in the cool waters of the North Atlantic, characterized by gradual reduction in CS_2 with depth, and another in the warm waters of the North Pacific central gyre, showing the coexistence of subsurface CS_2 and chlorophyll maxima.

Solar UV-initiated photochemical reactions were identified as a significant source for oceanic CS_2 . Apparent quantum-yield spectra of CS_2 photo-production were determined using water samples collected in the Northeast Atlantic. The photo-production rate of CS_2 is positively correlated with absorbance at 350 nm, suggesting that the reactions are mediated by coloured dissolved organic matter. Laboratory irradiations confirmed that cysteine and cystine are efficient precursors of CS_2 and that OH radicals are likely to be important intermediates. Both the field survey and laboratory work point to similar mechanisms for photochemical production of CS_2 and OCS. The total amount of photochemically formed CS_2 in the ocean was estimated to be 0.29 Tg CS_2 yr⁻¹.

CS_2 data were collected from axenic monocultures of six species of marine phytoplankton: *Chaetoceros calcitrans*, *Phaeodactylum tricorutum*, *Phaeocystis* sp., *Porphyridium purpureum*, *Synechococcus* sp. and *Isochrysis* sp.. For a period of between two weeks and forty days, substantial accumulation of CS_2 was found in the cultures of *C. calcitrans*, *P. tricorutum* and *Phaeocystis* sp., whereas the change of CS_2 concentration in the other cultures was insignificant. *C. calcitrans* has a potential for CS_2 production about 10 times higher than *P. tricorutum* or *Phaeocystis* sp.. CS_2 formation was strongly dependent on the growth stage of the cultured species. More investigation is needed to elucidate the mechanisms responsible for CS_2 production by marine phytoplankton.

Abbreviations and Symbols

Φ	quantum yield
Φ_{CS_2}	quantum yield of CS_2
α	attenuation coefficient of the medium (Chapter 2)
η	dynamic viscosity of water
α	enhancement factor due to chemical reaction (Chapter 4)
ϵ	molar absorptivity of the chemical
σ	standard deviation
σ_t	density
λ	wavelength
χ^2	mean-squared error
ΔC	concentration difference between gas phase and water phase
μg	microgram (1 μg = 10^{-6} gram)
μL	microlitre (1 μL = 10^{-6} litre)
μm	micrometre (1 μm = 10^{-6} metre)
μM	micromolar = micromoles per litre (1 μM = 10^{-6} moles per litre)
μmol	micromole (1 μmol = 10^{-6} mole)
A	area
a_{CDOM}	absorption coefficient of coloured dissolved organic matter
a_{ph}	absorption coefficient of phytoplankton
a_{w}	absorption coefficient of pure water
b_{msw}	molecular scattering coefficient of seawater
C	molar concentration of the chemical
C_{a}	concentration in air
CDOM	coloured dissolved organic matter
Chl- <i>a</i>	chlorophyll- <i>a</i>

CNN	Cloud condensation nuclei
COADS	Comprehensive Ocean-Atmosphere Data Set
CPS	controlled power system
C_w	concentration in water
d	day
D	diffusion coefficient
DMDS	Dimethyl disulphide
DMS	Dimethyl sulphide
DMSO	Dimethyl sulphoxide
DMSO₂	Dimethyl sulphone
DMSP	Dimethylsulphonium propionate
DOM	dissolved organic matter
D_w	vertical eddy diffusivity
ECD	electron capture detector
F	gas flux between the ocean and atmosphere
F_c	fraction of light absorbed by the chemical of interest
fmol	femtomole (1 fmol = 10⁻¹⁵ mole)
FPD	flame photometric detector
F_s	fraction of light absorbed by the reacting system
g	gram
GC	gas chromatography
Gg	gigagram (1 Gg = 10⁹ grams)
GSH	glutathione
H_s	Henry's law constant in seawater
H_d	Henry's law constant in distilled water
hr	hour
I(0)	light intensity at the sea surface

I(z)	light intensity at depth z
I₀	incident light intensity
I_{C_{DOM}}	light absorbed by coloured dissolved organic matter
ID	inner diameter
K	exchange velocity
K_a	exchange velocity in the air diffusion layer
kg	kilogram (1 kg = 10³ grams)
K_s	Setchenow coefficient
K_w	exchange velocity in the water diffusion layer
L	litre
m	metre
M	molar = moles per litre
M_w	molar weight of water
MeSH	Methyl mercaptan
min	minute
mL	millilitre (1 mL = 10⁻³ litre)
MS	mass spectrometry
MSA	Methane sulphonic acid
n	number of samples or observations
nm	nanometre (1 nm = 10⁻⁹ metre)
OD	Outer diameter
P_{CS₂}	photo-production rate of CS₂
P(z)	photo-production rate at depth z
pM	picomolar = picomoles per litre (1 pM = 10⁻¹² moles per litre)
pmol	picomole (1 pmol = 10⁻¹² mole)
ppmv	parts per million by volume

pptv	parts per trillion by volume
PSCs	Polar stratospheric clouds
psu	practical salinity unit
r	correlation coefficient
S	Sulphur
s	second
Sc	Schmidt number
SD	standard deviation
SST	sea surface temperature
t	temperature in Celsius (Chapter 3 and Chapter 4)
t	time (Chapter 5)
T	temperature in Kelvin
Tg	teragram (1 Tg = 10¹² grams)
u	spot wind speed
u_{av}	long -term average wind speed
UHP	ultra high purity
UV	Ultraviolet
V	molal volume (Chapter 4)
V	volume (Chapter 2)
x	association factor of water
yr	year
z	depth

Acknowledgements

I thank all the members of my committee for their advice, support and criticism generously provided throughout this work. I am particularly indebted to Robert Moore for identification of a rewarding field of study, and for his encouragement and many enlightening discussions. The guidance given by William Miller is also gratefully acknowledged. Many thanks are due to: Stewart Niven for his technical assistance; Michael Scarratt for his help and collaboration in the phytoplankton culture experiments; Walter Judge who operated the CTD during the *Challenger* cruise; Roy Lowry for providing the underway surface data for the *Challenger* expedition; the Bedford Institute of Oceanography for use of the Knudsen bottles; the scientists, officers and crew members aboard CSS *Hudson*, RSS *Challenger* for their collaboration during the field investigations. I express my appreciation to Youlian Pan who provided the filtrates of *Nitzschia frustula* and *Chlamydomonas plethora*.

This work was supported by grants from the National Science and Engineering Research Council to Robert Moore and William Miller, and by Killam Memorial Scholarships and Dalhousie Graduate Fellowships.

Chapter 1 Introduction

1.1 Sources of natural sulphur gases in the atmosphere

Volatile sulphur species that are emitted naturally to the atmosphere from the earth's terrestrial and aquatic environments include dimethyl sulphide (DMS), sulphur dioxide (SO_2), hydrogen sulphide (H_2S), carbonyl sulphide (OCS), carbon disulphide (CS_2) and other minor compounds (e.g. methyl mercaptan (MeSH) and dimethyl disulphide (DMDS)). With the exception of sulphur dioxide (SO_2), which has a sulphur oxidation state of IV and a natural source predominantly from volcanic eruptions [Andreae, 1990], most naturally occurring sulphur gases have lower sulphur oxidation states (-II or -I), and production of these species is directly or indirectly related to biological activities [Charlson et al., 1987]. According to an estimate made by Andreae [1990], the magnitude of natural sulphur emissions into the atmosphere could be as high as that of the gaseous sulphur released from human activities, which is almost exclusively in the form of SO_2 from burning of fossil fuels. Table 1.1 shows estimates of natural sulphur emissions given by Andreae [1990]. Although large uncertainties may exist in these estimates, due to technical limitations in measuring gas fluxes and restricted spatial and temporal coverage of relevant data, several points can be made here: 1) biogenic compounds, rather than SO_2 from volcanic activities, comprise the bulk of natural sulphur emissions, 2) oceans release to the atmosphere much more gaseous sulphur than do the continents, and 3) DMS is the dominant oceanic sulphur species.

1.2 DMS and tropospheric sulphate aerosols

Figure 1.1 illustrates the chemical and physical transformations of biogenic sulphur gases in the atmosphere. In the troposphere, DMS and other reduced sulphur species are oxidised, mainly by OH radicals, to SO_2 and other intermediate

Table 1.1 Flux estimates of natural sulphur gases

	SO ₂	H ₂ S	OCS	DMS	CS ₂	Other	Total
Volcanoes	7.36-9.28	0.39	0.0096	-	0.0096	?	9.6-12.8
Soils and plants	-	3.2-9.6	±0.64	0.19-3.84	0.64-0.8	0.96	4.8-12.8
Coastal wetlands	-	0.96	0.13	0.64	0.064	0.13	1.92
Biomass burning	2.56	?	0.096	-	?	?	≥ 2.56
Oceans	-	1.6-6.4	0.32	19-52.1	0.32	?	35.2-57.6
Total	9.6-12.8	6.4-19.6	0-1.28	19-54.4	0.96-1.28	1.1	38.4-89.6

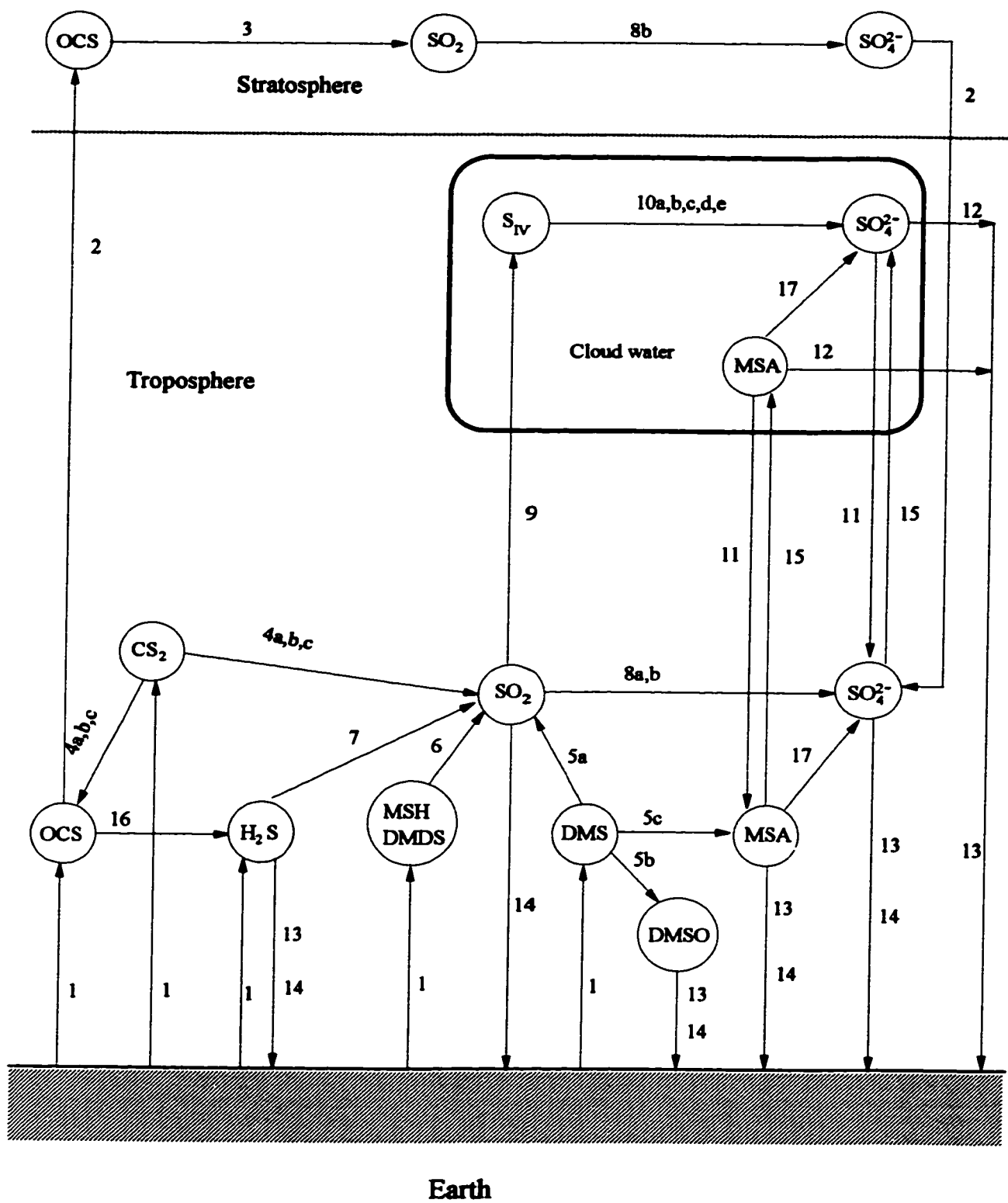
Flux estimates are in Tg S (sulphur) yr⁻¹ (1 Tg = 10¹² grams)

Figure 1.1 The chemical and physical transformations of biogenic sulphur in the atmospheric cycle. Circles are chemical species, the box represents cloud-liquid phase. This figure is modified from Charlson et al. [1992].

DMS = CH_3SCH_3 ; DMDS = CH_3SSCH_3 ; $\text{S}_{\text{IV}} = (\text{SO}_2)_{\text{aq}} + \text{HSO}_3^- + \text{SO}_3^{2-} + \text{CH}_2\text{OHSO}_3^-$;
 DMSO = CH_3SOCH_3 ; MSA = $\text{CH}_3\text{SO}_3\text{H}$.

1. Surface emissions
2. Tropospheric/stratospheric exchange
3. $\text{OCS} + h\nu \rightarrow \text{S} + \text{CO}$
 $\text{S} + \text{O}_2 \rightarrow \text{SO} + \text{O}$
 $\text{SO} + \text{O}_2 \rightarrow \text{SO}_2 + \text{O}$
- 4a. $\text{CS}_2 + \text{OH} \rightarrow \text{CS}_2\text{OH}$
 $\text{CS}_2\text{OH} \rightarrow \text{multistep} \rightarrow \text{OCS} + \text{SO}_2$
- 4b. $\text{CS}_2 + h\nu \rightarrow \text{CS}_2^*$
 $\text{CS}_2^* + \text{O}_2 \rightarrow \text{CS} + \text{SO}_2$
 $\text{CS} + \text{O}_2 \rightarrow \text{OCS} + \text{O}$
 $\text{CS} + \text{O}_3 \rightarrow \text{OCS} + \text{O}_2$
- 4c. $\text{CS}_2 + \text{O} \rightarrow \text{OCS} + \text{S}$
- 5a. $\text{CH}_3\text{SCH}_3 + \text{OH} \rightarrow \text{multistep} \rightarrow \text{SO}_2$
- 5b. $\text{CH}_3\text{SCH}_3 + \text{OH} \rightarrow \text{multistep} \rightarrow \text{CH}_3\text{SOCH}_3$
- 5c. $\text{CH}_3\text{SCH}_3 + \text{OH} \rightarrow \text{multistep} \rightarrow \text{CH}_3\text{SO}_3\text{H}$
6. $\text{CH}_3\text{SH} + \text{OH} \rightarrow \text{multistep} \rightarrow \text{SO}_2$
7. $\text{H}_2\text{S} + \text{OH} \rightarrow \text{multistep} \rightarrow \text{SO}_2$
- 8a. $\text{SO}_2 + \text{OH} \rightarrow \text{HSO}_3^-$
 $\text{HSO}_3^- + \text{O}_3 \rightarrow \text{HO}_2 + \text{SO}_3$
 $\text{SO}_3 + \text{H}_2\text{O} \rightarrow \text{H}_2\text{SO}_4$
- 8b. $\text{SO}_2 \rightarrow \text{SO}_4^{2-}$ (heterogeneous reaction)
9. $(\text{SO}_2)_{\text{g}} \leftrightarrow (\text{SO}_2)_{\text{aq}}$
 $(\text{SO}_2)_{\text{aq}} + \text{H}_2\text{O} \rightarrow \text{HSO}_3^- + \text{H}^+$
 $\text{HSO}_3^- \leftrightarrow \text{H}^+ + \text{SO}_3^{2-}$
- 10a. $\text{CH}_2(\text{OH})_2 + \text{HSO}_3^- \leftrightarrow \text{H}_2\text{O} + \text{CH}_2\text{OHSO}_3^-$
- 10b. $(\text{H}_2\text{O}_2)_{\text{g}} \leftrightarrow (\text{H}_2\text{O}_2)_{\text{aq}}$
 $\text{HSO}_3^- + (\text{H}_2\text{O}_2)_{\text{aq}} \rightarrow \text{multistep} \rightarrow \text{H}^+ + \text{SO}_4^{2-}$
- 10c. $(\text{O}_3)_{\text{g}} \leftrightarrow (\text{O}_3)_{\text{aq}}$
 $\text{HSO}_3^- + (\text{O}_3)_{\text{aq}} \rightarrow \text{multistep} \rightarrow \text{H}^+ + \text{SO}_4^{2-}$
11. Evaporation
12. Cloud water rainwater
13. Wet deposition
14. Dry deposition
15. Cloud nucleation
16. $\text{OCS} + \text{OH} \rightarrow \text{multistep} \rightarrow \text{H}_2\text{S}$
17. MSA $\rightarrow \text{SO}_4^{2-}$ by some mechanism
- 10d. $(\text{OH})_{\text{g}} \leftrightarrow (\text{OH})_{\text{aq}}$
 $\text{HSO}_3^- + (\text{OH})_{\text{aq}} \rightarrow \text{multistep} \rightarrow \text{H}^+ + \text{SO}_4^{2-}$
- 10e. $\text{HSO}_3^- + \text{O}_2 \rightarrow \text{multistep} \rightarrow \text{H}^+ + \text{SO}_4^{2-}$

Figure 1.1



species, such as methane sulphonic acid (MSA), dimethyl sulphoxide (DMSO). Through reactions mainly with OH (dry conditions) and hydrogen peroxide (H_2O_2) (wet conditions), SO_2 is then further oxidised to sulphuric acid which forms sulphate aerosols. Methane sulphonates which may be transformed to sulphates by some unknown mechanism [Charlson et al., 1992].

Sulphate aerosols are an important component of tropospheric aerosols that are considered to exert significant influence on climate through perturbation of the earth's radiation balance and through alteration of cloud properties. Aerosols reflect incoming solar radiation back to space, leading to cooling both at the ground and in the atmosphere. In the meantime, aerosols also absorb incoming (short wave) and outgoing (long wave, IR) radiation, and thus cause warming in the atmosphere and energy transfer from the ground to the atmosphere. Whether aerosols cause a net cooling or warming effect on the earth/atmosphere system depends on their composition, size distribution, and the albedo of the underlying surface. Darker particles (e.g. black carbon) absorb light more efficiently than brighter ones; aerosols between 0.1-1 μm in diameter are the major light-scattering particles in the atmosphere; aerosols result in cooling if they have a higher albedo than the underlying surface, or cause warming if they are more opaque than the underlying surface. The overall direct effect of the tropospheric aerosols is thought to be cooling. It is estimated that this effect corresponds to a radiative forcing of -4.8 W m^{-2} , of which -1.84 W m^{-2} results from sulphate aerosols, including -0.78 W m^{-2} from the natural sulphate component [Andreae, 1995]. The relative contribution from sulphate aerosols to the total negative radiative forcing is very high considering that sulphates account for only 11% of the total global aerosol burden (29 Tg).

In addition to their direct radiative effect, sulphate aerosols also indirectly influence climate by promoting formation of cloud droplets and by modifying

cloud properties. In air free of aerosol particles, cloud droplets formation from water vapour is difficult because an interfacial energy barrier, associated with the sharp curvature of the incipient droplet, is too high to be overcome under normal humidity in clouds which rarely exceeds 101%. However, cloud droplets can be formed relatively easily in the presence of cloud condensation nuclei (CCN), which substantially reduce the energy barrier inhibiting the formation of water droplets. Only wettable or soluble aerosol particles can act as CCN, among which sulphate aerosols are the dominant component in both remote and polluted environments [Charlson et al., 1992 and references therein]. Therefore, sulphate aerosols play an extremely important role in cloud formation.

Moreover, a variation in CCN concentration may alter cloud albedo and precipitation. Simultaneous measurements of CCN and cloud droplet concentrations indicate that the two terms are positively correlated, although their relationship is far from linear [Andreae, 1995 and references therein]. Thus, given a constant liquid water content in a cloud, an increase in CCN concentration leads to an increase in cloud droplet number and a corresponding reduction in droplet size which, in turn, increases cloud albedo and causes cooling. By reducing the size of cloud droplets, an increase in CCN concentration also diminishes the probability that a cloud droplet evolves into a rain droplet. This results in less precipitation, longer lifetimes of cloud droplets, and hence an increase in cloud albedo. Clouds also cause warming by absorbing incoming short wave energy and outgoing long wave energy. But, the warming effect caused by an increase in CCN concentration is much smaller than the cooling effect since clouds are essentially opaque to IR and an increase in droplet number causes little additional absorption. Andreae [1995] pointed out that the cooling effect due to an increase in CCN concentration is strongest in the least-polluted areas of the world, i.e. the remote ocean areas where CCN concentration is relatively low. Charlson et al. [1987]

estimated that a 30% increase in CCN concentration over the ocean could increase the planetary albedo by 0.005 averaged over the entire earth. This change in the planetary albedo is equivalent to a decrease of 1.3 K in global mean surface temperature, which corresponds to one third of the increase in surface temperature predicted for a doubling of atmospheric CO₂ [Charlson et al., 1987 and references therein].

Charlson et al. [1987] demonstrated that the majority of CCN in the unpolluted marine atmosphere are sulphate aerosols that result from oxidation of DMS emitted from the ocean. Oceanic DMS is mainly a decomposition product of an osmo-regulatory substance, dimethylsulphonium propionate (DMSP), synthesised by certain marine algae. DMS production by algae is highly species-specific and changes greatly under external stress (e.g. salinity change, physical disturbance, exposure to atmosphere) [Andreae, 1990]. Ventilation to air, photo-oxidation by solar radiation [Shooter and Brimblecombe, 1986; Shooter and Brimblecombe, 1989; Kieber et al., 1996] and microbial consumption [Kiene and Bates, 1990] are the dominant removal processes for DMS in seawater. Because of the complexity involved in the production and loss of DMS, no simple, linear relationship has ever been found between the distribution of DMS and that of phytoplankton abundance (e.g. chlorophyll-a concentration) or primary productivity (e.g. ¹⁴C uptake rate). High levels of DMS, and hence elevated emission rates of DMS to the atmosphere, were frequently found in the warmest, most saline and most intensely irradiated waters (equatorial and tropical regions, and subtropical gyres) where primary production rates are relatively lower than in temperate waters [Charlson et al., 1987; Andreae, 1986; Andreae, 1990]. This unusual behaviour is one of the cornerstones underlying the hypothesis proposed by Charlson et al. [1987]: a biofeedback loop that encompasses marine phytoplankton, reduced sulphur gases (mainly DMS) and CCN could be one of the important factors that regulate the

earth's climate. In this loop, an increased atmospheric temperature as a result of enhanced solar input and/or addition of green-house gases causes an increase in surface seawater temperature; the warming of surface seawater leads to an increase in DMS production by phytoplankton and its emission rate to air, and hence an increase in the density of sulphate aerosols. As has been discussed above, an increase in the abundance of sulphate aerosols reduces incoming solar radiation and causes cooling at the earth's surface. On the other hand, lowered temperature and reduced solar radiance would, according to the hypothesis, suppress DMS production in the ocean, especially in warm waters, which then would mitigate the cooling effect.

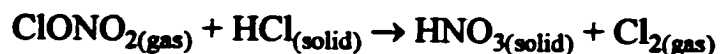
1.3 OCS and stratospheric aerosols

Table 1.1 shows that OCS emission is a minor contribution to the total atmospheric sulphur budget. Carbonyl sulphide is, however, the most stable and longest-lived (lifetime ~1 year or more) reduced sulphur gas in the atmosphere [Khalil and Rasmussen, 1984; Carroll, 1985]. As a result, OCS has a high and fairly uniform concentration (average, 500 ± 50 pptv) in the troposphere [Khalil and Rasmussen, 1984; Rinsland et al., 1992; Bandy et al., 1992; Johnson and Bates, 1993]. Carbonyl sulphide is actually the largest reservoir of atmospheric sulphur and the only sulphur species that is transported into the stratosphere during volcanically quiescent periods. Once in the stratosphere, OCS photo-dissociates rapidly, and oxidation of the photochemical product (SO_2) is believed to be responsible for the maintenance of the nonvolcanic stratospheric sulphate aerosols (Figure 1.1) [Crutzen, 1976; Hofmann, 1990; Engel and Schmidt, 1994]. This background sulphate aerosol mass is strongly, but episodically perturbed by large volcanic eruptions which inject precursor gases, such as SO_2 and OCS, into the stratosphere [Mohnen, 1990].

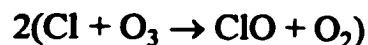
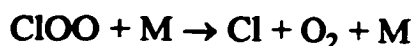
Like sulphate aerosols in the troposphere, stratospheric sulphate aerosols also affect the earth's radiation balance by interacting with solar and terrestrial radiation. Stratospheric sulphate aerosols induce cooling at the earth's surface by reflecting incoming solar radiation back to space, while causing warming in the stratosphere where the aerosols reside by absorbing incoming short wave and outgoing IR [McCormick, 1993 and references therein]. One of the fundamental differences between stratospheric sulphate aerosols and their tropospheric counterparts is that, due to lack of precipitation in the stratosphere, the former have a much longer residence time than the latter. This feature enables stratospheric aerosols to affect the earth's radiative balance on longer time scales.

Stratospheric sulphate aerosols also catalyse ozone destruction through their involvement in heterogeneous reactions and, thus, influence the solar ultraviolet (UV) flux reaching the earth's surface. Stratospheric ozone is chemically destroyed, mainly by reaction with the HO_x , NO_x and ClO_x families. In the presence of sulphate aerosols, NO_x is converted to nitric acid (HNO_3), a relatively stable reservoir species of NO_x , which increases the concentration of ClO_x and HO_x by reducing the abundance of ClONO_2 and the destruction rate of HO_x , respectively. As the increased ozone loss resulting from the increased ClO_x and HO_x can more than compensate for the reduced ozone destruction due to the decrease in the concentration of NO_x , the net ozone loss rate is increased [Wennberg et al., 1994]. Furthermore, sulphate aerosols are involved in the formation of polar stratospheric clouds (PSCs) that induce dramatic springtime ozone depletion over the Antarctic and less frequently over the Arctic [Brune et al., 1991]. Poole et al. [1988] suggested that PSCs are formed in three stages: (1) formation of supercooled liquid sulphate aerosols; (2) deposition of HNO_3 and H_2O (as $\text{HNO}_3 \cdot 3\text{H}_2\text{O}$) vapours (above the local frost point) onto frozen aerosol nuclei, producing type I PSCs; (3) coupled deposition of $\text{HNO}_3 \cdot 3\text{H}_2\text{O}$ and pure

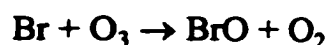
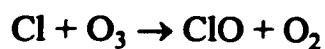
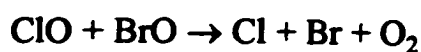
water ice (below the local frost point) onto type I PSCs, forming type II PSCs. When air parcels containing ClONO_2 are exposed to PSCs, ClONO_2 reacts with HCl that is absorbed onto PSCs:



The shift of reactive nitrogen to relatively stable HNO_3 and its subsequent deposition with PSC particles to lower altitudes makes more chlorine stay in the reactive form (ClO_x) which can destroy ozone. In the meantime, the resulting Cl_2 is rapidly photolysed to chlorine atoms which then react with ozone to produce ClO . As the concentration of ClO increases, a more efficient, self-catalysing, ozone-destroying cycle is created [Brune et al., 1991]:



where M is molecular nitrogen or oxygen. Another important sequence for ozone loss involves ClO and BrO :



The above schemes are the so-called PSC-perturbed ozone-loss mechanisms that are supposed to be responsible for the observed "ozone hole" over the Antarctic.

1.4 Atmospheric CS_2

As in the case of OCS , CS_2 emission to the atmosphere is also considered to be a minor component in the global sulphur budget (Table 1.1). The stimulus for studying the atmospheric chemistry of CS_2 mainly arises from its potential role as a major precursor for carbonyl sulphide (OCS) [Barns et al., 1983; Khalil and

Rasmussen, 1984; Chin and Davis, 1993], thus influencing indirectly the earth's climate. CS₂ conversion is estimated to account for 26% of the total OCS input to the atmosphere, making it the largest source for OCS [Chin and Davis, 1993]. Carbonyl sulphide is generated when CS₂ is oxidised by OH radicals, by oxygen (O(³P)) atoms, and by direct photo-oxidation (Figure 1.1) [Logan et al., 1979; Sze and Ko, 1979; Sze and Ko, 1980; Bandy et al., 1981; Wine et al., 1981; Wine and Ravishankara, 1982; Jones et al., 1983]; of these reactions, the one with OH radicals is predominant [Chin and Davis, 1993]. Oxidation of CS₂ produces SO₂ along with OCS, with the molar conversion factor to OCS being 0.81 ± 0.06 [Chin, 1992]. Carbon disulphide is believed to be a minor source for atmospheric SO₂ [Wine et al., 1981]. However, due to convection within clouds and its relatively long lifetime (~7 days), the possibility cannot be excluded that oxidation of CS₂ might make a significant contribution to SO₂ formation in the mid and upper troposphere [Chatfield and Crutzen, 1984].

Measurements of atmospheric CS₂ were first made in 1977 when Sandalls and Penkett [1977] conducted a field survey near Harwell, England. Table 1.2 lists the concentrations of atmospheric CS₂ measured by various research groups. The carbon disulphide mixing ratio in the free troposphere is mostly below 10 parts per trillion by volume (pptv), except Carroll's [1985] values which are unusually high compared to the others. The concentration in the boundary layer exhibits strong geographical dependence with the remote marine boundary layer frequently containing much less CS₂ than the boundary layer over coastal regions or the land (Table 1.2). The high content of atmospheric CS₂ found near or over the continents may result from anthropogenic release [Bandy et al., 1993; Johnson and Bates, 1993], biomass burning [Bandy et al., 1993] or elevated emission of this compound from the underlying environments [Kim and Andreae, 1987a]. The

Table 1.2 Summary of measurements of atmospheric CS₂

References	Concentrations		Layer in the troposphere	Locations
	pptv			
Sandalls and Penkett [1977]	20-200		BL	Near Harwell, England
Maroulis and Bandy [1980]	20-30		BL	East coast of North America
and Bandy et al. [1981]	2-10		FT	
Carroll [1985]	50 ± 46 (11-166)		FT	East coast of the United States
Tucker et al. [1985]	5 ± 3		FT	42°N in central N. America to 43°S in Chile
Bandy et al. [1986]	50		BL	Wallops Island, Virginia
Kim and Andreae [1987a]	5 (1-10)		BL	Open ocean of N. Atlantic
	28 ± 23 (4-94)		BL	Coastal areas of N. Atlantic
	69 ± 63 (7-184)		BL	Estuaries of N. Atlantic
Thornton and Bandy [1993]	1-8		BL	Central Pacific
Bandy et al. [1993]	< 3		BL	NW South Atlantic
	0.5-5		FT	Western Atlantic
Johnson and Bates [1993]	< 2		BL	Open Ocean of the Atlantic
	9		BL	Coastal areas of the Atlantic

BL is boundary layer and FT is free troposphere.

concentration in the remote marine boundary layer is generally considered to be of the order of a few pptv.

1.5 Sources and sinks of atmospheric CS₂

1.5.1 Anthropogenic sources

Present estimates of sources and sinks for atmospheric CS₂, together with the OCS data, are shown in Table 1.3. Human activities release the largest amount of CS₂ to the atmosphere, making up ~58% of the total source strength. Anthropogenic sources for atmospheric CS₂ include production by the chemical industry, automobile exhaust, and sulphur recovery processes. The chemical industry is the dominant source (0.31 Tg yr⁻¹), accounting for 99% of the total man-made input [Chin and Davis, 1993]. The largest single industrial use of CS₂ is in the manufacture of viscose rayon fibres, where CS₂ is used as a solvent carrier to form xanthate crumbs from alkali cellulose and is liberated during the spinning process [Avilova et al., 1979]. Production of carbon tetrachloride and cellophane film also consume a large amount of CS₂. Used as a direct reactant, chemical intermediate, or solvent, CS₂ plays an important role in the production of pesticides, drugs, rubber and other polymers [Reid, 1962; Lay et al., 1986].

A small amount of CS₂ is also released from automobiles and sulphur recovery processes. Sulphur recovery here refers to the conversion of sulphur compounds (mainly H₂S) from oil refineries and natural gas processing to elemental sulphur. Carbon disulphide is formed during sulphur recovery due to the presence of hydrocarbons and part of it escapes to the atmosphere [Peyton et al., 1976].

1.5.2 Emission from land

Land sources refer here to soils, marshes, volcanoes, and biomass burning. Biomass burning has both anthropogenic and natural components. Carbon

Table 1.3 Estimates of sources and sinks for tropospheric CS₂ and OCS

	OCS Tg yr ⁻¹	CS ₂ Tg yr ⁻¹
Sources		
Soils and marshes	0.27 (0.14-0.52)	0.023 (0.012-0.045)
Volcanoes	0.02 (0.006-0.09)	0.02 (0.006-0.09)
Biomass burning	0.14 (0.04-0.26)	-
Ocean	0.32 (0.16-0.64)	0.18 (0.09-0.36)
Anthropogenic	0.04 (0.03-0.06)	0.313 (0.162-0.476)
CS ₂ oxidation	0.34 (0.17-0.61)	Not a source
DMS oxidation	0.17 (0.10-0.28)	No estimates
Total	1.3 (0.65-2.5)	0.54 (0.27-0.97)
Sinks		
Reaction with OH	0.13 (0.02-0.8)	0.54 (0.27-0.97)
Reaction with O	0.015 (0.009-0.026)	negligible
Photolysis	0.029 (0.020-0.040)	negligible
Vegetation uptake	0.43 (0.16-1.0)	No estimates
Open ocean	0.032 (0.010-0.054)	Not a sink
Total	0.64 (0.22-1.9)	0.54 (0.27-0.97)

Data are from Chin and Davis [1993], except for DMS source for OCS, which is from Barnes et al. [1994], and open ocean sink for OCS, which is from Weiss et al. [1995a]

disulphide emissions from soils, marshes, and volcanoes account for only 8% of the estimated total flux (Table 1.3). Biomass burning is suspected to generate CS₂ [Bandy et al., 1993], but no measurements for this production have been reported. Although some plants are known to emit CS₂ [Aneja and Cooper, 1989], relevant data about this pathway are too sparse to identify whether land vegetation as a whole is a net source or sink of atmospheric CS₂ [Chin and Davis, 1993]. Taylor et al. [1982] and Stedman et al. [1984] reported production of CS₂ (and also OCS) by chemical decomposition of pyrite and other sulphide minerals in the presence of oxygen, water and organic matter. Their results imply that natural metal sulphides in oxygenated aquatic or moist environments could be possible precursors for CS₂ and OCS. Extrapolation from the results of Stedman et al [1984] gives an annual release of 0.0015 Tg CS₂ and 0.0012 Tg OCS to the atmosphere from chemical decomposition of pyrite, which are negligible compared with the total land-source strengths of these two species.

1.5.3 Emission from oceans

The ocean is considered to deliver 33% of the total CS₂ input to the atmosphere (Table 1.3). Lovelock [1974] made the first measurements of CS₂ in the Atlantic and reported a concentration (mean \pm SD) of 14 ± 4 pM S (picomol sulphur per litre) for surface waters in the open ocean. The next significant work on oceanic CS₂ was done by Kim and Andreae [1987, 1992], who conducted three field programs in the North Atlantic (25-44°N, 66-81°W) from April to September, 1986. They determined concentrations of 16 ± 8 pM S in offshore waters and 33 ± 19 pM S in coastal and shelf waters. Concentrations in anaerobic environments, such as stagnant bays, estuaries, and saline marshes, were found to be 10 to more than 100 times higher than in the open ocean [Lovelock, 1974; Bandy et al., 1982; Jørgensen and Okholm-Hansen, 1985; Turner and Liss, 1985; Kim and Andreae,

1987a, 1992; Wakeham et al., 1987]. Calculations using the above CS₂ data and Henry's law constants, provided by Elliott [1989], show that the atmospheric CS₂ concentration at equilibrium with seawater should be ~70 pptv in the remote marine boundary layer and ~130 pptv over coastal waters, whereas field atmospheric measurements indicate only a few pptv in air over the open ocean and tens of pptv over coast regions (see section 1.4). Therefore, marine waters are highly supersaturated in CS₂ relative to the atmosphere, and the ocean acts as a source for atmospheric CS₂. Using the data obtained in the mid-latitudes of the North Atlantic, Kim and Andreae [1987a] arrived at an oceanic emission rate of 0.26 (0.13-0.52) Tg CS₂ yr⁻¹. Taking into account possible seasonal and diurnal variations that are not included in Kim and Andreae's estimate, Chin and Davis [1993] estimated the oceanic flux to be 0.18 Tg CS₂ yr⁻¹. Andreae [1990] reported a value of 0.38 Tg CS₂ yr⁻¹ (Table 1.1), but no information was given on how this estimate had been obtained.

1.5.4 Sinks

Carbon disulphide in the troposphere is predominantly destroyed by its reaction with OH radicals. Direct photo-oxidation, following absorption of solar ultraviolet radiation by CS₂, was considered to be a significant sink for tropospheric CS₂ [Wine et al., 1980; Jones et al., 1983]. A more recent study, however, shows that this destruction pathway is negligible because of low photolysis rates of CS₂ [Chin, 1992]. Reaction with the oxygen atom, O(³P) is also a negligible sink for CS₂ due to the extremely low concentration of O(³P) in the troposphere [Chin and Davis, 1993].

1.6 Potential sources for oceanic CS₂

1.6.1 Marine sediments

Andreae [1986] suggested that CS₂ in anoxic aquatic environments could be formed by fermentation reactions of organo-sulphur compounds and by reactions of organic matter with dissolved polysulphides originating from bacterial dissimilatory sulphate reduction. This proposition can explain the highly elevated concentrations of CS₂ (from ~200 pM S to ~ 2 nM S) found in sediment porewaters, stagnant bays [Lovelock, 1974], coastal and estuarine waters [Bandy et al., 1982; Turner and Liss, 1985; Kim and Andreae, 1992], and salt marshes [Adams et al., 1981; Steudler and Peterson, 1984] where anaerobic microbial processes may prevail. It also fits well with the observation that a strong concentration gradient of CS₂ coincides with an O₂-H₂S transition zone in a stratified coastal salt pond [Wakeham et al., 1987]. As circumstantial evidence for Andreae's hypothesis, production of CS₂ by microbial decomposition of sulphur-containing amino acids in soils is well documented [Skipper and Westermann, 1974; Banwart and Bremner, 1975a,b]. It has been suggested that much of the CS₂ found in coastal waters could be a result of diffusion of this compound from the porewaters of underlying sediments [Andreae, 1986]. In addition to CS₂, other volatile sulphur compounds have been observed in anoxic sediments. Kiene [1988] observed the evolution of DMS and methyl mercaptan during incubations of anoxic sediment slurries. Zhang et al. [1988] found that the concentrations of OCS in porewaters of the Chesapeake Bay sediments are 20-1000 times higher than those in the overlying water column. Zhang et al. [1988] also presented evidence that OCS production in the sediments is coupled to microbial sulphate reduction. The mechanisms responsible for CS₂ production in sediments remain to be understood.

1.6.2 Marine phytoplankton

Marine phytoplankton, which are ubiquitous in the ocean, have been shown to produce a suite of atmospherically reactive trace gases, such as dimethyl sulphide, methyl halides, non-methane hydrocarbons. As stated previously, production by marine algae is the major source for oceanic DMS. Keller et al. [1989] examined more than one hundred and twenty individual clones of phytoplankton, representing twelve algal classes. Their results indicate that whereas many phytoplankton species have the capability to produce DMS, the dominant producers are dinoflagellates and prymnesiophytes, including coccolithophores.

Aside from the clear taxonomic pattern of DMS production, DMS formation may also be strongly dependent on the physiological states of algae. Turner et al. [1988] demonstrated that the release of DMS and DMSP by *Emiliana huxleyi* occurs mainly during cell senescence. A number of research groups have studied the production of methyl halides in laboratory phytoplankton cultures. Tait and Moore [1995] reported production of methyl chloride in xenic diatom cultures, possibly via chemically or bacterially mediated reactions of algal organic compounds. In more recent studies, Scarratt and Moore [1996 and 1997] examined production of methyl chloride and methyl bromide in both xenic and axenic phytoplankton cultures. The species tested include diatoms (*Chaetoceros calcitrans*, *Phaeodactylum tricorutum*, and *Thalassiosira weissflogii*), prymnesiophytes (*Phaeocystis* sp., *Isochrysis* sp., and *Emiliana huxleyi*), blue-green algae (*Synechococcus* sp.), prasinophytes (*Tetraselmis* sp.), dinoflagellates (*Prorocentrum* sp.), and the Rhodophyceae (*Porphyridium* sp.). Methyl chloride is produced in all the tested species and methyl bromide in all but two cultures (*Tetraselmis* sp. and *Isochrysis* sp.). The organisms tend to produce the two compounds predominantly in stationary phase. No consistent difference in production rates between xenic and axenic cultures was observed. Production of

methyl iodide in phytoplankton cultures has been reported by Manley et al. [1997]. In all cases, biomass-based production rates of methyl halides obtained from laboratory cultures can only account for a small fraction of their production estimated for the global oceans. Nevertheless, as stated by these authors, large uncertainties may arise from scaling the results from bottle cultures to the real ocean since only a limited number of species have been tested under conditions that are very different from field situations. Production of non-methane hydrocarbons by phytoplankton have been observed in several cases [Bonsang et al., 1992; Moore et al., 1994; Milne et al., 1995; McKay et al., 1996], but the contribution of this source to the total oceanic production of non-methane hydrocarbons remains unknown.

As marine algae have the capability of producing various volatile compounds, it is reasonable to assume that they are potential candidates for CS₂ production in the sea. Lovelock [1974] first explored such a possibility and reported no release of CS₂ from the algal species that he had examined. Unfortunately, details of the species tested and experimental conditions were not given. Since then no further studies of this potential source have been reported. Recently, some phytoplankton species have been shown to be able to produce a variety of reduced sulphur gases, in addition to DMS. Walsh et al. [1994] observed production of H₂S in unialgal cultures of six marine phytoplankton species and found that bacteria are not important in the formation of this compound in the cultures. Tsuchiya et al. [1992] incubated ten strains of the freshwater blue-green alga, *Microcystis*, and detected the formation of volatile organic sulphur compounds. The identified compounds are isopropyl mercaptan, isopropyl disulphide, methyl isothiocyanate, isopropyl methyl sulphide, and isopropyl methyl disulphide. It should be noted that isothiocyanates are direct precursors of CS₂ and OCS [Challenger, 1959]. Caron and Kramer [1994] reported the production of volatile sulphur compounds in

freshwater algal cultures. The identified compounds are MeSH, DMS, DMDS, H₂S, OCS and CS₂. In view of these observations, a re-assessment of the possibility of CS₂ production by marine phytoplankton may be useful.

1.6.3 Photochemical production

Thornton and Bandy [1991] observed diurnal variations in atmospheric CS₂ levels over the equatorial oceans, with lower concentrations at night or in the early morning and higher concentrations during daytime. They, thus, speculated on the existence of a photosynthetic source in the sea surface, although a light- or temperature-dependent abiotic source may cause a similar phenomenon. Staubes et al. [1989] showed that emission of CS₂ from soils is positively correlated with solar irradiance at the earth's surface. The observations made by these two groups suggest the possibility of photochemical CS₂ production in marine waters. This pathway has been confirmed by this thesis. The following is a brief account of the influence of photochemical processes on aquatic ecosystems and the importance of coloured dissolved organic matter in aquatic photochemistry.

Sunlight-initiated chemical processes in natural waters play an important role in biogeochemical cycling of carbon, sulphur, nitrogen and trace metals. Photochemical processes convert biologically refractory organic matter to carbon dioxide [Miller and Zepp, 1995], carbon monoxide [Conrad et al., 1982; Valentine and Zepp, 1993], or other more biodegradable substances [Kieber, et al., 1989; Kieber et al., 1990]. It has been proposed that photo-degradation of dissolved organic matter (DOM) may control the loss of terrestrially derived organic carbon in the sea [Miller, 1994 and references therein]. Photoproduction of carbon monoxide in the ocean may be a significant source for this compound to the marine atmosphere [Conrad et al., 1982]. The reaction of carbon monoxide with OH radical is the major sink of these radicals in the atmosphere [Thompson and

Cicerone, 1986]. Photochemistry also exerts a significant effect on the sulphur cycle in the ocean. The major formation pathway for oceanic OCS is the photodegradation of organosulphur compounds [Zepp and Andreae, 1995; Flock et al., 1997]. On the other hand, DMS [Shooter and Brimblecombe, 1989] and H₂S [Pos et al., 1997] are photochemically oxidised in seawater, which reduces their emissions to the atmosphere. The nitrogen cycle is affected through direct photolysis of substances such as nitrate and nitrite ions [Zafiriou and True, 1979a,b,c]. In addition, photochemical transformations of organic matter in natural waters may release inorganic combined nitrogen, potentially critical to ecosystems in which primary production is nitrogen limited [Bushaw, et al., 1996]. Finally, photochemical processes strongly influence the distribution and redox chemistry of biologically active metals such as iron, copper, and manganese [Sunda et al, 1983; Moffett and Zika, 1987; Miller et al., 1995]. Photo-reduction of iron and manganese oxides helps to make these elements available to biota and, thus, has an important effect on biological activity in parts of the ocean where productivity depends on the bioavailability of these metals.

Absorption of sunlight by chromophores is essential to trigger photochemical reactions in natural waters. The dominant source for naturally occurring chromophores is the "coloured" components of dissolved organic matter (CDOM) although there are other types of chromophores present in natural waters, including trace organic compounds, inorganic substances (e.g. nitrate and nitrite), and transition-metal complexes. CDOM, variously known as gelbstoffe, yellow substance, or humic substances, is a chemically complex, ill-defined mixture of anionic organic compounds generated by the decay of plant organic matter. The absorption spectra of CDOM are usually featureless, showing approximately exponential decrease with increasing wavelength throughout the ultraviolet and visible regions of the spectrum. A simple linear relationship has frequently been

shown to exist between many photochemical processes (e.g. photoproduction of CO, CO₂, OCS, and low-molecular-weight carbonyl compounds) and absorption of light by CDOM at a particular wavelength [Uher and Andreae, 1997; Valentine and Zepp, 1993; Miller and Zepp, 1995]. Miller [1994] suggests that the similarities may be due to common chromophores or a common photochemical pathway in the observed photochemical reactions.

Photochemical processes in natural waters usually involve the formation and destruction of reactive transient intermediates, and a major portion of these species are free radicals. Because of the presence of oxygen, the most important transient intermediates in natural waters are arguably the reactive oxygen species, which include singlet oxygen (¹O₂), superoxide (O₂⁻), hydrogen peroxide (H₂O₂), OH radical, and peroxy radicals (RO₂). These species mainly originate from reactions initiated directly or indirectly by the excited (singlet and triplet) states of CDOM that are formed through absorption of solar radiation [Blough and Zepp, 1995]. The only known source of ¹O₂ in natural waters is through energy transfer from the excited triplet states of CDOM to oxygen [Blough and Zepp, 1995]. Superoxide is known to be produced mainly from CDOM, though the precise mechanisms are unclear [Blough and Zepp, 1995]. The principal source of H₂O₂ is the dismutation of O₂⁻ which, as pointed out previously, results from photochemical transformations of CDOM. Cooper et al. [1988] showed that ultraviolet radiation is most effective at inducing H₂O₂ formation. Photolysis of CDOM provides the major source for the OH radical in seawater [Mopper and Zhou, 1990]. Photolysis of nitrate and nitrite [Zafiriou and True, 1979a,b,c] and reduction of H₂O₂ by transition metals [Zepp et al., 1992] may also contribute significantly to OH production in waters with sufficiently high levels of nitrate, nitrite or transition metals. Our knowledge concerning RO₂ radicals in seawater is scarce. Blough and Zepp [1995] proposed that RO₂ radicals are produced via the

addition of oxygen to primary radicals that are generated photochemically from CDOM.

Reactions of reactive oxygen species with sulphur-containing compounds may be an important source for sulphur-centred radicals in seawater. Flock et al. [1997] suggested that O_2^- , OH radical and the hydrogen peroxide conjugate base (HO_2^-) can abstract a hydrogen atom from thiols and lead to the formation of thiyl radicals ($RS\cdot$). In addition to its direct reaction with thiols, the OH radical also reacts with bromide and carbonate to produce dibromine radicals (Br_2^-) and carbonate radicals (CO_3^-). Both Br_2^- and CO_3^- are highly reactive with organo-sulphur compounds and may act to generate $RS\cdot$ [Pos et al., 1998]. Addition reactions of $RS\cdot$ to carbonyl groups are postulated to be responsible for OCS production in marine waters [Flock et al., 1997; Pos et al., 1998]. As will be discussed in Chapter 6, photochemical processes generating OCS and CS_2 may be related to each other; therefore, information on the mechanisms for OCS photoproduction may provide useful clues to study the mechanisms for photochemical CS_2 formation.

1.7 Conclusions

Table 1.3 shows that the known total source strength of atmospheric OCS is ~ 50% higher than the sum of all its known sinks. This unbalanced budget indicates that either the sources are overestimated or the sinks are underestimated. The most extensively studied source of atmospheric OCS has been the ocean where OCS is produced through photochemical and thermal reactions [Flock et al., 1997], and possibly microbial processes as well [Cutter and Radford-Knoery, 1993]. However, relatively little effort has been made to refine the estimates of other sources, particular for the source from CS_2 conversion. Carbon disulphide oxidation is currently considered to be the largest OCS source, but large uncertainties exist in this assessment due to our very limited knowledge about the

source strengths of atmospheric CS₂. Although the total amount of CS₂ consumed by the chemical industry can be evaluated with a rather high certainty, the procedure used by Chin and Davis [1993] in deriving the amount of CS₂ that escapes from industrial applications is essentially speculative. In regard to the emission rates of CS₂ from oceans, the work of Kim and Andreae [1987a, 1992] is the only well-documented field analysis of CS₂ in seawater. Their measurements are, however, restricted to the mid-latitudes of the North Atlantic and, thus, may not be representative of other ocean areas. Investigations covering water bodies with wider ranges of biological, physical, and meteorological properties are needed to refine the flux estimate of oceanic CS₂.

An elucidation of oceanic sources of CS₂ is essential for establishing an alternative and independent means of making ocean-to-atmosphere flux assessment of this compound based on mass balance, instead of on saturation ratios and wind speeds. This would also further our understanding of the cycling of sulphur within the ocean. Compared with our understanding of the concentration and distribution of CS₂ in seawater and its efflux to the atmosphere, even less is known of the processes that form CS₂ in the ocean. Current data only suggest that production of CS₂ by anaerobic microbial processes in marine sediments and anoxic waters is highly plausible. Information on other potential biotic or abiotic sources are either conflicting or lacking.

Through field surveys and laboratory studies, this thesis is directed at re-evaluation of the ocean-to-atmosphere flux of CS₂ and identification of sources for this compound in marine waters. Chapter 2 describes the major analytical and experimental methods. In Chapter 3, the spatial distributions of CS₂ in the ocean are discussed using data obtained from three ocean cruises in the Northwest Atlantic, the Northeast Atlantic, and the Pacific Ocean. Chapter 4 evaluates the ocean-to-atmosphere fluxes of CS₂, using the data collected from the

aforementioned three field surveys, and compares the flux estimates from this work with those of other research groups. Chapter 5 reports production of CS₂ in laboratory cultures of some marine phytoplankton species and its potential contribution to forming CS₂ in the ocean. This project confirms for the first time that photochemical reactions in marine waters are an important source for oceanic CS₂ production. Full spectrum and wavelength-dependent irradiations were conducted during the eastern Atlantic expedition. Photoproduction rates of CS₂ from this work were extrapolated to the global ocean. A brief exploration was made into possible mechanisms for photoproduction of CS₂ and the relationship between photochemical formation of CS₂ and OCS. The photochemical issues are addressed in Chapter 6. A summary and directions for future studies are given in Chapter 7.

Chapter 2 Methods

2.1 Water Sampling

2.1.1 Sampling locations

Water samples were taken during three cruises covering the areas of the Northwest Atlantic (Figure 2.1a), the Pacific Ocean (Figure 2.1b) and the Eastern Atlantic off Ireland (Figure 2.1c). The Northwest Atlantic survey was carried out on the Canadian Scientific Ship (CSS) *Hudson* from July 6 to July 23, 1995. The ship's track covered three major areas: (1) the continental shelves of Nova Scotia, Newfoundland and southern Labrador, (2) the Labrador Sea along a World Ocean Circulation Experiment (WOCE) hydrographic line, and (3) the open North Atlantic along a meridional section between Greenland and the Sargasso Sea. The Pacific expedition was conducted on the National Oceanic and Atmospheric Administration Ship (NOAAS) *Discoverer* from October 11 to November 10, 1995. The cruise track started from Seattle, USA, passed by Hawaii, then proceeded along the 160°W meridional line to ~30°S, and finally headed towards Hobart, Australia. The Northeast Atlantic voyage was aboard on the British Royal Research Ship (RRS) *Challenger* from June 6 to July 4, 1996. The sampling area was confined within 51.5°-54.5°N and 9°-13°W, off the west coast of Ireland. Sampling locations and other related information for the *Challenger* cruise are shown in Table 2.1.

2.1.2 Sample collection

A variety of sampling techniques were used for seawater collection during this project. Surface water was taken with a steel bucket; vertical profile samples were collected using Niskin bottles, Knudsen bottles, and a submersible pump. Niskin and Knudsen bottles were triggered at 5 m and the submersible pump sampled

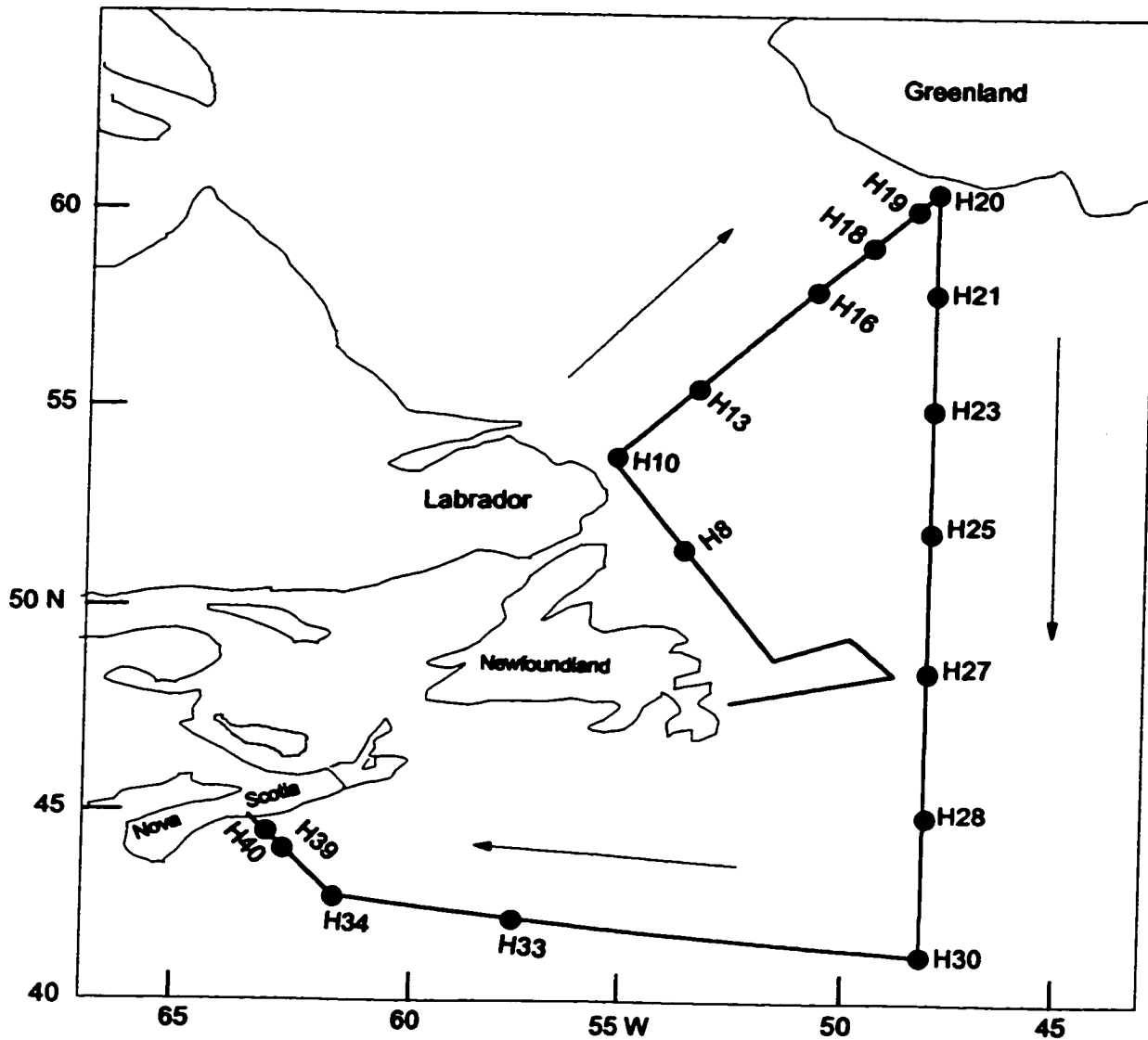


Figure 2.1a Cruise track and station positions of CSS *Hudson* in the Northwest Atlantic, July 6 to July 23, 1995.

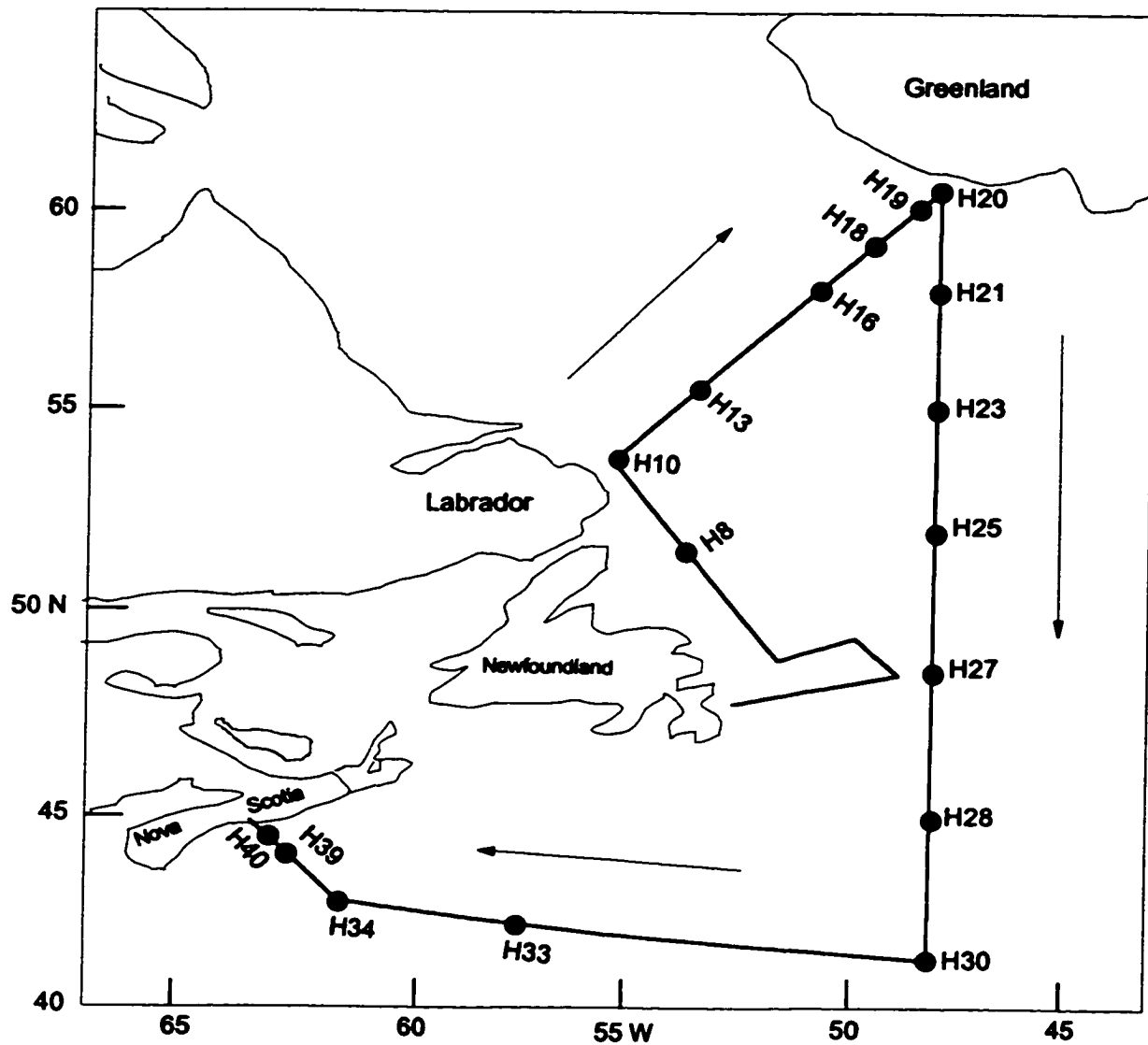


Figure 2.1b Cruise track and station positions of NOAA's *Discoverer*, October 11 to November 10, 1995.

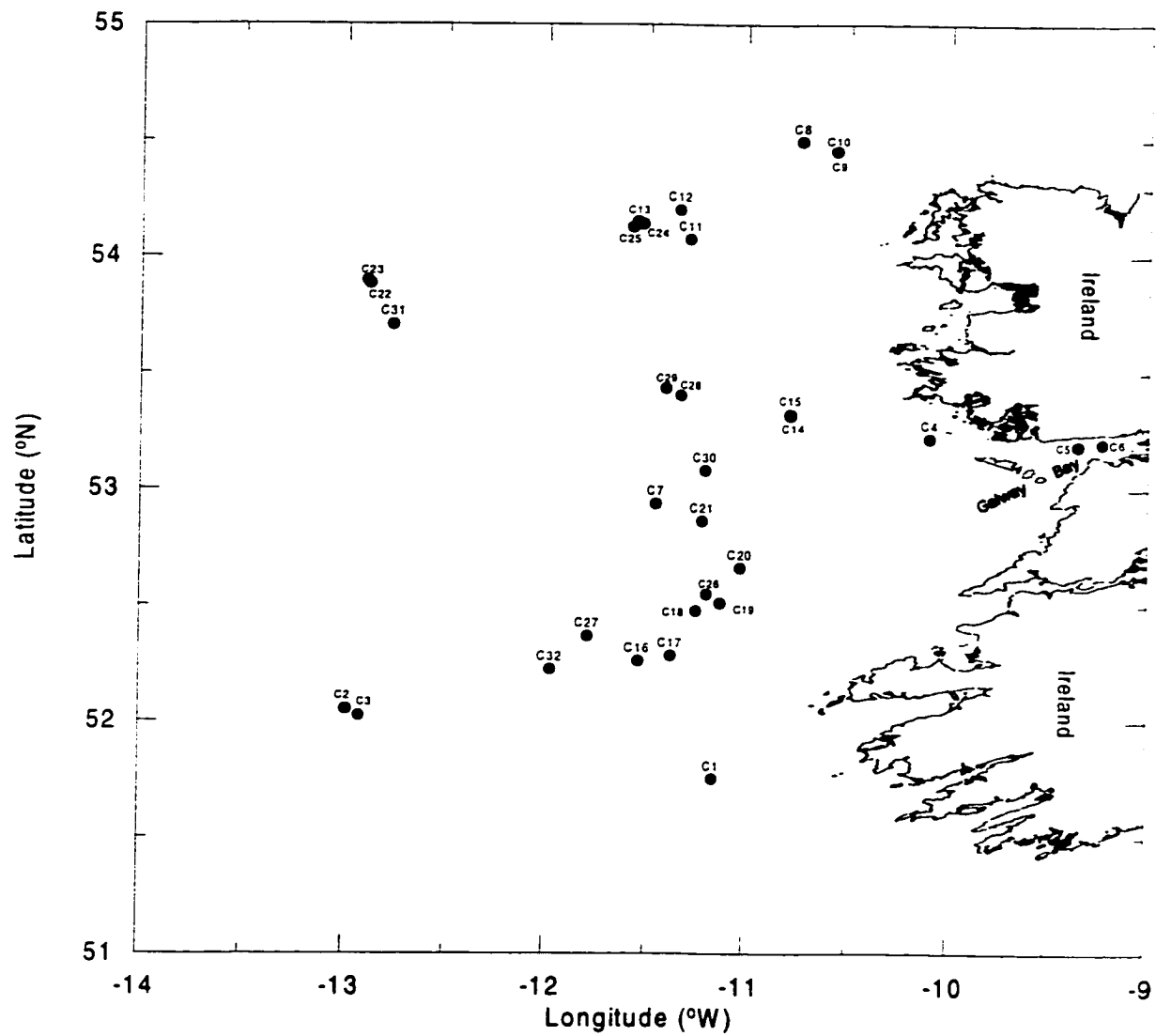


Figure 2.1c Station positions of RRS *Challenger*, June 6 to July 4, 1996.

Table 2.1 Description of the RSS *Challenger* cruise showing sampling time, locations and methods, and irradiation mode for studies on photoproduction of CS₂

Date day/month	Time GMT	Station Number	Latitude °N	Longitude °W	Water depth m	Sampling Method	Irradiation Mode
9/06	10:14	C1	51.754	11.154	185	KB	
10/06	08:33	C2	52.053	12.989	753	KB	
11/06	08:34	C3	52.024	12.922	807	KB	
13/06	08:31	C4	53.222	10.100		Bucket	FSI
13/06	11:44	C5	53.192	9.344		Bucket	FSI
13/06	14:21	C6	53.202	9.224		Bucket	
14/06	08:18	C7	52.940	11.456	139	KB	FSI
15/06	08:17	C8	54.498	10.733	312	KB	FSI
15/06	13:00	C9	54.457	10.568	160	KB	
15/06	13:03	C10	54.457	10.569		Bucket	WDI
16/06	08:31	C11	54.077	11.290	280	KB	
17/06	08:19	C12	54.203	11.344	362	KB	
17/06	14:00	C13	54.155	11.558		Bucket	WDI
18/06	08:30	C14	53.320	10.779		Bucket	WDI
18/06	08:32	C15	53.326	10.778	125	KB	
19/06	08:02	C16	52.263	11.539	184	KB	FSI
19/06	15:30	C17	52.286	11.375		Bucket	WDI
20/06	08:06	C18	52.479	11.245	137	KB	FSI
20/06	12:00	C19	52.513	11.119		Bucket	WDI
21/06	08:06	C20	52.664	11.023	133	KB	FSI
21/06	14:00	C21	52.866	11.216		Bucket	WDI
22/06	08:06	C22	53.885	12.881	387	KB	FSI
22/06	09:30	C23	53.897	12.894		Bucket	WDI
23/06	08:09	C24	54.143	11.531	363	KB	FSI
23/06	13:00	C25	54.130	11.582		Bucket	WDI
24/06	08:17	C26	52.551	11.191	134	KB	
25/06	07:40	C27	52.369	11.788		Bucket	WDI
26/06	08:18	C28	53.406	11.332	145	KB	
26/06	10:20	C29	53.437	11.409		Bucket	WDI
27/06	11:47	C30	53.084	11.202	135	KB	
30/06	10:31	C31	53.708	12.768	269	KB	
02/07	08:16	C32	52.226	11.971	490	KB	WDI

KB is Knudsen bottle. FSI is full spectrum irradiation, and WDI is wavelength-dependent irradiation (see section 2.3 for detailed description).

over a depth range from 2 m to 100 m. We had mixed success in using Niskin bottles as samplers. Water samples collected with the Niskin bottles during the *Hudson* cruise were found to be heavily contaminated with CS₂. Water samples taken with these bottles gave concentrations up to 40 times higher than those collected by the bucket or the pump. However, surface water samples that were collected with Niskin bottles during the *Discoverer* cruise gave reasonable CS₂ concentrations when compared with the available bucket samples. The two methods agreed with each other to better than 8%. Other research groups had similar experience in using standard or Go-Flo Niskin bottles to collect water samples for OCS or CS₂ measurements. Kim and Andreae [1987a] reported no observable CS₂ contamination in samples taken with Go-Flo bottles, while Johnson and Harrison [1986] encountered severe OCS contamination with Niskin and Go-Flo samplers. Cutter [personal communication, 1995] and Andreae et al. [1991] found that old Go-Flo bottles that are repaired with polyvinyl chloride (PVC) cement are highly OCS-contaminating. Thus, PVC cement appears to contain sulphur compounds that may release CS₂ and OCS in aqueous media. Because of the contamination problem from the Niskin bottles, profile samples during the *Hudson* cruise were collected using the submersible pump. Surface water samples from the pumping system were checked against the bucket samples, and the differences between the two methods were below 10%.

One-litre stainless steel Knudsen bottles were used for taking water samples during the *Challenger* cruise. Prior to the field trip, the rubber seals in these bottles were replaced with Teflon, and the bottles were checked for CS₂ contamination. This involved filling the bottles with deionized water (Nanopure UV), and analysing aliquots of this water at intervals of ~2 hours. No significant change of CS₂ concentration was observed for a test period of 12 hours. Cross-checks

between the bucket and Knudsen-bottle samples indicated that the difference between the two methods was within 5%.

2.1.3 Sample transfer

Bulk water samples collected by the bottles, the bucket or the pump were drawn into 100-mL ground glass syringes (Popper) with Luer-Lok fittings. The syringe was connected to a sampling-bottle spigot using a stainless steel needle tubing (8 cm long, 0.32 cm OD), or in the case of drawing water from the bucket or the pump hose, the syringe was fitted with a long steel needle (22.5 cm long, 0.32 cm OD). The syringe was rinsed 2-3 times with the sampled water before finally drawing the sample. To minimise possible artefacts arising from gas exchange between the ambient air and the water in the sampling-bottles, water samples were drawn immediately after the bottles were brought aboard. Direct sunlight was avoided during sample transfer to prevent photochemical processes, which could affect the concentration of CS₂ in the samples.

2.1.4 Sample storage

Prior to analysis, the syringes were stored in a bath of cold, flowing seawater (*Hudson* cruise), or in a bucket of freshly collected surface seawater (all other cruises). The bath was kept in the dark, and the bucket in dim light (cool-white fluorescent tubes), in order to minimise photochemical interference. Keeping the syringes in seawater was intended to reduce the rate of CS₂ diffusion that could occur along the syringe barrels and to prevent the syringe plungers from becoming jammed by salt crystals. The samples were analysed usually within 6 hours of their collection. Figure 2.2 shows the result of a test for storage effects for a bucket sample from the *Challenger* cruise. During this test, the same procedure as described in section 2.1.3 was used for sample transfer, and the syringes were

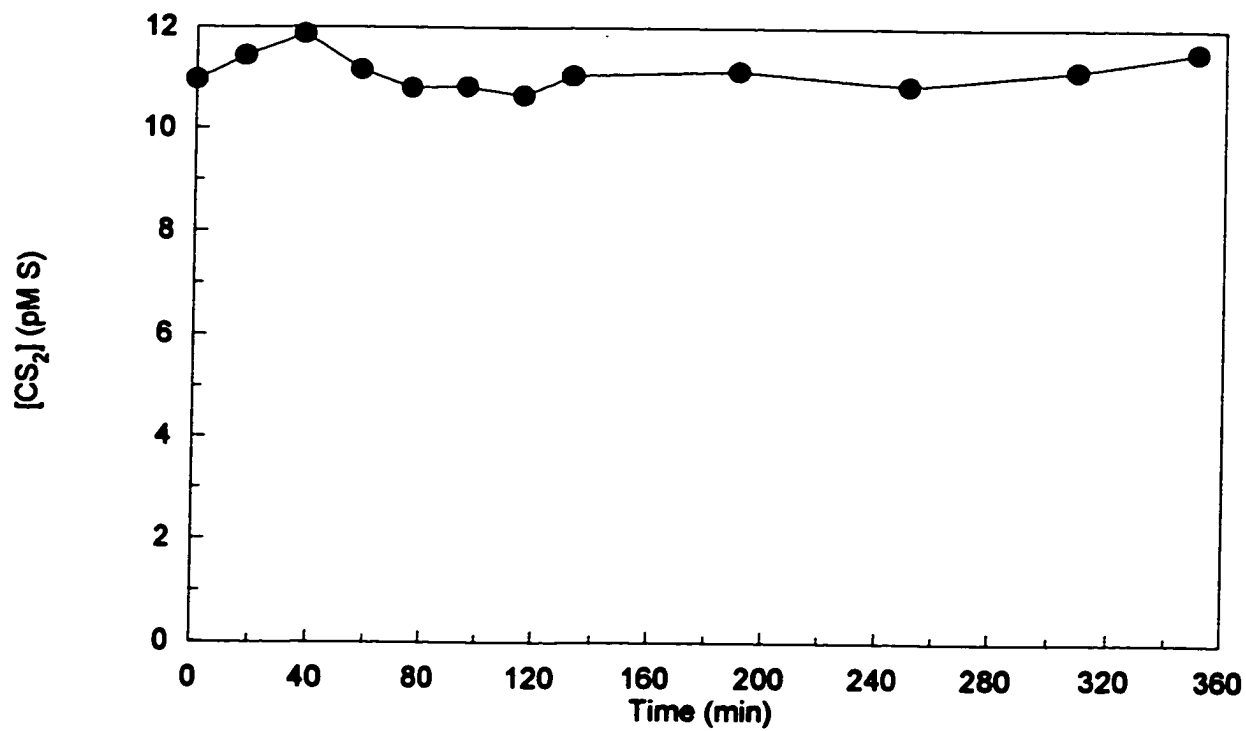


Figure 2.2 Test of sample storage effect. Water was collected with a steel bucket at 53.7°N and 12.8°W in the Eastern Atlantic off the west coast of Ireland. See text for detailed description of sample transfer and storage.

stored in a bucket of seawater. Water samples were analysed using purge-and-trap pre-concentration coupled to a GC/MS system (see section 2.2). The mean concentration of 12 subsamples that were measured sequentially over a period of ~6 hours was 11 pM S with a standard deviation of 3%. While the possibility of production and loss processes in the syringes cannot be excluded, no systematic changes in concentration were observed.

2.2 Analysis of carbon disulphide

2.2.1 Introduction

The first measurements of CS₂ in seawater were made by Lovelock [1974] by gas chromatography and electron capture detection (GC/ECD). Unfortunately, no details of the analytical procedure were revealed. Analytical techniques published afterwards generally contain three operational steps: pre-concentration, separation and detection. Sample pre-concentration is needed because of extremely low concentrations of CS₂ (pM levels) encountered in most natural waters. Carbon disulphide is stripped out from seawater with a ultra high purity (UHP) gas stream of helium or nitrogen and is then pre-concentrated with a cryogenic freeze-out loop [Staubes and Georgii, 1993] or with an adsorption tube [Kim and Andreae, 1987b].

A GC column is usually employed to separate CS₂ from other volatile species, though some types of columns cannot separate CS₂ efficiently and, thus, produce severe peak interference [Kim and Andreae, 1987b]. With high selectivity for sulphur compounds, flame photometric detection (FPD) is widely used for analysing reduced sulphur species, such as DMS, OCS, H₂S and CS₂ [Bremner and Banwart, 1974; Kim and Andreae, 1987b; Bandy et. al., 1993; Staubes and Georgii, 1993]. However, FPD suffers from a squared response to the concentration of a sulphur-containing analyte, which limits its ability to measure

extremely low sulphur contents. By combining Carbosieve adsorbent pre-concentration and FPD, Kim and Andreae [1987b] obtained a detection limit of 4 pmol S, corresponding to about 2 pM S in a 2-L sample. Although this detection limit is sufficiently low to measure CS₂ in seawater, the efficiency of this method is restricted by a relatively long purging time (30 min) and a high flow rate of purging gas (650 mL min⁻¹), which result from large volumes of water sample being pre-concentrated. During an expedition to the Antarctic region, Staubes and GeorgII [1993] failed to detect the presence of CS₂ in most of their water samples, using cryogenic pre-concentration and GC/FPD with a detection limit of 13 pM S. This is not surprising since their instrumental detection limit is probably above the concentrations of CS₂ occurring in the investigated waters. In an effort to develop a method for measuring DMS in surface ocean waters, Johnson and Lovelock [1988] devised a new technique in which reduced sulphur species were fluorinated with fluorine gas on a heated silver catalyst after GC separation and prior to electron capture detection. They obtained a detection limit of 0.92 fmol S s⁻¹ (femtomoles per second) for CS₂, the lowest ever reported. Described below are two alternative analytical methods developed during this project. One of them used oxygen-doped electron capture detection, while the other used mass selective detection. Both methods employed a purge-and-trap system for pre-concentration and GC columns for separation.

2.2.2 Purge and trap pre-concentration

A schematic diagram of the purge-and-trap device from this study is shown in Figure 2.3. The system contained three rotary valves (Valco), a sampling pipette (40 mL), a glass purge vessel and a cryotrap. Among the three valves two were eight-way (V1 and V2) and one was four-way (V3). By selecting appropriate settings of the three valves, sample loading, stripping, and trapping or desorbing

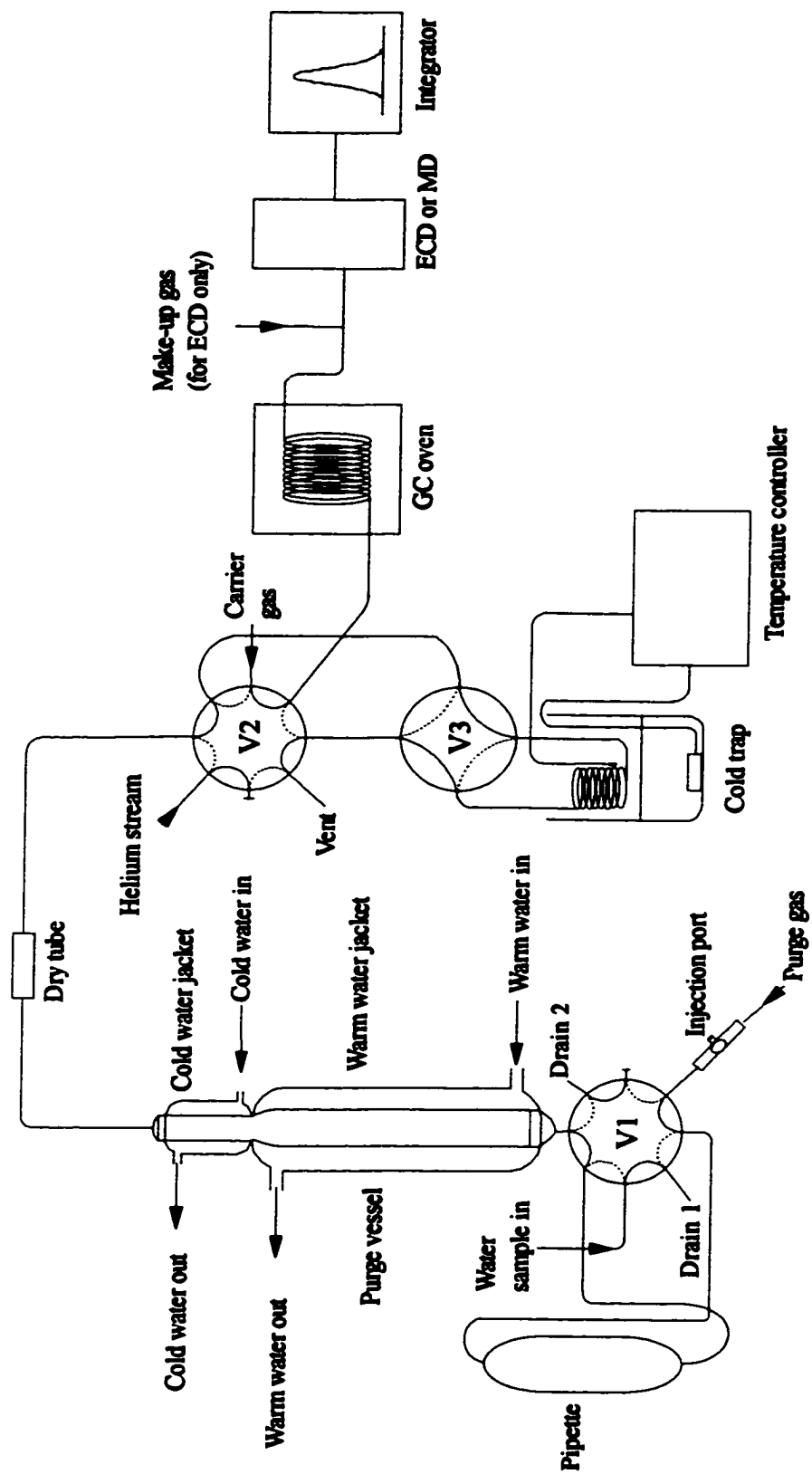


Figure 2.3 Purge-trap pre-concentration interfaced with oxygen-doped GC/ECD or GC/MS

operations could be achieved. V1 and V2 were manually operated during sample loading, while V2 and V3 were controlled by a computer program during purging, trapping and desorbing. During sample loading, V1 and V2 were set to the dotted line positions while V3 was in the solid line position. A water sample, contained in a 100 or 50-mL Pyrex syringe, was manually introduced into the glass sampling pipette through the sample inlet. The volume of the sample was set to 40 mL by overflow via drain outlet 1. While the water sample was being loaded, an UHP helium stream (40 mL min^{-1}), passing through V2, drove out the previously purged water in the purge vessel via drain outlet 2. After the completion of sample loading, V1 and V2 were switched to the solid line, and the system entered the stripping and trapping stage. An UHP helium stream (40 mL min^{-1}), passing through V1, pushed the seawater in the pipette into the purge vessel. The water sample was purged by the helium stream flowing through fritted glass bubblers at the bottom of the purge vessel. The purge vessel was jacketed with water at $\sim 40^\circ\text{C}$ in order to accelerate the stripping process. The moisture content of the purge gas was reduced by passing the gas stream through a short tube jacketed with water at $\sim 1^\circ\text{C}$ and then through a 4-cm long drying tube containing magnesium perchlorate. Carbon disulphide and other volatile gases were cryogenically trapped from the dried purge stream into a 30-cm long stainless steel tube held at -150°C over liquid nitrogen. At the end of the purge cycle (12 min), V3 was changed to the dotted line position, isolating the trapped compounds from the purge gas. An electric current was instantly transmitted to the trap, and this heated the trap to $\sim 15^\circ\text{C}$. Eleven seconds later, an UHP helium flow (5 mL min^{-1}) was introduced through the trap for 10 s following the switch of V2 to the dotted line position and of V3 subsequently to the solid line position. CS_2 and other species were transported by the carrier gas to GC columns where CS_2 was separated from other compounds. While the desorbed CS_2 was being analysed, the next water sample was loaded

and purged. Water samples were passed through a pre-combusted in-line GF / F filter during injection.

2.2.3 Oxygen-doped GC/ECD

An oxygen-doped GC/ECD system was highly sensitive to CS₂; thus, CS₂ in seawater could be readily separated and determined using this system, combined with purge-and-trap pre-concentration. The potential application of the method to CS₂ was discovered by Dr. R. M. Moore during the use of the procedure for measuring methyl chloride in seawater. Oxygen-doping was used to enhance the sensitivity of the ECD to methyl chloride [Grimsrud and Miller, 1978].

A pair of fused-silica capillary columns (J&W Scientific DB-624, film thickness, 3.0 µm) of 30 and 70 m length were used, the first of these being back-flushed after the desired volatile species had passed onto the second. The column temperature was initially 35°C and was increased ultimately to 60°C at a rate of 10°C min⁻¹. The detector was operated at 300°C. A make-up gas, composed of UHP nitrogen and 0.22% oxygen (by volume), was continuously supplied to the GC/ECD. The make-up gas flow was adjusted to give a final total flow rate (carrier gas plus make-up gas) of 30 mL min⁻¹. Carbon disulphide was detected by the oxygen-doped ECD and its signals were recorded by a computer, using a Varian Star software package.

Identification of CS₂ was made by comparing the retention times of a secondary liquid CS₂ standard (see section 2.2.5) with those of water samples. The CS₂ peak eluted in around 11.5 min.

Figure 2.4 shows two chromatograms: one was for an open ocean water sample (Labrador Sea), and another for a coastal water sample (the Northwest Arm of Halifax, Nova Scotia, Canada). Figure 2.5 illustrates a typical calibration curve obtained using a standard addition method. Microliter amounts of the secondary

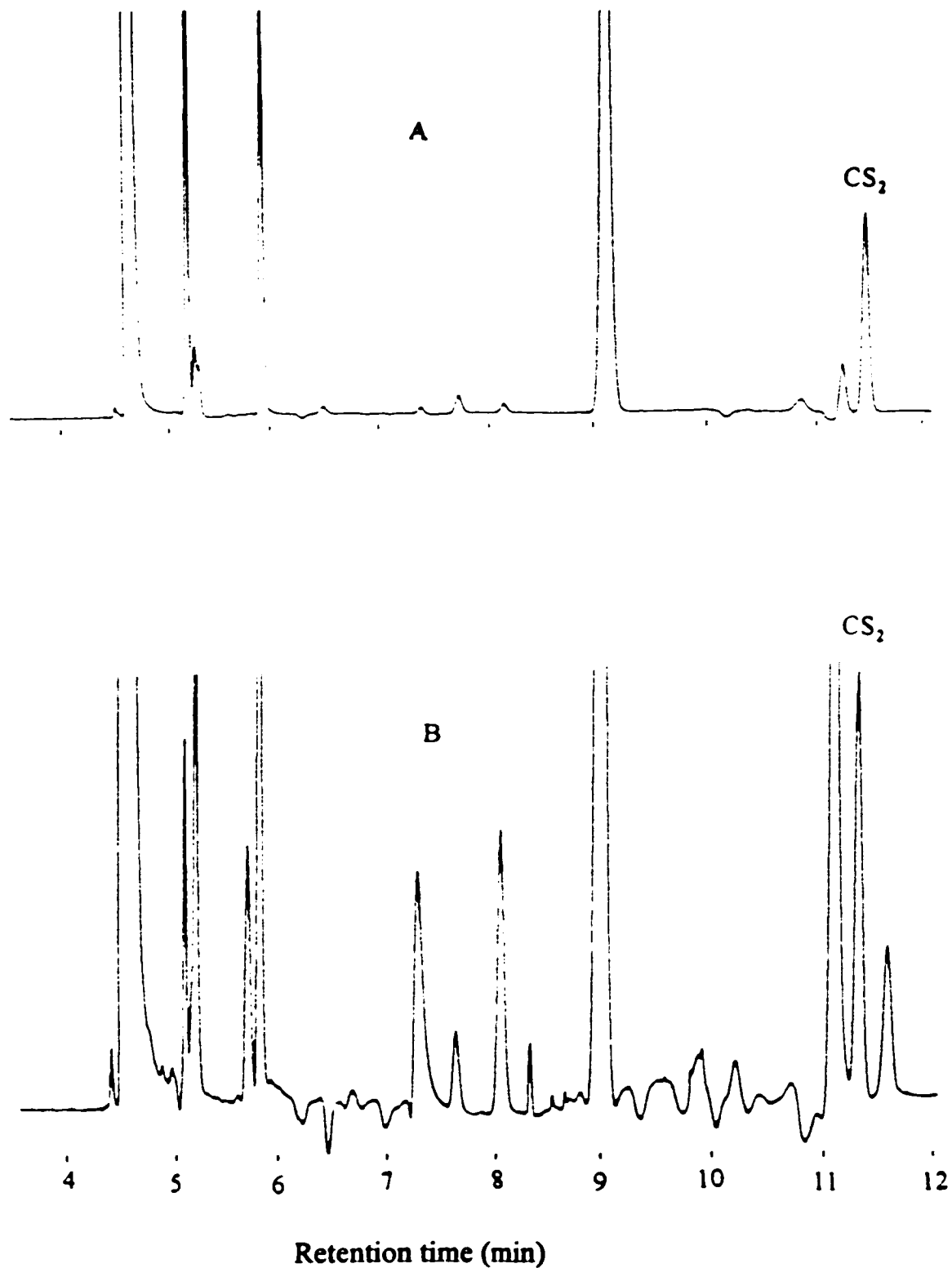


Figure 2.4 Chromatograms from (A) offshore water in Labrador Sea and (B) coastal water in the Northwest Arm of Halifax, Nova Scotia, Canada.

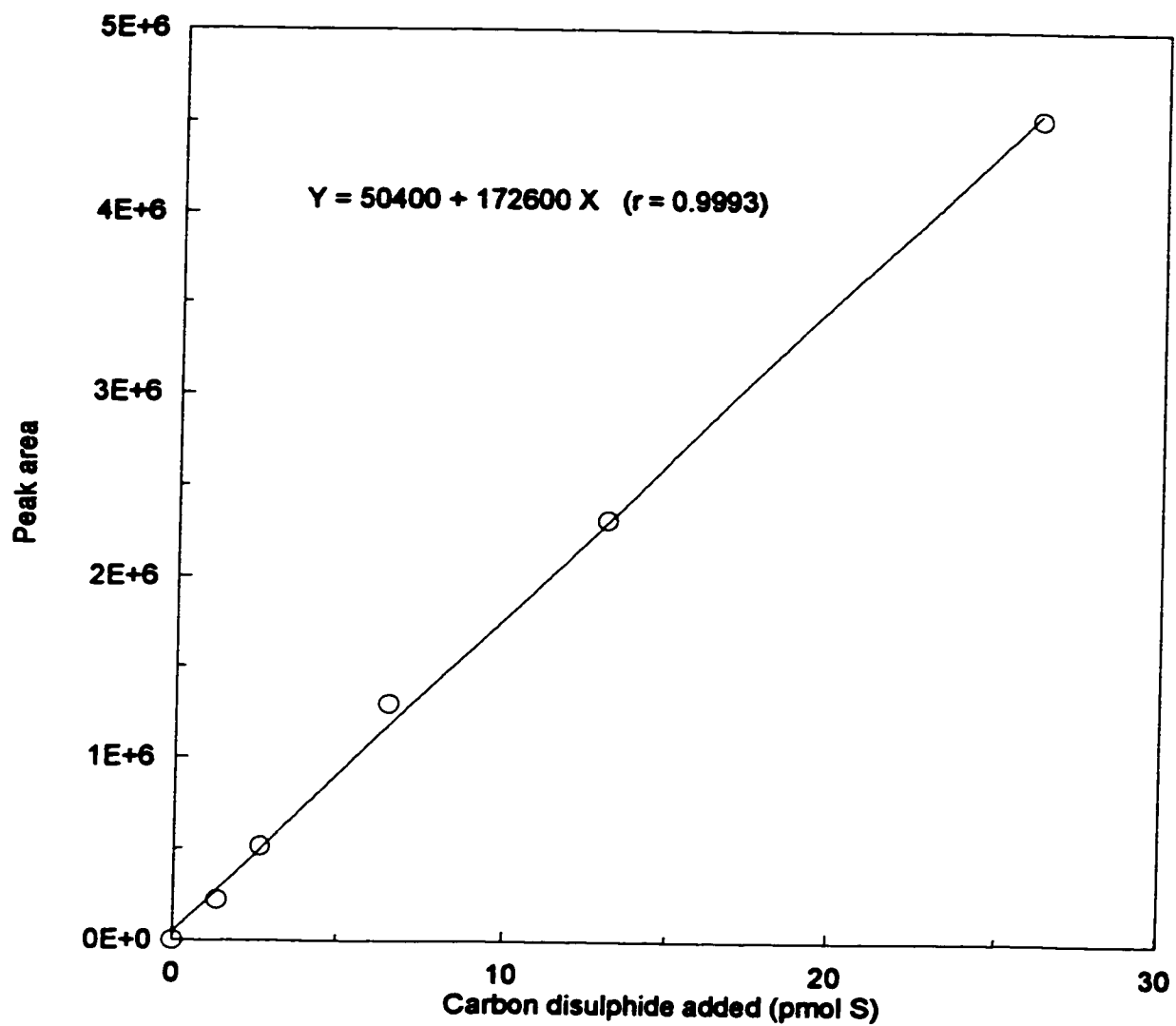


Figure 2.5 Typical calibration curve of the oxygen-doped GC/ECD

standard were injected, via a septum port, into 40 mL aliquots of 0.45- μm filtered seawater samples contained in the purging vessel at the start of the purging process. The linearity of the oxygen-doped ECD, expressed as the slope of the least-square linear fit for the calibration points (logarithmic scale), was 0.996. The oxygen-doped ECD showed linear response up to at least 26 pmol S, corresponding to an aqueous concentration of 650 pM S (for a 40 mL sample), which is broader than that of the system reported by Kim and Andreae [1987b] (linear up to 300 pM S), and covers the CS₂ levels occurring in most marine waters. The detection limit of the oxygen-doped GC/ECD, in terms of the equivalent amount of CS₂ to a peak area of twice the instrumental noise, was ~60 fmol S, or 12 fmol S s⁻¹ (the above defined detection limit divided by the half-peak width in seconds). This value was almost 70 times lower than that of the GC/FPD (4 pmol S) [Kim and Andreae, 1987b], but still ~12 times higher than that of the GC/ECSD (0.92 fmol S s⁻¹) [Johnson and Lovelock, 1988]. The sensitivity of the oxygen-doped ECD, given as the slope of the peak response plotted against the amount of CS₂ injected, was 38.5 millivolts per pmol S.

The accuracy of this analytical system could not be directly determined due to lack of certified CS₂ standards in aqueous media. Thus, the accuracy was evaluated from the recovery rates of 8 replicates of 10- μL of the secondary standard using the method of standard addition. The mean recovery rate was ~106% (Table 2.2). The reproducibility of the method was also assessed by the measurements of the 8 replicates. The results (Table 2.2) indicate that the precision of the system, in terms of relative standard deviation, was ~8%.

For comparison, the linearity, detection limit and sensitivity of the non-doped ECD was also investigated. Although the linearity was excellent (1.0), its detection limit (2 pmol S) was higher and sensitivity (0.14 millivolts per pmol S) was much lower than those of the oxygen-doped ECD. Overall, a 275-fold enhancement of

Table 2.2 Precision and recovery of standard additions (13.1 pmol S) to seawater samples measured by the oxygen-doped GC/ECD

Sample Number	Measured CS₂ pmol S	Recovery %
1	13.10	100.3
2	15.42	118.1
3	15.22	116.5
4	14.98	114.7
5	13.76	105.4
6	13.34	102.1
7	13.18	100.9
8	11.88	91.0
Mean ± SD	13.86 ± 1.16	106.1 ± 8.4

sensitivity was provided by the introduction of oxygen-doping. Due to the high sensitivity and low detection limit of the oxygen-doped GC/ECD, a small volume of water sample (40 mL), short purging time (12 min) and low purging flow rate (40 mL min⁻¹) were needed, displaying advantages over the GC/FPD system [Kim and Andreae, 1987b].

2.2.4 GC/MS

A gas chromatography-mass selective detection system (Fisons GC8000 and MD800) was installed in August 1994. It was fitted with the purge-and-trap unit as described in section 2.2.2. Carbon disulphide was monitored at the mass to charge ratio of 76, and the retention time of this species was confirmed by running a gas sample of pure CS₂ diluted in pure nitrogen. Carbon disulphide peaks emerged around 11 min. The volatile compounds were separated using a pair of DB-624 columns (100 m, ID, 0.53 mm, film thickness, 3 µm) connected in series. Undesired compounds were discarded by backflushing from the first column. The temperature of the GC column started at 35°C and increased to 60°C at a rate of 10°C min⁻¹.

The linear response of the system was up to at least 24 pmol S, equivalent to 600 pM S in a 40-mL sample. The detection limit, defined as 3σ of 17 blanks determined during the *Challenger* cruise, was 1.5 pM S. The mean value of the 17 blanks corresponded to 0.5 pM S, and the maximal blank was equivalent to 1.6 pM S. The blank measurements integrated over that part of the baseline that exhibited a signal for CS₂ during seawater sample measurements.

The reproducibility of the system was evaluated by sequentially measuring 6 replicates of a water sample collected at 100 m depth and 8 replicates of a surface water sample. Both the surface and subsurface samples were collected in the eastern Atlantic off Ireland (the *Challenger* cruise). At a level of ~11 pM S, the

relative standard deviations were 1.4% for measurements of the 100-m sample and 3.3% for those of the surface sample. Ideally, the precision should be determined with replicate samples that contain exactly the same amount of CS₂. In reality, this could not be achieved due to possible biological and/or chemical processes that affected CS₂ concentrations in the tested samples. In this regard, the subsurface sample was probably better than the surface sample because biological activity at depth in the ocean is presumably lower than at the surface. This partly accounts for the better reproducibility obtained for the subsurface sample.

On account of its extremely high specificity, the GC/MS system was employed to analyse CS₂ except for the laboratory cultures of the marine algal species, *Chaetoceros calcitrans*, *Synechococcus* sp. and *Isochrysis* sp. Measurements of CS₂ for these cultures were made using the oxygen-doped GC/ECD as the GC/MS was not available when these experiments were undertaken.

2.2.5 Carbon disulphide standards

Liquid CS₂ standards were gravimetrically prepared. Microliters of pure CS₂ (Fisher Scientific) were drawn into a clean 10- μ L glass syringe (Hamilton). The syringe was weighed with the head of its needle blocked by a septum to prevent evaporation of CS₂. The syringe was weighed again after the CS₂ was injected into 10 mL of pure ethylene glycol contained in a 10-mL glass flask. The difference of the two weights was the amount of CS₂ injected. Immediately after the injection, the flask was tightly sealed, vigorously shaken, and stored in a freezer in order to maintain the stability of the standard. A secondary standard with μ M levels of CS₂ was made by diluting microliter amounts of the primary standard with 50 mL of pure methanol. The validity of this method has been confirmed by Kim and Andreae [1987b].

A gaseous standard of CS₂ was gravimetrically made using the set-up shown in Figure 2.6. Major parts of the set-up included an UHP nitrogen supply cylinder (C1), a 29.5-L Aculife-treated aluminium cylinder (SRL Scott) (C2) for containing the CS₂ standard, a vacuum pump, and a cold trap to prevent potential contamination of organic compounds from the pump. Other parts were two on/off valves (V1 and V2), a glass injection port, and a pressure regulator on C1. All the tubing was made of stainless steel.

The procedure for making the standard involved the following steps:

- 1) Left C2 and V2 on while V1 and C1 off; evacuated C2 for a certain period of time and weighed it; evacuated C2 again until its weight became constant.
- 2) Isolated C2 and switched on V1; evacuated the tubing between C1 and C2.
- 3) Shut off V2 and turned on C1 and C2; adjusted the pressure regulator on C1 and allowed a relatively small flow of nitrogen from C1 to C2; injected 3.57 mg of CS₂ via the septum port; waited for ~15 min.
- 4) Isolated C2 and C1; replaced the glass sample port with a stainless steel tubing; switched on V2 and evacuated the tubing between C2 and C1.
- 5) Switched off V2 and turned on C1 and C2; adjusted the pressure regulator and allowed a high flow of nitrogen from C1 to C2 until a desired pressure in C2 was reached.
- 6) Weighed C2 again

The amount of nitrogen transported from C1 to C2 was 911.1 grams. The concentration of CS₂ was calculated to be 2.89 ppmv S. The gas standard was cross-checked against a freshly prepared liquid standard. The concentration obtained from the cross-check was 2.98 ppmv with a standard deviation of 3% (n = 4, two 50 mL replicates and two 100 mL replicates), in good agreement with the gravimetrically calculated value. A 2.89 ppmv of isoprene standard was made using the identical procedures and contained in the CS₂ standard cylinder.

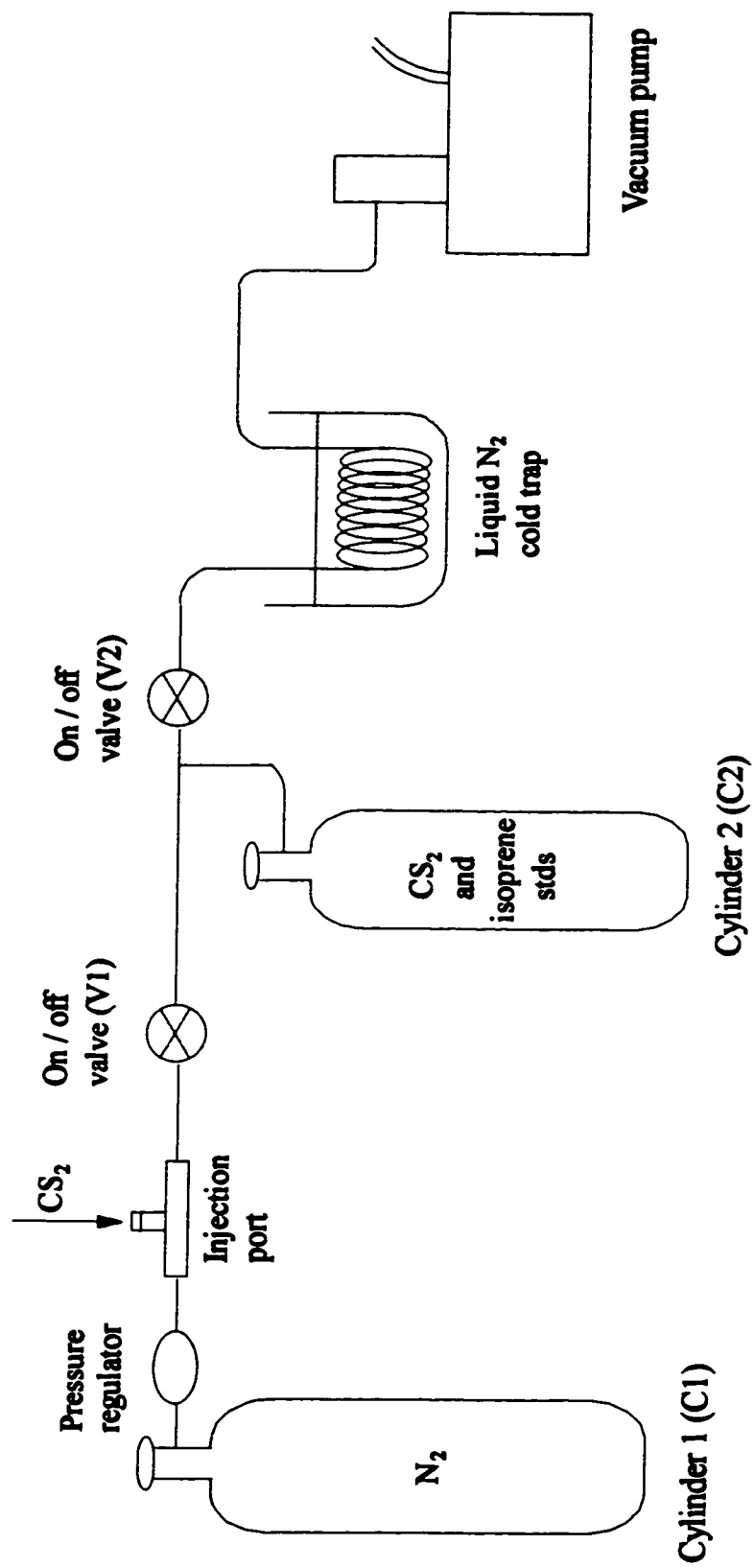


Figure 2.6 Schematic diagram for preparation of carbon disulphide gas standard

The gaseous standard was used for calibrations throughout this work except for the *Hudson* cruise and for the laboratory cultures of the marine algal species, *Chaetoceros calcitrans*, *Synechococcus* sp. and *Isochrysis* sp.. Calibration curves were constructed by injecting volumes of the gaseous standard between 10 and 50 μL via a septum port (Figure 2.3) using Hamilton syringes. If the liquid standards were used, the standard addition method as described was employed.

2.3 Photochemical Studies

2.3.1 Irradiation vessels and sample transfer

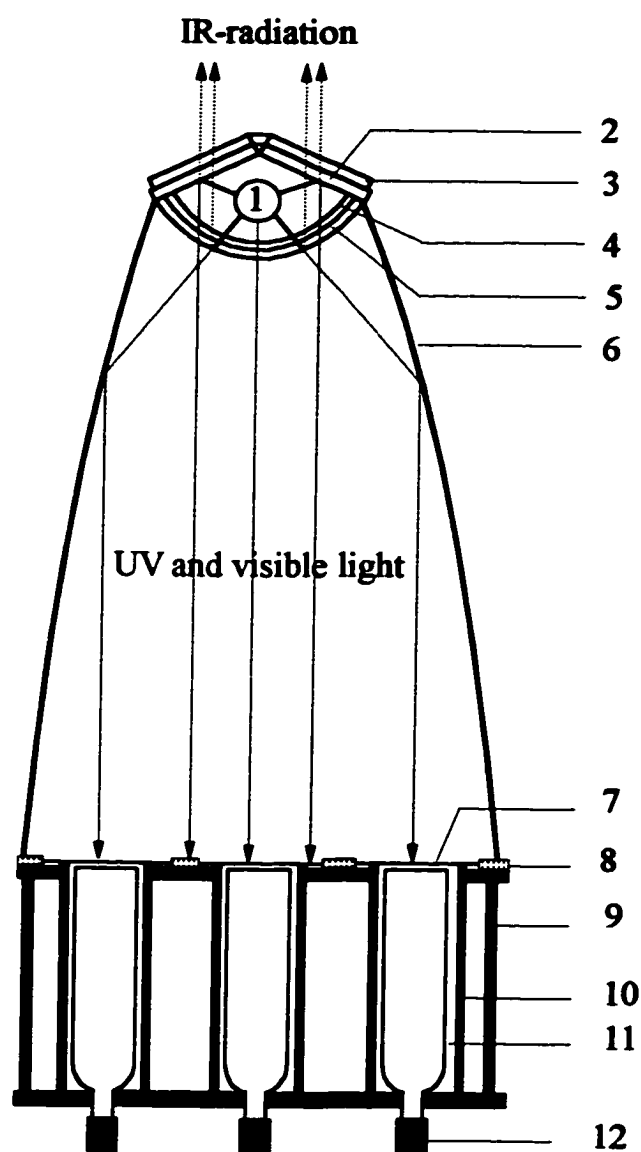
Studies on photochemical production of CS_2 were conducted during the *Challenger* expedition. The sample locations are shown in Table 2.1. Six quartz ampoules were constructed as irradiation vessels. Each ampoule measured 12-cm long (excluding a neck that was 3-cm long, 0.6 cm OD and 0.2 cm ID), 2.7-cm OD and 2.5-cm ID. The light-facing end of the ampoule was a 0.16-cm-thick quartz window. The ampoules were cleaned by soaking them in chromic acid for 24 hours, and then thoroughly rinsed using deionized water (Nanopure UV). Water samples for photochemical studies were drawn from the bucket or the Knudsen bottles into the 100-mL ground glass syringes and then transferred to the ampoules. Sample transfer was conducted at the upwind side of the ship and direct sunlight was avoided by covering the ampoules and syringes with aluminium foil. The syringe was fitted with a 1-inch ID steel syringe filter holder that was further connected to a steel needle to facilitate the transfer. The syringe holder contained a pre-combusted 0.7- μm GF/F glass fibre filter (Whatman) to remove particulate matter. Immediately prior to the sample transfer, the ampoule was flushed with ambient air and rinsed with the water sample. The 0.7- μm filter should eliminate all algal cells, but not all bacteria. Thus, a microbial production or consumption cannot be ruled out absolutely. However, dark controls illustrated that the effect of

bacteria, if any, was negligible over the length of the irradiation time for most of the water samples (see Chapter 6).

2.3.2 Full-spectrum irradiation

The irradiation system is shown schematically in Figure 2.7. Solar-simulated full-spectrum irradiation was conducted using a modified SUNTEST CPS solar simulator (Hereaus DSET Laboratories). The solar simulator was supported above the bench to allow an aluminium tray holding the quartz ampoules to be attached to two aluminium plates sitting at the bottom of the light chamber. Each plate has corresponding holes to permit light transmission from the solar simulator into the ampoules. The exterior wall of each ampoule was wrapped with black foam. A small electric fan was used for dissipating heat generated during the irradiations.

The light source was a xenon arc lamp with an adjustable output from 400 to 765 W m^{-2} between 300 and 800 nm. Three specially fabricated mirrors surrounded the lamp, which worked together to allow passage of UV and visible radiation to the exposure compartment while reducing the infrared component. The spectral distribution of the xenon arc lamp is probably closest to sunlight at the earth's surface when compared with the other artificial light sources employed in environmental photochemistry [Miller and Zepp, 1983]. It should be noted, however, that the xenon arc lamp still emits a small amount of radiation below 290 nm which is not present in sunlight. A supplementary filter made of special window glass (called "lamp filter" hereafter) was, therefore, placed just below the lamp in the solar simulator to remove the short UV radiation. A parabolic reflector served to collimate the light emitting from the lamp and reduce inhomogeneous distribution of radiation over the specimen surface.



1. Xenon lamp	6. Parabolic reflector
2. UV mirror	7. Cut-off filters
3. Light mirror	8. Aluminum plates
4. Lamp filter	9. Aluminum tray
5. Quartz glass	10. Black foam
dish with selective reflecting coating	11. Quartz ampoules
	12. Swagelok fittings

Figure 2.7 Schematic representation of the cross section of the irradiation system.

2.3.3 Wavelength-dependent irradiation

The experimental set-up for wavelength-dependent irradiation was identical to the one used for full-spectrum irradiation with the exception of a few modifications. The modifications were (1) six successive sharp cutoff light filters (Oriel, 2 inches in diameter) were placed between the two aluminium plates (Figure 2.7) and (2) the lamp filter was removed to allow more UV to reach the irradiation vessels. The Schott model numbers of the cutoff filters are WG305 (286 nm), WG320 (302 nm), WG345 (337 nm), GG385 (362 nm), GG420 (407nm) and GG475 (468 nm). The numbers in parentheses are the wavelengths at which the transmittances of the filters are approximately 1%. Hereafter, these wavelengths will be referred to as cutoff wavelengths. Five quasi-monochromatic transmittance bands can be defined for wavelength studies using the mathematical differences between successive sharp cutoff light filters. For these studies the following combinations were used: WG305-WG320, WG320-WG345, WG345-GG385, GG385-GG420 and GG420-GG475. The transmittance spectra of the filters and the resultant bands are presented in Figure 2.8. CS₂ quantum yield in this study was defined by dividing the difference between the photoproduction rates (in $\mu\text{mol S sec}^{-1}$) of two successive cutoff filters by the rate of light absorption by CDOM (in $\mu\text{Einsteins sec}^{-1}$) within the corresponding quasi-monochromatic transmittance band. The solar simulator was set to maximal output for both the full-spectrum and wavelength-dependent irradiations.

2.3.4 Quantification of light Intensity

The output of the xenon lamp and the integrated light intensities inside the ampoules were quantified using the potassium ferrioxalate ($\text{K}_3\text{Fe}(\text{C}_2\text{O}_4)_3$) actinometer, which was developed by Parker and Hatchard [1956] and described more recently by Leifer [1988] and Murov [1993]. The potassium ferrioxalate

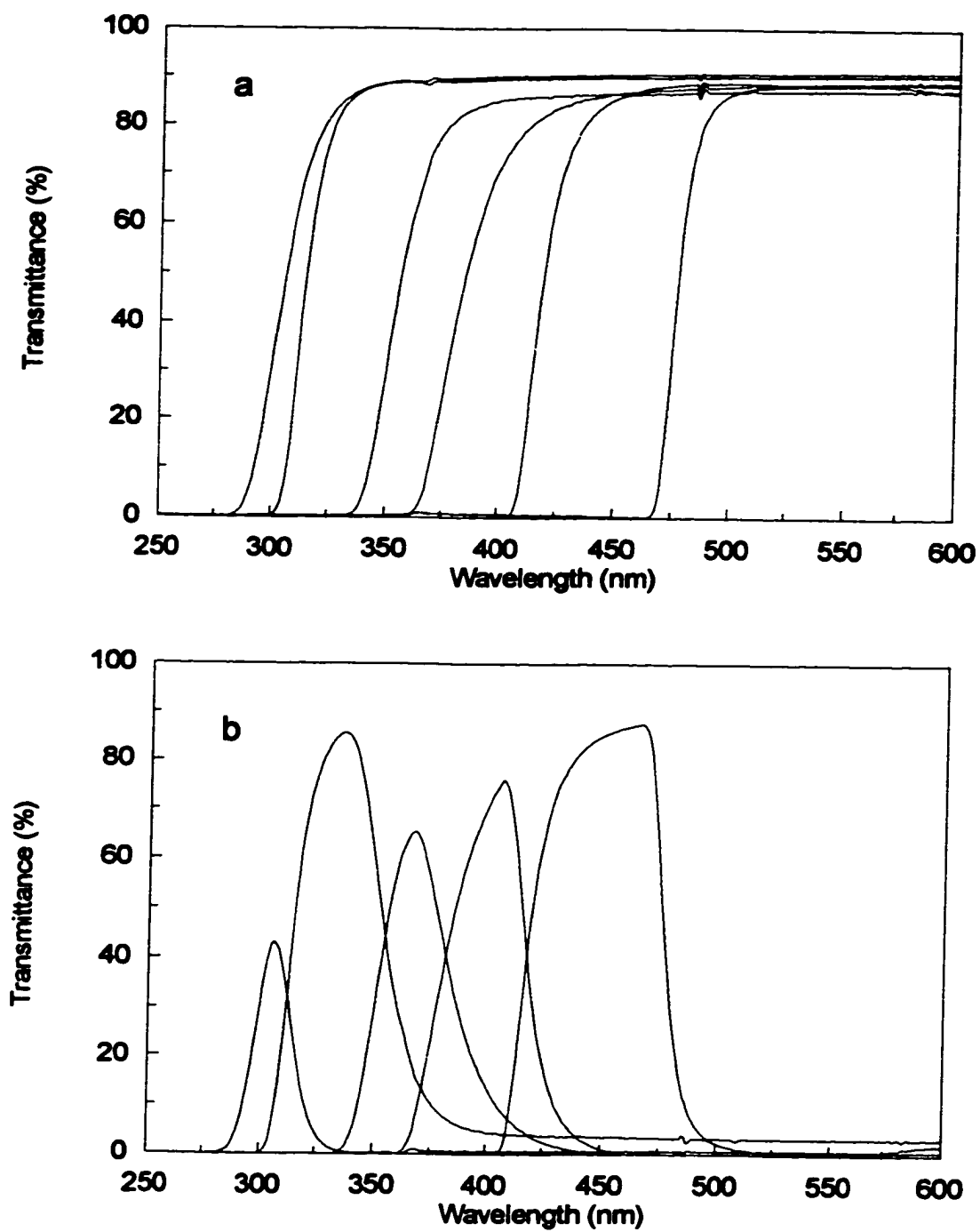
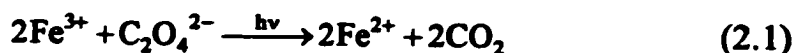


Figure 2.8 (a) Transmittance curves of six cutoff long pass light filters; (b) five quasi-monochromatic transmittance bands resulting from the mathematical difference between the six cutoff filters.

system is simple to operate, and very sensitive over a wide range of wavelengths of environmental importance. When sulphuric acid solutions of $K_3Fe(C_2O_4)_3$ are irradiated in the range from 250 to 577 nm, simultaneous reduction of iron to the ferrous state and oxidation of oxalate occur. The net photochemical reaction is



The concentration of the product Fe^{2+} was determined spectrophotometrically through its complexation with ferrozine [Stookey, 1970]. The quantum yields of Fe^{2+} formation ($\Phi(\lambda)$) and fractions of light absorption ($F_c(\lambda)$) of a 0.006 M ferrioxalate over 1 cm pathlength have been accurately determined, and are plotted in Figure 2.9 using the tabular data of Leifer [1988]. A piece-wise linear regression of Leifer [1988] data was used to estimate $\Phi(\lambda)$ and $F_c(\lambda)$ over the spectrum from 250 to 550 nm.

The irradiance impinging on a reaction system can be calculated, based on the theoretical considerations presented in Leifer [1988] with the following mathematical expression:

$$-(d[C]/dt)_d(\lambda) = 10^{-3} \Phi_d(\lambda) I_0(\lambda) (A/V) F_s(\lambda) F_c(\lambda) \quad (2.2)$$

where $(d[C]/dt)_d(\lambda)$ denotes the rate of chemical (here Fe^{3+}) concentration change ($M s^{-1}$) for a direct photochemical reaction at wavelength λ in nm, $\Phi_d(\lambda)$ is the quantum yield, $I_0(\lambda)$ is the incident light intensity in $\mu\text{Einstein cm}^{-2} s^{-1}$, A and V are the exposure area (cm^2) and volume (cm^3) of the reaction vessel, respectively, $F_s(\lambda)$ is the fraction of light absorbed by the reacting system, and $F_c(\lambda)$ is the fraction of light absorbed by the chemical of interest, here $K_3Fe(C_2O_4)_3$. $F_s(\lambda)$ and $F_c(\lambda)$ are given as below

$$F_s(\lambda) = 1 - 10^{-(\alpha(\lambda) + \epsilon(\lambda) [C]) L} \quad (2.3)$$

$$F_c(\lambda) = \epsilon(\lambda) [C] / (\alpha(\lambda) + \epsilon(\lambda) [C]) \quad (2.4)$$

where $\alpha(\lambda)$ is the attenuation coefficient of the medium (water) in cm^{-1} , $\epsilon(\lambda)$ is the molar absorptivity of the chemical in $M^{-1} \text{cm}^{-1}$, and L is the optical pathlength in

cm. The stoichiometry of reaction (2.1) indicates that the loss rate of Fe^{3+} is identical to the production rate of Fe^{2+} .

Figure 2.9 indicates that essentially all the incident light in the range 250 to 450 nm is absorbed by a 0.006 M $\text{K}_3\text{Fe}(\text{C}_2\text{O}_4)_3$ solution within 1-cm pathlength. The absorbance, $(\alpha(\lambda) + \epsilon(\lambda) [\text{C}]) L$, in this wavelength range is greater than 2 and $\epsilon(\lambda) [\text{C}]$ is much greater than $\alpha(\lambda)$. This leads to both $F_s(\lambda)$ and $F_c(\lambda)$ being essentially unity and reduces equation (2.2) to

$$-(d[\text{C}] / dt)_d(\lambda) = 10^{-3} \Phi_d(\lambda) I_0(\lambda) (A / V) \quad (2.5)$$

This equation can be used to calculate $I_0(\lambda)$ for light that is completely absorbed by the actinometer. Using the absorbance data provided by Murov [1993], calculation indicates that, for a 0.15 M and 12-cm thick $\text{K}_3\text{Fe}(\text{C}_2\text{O}_4)_3$ actinometer, the applicability of equation (2.5) can be extended up to 506 nm. For light beyond 506 nm, equation (2.2) should be employed, and the fractions of light absorbed can be derived from Murov [1993].

Equations (2.2) and (2.5) allow straightforward calculation of irradiance for experiments done with monochromatic irradiation. They are, however, not directly applicable to experiments done with full-spectrum irradiation, as is the case in this study. To resolve this problem, an approach developed by Miller [1990] is adopted, and a simplified version of its principle is given below. The change of measured $[\text{Fe}^{2+}]$ in full-spectrum irradiation results from the entire active spectrum and can be defined as

$$d[\text{Fe}^{2+}] / dt = \sum_{\lambda} [-(d[\text{C}] / dt)_d(\lambda)] = -(d[\text{C}] / dt)_d \quad (2.6)$$

Equation (2.6) can be rewritten for multi-wavelength irradiation,

$$-(d[\text{C}] / dt)_d = 10^{-3} \sum_{\lambda} \Phi_d(\lambda) I_0(\lambda) (A / V) F_s(\lambda) F_c(\lambda) \quad (2.7)$$

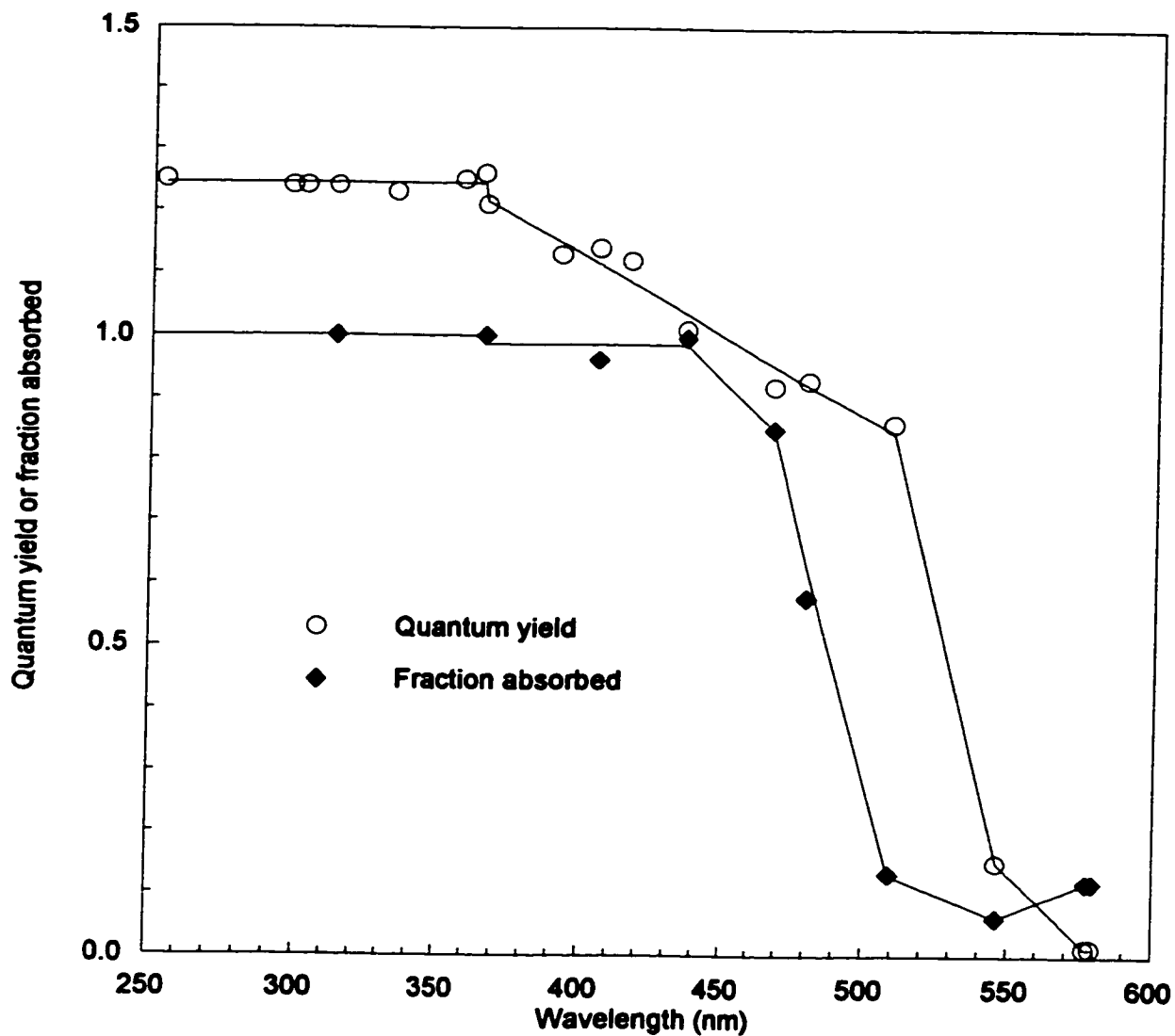


Figure 2.9 Quantum yield and fraction of light absorbed from 250 to 600 nm for a 0.006 M ferrioxalate actinometer over a 1-cm pathlength. Solid lines are best fit linear regressions of data compiled by Leifer [1988]. This figure was adapted from Miller [1990].

To determine the spectral quality and the total light intensity for the solar simulator over the entire active wavelength (250-578 nm), the spectral composition of the xenon lamp is assumed to be constant regardless of the aging of the lamp. This assumption is supported by documents and data supplied by DSET. In that case, the relative spectral irradiance ($r(\lambda)$) of the lamp, which was determined on a 2-nm interval by the manufacturer, also remains constant. Equation (2.7) can be rewritten to (2.8) by assigning the total irradiance from 250 to 578 nm to be I_0 ,

$$-(d[C]/dt)_d = 10^{-3} \sum_{\lambda} \Phi_d(\lambda) I_0 r(\lambda) (A/V) F_s(\lambda) F_c(\lambda) \quad (2.8)$$

Only I_0 is unknown in equation (2.8) and hence can be calculated,

$$I_0 = \frac{10^3 [-(d[C]/dt)_d]}{\sum_{\lambda} \Phi_d(\lambda) r(\lambda) (A/V) F_s(\lambda) F_c(\lambda)} \quad (2.9)$$

Following the procedures in Murov [1993], two stock solutions were prepared for the actinometer experiments: 1) 0.2064 M ferric sulphate, $Fe_2(SO_4)_3$ in 0.14 M H_2SO_4 , and 2) 1.2384 M potassium oxalate, $K_2C_2O_4$. Just before the experiments these two solutions were mixed thoroughly and diluted with deionized water (Nanopure UV) to obtain a 0.15 M $K_3Fe(C_2O_4)_3$ solution. The solution was then transferred into the quartz ampoules and irradiated with the solar simulator. Figure 2.10 shows the change of Fe^{2+} concentrations with irradiation time for the full-spectrum actinometer experiments. Each panel displays the result from a specific irradiation vessel. The $[Fe^{2+}]$ in each vessel showed a good linear relationship with irradiation time. However, some variation in the rate of $[Fe^{2+}]$ change was observed for different vessels with the ampoules closer to the centre of the aluminium tray showing higher values than those farther away from the centre. This variation was most likely due to the difference in the horizontal location that each vessel occupied, implying that the radiation from the light source was not

Figure 2.10 Fe(II) concentration as a function of irradiation time during full spectral exposures. Solid lines are the least-squares linear fits to the data points.

The regression equations are as follows:

$$\text{Ampoule 1: } [\text{Fe(II)}] = 79.32 + 436.57 t \quad (r^2 = 0.9894)$$

$$\text{Ampoule 2: } [\text{Fe(II)}] = 5.238 + 490.08 t \quad (r^2 = 0.9992)$$

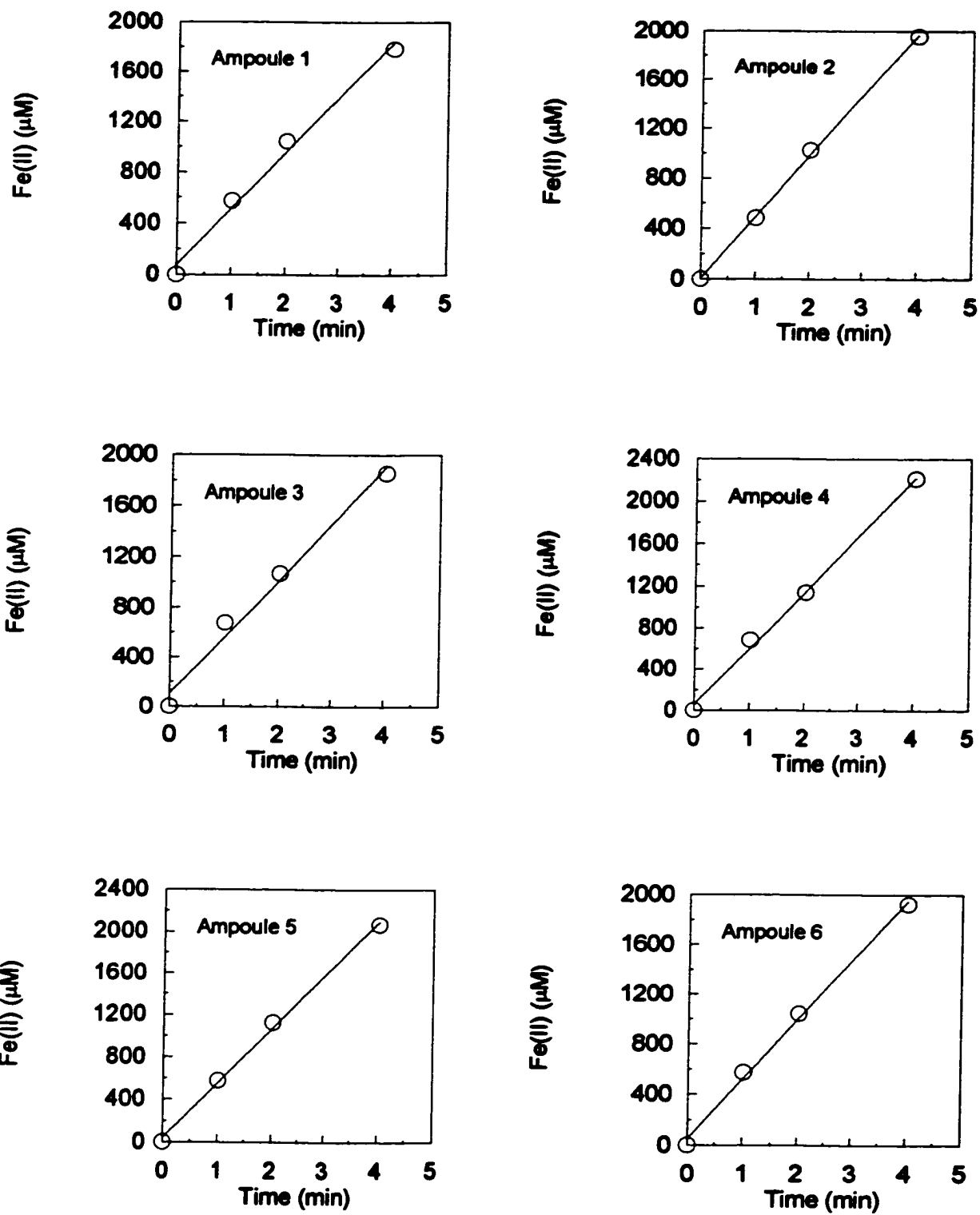
$$\text{Ampoule 3: } [\text{Fe(II)}] = 109.66 + 447.63 t \quad (r^2 = 0.9833)$$

$$\text{Ampoule 4: } [\text{Fe(II)}] = 57.94 + 538.70 t \quad (r^2 = 0.9960)$$

$$\text{Ampoule 5: } [\text{Fe(II)}] = 41.46 + 511.48 t \quad (r^2 = 0.9975)$$

$$\text{Ampoule 6: } [\text{Fe(II)}] = 50.35 + 472.74 t \quad (r^2 = 0.9967)$$

Figure 2.10



homogeneously distributed over the specimen surface even though a parabolic reflector was used. After correction for the filtration by the quartz window, the average incident light intensity measured with the ferrioxalate actinometer was $0.158 \mu\text{Einsteins cm}^{-2} \text{ s}^{-1}$ with a relative standard deviation of 7%. The largest irradiance ($0.171 \mu\text{Einsteins cm}^{-2} \text{ s}^{-1}$) was found in the vessel closest to the centre, which was 15% lower than the value ($0.202 \mu\text{Einsteins cm}^{-2} \text{ s}^{-1}$) provided by DSET for the corresponding spectral range (250-578 nm). The DSET's measurement was made at the centre of an aluminium specimen tray using an OMAR-II system. The difference between this study and DSET could partly be due to the difference in the position at which the irradiance was measured, and partly because the specimen tray, attached to the bottom of the solar simulator during the DSET's measurement, reflects more light than does the tray used in this study.

The spectral output distribution of the solar simulator was obtained by multiplying the total light intensity determined with ferrioxalate actinometry by the relative spectral irradiance provided by DSET. In Figure 2.11, a comparison is made of the output spectrum of the solar simulator with that for midday, mid-summer sunlight at 40°N [Zepp and Cline, 1977]. The solar simulator closely approximated the solar spectrum for UV and visible light with the exception of elevated spikes over the wavelength range from 450 to 500 nm.

Quantification of light intensity for wavelength-dependent irradiation was also done using ferrioxalate actinometry. The procedure was similar to that for the full-spectrum irradiation except that the lamp filter was removed and the light filters were placed between the two aluminum plates (Figure 2.7). Because of the inhomogeneity of radiation distribution, the rate of $[\text{Fe}^{2+}]$ change under the WG305 filter (cutoff at 286 nm) was found to be appreciably lower than that under the WG320 (cutoff at 302 nm) filter. In order to correct for the effect of non-

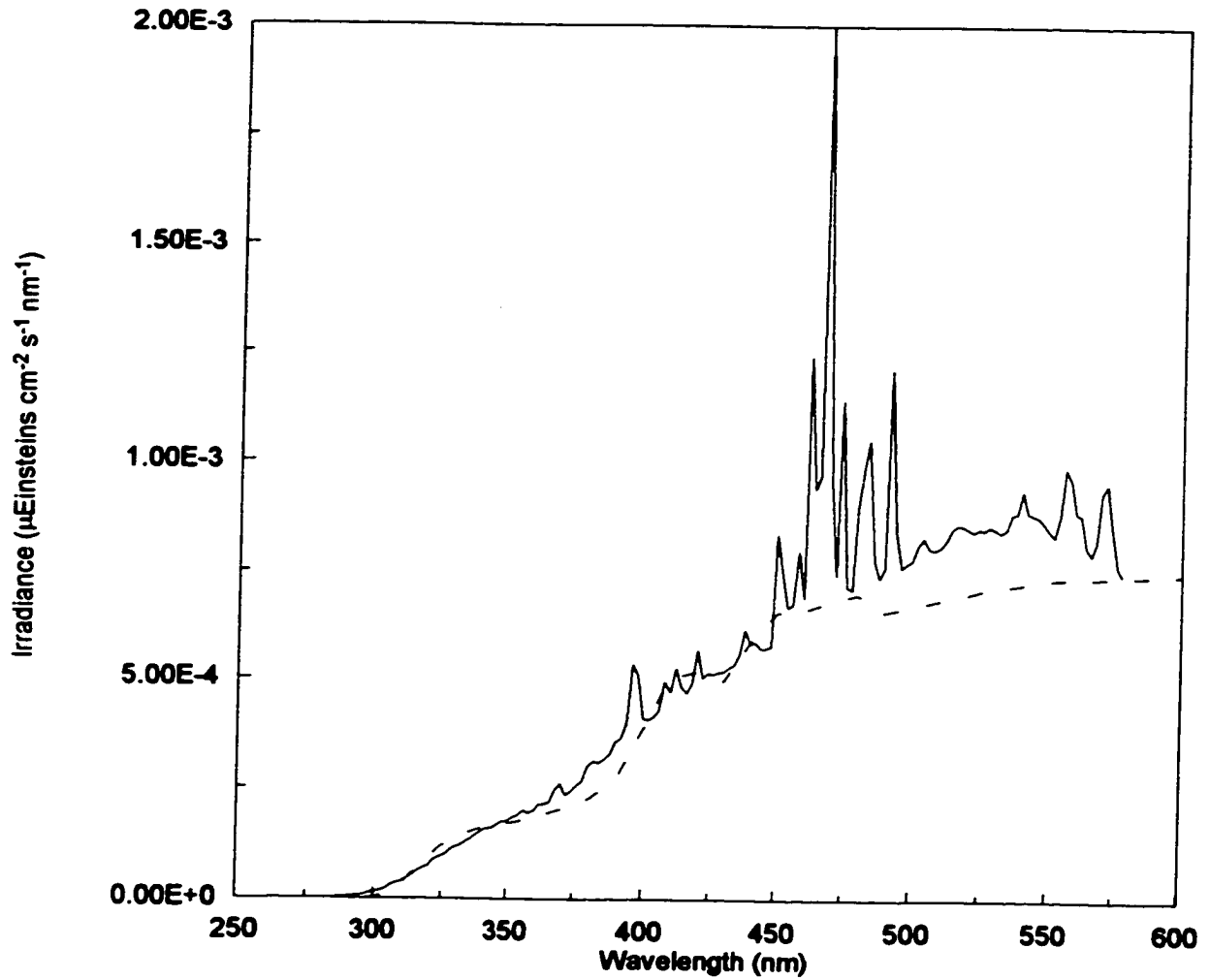


Figure 2.11 Output spectrum of the solar simulator (solid line). Dashed line is the solar spectrum for mid-day, mid-summer sunlight at 40°N [Zepp and Cline, 1977].

uniform radiation distribution, the rate of $[\text{Fe}^{2+}]$ change for each vessel was determined with the WG305 filter in place. A correction factor for each vessel was then obtained by dividing the rate of $[\text{Fe}^{2+}]$ change for that vessel by the lowest rate of $[\text{Fe}^{2+}]$ change observed. Table 2.3 shows the rate of $[\text{Fe}^{2+}]$ change as a function of cutoff wavelength before and after correction for the effect of non-uniform light distribution. The differential spectral irradiance between the successive light filters was obtained using the relative light intensity for the bare lamp as provided by DSET, the transmittance data of the light filters and the integrated irradiance in each vessel determined with the chemical actinometer (Figure 2.12). In this calculation, the relative light intensity within the exposure compartment is assumed to be constant, irrespective of non-uniform distribution of the integrated irradiance. The long tails of the first two light bands in Figure 2.12 result from the discrepancy between the maximal transmittances of filters WG305, WG320 and WG345 (see Figure 2.8). Calculations made using the determined CS_2 quantum-yield spectra indicate that the contributions of the two tails (longer than 345 nm for the first and longer than 390 nm for the second) to the total CS_2 generation from each of the bands are negligible (<1%).

2.3.5 Measurement of optical absorbance

Water samples for optical absorbance measurement were passed through acid-cleaned 0.2- μm nylon filteres (Millipore) immediately after collection from the Knudsen bottles or the bucket. The samples were then stored in 100-mL glass bottles and refrigerated (2°C). The glass bottles had been combusted at 670°C for ~12 hrs in a Muffle furnace (Barber-Colman), soaked in 0.5-M HCl for 24 hrs and finally thoroughly rinsed with deionized water (Nanopure UV). The water samples were subsequently transported to Dalhousie University for absorbance measurement using an HP 8453 diode array spectrophotometer fitted with a 10-cm

Table 2.3 Rate of Fe(II) change ($\mu\text{M min}^{-1}$) before and after correction for non-uniform distribution of incident light in the solar simulator.

Cutoff λ nm	Rate of Fe(II) change		correction factor
	Before correction	After correction	
286	481.7	454.4	1.060
302	536.8	442.4	1.213
337	438.2	423.0	1.036
362	369.7	369.7	1.000
407	305.5	255.1	1.198
468	106.8	106.4	1.004

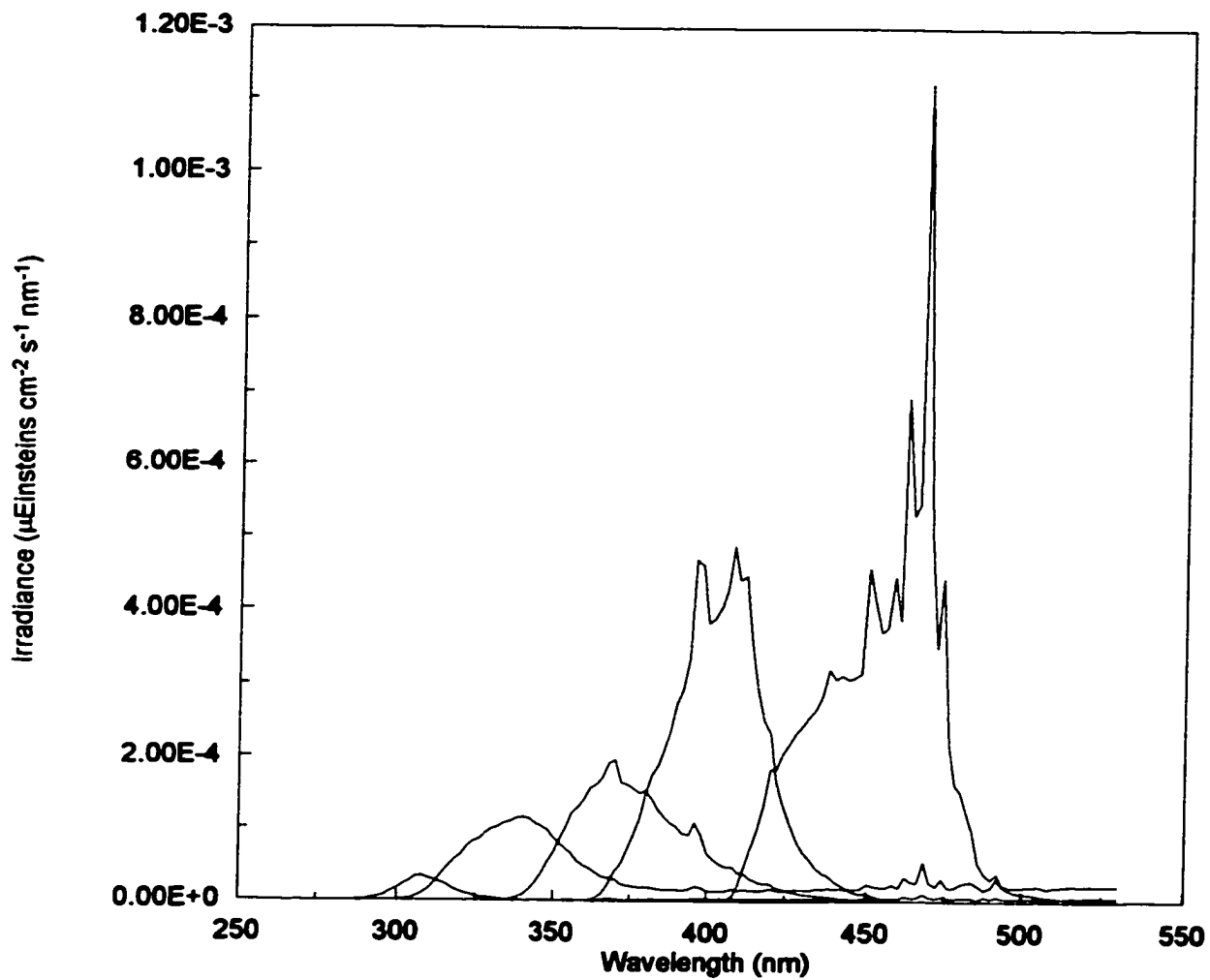


Figure 2.12 Differential spectral irradiance between the successive sharp cutoff light filters.

quartz cell. Absorption spectra were measured with a spectral resolution of 1 nm and referenced by purified water from a Nanopure UV system. Correction was made for the refractive index effect by deducting the average apparent absorption from 700 to 800 nm [Blough et al. 1993].

2.4 Laboratory culture experiments*

2.4.1 Cultures

Isolates of *Chaetoceros calcitrans*, *Synechococcus* sp., *Phaeodactylum tricorutum* and *Isochrysis* sp. were obtained from the Provasoli-Guillard National Center for Culture of Marine Phytoplankton, Boothbay Harbor, ME, USA, *Porphyridium purpureum* from the Culture Collection for Algae and Protozoa, Dunstaffnage Marine Laboratory, Oban, Scotland, UK, and *Phaeocystis* sp. from Jacqueline Stefels of the University of Groningen, Netherlands [Stefels and van Boekel, 1993]. An index of cultures is shown in Table 2.3. All the experimental cultures were grown in GF/F-filtered seawater collected in Labrador Sea (250 m depth) and used modified *f*-medium [Guillard and Ryther, 1962]. Prior to autoclaving, all the media were bubbled for 24 hours with CO₂-enriched (5000 ppmv) UHP air to reduce the level of naturally occurring CS₂ and lower the pH to ~7.2 to prevent precipitation of nutrients during autoclaving.

2.4.2 Culture apparatus

The culture vessels were made of Pyrex glass and designed for growing phytoplankton in a controlled environment while allowing the sampling compounds of interest in the gas phase. Figure 2.13 shows a schematic illustration

* This work was conducted in collaboration with Dr. M. G. Scarratt, who was then a postdoctoral fellow of Dr. R. M. Moore, and was examining the significance of production of halogenated carbon compounds (especially methyl chloride and methyl bromide) from marine phytoplankton cultures.

Table 2.4 Cultures and species examined

Culture	Species	Strain	Temp. (°C)	Medium type
01Ccal	<i>Chaetoceros calcitrans</i>	CCMP1315	18	f/8 (45 µM nitrate)
02Syn	<i>Synechococcus</i> sp.	CCMP1334	18	f/8 (45 µM nitrate)
03Tiso	<i>Isochrysis</i> sp.	CCMP1324	18	f/8 (45 µM nitrate)
04Con	Control for cultures 01-03		18	f/8 (45 µM nitrate)
05Ppur	<i>Porphyridium purpureum</i>	CCAP1380/3	18	f/8 (45 µM nitrate)
06Ppur	<i>Porphyridium purpureum</i>	CCAP1380/3	18	f/8 (45 µM nitrate)
07Con	Control for culture 05-06		18	f/8 (45 µM nitrate)
08Phcys	<i>Phaeocystis</i> sp.		15	f/8 (25 µM nitrate)
09Phcys	<i>Phaeocystis</i> sp.		15	f/8 (25 µM nitrate)
10Ptri	<i>Phaeodactylum</i> <i>tricornutum</i>	CCMP630	15	f/8 (25 µM nitrate)
11Ptri	<i>Phaeodactylum</i> <i>tricornutum</i>	CCMP630	15	f/8 (25 µM nitrate)
12Con	Control for cultures 08-11		15	f/8 (25 µM nitrate)

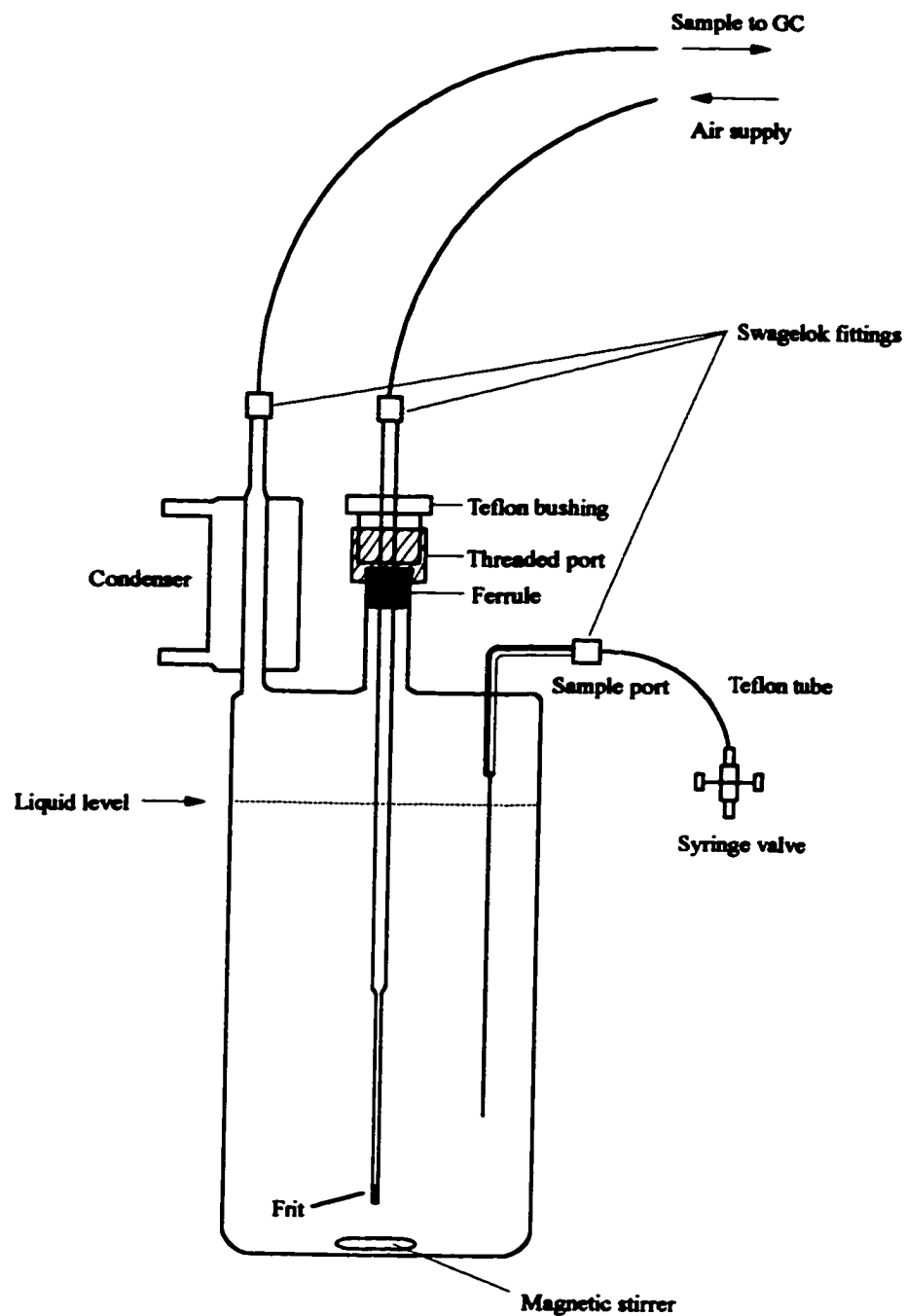


Figure 2.13 Schematic diagram of the glass culture vessel showing air inlet port, sample port, condenser and connection to gas chromatograph. This figure was adapted from Scarratt and Moore [1996].

of the culture vessel. The vessel contained ~1 L of culture medium with ~190 mL of headspace available. A fine glass frit (Ace Glass type D, 5 × 10 mm) was used to sparge the vessel with CO₂-enriched (5000 ppmv) UHP air. Gas samples were carried by an exhaust tube, and the moisture content of the gas stream was reduced by a condenser. Inserted through a third port in the vessel was a Teflon sampling tube fitted with a Mininert syringe valve (Alltech) for withdrawing culture samples without introduction of atmospheric contamination. A 2.5-cm Teflon-coated magnetic bar was used to stir the culture with the stirring speed kept as low as possible to minimise the damage to the algal cells. Up to six culture vessels could be grouped together in a temperature-controlled water bath.

2.4.3 Inoculation

The medium-filled culture vessels and rotary valves were assembled and autoclaved as a single unit. During autoclaving, the exhaust ports were capped with cotton-filled glass vials to prevent particulate or bacterial contamination, while allowing pressure equilibration in the culture vessels. After autoclaving, the vessels were allowed to cool, and then immersed in the water bath. Each vessel was sparged for 12 hours with the CO₂-enriched UHP air stream (50 mL min⁻¹) to remove any residual volatile compounds and lower the pH to redissolve any precipitate formed during autoclaving. Inoculations for *Phaeocystis sp.* and *P. tricornutum* were made via the Teflon sampling tube. All other inoculations were made using a pre-sterilised glass syringe (Popper Perfektum) with a long needle inserted through the exhaust port for all the cultures. To prevent contamination from the ambient air, the sparge stream was flowing while the inoculations were conducted. Half mL of inoculum was injected for *P. tricornutum* and 5 mL for all the other cultures. The cultures were illuminated by four fluorescent tubes

(*Sylvania cool-white*) with a diel light/dark cycle of 17/7 and an irradiance of $\sim 120 \mu\text{Einsteins m}^{-2} \text{s}^{-1}$, as measured with a submersible scalar radiometer (Li-Cor).

2.4.4 Culture sampling

Culture samples were withdrawn through the Teflon sampling tube with a sterile plastic syringe. Samples were taken daily in the early stage of growth and every few days in stationary phase. Sample volume was 15 mL and was subdivided for the following analyses.

Cell or bacterial population density was determined by epifluorescence microscopy on filtered, acridine orange stained samples (2 mL). Twenty fields were counted on duplicate slides and the results averaged. Chlorophyll-*a* (Chl-*a*) samples (2 mL) were filtered onto 25-mm GF/C discs and measured with the method of Parsons et al. [1984], using a Turner Designs (Model 10-005R) fluorometer. Medium pH (1 mL sample) was determined using a Fisher Accumet Model 320 hydrogen electrode and meter. An autoanalyser [Grasshoff and Almgren, 1976] was employed to assess nutrient concentrations (nitrate and phosphate) on a filtered 10 mL sample.

2.4.5 Gas sampling

Gas samples were taken every few days and carried by the exhaust tube to a sampling loop. The gas stream passing through the sampling loop could be isolated and injected into the cryotrap and then analysed by the oxygen-doped GC/ECD or the GC/MS. Sample volume was 80, 40 or 6 mL, depending on the concentrations of measured compounds in the vessels. Equilibrium between the gas and the liquid phases was assured by sparging the vessel for 2-4 min with CO₂-enriched (5000 ppmv) UHP air at a flow rate of 50 mL min⁻¹. The flow rate was controlled with mass flow controllers (Tylan) and manually-operated rotary valves (Valco). The

oxygen-doped GC/ECD was used for analysing samples from the cultures of *C. calcitrans*, *Synechococcus* sp. and *Isochrysis* sp.. For all the remaining cultures, analysis was done using the GC/MS. A technical failure of the GC/MS resulted in a 2-week interruption (between day 13 and 27) of sampling for the cultures of *P. tricornutum* and *Phaeocystis* sp.

The measured concentration of CS₂ in the headspace is converted to the concentration in the liquid phase using the Henry's law constants for this compound [Elliott, 1989]. The total CS₂ amount in each vessel is, thus, obtained by summing the amounts in the headspace and the culture medium. Corrections are made for CS₂ loss by sampling and sparging, and also for changes in the culture and headspace volumes.

2.5 Water temperature, salinity, wind speed, and Chl-*a*

During all the ocean investigations, seawater temperature and salinity were recorded by a conductivity-temperature-depth (CTD) profiler attached to a rosette or hydrowire, or in the case of bucket samples, temperature was measured using a thermocouple. Surface water temperature and salinity during the *Challenger* cruise were monitored with a resolution of 1 min using a TSG-103 thermosalinograph (Ocean Data Equipment Corporation). Chl-*a* concentration during the *Hudson* and *Discoverer* cruises was determined by fluorometry on acetone extracts [Holm-Hansen et al., 1965] calibrated by high pressure liquid chromatography [Head and Horne, 1993]. During the *Challenger* cruise surface fluorescence was measured at 1 min interval with a Chelsea Instruments Aquatracka fluorometer. Subsurface fluorescence measurements were made with a Seatech fluorometer mounted on a CTD unit. The fluorescence data were converted to chl-*a* concentrations using a calibration equation established by correlating fluorometrically assayed extracted chl-*a* values with the contemporaneous fluorometer voltages. Wind speeds were

recorded using anemometers during the *Discoverer* and *Challenger* cruises, but visually estimated by during the *Hudson* cruise. Thus, the *Hudson* wind speed data are approximations only.

Chapter 3 Carbon Disulphide Distributions in the Oceans

3.1 Carbon disulphide in surface water

3.1.1 Concentrations

Carbon disulphide in seawater was measured during three cruises in the North Atlantic and the Pacific Ocean. The surface water concentrations of CS₂ for each sampled area are shown in Table 3.1. Relative to open ocean waters, higher concentrations were observed in coastal waters. The concentration in near-shore waters off Nova Scotia (stations H39 and H40) and Greenland (stations H19 and H20) ranged from 18 to 35 pM S and averaged 26 pM S. Samples taken near or within Galway Bay, Ireland (stations C4, C5, C6, C14 and C15) showed a concentration range from 20 to 48 pM S with a mean value of 33 pM S. The overall mean concentration (30 pM S) in the coastal areas was more than twice that found in the open ocean waters (13 pM S). The mean concentrations in the open ocean for the three cruises fell in a fairly narrow range (12 to 15 pM S), whereas the concentration ranges for the *Hudson* (8-26 pM S) and *Discoverer* (7-28 pM S) cruises were significantly greater than the range for the *Challenger* cruise (8-18 pM S). This observation could result from wider ranges of physical and biological properties spanned by the *Hudson* and *Discoverer* transects (see Chapter 2, Figures 2.1a-c). Pooling the coastal and open ocean data together, the concentration observed in this study averaged 15 pM S and ranged from 8 to 48 pM S.

Lovelock [1974] made CS₂ measurements in the waters off the Beara peninsula in western Ireland and in the open Atlantic. He reports the mean concentrations to be 21 ± 12 pM S ($n = 8$) and 14 ± 4 pM S ($n = 35$) in the coastal and open ocean waters, respectively. This is in good agreement with the results from this study. Kim and Andreae [1987a] conducted three field surveys in the North Atlantic (25°

Table 3.1 CS₂ concentrations (pM S) in surface waters

Area	Research vessel	n	Concentration Mean \pm SD	Concentration Range
<i>Coastal waters</i>				
NW Atlantic	<i>Hudson</i>	4	26 \pm 7	18-35
NE Atlantic	<i>Challenger</i>	4	33 \pm 12	20-48
Overall		8	30 \pm 10	18-48
<i>Open ocean</i>				
NW Atlantic	<i>Hudson</i>	13	13 \pm 5	8-26
NE Atlantic	<i>Challenger</i>	27	12 \pm 2	8-18
Pacific	<i>Discoverer</i>	17	15 \pm 6	7-28
Overall		57	13 \pm 4	7-28

-44°N, 66°-81°W) off the east coast of the United States from April to September, 1986. They obtained a mean surface concentration of 16 ± 8 pM S ($n = 95$) in offshore waters, and of 33 ± 19 pM S ($n = 110$) in coastal waters. The values of Kim and Andrea [1987a] are slightly higher than both those of Lovelock [1974] and of this study, probably due to the difference in the geographic coverage. Kim and Andreae [1987a] limited their investigations to the mid-latitudes of the North Atlantic, while the areas explored by the other two groups covered waters in the southern hemisphere and higher latitudes of the North Atlantic. On the other hand, Kim and Andreae [1987a] made many more observations (particularly for coastal waters) than did Lovelock [1974] and this work. Thus, for their specific study region, the data from Kim and Andreae [1987a] may be more representative.

3.1.2 Carbon disulphide and sea surface temperature

Figures 3.1a-c show the patterns of CS₂ distributions with those of sea surface temperature (SST). Wide ranges of SST were encountered during the *Hudson* (0.6°-23.3°C) and *Discoverer* (15.1°-28.8°C) cruises while SST remained within a rather narrow range (12.0°-14.6°C) during the *Challenger* cruise since the ship moved within a relatively small area. Visual examination of the plots indicates that data points obtained at the coastal stations for the *Hudson* cruise greatly deviate from the general trend found for the open ocean waters. For this reason, a plot that excludes the coastal data is also presented for this cruise and description of this data set was focused on the open ocean stations. The graphs for the *Hudson* and the *Discoverer* cruises (Figures 3.1a-b) clearly show that CS₂ was more abundant in warm waters than in cool waters. The CS₂ concentration was more than doubled crossing from the cool Labrador Sea waters into the warm Gulf Stream waters (stations H30 and H33). Similarly, the concentration of CS₂ in the Pacific Ocean decreased almost four times from the warm equatorial and tropical waters to the

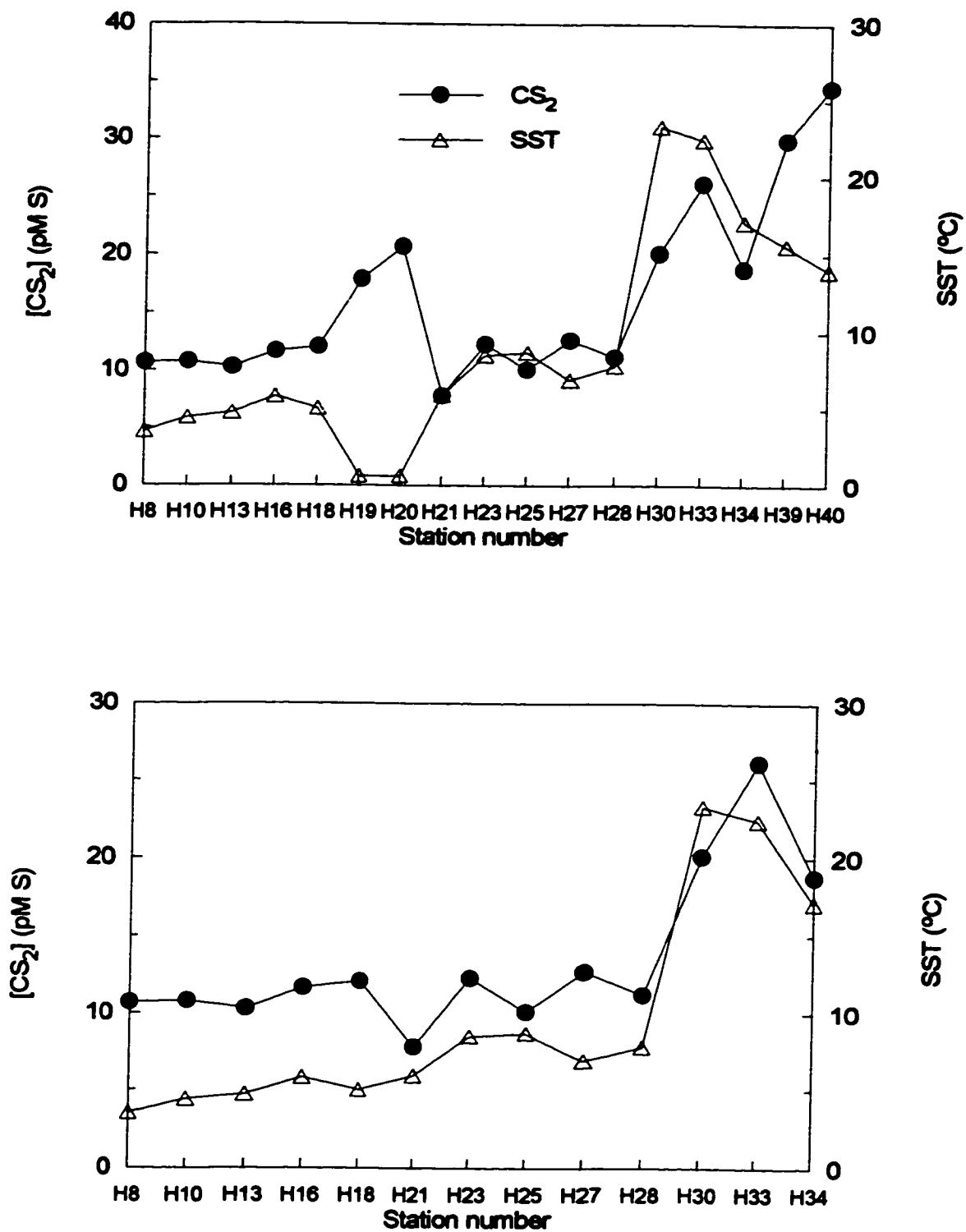
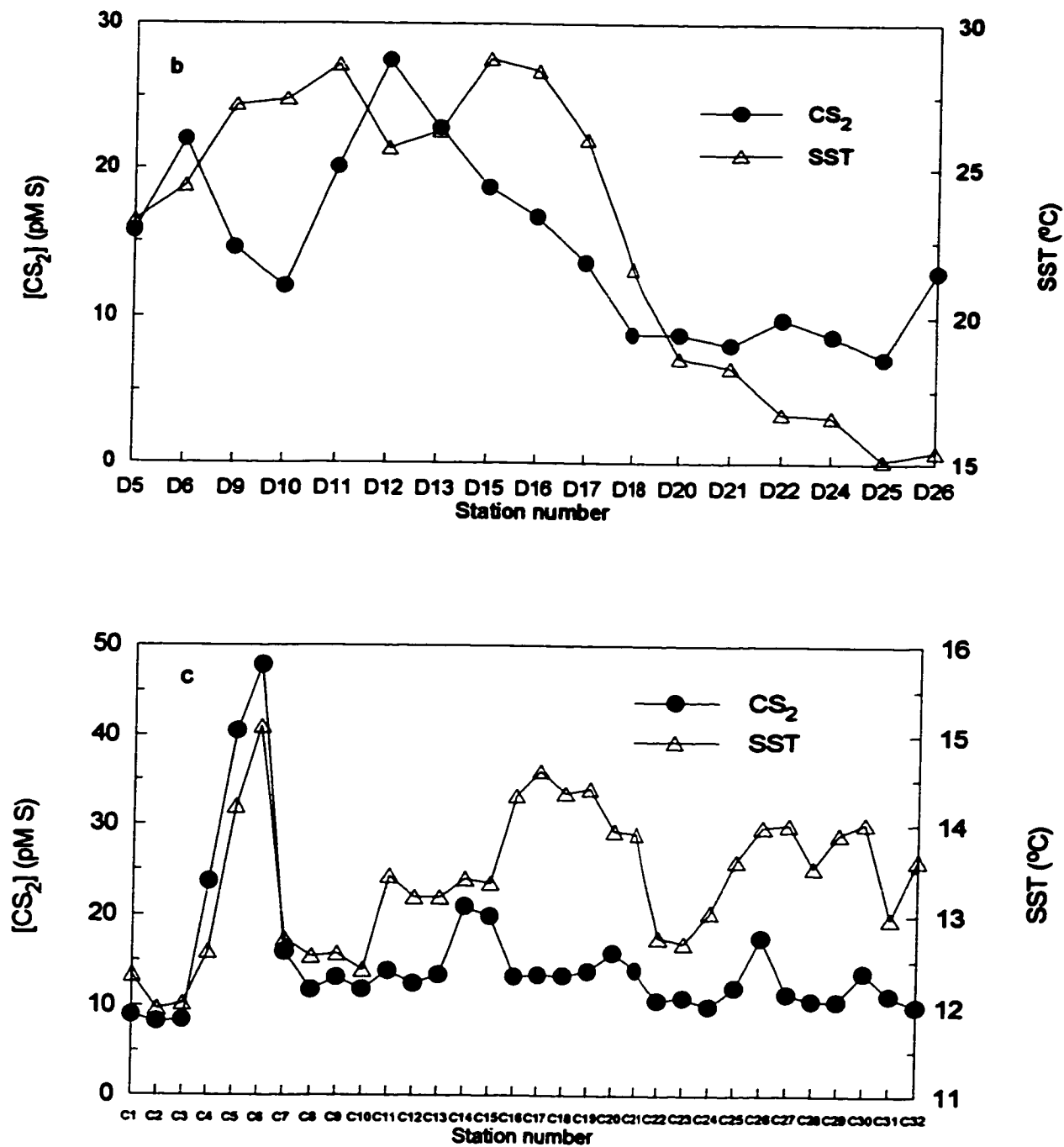


Figure 3.1a Concentration of CS_2 and temperature in surface water along the cruise track of *Hudson*. Lower panel excludes the coastal stations.



Figures 3.1b-c Concentration of CS₂ and temperature in surface water along the cruise tracks of *Discoverer* (b) and *Challenger* (c).

cool temperate waters in the southern hemisphere. Elevated CS₂ levels in the warm Gulf Stream waters were also reported by Kim and Andreae [1987a]. Although SST from the *Challenger* cruise was restricted to a small range, the general distribution pattern of CS₂ was still similar to that of the SST.

Linear regression analysis between CS₂ and SST generates the following relations:

$$\text{Hudson cruise } [CS_2] = 6.9 + 0.7 t, r = 0.918, n = 13 \quad (3.1)$$

$$\text{Discoverer cruise } [CS_2] = -3.8 + 0.8 t, r = 0.676, n = 17 \quad (3.2)$$

$$\text{Challenger cruise } [CS_2] = -52.3 + 5.0 t, r = 0.474, n = 32 \quad (3.3)$$

where [CS₂] is the concentration of CS₂ in pM S, t is sea surface temperature in degrees Celsius, r is the correlation coefficient and n is the number of observations. All three equations show significant positive correlation between the CS₂ concentration and SST at 1% significance level. Because of lack of low temperature (<10°C) data in deriving Equations 3.2 and 3.3, the two equations predict negative concentrations in cold waters, which is obviously unrealistic. Equation 3.1 is more representative than the other two since it was obtained from a data set covering both cold and warm waters. However, this equation suffers from scarcity of intermediate water temperatures (10°-15°C). Pooling all the open ocean data from the three cruises, a significant correlation between CS₂ and SST still exists:

$$[CS_2] = 7.5 + 0.4 t, r = 0.576, n = 57$$

During an investigation of waters off the eastern United States, Kim and Andreae [1992] found a positive correlation between CS₂ concentration and SST in oceanic waters, but a negative correlation for some shelf waters. These authors also reported that the correlation between the two terms is appreciably improved if Chl-*a*-normalised CS₂ concentration is used. Application of this technique does not improve the correlations for the present data. Instead, the correlation deteriorates

substantially compared with that using the non-normalised data. This may imply that phytoplankton is probably not the major factor that controls the surface concentrations of CS₂ during the present study.

3.1.3 Carbon disulphide and salinity

Figures 3.2a-c display the distributions of CS₂ concentration and surface water salinity along the cruise tracks. The *Hudson* cruise provides somewhat confused information on the relationship between CS₂ and salinity. The data set presents a roughly inverse covariance between CS₂ and salinity with two exceptions. One of the exceptions is the Gulf Stream water (stations H30 and H33) which was distinguished by its high salinity and high abundance of CS₂. Another exception is the near-shore waters off Newfoundland and Labrador (stations H8 and H10). Salinity was relatively low at the two locations. However, unlike other coastal stations, these two sites did not show elevated CS₂ concentrations compared with the adjacent open sea stations. A good inverse correlation explains for the remaining data points:

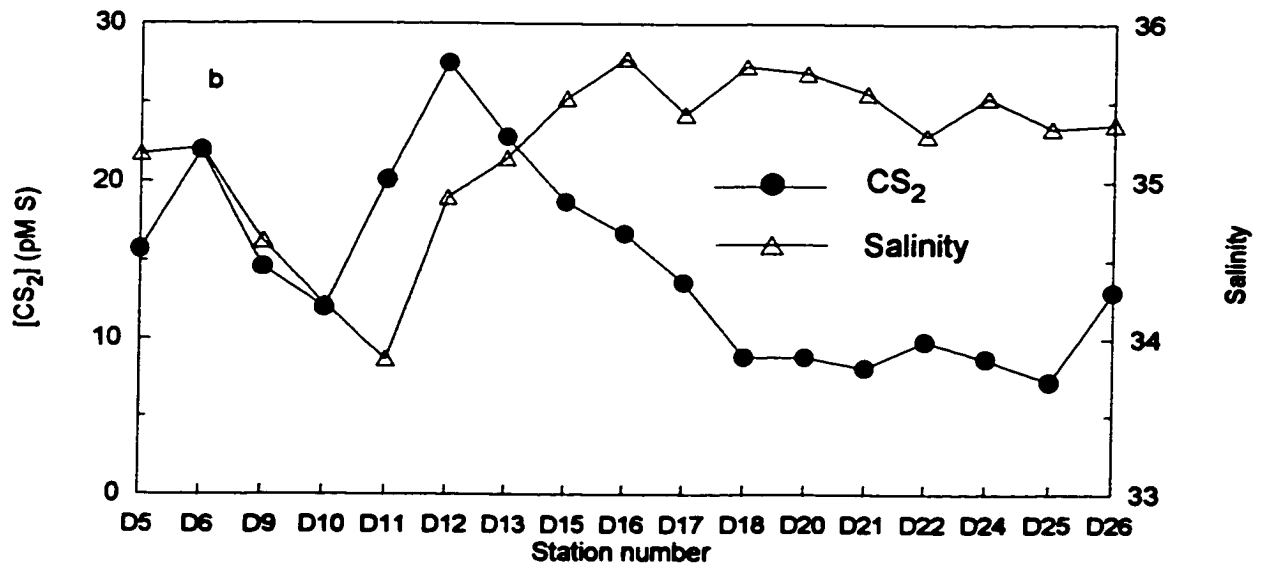
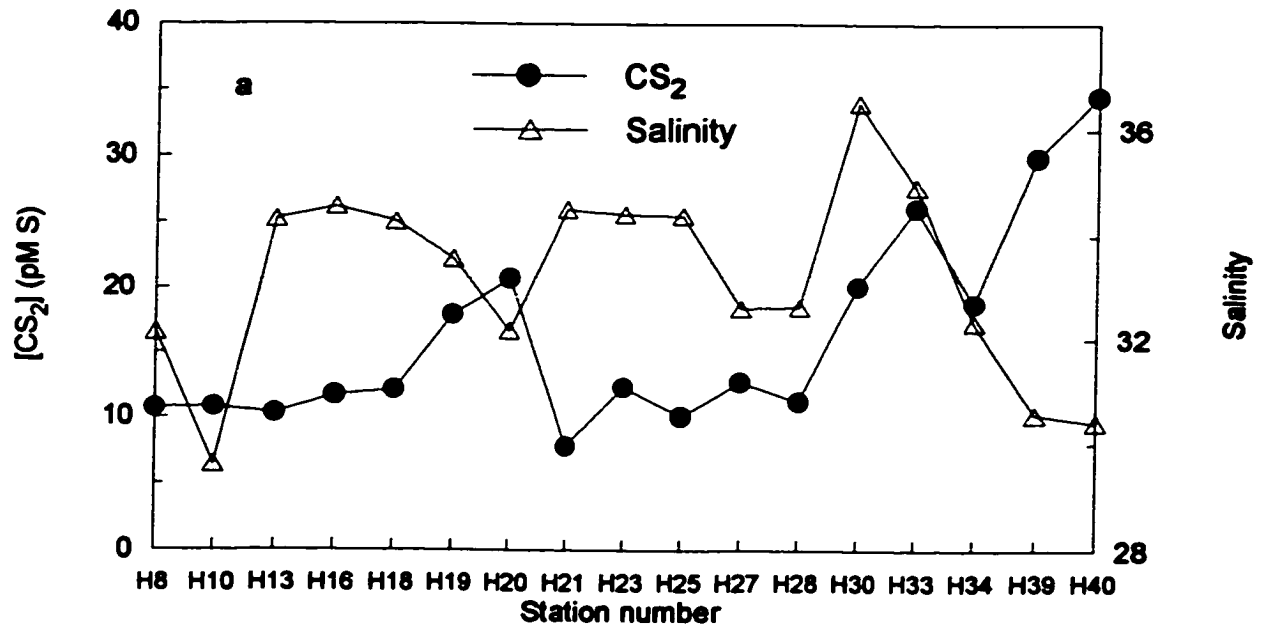
$$[\text{CS}_2] = 179.5 - 4.9 S, r = -0.899, n = 13$$

where S is salinity on the practical salinity scale. No consistent relationship between the CS₂ concentration and salinity exists for the Pacific Ocean data (Figure 3.2b).

For the *Challenger* cruise (Figure 3.2c), a negative correlation between CS₂ concentration and salinity is evident and the result of a linear regression is

$$[\text{CS}_2] = 841.9 - 23.4 S, r = -0.963, n = 32$$

Nevertheless, it must be noted that there are only three data points available with relatively low salinities (34.0-34.8). The three points were acquired at stations C4, C5, C6 that were in the north Sound of Galway Bay and possibly influenced by freshwater that runs into the bay. It is difficult to ascertain whether or not the data



Figures 3.2a-b Concentration of CS_2 and salinity in surface water along the cruise tracks of *Hudson* (a) and *Discoverer* (b).

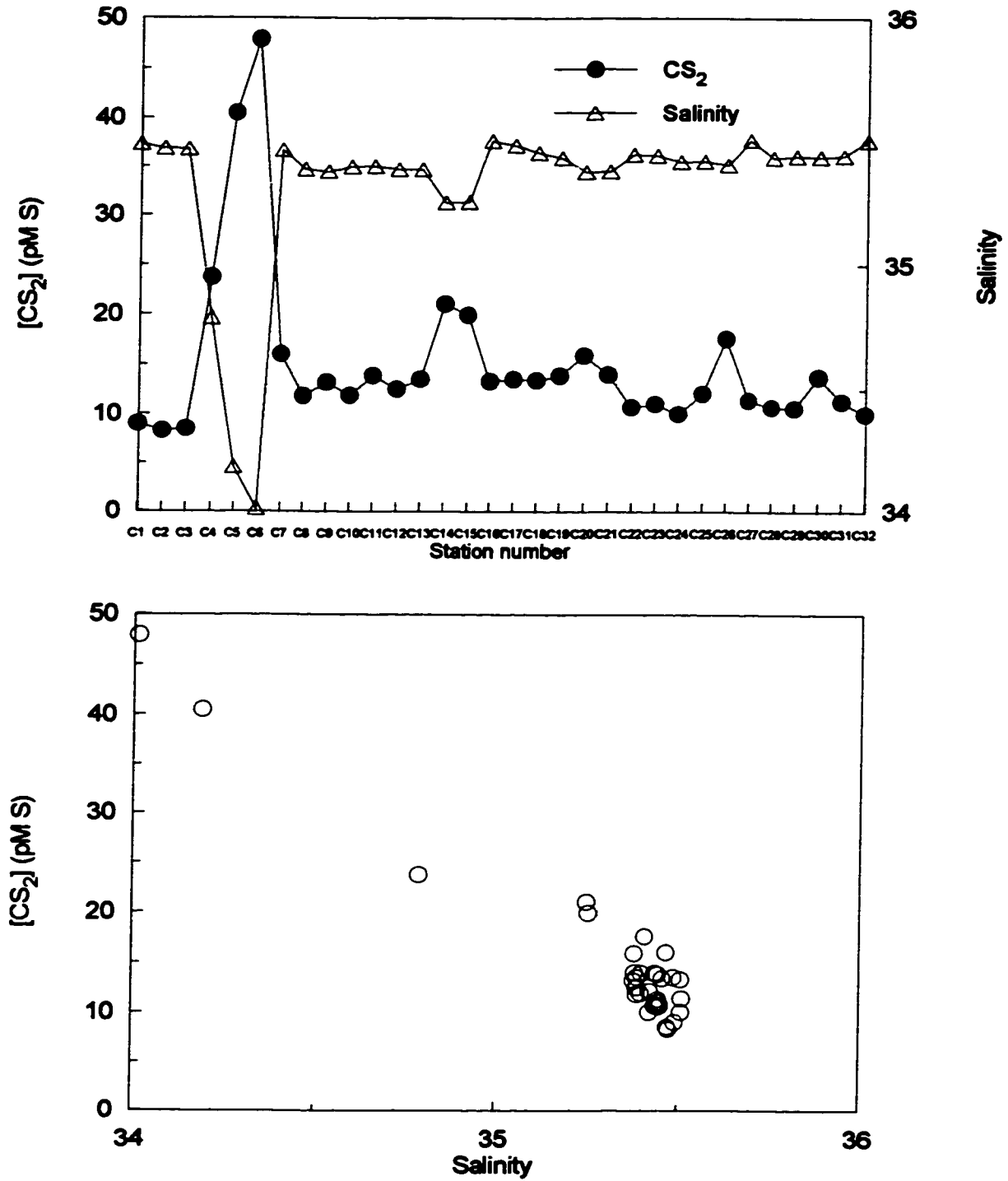


Figure 3.2c Concentration of CS_2 and salinity in surface water along the cruise track of *Challenger* (upper panel), and scatter plot of CS_2 concentration against salinity for the data from the upper panel (lower panel).

obtained from these locations could be representative of the surrounding coastal region. The majority of the *Challenger* data set is restricted to a salinity range from 35.3 to 35.5. To further illustrate the inverse trend between CS₂ concentration and salinity, the distributions of CS₂ concentration and salinity along a transect are shown in Figure 3.3. This transect runs from Galway Bay (station C6) to the open ocean (station C22). The change of CS₂ concentration nearly mirrored that of salinity.

3.1.4 Carbon disulphide and Chl-*a*

Figures 3.4a-c show the distribution patterns of surface water concentrations of CS₂ and Chl-*a*. No consistent relationship exists between CS₂ and Chl-*a* for the *Hudson* and *Challenger* cruises. This is true even if the coastal data points are removed. A notable feature for the *Hudson* data is high CS₂ concentrations found in the Gulf Stream waters (stations H30 and H33) which were characterised by extremely low Chl-*a* concentrations (<0.19 mg m⁻³) as well as high temperature and salinity. For the *Discoverer* cruise, however, an approximate covariation between the two parameters is evident with a few exceptions, particularly for stations D24-D26. Without considering the data points of these three stations, CS₂ concentration exhibits a significant positive correlation with Chl-*a* concentration:

$$[\text{CS}_2] = 8.4 + 70.3 [\text{Chl-}a], r = 0.760, n = 14$$

where [Chl-*a*] stands for Chl-*a* concentration in mg m⁻³. Kim and Andreae [1992] did not find meaningful correlation between CS₂ and Chl-*a* for most of the waters that they had surveyed in the Northwest Atlantic. The findings from the present study are generally in accordance with the results of Kim and Andreae [1992].

3.1.5 Discussion

Several implications can be drawn from the distribution of CS₂ in surface water

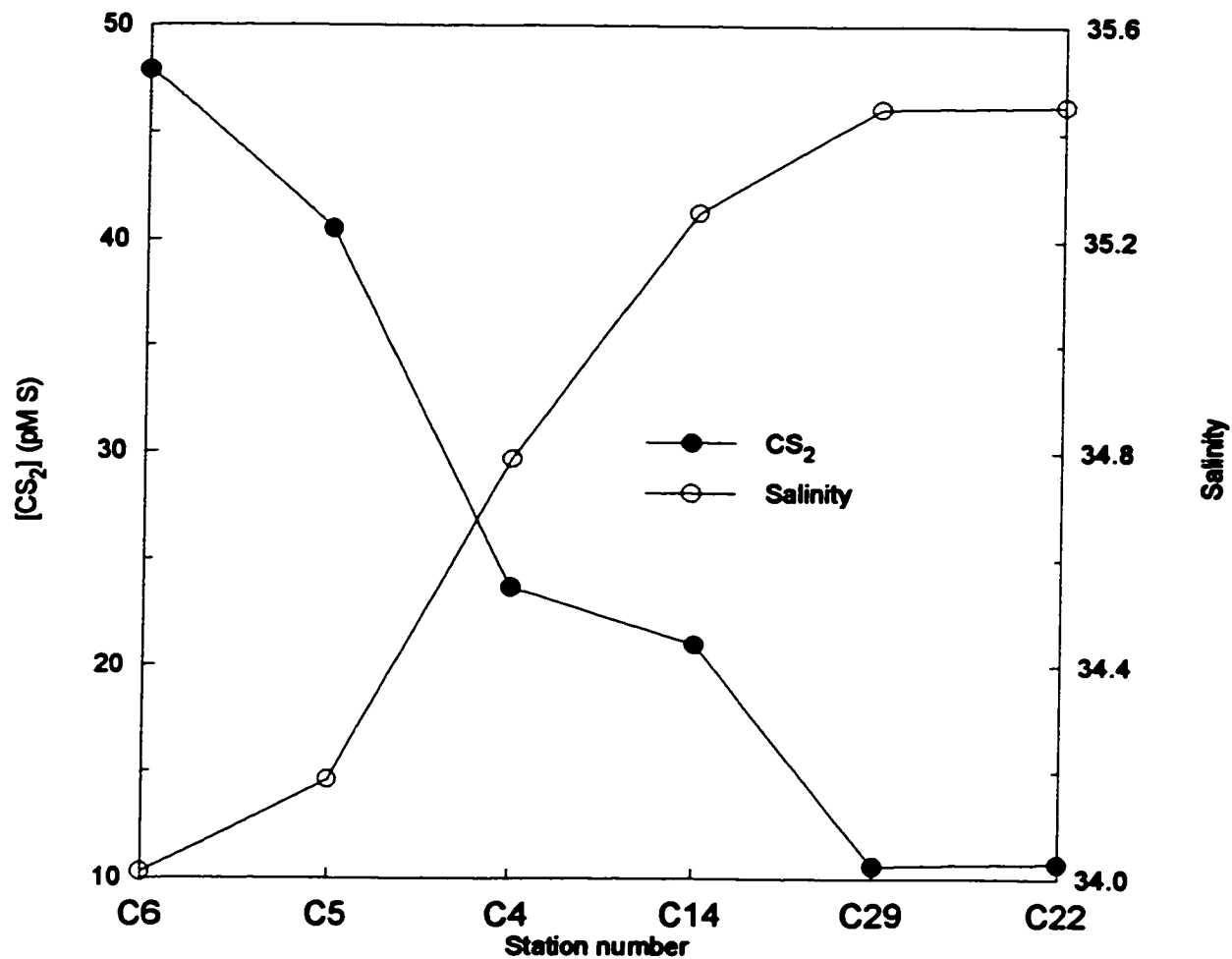
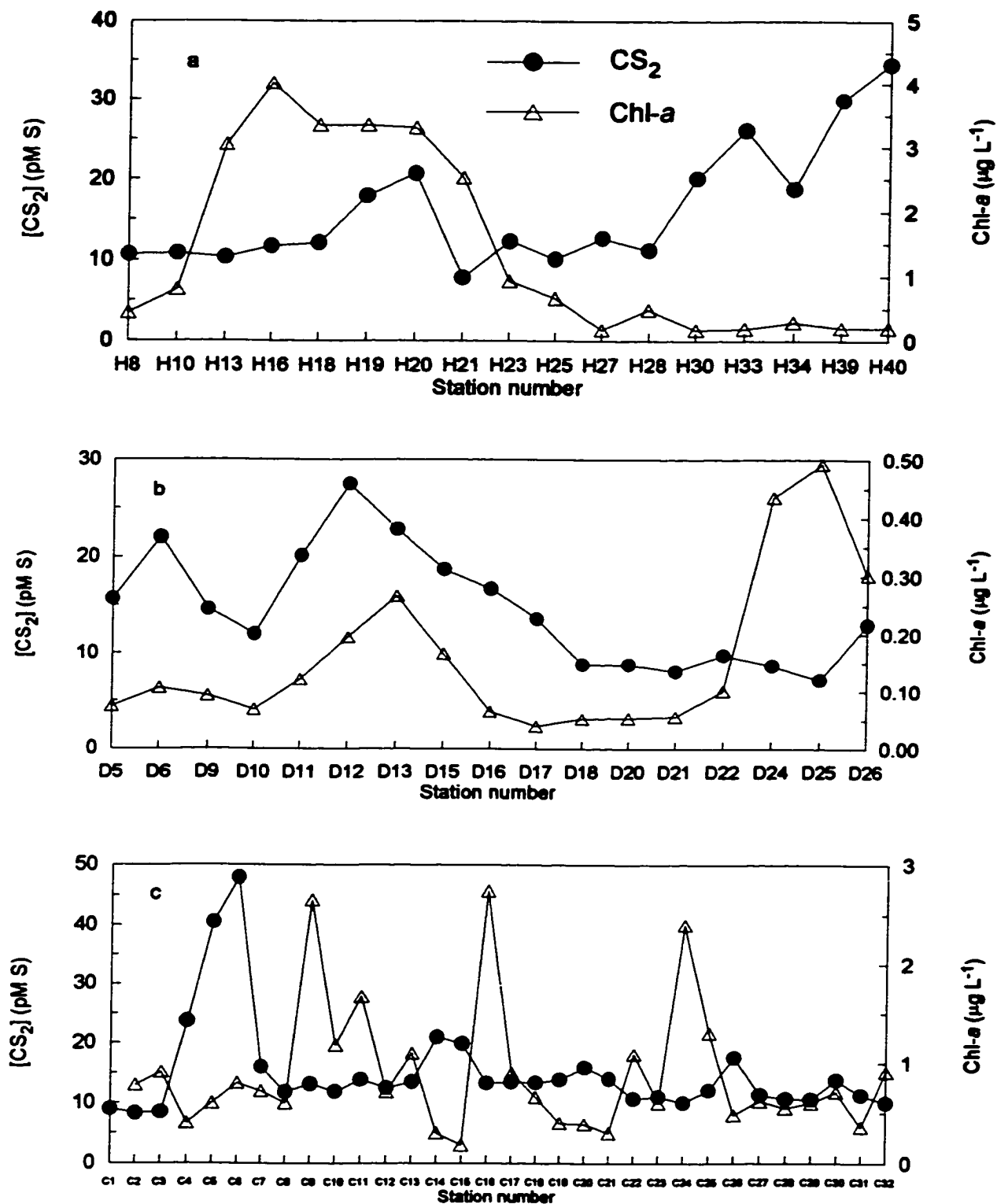


Figure 3.3 Concentration of CS_2 and salinity in surface water along a transect from Galway Bay, Ireland to the open North Atlantic. Data are from the *Challenger* cruise.



Figures 3.4a-c Concentration of CS_2 and Chl-*a* in surface water along the cruise tracks of *Hudson* (a), *Discoverer* (b) and *Challenger* (c).

and its relationship with the hydrographic parameters. The observed elevation of CS₂ concentration in coastal waters suggests that mechanisms controlling the behaviour of CS₂ in coastal waters may be different from those in open ocean waters, or that these mechanisms work at different rates in the two water bodies.

Coastal areas contain relatively large amounts of particulate organic matter originating from terrestrial runoff, aeolian transport and marine primary production. A significant portion of the particulate matter may deposit to the sea floor before it is carried to the open sea and destroyed by biological and chemical degradation. Thus, coastal sediments are usually enriched with organic matter, which facilitates the formation of anoxic environments in the sediments. Biological and/or chemical processes under anaerobic conditions have been frequently suggested to be responsible for producing a suite of volatile sulphur compounds, such as CS₂, DMS and OCS [Lovelock, 1974; Andreae, 1986; Wakeham et al., 1987; Cutter and Radford-Knoery, 1993; Zhang et al., 1998]. As the lifetime of CS₂ in seawater with respect to its chemical destruction is on the order of years or even longer [Elliott, 1990], CS₂ may be transported from the sea floor to the surface. The green-brownish water colour found in Galway Bay during our field survey was indicative of a high level of organic matter in the bay area and, thus, a low content of oxygen in both the sediments and overlying waters. Hence, anaerobic processes could be an important factor contributing to the high concentration of CS₂ in the bay.

Diffusion of CS₂ from sediments to deep waters is possible in the open ocean. However, the sedimentary source probably has little effect on the concentration of CS₂ in surface waters of the open ocean since the oceanic mixing time scale (~1000 yrs) is much longer than the lifetime of CS₂.

The elevated concentrations of CS₂ in coastal waters might also be connected to high levels of biological activity in near-shore areas. During this thesis work, I

collected CS₂ data from axenic monocultures of six species of marine phytoplankton: *Chaetoceros calcitrans*, *Phaeodactylum tricorutum*, *Phaeocystis* sp., *Porphyridium purpureum*, *Synechococcus* sp. and *Isochrysis* sp.. Of the tested species, *C. calcitrans*, *P. tricorutum* and *Phaeocystis* sp. showed the capability of producing CS₂ while the other species did not. CS₂ formation in the cultures of *C. calcitrans* and *Phaeocystis* sp. was faster in stationary phase than in log phase. In contrast, the *P. tricorutum* culture showed higher formation rates in log phase. Therefore, CS₂ production by phytoplankton in the sea is highly species-specific and dependent on physiological states of the algae. This may partly explain why clear relationships between concentrations of CS₂ and bulk phytoplankton biomass, such as Chl-*a*, are usually not observed in field surveys. For the *Hudson* and *Challenger* cruises, the Chl-*a* concentrations at the coastal stations were near or below the average Chl-*a* levels for the two investigations, suggesting that primary production at those locations was not higher than that in the open ocean. It is unknown whether the sampled coastal waters contained abundant algal species that are prolific producers of CS₂.

Solar UV-induced photochemical processes are another route for CS₂ formation in seawater. Results from the irradiation experiments conducted during the *Challenger* cruise indicate that the photoproduction rate of CS₂ is positively correlated with the absorptivity of CDOM at 350 nm, suggesting the involvement of CDOM in this production. Coastal waters dominated by terrestrial CDOM are thought to be more photochemically reactive than open ocean waters that mainly contain marine CDOM [Kieber et al., 1990; Dister and Zafiriou, 1993; Qian and Mopper, 1997]. Higher concentrations of CS₂ observed in coastal waters relative to the open oceans are probably caused in part by enhanced photoproduction of the compound in coastal areas. For instance, the photoproduction rate of CS₂ measured with water samples taken from the Northwest Arm of Halifax, Nova

Scotia, Canada was almost three times higher than that measured with the open ocean samples collected at station H33 during the *Hudson* cruise. This is consistent with the observation that the concentration in the Northwest Arm (>73 pM S) was much higher than that at station H33 (26 pM S).

An interesting finding from this study is that the concentration of CS₂ in warm and oligotrophic waters (tropical and subtropical gyres) is significantly higher than that in cool and biologically more productive waters (temperate and subarctic regions). This observation may be due to the fact that the warm waters are more intensely irradiated by solar radiation and, thus, more CS₂ is photochemically formed. Using the quantum yield data and absorption spectra of CDOM obtained during the *Challenger* cruise, I have estimated the CS₂ photoproduction rates for different latitudinal zones (see Chapter 6, section 6.6). The mean photoproduction rate of CS₂ in waters between 0° and 30°N ($40 \mu\text{mol S m}^{-2} \text{yr}^{-1}$) is almost twice that in waters between 40° and 70°N ($21 \mu\text{mol S m}^{-2} \text{yr}^{-1}$). The quantum yield and CDOM absorption data obtained from a small region of the Northeast Atlantic are assumed to be representative of other ocean areas for this assessment, which may not be necessarily true. Significant uncertainties may, therefore, exist in assessing the difference in the photoproduction between the warm and cool waters. Oligotrophic waters are enriched with DMS and its metabolic precursor, DMSP [Andreae, 1990]. Kiene [1996] demonstrated that microbial degradation of dissolved DMSP in oxic seawater can produce MeSH as well as DMS. MeSH has been shown to be a weak precursor for OCS photoproduction in seawater [Flock and Andreae, 1996; Flock et al., 1997]. It is possible that photo-degradation of MeSH might also produce CS₂. More study is needed to elucidate if the production of CS₂ is related to the production of DMSP in these waters.

The inverse correlation between CS₂ concentration and salinity is probably a combined result of physical mixing and enhanced photo-production of CS₂ in

freshwater relative to marine waters. That CS₂ concentration is positively correlated with SST for the *Challenger* data set is probably additional evidence for the involvement of physical processes, since relatively high temperatures were found at the coastal stations, particularly those within Galway Bay. The significance of horizontal transport of CS₂ can be evaluated by comparing the advective rate of CS₂ with its loss rates due to chemical destruction and emission to the atmosphere. The horizontal concentration gradient observed between stations C6 and C30 was 0.22 pM S km⁻¹. If the horizontal advection velocity in this area falls between 0.1 and 1 m s⁻¹, the advective rate would be in the range 690 to 6900 pM S yr⁻¹.

Carbon disulphide is chemically decomposed through hydrolysis and its reaction with the hydrogen peroxide conjugate base HO₂⁻ [Elliott, 1990]. The rate constant at room temperature is 1.0 × 10⁻³ M⁻¹ s⁻¹ for CS₂ hydrolysis and 20.4 M⁻¹ s⁻¹ for its reaction with HO₂⁻ [Elliott, 1990]. The concentration of HO₂⁻ is calculated from the concentration of H₂O₂ and its dissociation constant (2 × 10⁻¹²) provided by Evans and Uri [1949]. Assuming that pH = 8 and [H₂O₂] = 1 μM, the lifetime of CS₂ with respect to its chemical destruction is estimated to be 6.4 years. The chemical removal rate would then be 8 pM S yr⁻¹ at station C6 and 2 pM S yr⁻¹ at station C30, which are negligible compared with the advective rates.

The emission rates to the atmosphere are estimated using Liss and Slater's [1974] film model which expresses the gas flux as the product of the exchange velocity and a concentration difference term: (C_w - C_a / H). Here C_w is the concentration in water that has been measured in this work; C_a (pM S) is the concentration in air, and H is the Henry's law constant. The concentration in air is derived from the reported mixing ratio of ~10 pptv for coastal regions [Johnson and Bates, 1993], and the Henry's law constant is taken from Elliott [1989]. The exchange velocity is calculated using the formula given by Wanninkhof [1992] for long-term average

wind speeds. The estimated sea-to-air fluxes are $58 \mu\text{mol S m}^{-2} \text{ yr}^{-1}$ at station C6 and $17 \mu\text{mol S m}^{-2} \text{ yr}^{-1}$ at station C30. The depth of the surface mixed layer was 17 m at station C30 and is assumed to be 10 m at station C6. The calculated loss rates at stations C6 and C30 due to ventilation to the atmosphere are 5800 and 1000 pM S yr^{-1} , respectively. These two values are within the range of the advective rate. Horizontal advection could, therefore, constitute a significant sink for CS_2 in the bay and a source for this compound in the near-bay waters.

Biological consumption of CS_2 in seawater has not been reported. However, bacterial decomposition of CS_2 appeared to occur in Galway Bay. Two water samples (0.7 μm -filtered) collected from stations C4 and C5 were incubated in the dark for 30 min. The concentration of CS_2 decreased by 1 pM S in the sample from station C4 and 3 pM S in the sample from station C5. The results from these two incubations suggest the lifetime of CS_2 in the bay to be only ~ 10 hours. In that case, the chemical/biological removal rate would be 42000 pM S yr^{-1} at station C6, which leads to the advective rate being inconsequential as a sink at this locality.

3.2 Vertical distribution

3.2.1 Elevated surface concentration

Elevated surface concentrations of CS_2 were observed for all the depth profiles obtained in the Northeast Atlantic and a few in the Northwest Atlantic and the Pacific Ocean. Examples of this type of profile, together with the corresponding distributions of temperature and Chl-*a*, are illustrated in Figures 3.5. All the temperature profiles were strongly stratified with shallow surface mixed layers (≤ 2.5 to ~ 40 m).

The influence of surface mixing on the vertical distribution of CS_2 is illustrated by the profiles at stations C8, C24 and C32 (Figure 3.5). Station C8 exhibited a very thin surface mixed layer (≤ 2.5 m). Accordingly, high gradients of CS_2

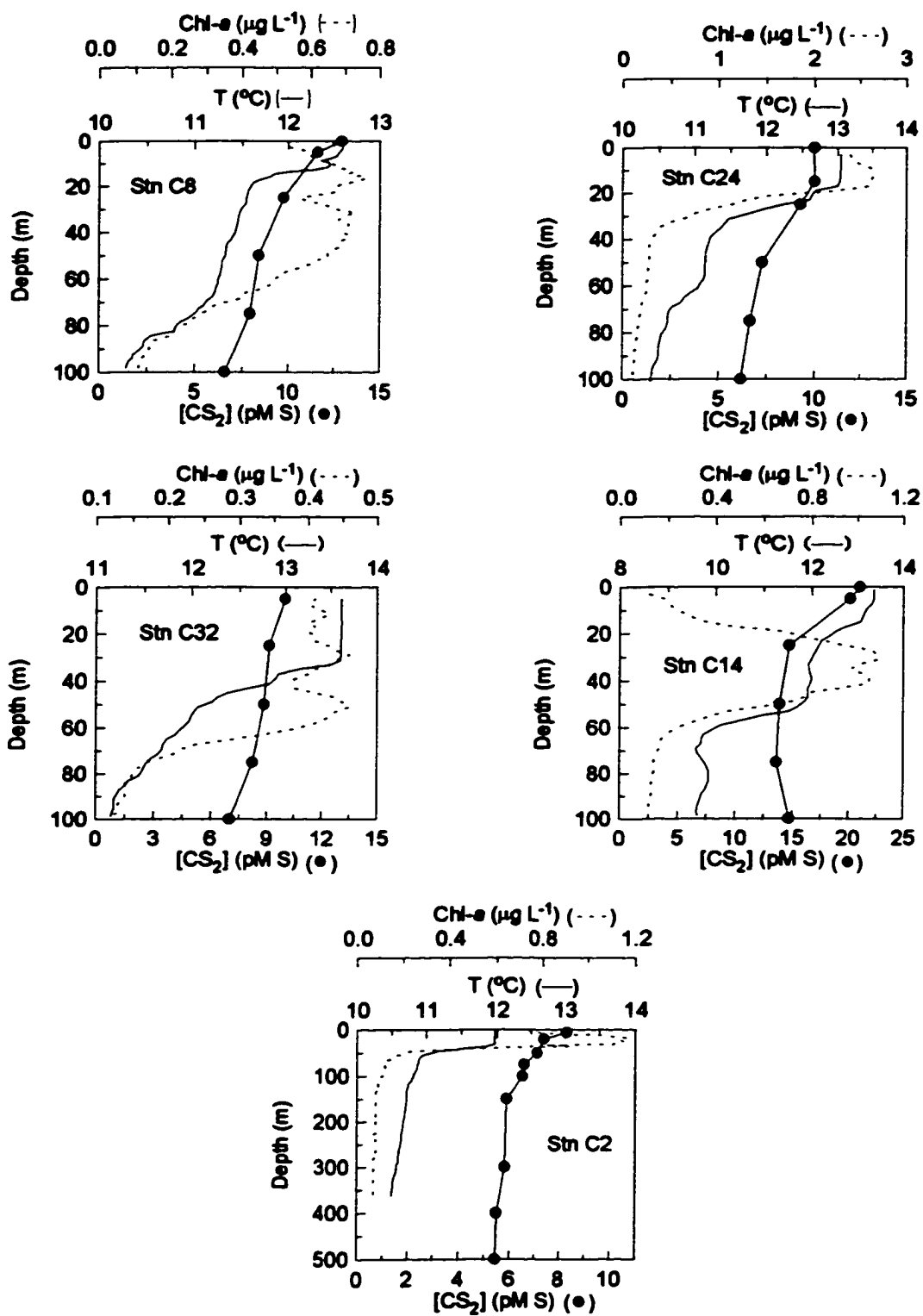


Figure 3.5 Representative profiles obtained in the Northeast Atlantic.

concentration in the surface layer were observed at this station. By contrast, strong surface mixing at station C24 was accompanied by homogeneous distribution of CS₂ in the upper layer of the water column. However, weak concentration gradients were still discernible within the surface mixed layers at some locations (e.g. station C32 in Figure 3.5). Thus, turbulent mixing in the surface layer was not always able to prevent the formation of vertical concentration gradients.

The decrease in CS₂ concentration with depth suggests net production of this compound in the surface and net destruction at depth. Consistent with the observations by Kim and Andreae [1992], most of the CS₂ profiles presented here did not resemble those of Chl-*a* which often showed subsurface maxima. In marked contrast, isoprene, which is known to be emitted by both land [Rasmussen and Khalil, 1988 and references therein] and marine plants [Moore et al., 1994; Milne et al., 1995], consistently showed distributions similar to those of Chl-*a* throughout the waters that we sampled in the North Atlantic [Moore and Xie, unpublished data].

Photochemical production of CS₂, which is induced by solar-UV radiation and, thus, restricted to the upper layer of the water column, was at least partly responsible for the pronounced high levels of the sulphur species in the surface. Depth profiles similar to those of CS₂ are frequently observed for a variety of gases with a photochemical source in seawater, such as carbon monoxide (CO) [Conrad et al., 1982; Kettle, 1994; Johnson and Bates, 1996], hydrogen peroxide (H₂O₂) [Palenik and Morel, 1988; Sikorski and Zika, 1993; Miller and Kester, 1994] and OCS [Flock and Andreae, 1996]. On the other hand, because of the distinct concentration gradients found between near-shore waters and the open ocean, horizontal advection and mixing might also play an important role in dictating the distribution of CS₂ within the water column.

Seven out of eighteen profiles (stations C5, C16, C18, C13, C24, C26, and C28) acquired in the Northeast Atlantic exhibited significant increases in CS₂ concentration with depth, following the initial decreasing trend in the subsurface (station C14 in Figure 3.5). Interestingly, all these stations are characterised by shallow water depths (less than 140 m), while the others had relatively greater depths (mostly over 200 m). The high content of CS₂ observed at depth was most likely caused by diffusional input of the compound from underlying sediments. Kim and Andreae [1992] reported similar features in CS₂ distribution in the Northwest Atlantic. Sedimentary input to overlying waters has also been observed for OCS [Cutter and Radford-Knoery, 1993; Zhang et al., 1998]. Station C2 (Figure 3.5) is the only location that was sampled down to more than 500 m. The data from this site indicate that CS₂ was detectable at a level of ~5 pM S below the euphotic zone, probably due to downward and upward diffusion from the surface and bottom, respectively.

3.2.2 Subsurface maxima

Distinct subsurface maxima of CS₂ concentration were observed at eight stations: three of them were located in waters off Nova Scotia (stations H33, H34 and H39) and the others were in the tropical and subtropical waters of the North Pacific (stations D5, D6, D9, D10 and D11). Figures 3.6 shows the vertical distributions of CS₂ concentration, Chl-*a* abundance and temperature at four localities off the coast of Nova Scotia. The upper layer of the water column at stations H34 and H39 was highly stratified with a mixed layer of less than 5 m thickness. In contrast, surface mixing was well developed down to ~20 m at station H33. A maximum in Chl-*a* was situated at ~40 m for stations H34 and H39. Station H33 showed a spike of chlorophyll fluorescence (no Chl-*a* concentration data available for this station) at ~50 m. The maximum CS₂ concentrations for

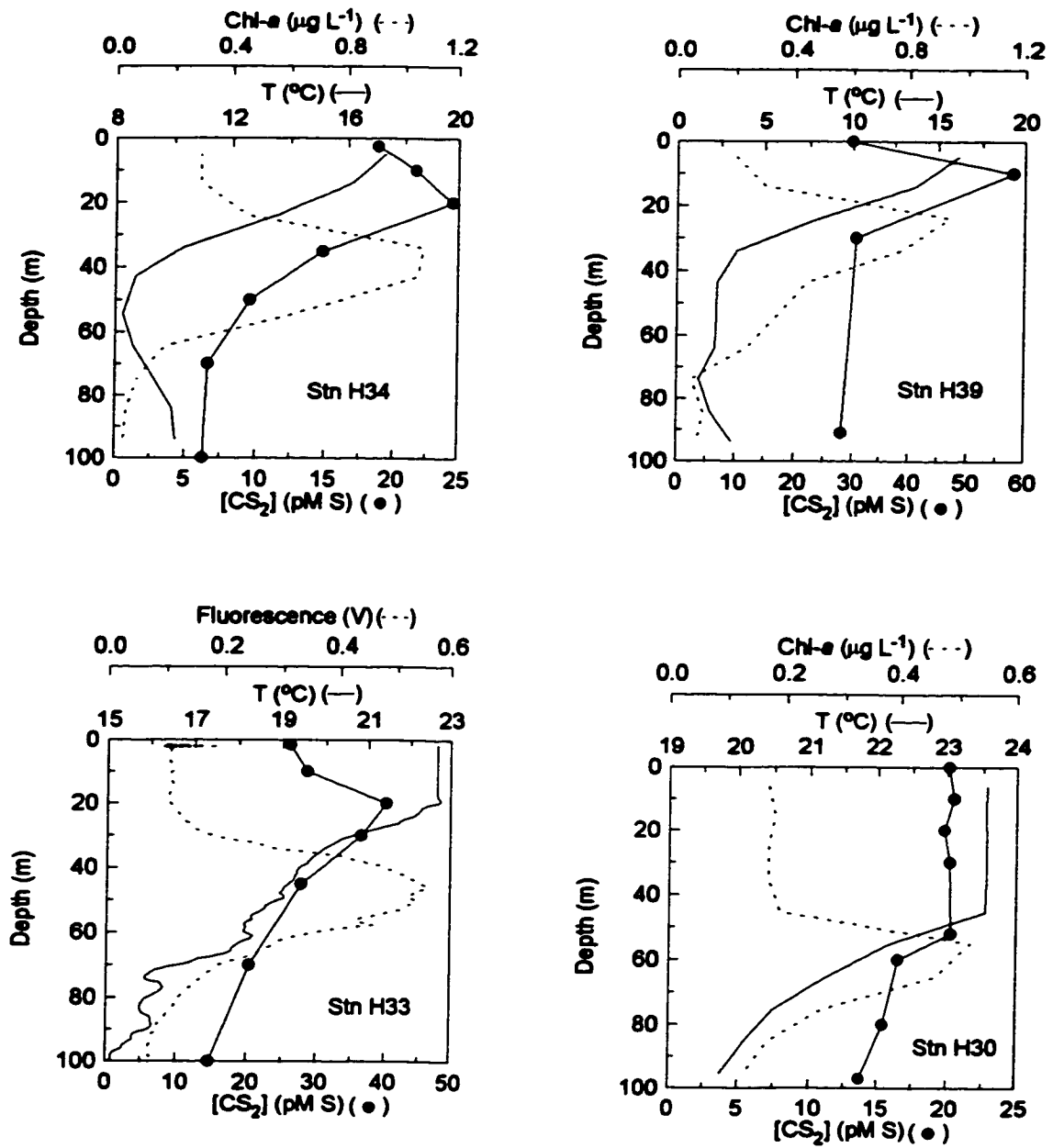


Figure 3.6 Vertical profiles obtained in waters off the coast of Nova Scotia.

stations H34 and H33 occurred at ~20 m, well above the depths of the corresponding Chl-*a* maxima. Also, the CS₂ peak at station H33 was noticeably below the base of the surface mixed layer. Station H39 showed an apparent CS₂ maximum at ~10 m. However, the depth of the real maximum might have been missed due to the coarse sampling resolution at this station.

The clear discrepancy between the depths of the CS₂ peaks and those of the Chl-*a* maxima may imply that the formation of the CS₂ peaks were not directly related to the underlying maxima in Chl-*a*. This argument was further supported by the profile obtained from station H30 (Figure 3.6) which, along with station H33, was in the warm and saline Gulf Stream waters. Compared with station H33, surface mixing reached a greater depth (~45 m) at station H30. Although a highly pronounced Chl-*a* maximum at station H30 was developed at ~55 m within the thermocline, an observable CS₂ peak was absent. The CS₂ peaks seen at stations H33, H34 and H39 possibly result from *in situ* production at depths (~20 m) where they were formed. Photo-production of CS₂ was observed in experiments using surface water samples collected at stations H33 and H39. Change of photo-production rate with depth is a function of the light field, the properties and distributions of CS₂ precursors and CDOM within the water column. Whereas UV radiation is extinguished rapidly during its transmission in the water column, highly elevated subsurface concentrations of the precursors and/or CDOM could still lead to pronounced photo-production at depth.

The vertical profiles from the tropical and subtropical waters in the North Pacific (stations D5, D6 and D10 in Figure 3.7) had similar hydrological structure and Chl-*a* distribution to those of the profiles at stations H30 and H33 (Figure 3.6) in the Gulf Stream waters. However, the North Pacific waters were characterised by broader surface mixed layers (down to ~80 m) and much deeper Chl-*a* maxima (down to ~100 m). Moreover, the North Pacific profiles showed distinct

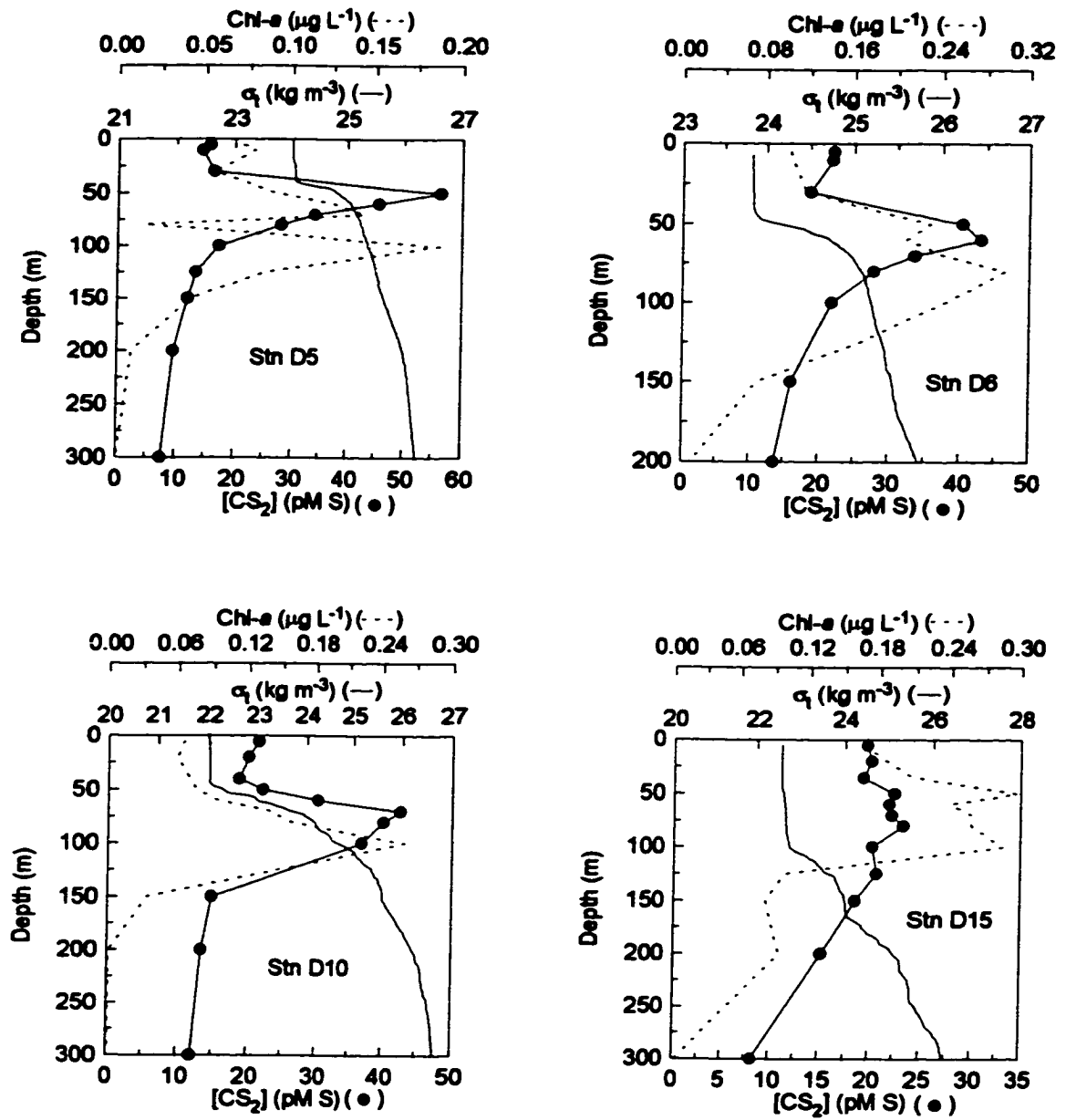


Figure 3.7 Representative profiles obtained in the Pacific Ocean.

subsurface CS₂ maxima within the pycnocline at the base of the mixed layer. Similar peaks were observed for other trace gases, such as methyl halides and isoprene [Moore and Groszko, 1997].

Instead of reflecting higher levels of plant biomass, the deep chlorophyll maximum is perhaps due to the abundant photosynthetic pigments produced by low-light adapted algal cells held in the stabilised layers [Taguchi et al., 1988; Moore et al., 1995]. The sharp pycnocline prevents the pigments from mixing vertically, thus resulting in the Chl-*a* peak. The stability within the density gradient can also account for the build-up of trace gases that are produced *in situ*. While the gases in the surface mixed layer can be easily ventilated to the atmosphere, the gases within the pycnocline are, however, subject to relatively low vertical mixing into the layers below and above. The gases within the pycnocline then tend to accumulate and have higher steady-state concentrations.

A conspicuous difference between waters north and south of station D11 was the deepening of the pycnocline in the southern waters. The surface mixed layer at station D15 extended to ~100 m, possibly close to or deeper than the base of the euphotic zone (Figure 3.7). As would be expected, this station did not show a Chl-*a* maximum below the mixed layer. The deepening of the mixed layer has also resulted in the disappearance of the maximum in CS₂ and other trace gases within the pycnocline. These observations imply that *in situ* production of the gases was mainly restricted to the euphotic zone and that the large increase in the concentrations of these gases within the pycnocline in waters north of station D11 might be associated with the biological activity leading to the Chl-*a* peak.

An attempt can be made to show whether photo-production alone could maintain the subsurface CS₂ maxima observed in the North Pacific waters. This evaluation requires estimating the photochemical and total production of the compound at the

depth of the CS₂ maximum. The photo-production rate in the water column is calculated using the following expression,

$$P(z) = \sum_{\lambda} \Phi(\lambda) I_{\text{CDOM}}(\lambda, z)$$

where

$P(z)$ = the photo-production rate ($\mu\text{mol S m}^{-2} \text{d}^{-1}$) at depth z (m) and was integrated over the wavelength range from 300 to 380 nm,

$I_{\text{CDOM}}(\lambda, z)$ = the irradiance ($\mu\text{Einsteins m}^{-2} \text{d}^{-1}$) absorbed by CDOM at depth z and wavelength λ (nm), and

$\Phi(\lambda)$ = the apparent quantum yield of CS₂ at wavelength λ and was derived from the *Challenger* data set using the Rundel method (see Chapter 6, section 6.5.2.2).

In this assessment, $\Phi(\lambda)$ is considered to be independent of depth. This implicitly assumes uniform distribution of the sulphur substrates for CS₂ photo-production in the water column, which may not necessarily be true. The underwater light field was obtained from the following empirical relationships between light attenuation and water depth:

$$\text{Log } I(z) = \text{Log } I(0) - 0.0690 z \quad \lambda = 308 \text{ nm}$$

$$\text{Log } I(z) = \text{Log } I(0) - 0.0526 z \quad \lambda = 320 \text{ nm}$$

$$\text{Log } I(z) = \text{Log } I(0) - 0.0370 z \quad \lambda = 340 \text{ nm}$$

$$\text{Log } I(z) = \text{Log } I(0) - 0.0196 z \quad \lambda = 380 \text{ nm}$$

where $I(0)$ and $I(z)$ stand for the irradiance at sea surface and depth z , respectively. These relationships are derived from the irradiance data collected by Johnson and Bates [1996] during field surveys in the Pacific Ocean waters that were similar in Chl-*a* concentrations to the Pacific Ocean waters that we investigated. The attenuation constants are linearly interpolated or extrapolated over a 2-nm interval to obtain the attenuation constants at wavelengths other than those listed above.

The water column is divided into a series of layers of water with a thickness $\Delta z = 0.5$ m. The total light absorbed by each layer was calculated using the above relationships between $I(z)$ and z . It is assumed that the fraction of light absorbed by CDOM is 84% which is an average value obtained from the *Challenger* cruise. The solar irradiance (averaged over 24 hours) at the Earth's surface, compiled by Leifer [1988] for mid-autumn at 20°N, is taken as $I(0)$. Figure 3.8 shows the simulated vertical profile of wavelength-integrated photo-production rate. The value at 50 m is ~1% of that at the surface. The potential photochemical formation rates at the depths of the subsurface CS_2 maxima are given in Table 3.2. The numbers in Figure 3.8 and Table 3.2 have been normalised to a volume equivalent to 1 m^2 by Δz (0.5 m), i.e. 0.5 m^3 .

The total production of CS_2 at the depths of subsurface CS_2 maximum can be estimated by equating it to the total loss occurring there, assuming that a steady state is achieved. The loss processes include chemical destruction (hydrolysis and reaction with H_2O_2), possible biological consumption, and eddy diffusion into the layers above and below. The potential biological consumption is ignored in assessing the total loss because no adequate knowledge about this pathway is available. Losses due to lateral diffusion or advection are assumed to be unimportant. The procedure for calculating the chemical destruction is described in section 3.1.5. In this case, pH was assumed to be 8.2 and the concentration of H_2O_2 to be 1 nM. Upward and downward flux of CS_2 caused by eddy diffusion can be computed using the following expression:

$$F_{\text{ed}}(z) = -D_w \frac{\partial[\text{CS}_2]}{\partial z}$$

where $F_{\text{ed}}(z)$ is the flux at depth z , D_w is a vertical eddy diffusivity, and $\frac{\partial[\text{CS}_2]}{\partial z}$ is the vertical concentration gradient of CS_2 . The loss rate (concentration change per

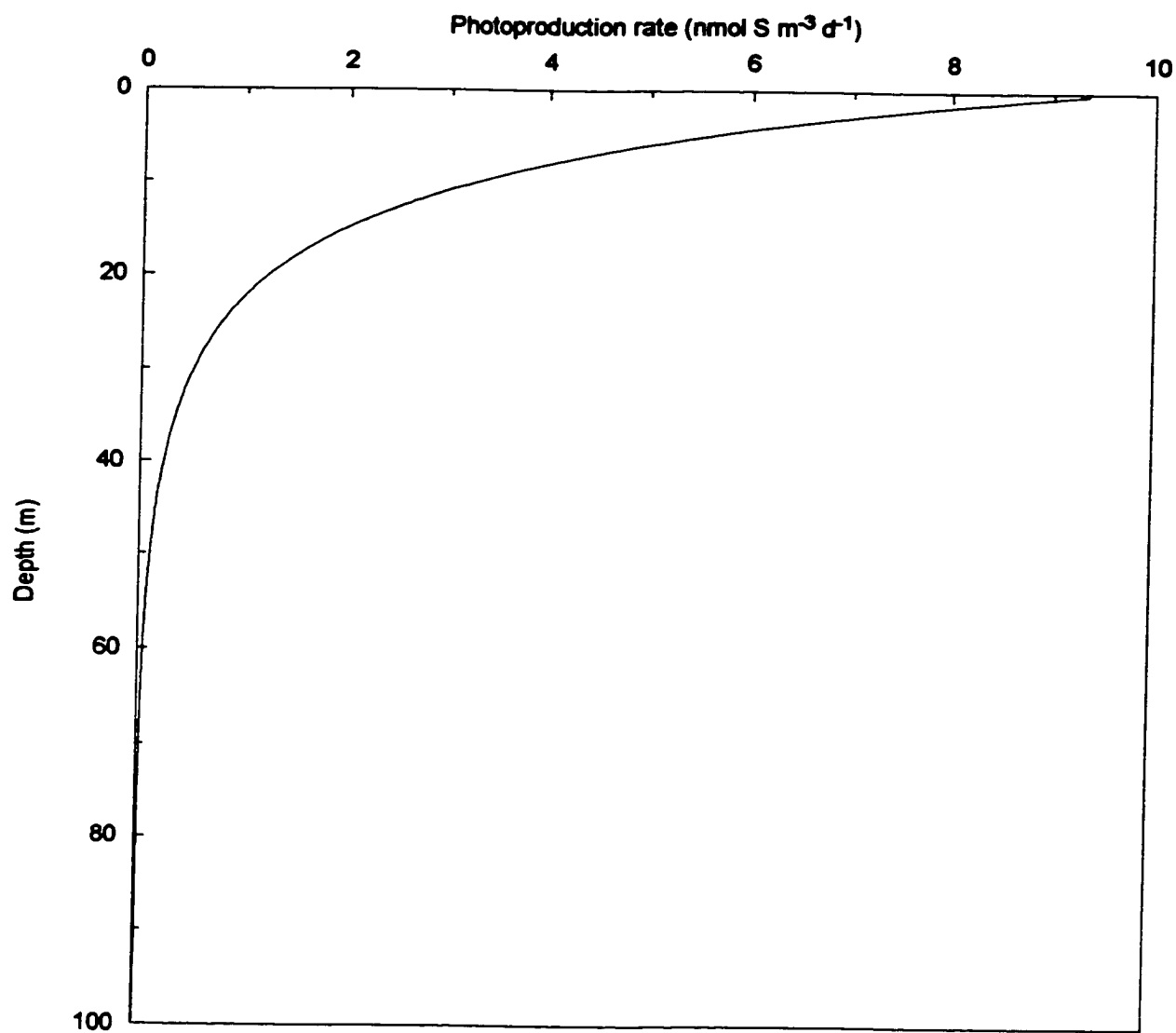


Figure 3.8 Modelled photo-production rate of CS₂ as a function of depth.

Table 3.2 Estimates of potential photo-production rates, chemical destruction rates at the depth of the subsurface CS₂ maximum, and the loss rates due to eddy diffusion just above the maximum

Station	z_{\max}	$[\text{CS}_2]_{\max}$	Chemical loss	Eddy diffusion	Total loss	Photochemical production
D5	50	60	3	30-126	33-129	39
D6	60	40	2	10-41	12-43	19
D9	80	40	2	5-22	7-24	5
D10	70	40	2	9-36	11-38	10

Here $[\text{CS}_2]_{\max}$ (pM S) is the concentration of CS₂ at the subsurface maximum, and z_{\max} (m) is the depth of the subsurface maximum. The units for all the production and loss terms are pM S yr⁻¹.

unit time) within a layer of Δz (here 0.5 m) is $\frac{F_{ed}(z) - F_{ed}(z \pm \Delta z)}{\Delta z}$.

The estimates of eddy diffusivity estimated for highly stratified waters vary widely. Using the temperature microstructure profiles measured in the centre of the subtropical gyre in the North Pacific, Gregg et al. [1973] estimated the eddy diffusivity in the main thermocline to be $\sim 8 \text{ m}^2 \text{ yr}^{-1}$, only about three times larger than the molecular diffusivity of heat. Lueck and Osborn [1986] reported similar values from the observations of kinetic energy dissipation in the Sargasso Sea. Based on the interannual change in temperature and density structure of the water column in the central North Pacific, White and Bernstein [1980] arrived at an eddy diffusivity in the range $630\text{-}1260 \text{ m}^2 \text{ yr}^{-1}$. More recently, Ledwell et al. [1993] suggested a value from 300 to $600 \text{ m}^2 \text{ yr}^{-1}$ based on the results from tracer release experiments in the North Atlantic. A range from 300 to $1260 \text{ m}^2 \text{ yr}^{-1}$ is used in this study to estimate the loss rates due to eddy diffusion.

The concentration gradient of CS_2 was calculated by fitting the concentration to a second order polynomial function of depth using the data points above and below the subsurface maximum separately. The fitted function forms are :

Above the subsurface maximum

Station D5 $[\text{CS}_2] = 23.5 - 1.5176 z + 0.0434 z^2, r^2 = 0.996, n = 4$

Station D6 $[\text{CS}_2] = 24.2 - 0.4893 z + 0.0140 z^2, r^2 = 0.909, n = 5$

Station D9 $[\text{CS}_2] = 16.9 - 0.3517 z + 0.0078 z^2, r^2 = 0.906, n = 5$

Station D10 $[\text{CS}_2] = 26.1 - 0.7133 z + 0.0133 z^2, r^2 = 0.964, n = 6$

Below the subsurface maximum

Station D5 $[\text{CS}_2] = 126.9 - 1.766 z + 0.0067 z^2, r^2 = 0.993, n = 7$

Station D6 $[\text{CS}_2] = 78.6 - 0.7895 z + 0.0023 z^2, r^2 = 0.951, n = 6$

Station D9 $[\text{CS}_2] = 65.8 - 0.4013 z + 0.0008 z^2, r^2 = 0.893, n = 6$

Station D10 $[\text{CS}_2] = 77.8 - 0.5622 z + 0.0011 z^2, r^2 = 0.961, n = 6$

The estimated loss rates are presented in Table 3.2. The data show that the photo-production rates are sufficient to balance the lower range of the total loss rates, but are smaller than the upper range of the total loss rates. Therefore, if the eddy diffusivity ($300 \text{ m}^2 \text{ yr}^{-1}$) reported by Ledwell et al. [1993] is representative of the North Pacific waters that we have sampled, photochemical production alone might be able to maintain the subsurface CS_2 maximum. Obviously, this is also true when the much smaller eddy diffusivities given by Gregg et al. [1973] and Lueck and Osborn [1986] are used. On the other hand, if the eddy diffusivity in this region reaches the upper end of the range ($1260 \text{ m}^2 \text{ yr}^{-1}$) reported by White and Bernstein [1980], other processes, such as biological activity or non-photochemical reactions, are needed to account for the imbalance between the photo-production and the total loss. However, it must be reiterated that the photochemical production rates estimated above are based on the assumption that the sulphur precursors and CDOM are evenly distributed in the water column. In reality, inhomogeneity of the distributions of the precursors and CDOM is likely since their formation is mostly connected to biological processes which are depth-dependent. If the concentrations of the sulphur substrates and CDOM are very high around the depths of the subsurface CS_2 maxima, the photo-production rates could be much greater than the values in Table 3.2.

3.3 Summary

Carbon disulphide concentrations were measured during three field programs in the North Atlantic and the Pacific Ocean. Coastal waters usually contained higher levels of CS_2 than did the open ocean waters. The mean concentrations were 30 and 13 $\mu\text{M S}$ in the sampled coastal and oceanic waters, respectively. The higher concentrations in coastal areas were possibly a consequence of substantial diffusional input from the underlying sediments and higher photo-production of

CS₂ in these waters. The negative correlation between CS₂ concentration and salinity in surface water suggests the importance of photochemical CS₂ formation in coloured freshwater. Horizontal advection may transfer a significant amount of CS₂ from near-shore waters to off-shore waters. No clear relationship was observed between CS₂ concentration and phytoplankton biomass (Chl-*a*). Warm waters in the tropical and subtropical gyres were highly enriched with CS₂ compared with cool temperate waters, which was probably a result of enhanced photo-production in the intensely irradiated waters.

Most of the vertical profiles obtained in cool temperate waters showed highly elevated levels of CS₂ in the surface and some of these profiles exhibited increasing concentrations near the bottom, suggesting the presence of CS₂ sources in surface water and sediments. Coexisting sharp subsurface maxima in CS₂ and Chl-*a* were observed for profiles in warm and oligotrophic waters. Because of the great uncertainty in the estimates of the vertical eddy diffusivity and lack of knowledge about the depth distribution of CS₂ precursors, modelling cannot unequivocally establish if photochemical production alone could maintain the subsurface CS₂ maxima observed in the central gyres in the North Pacific.

Chapter 4 Ocean-Atmosphere Exchange of Carbon Disulphide

4.1 Introduction

The two-layer stagnant film model proposed by Liss and Slater [1974] is widely employed to estimate gas exchange between air and water. This model assumes that the main bodies of air and water are well mixed and that gas transfer occurs by molecular diffusion through the gas and liquid phase interfacial layers. The model can be mathematically expressed as

$$F = K \Delta C$$

where F is the net gas flux, K is the total exchange velocity (also referred to as transfer coefficient or piston velocity) and ΔC is the concentration difference across the interfacial layer, which drives the gas exchange. A more specific expression for the concentration difference is

$$\Delta C = C_w - C_a / H$$

where C_w and C_a are the concentrations in water and air, respectively, and H is the gas-liquid partition coefficient which is often referred to as a dimensionless Henry's law constant. A positive ΔC indicates net gas transfer from water to air while a negative ΔC means net gas influx from air to water. The Henry's law constant is expressed as the ratio of the equilibrated concentration of gas in air to its concentration in unionised form in water.

The total exchange velocity is calculated from its individual components in the gas and liquid diffusional layers as follows:

$$1 / K = 1 / (\alpha k_w) + 1 / (H k_a)$$

where k_w and k_a are the exchange velocities in the water and air diffusion layers, respectively, and α is the enhancement factor due to chemical reaction. Many gases of interest in geochemical cycling, including CS_2 , have high H values and low chemical reactivity towards water. For these gases, k_w is the dominant factor

controlling the gas transfer and $\alpha \sim 1$, which leads to $K \approx k_w$ [Liss and Merlivat, 1974; Liss and Merlivat, 1986]. In order to estimate the net gas transfer between air and sea, we need to know the exchange velocity, the Henry's law constant for the gas of interest and the concentrations of the gas in air and seawater.

4.2 Henry's law constant for CS₂

De Bruyn et al. [1995] have determined the Henry's law constants for a suite of reduced sulphur species (DMS, H₂S, CS₂, OCS and MeSH) in distilled water in the range from 5° to 25°C. These authors defined Henry's law constant as the ratio of concentration in water to that in air and presented the data in the form

$$RT \ln H_d = A + BT$$

where R is the universal gas constant, A and B are fitted parameters in cal mol⁻¹ and cal K⁻¹ mol⁻¹, respectively, T is temperature in Kelvin, and H_d is Henry's law constant in distilled water and is in units of mole solute (mole solvent)⁻¹ atm⁻¹. The parameters A and B for CS₂ are 5500 and -32.2, respectively. If the data are converted to the dimensionless values and expressed as the ratio of concentration in air to that in water, the Henry's law constant for CS₂ (H'_d) can be calculated from the following equation:

$$H'_d = \frac{\exp(16.2 - 2768/T)}{4.55T}$$

De Bruyn et al. [1995] also measured the Setchenow coefficients (k_s) for the sulphur species to convert the Henry's law constants in distilled water to seawater values (H_s) using the formulation given by Clegg and Whitfield [1991]:

$$\text{Log}_{10} (H_s / H'_d) = k_s M$$

where M is the molarity of the ionic solution (0.725 for seawater with salinity ~ 35). The value of k_s for CS₂ at 5°C is 0.15 M⁻¹ and is not expected to exhibit

significant temperature-dependence [De Bruyn et al., 1995]. This k_s value is equivalent to a 28% salt effect.

Elliott [1989] measured the Henry's law constants for CS_2 in aqueous systems of varying temperature and ionic strength, including natural seawater (Table 4.1). The salt effect between seawater and distilled water ranges from 7 to 28% and averages 18%. Figure 4.1 shows the Henry's law constants for CS_2 in seawater from De Bruyn et al. [1995] and Elliott [1989]. Also included in this figure are the data calculated from the vapour pressures and solubilities of this compound [Washburn, 1928; Stephen and Stephen, 1963]. Obviously, Elliott [1989] presented the lowest Henry's law constants for CS_2 over the entire plotted temperature range, while the data from De Bruyn et al. [1995] are the highest below 15°C. In the range 5-25°C, De Bruyn et al.'s values are higher than Elliott's by an average of 41%.

The atmospheric CS_2 concentration in equilibrium with seawater can be calculated as a product of its Henry's law constant and water phase concentration. Using the Henry's law constants provided by Elliott [1989] and the seawater concentrations from the present study, the mean equilibrated concentration was 96.0 pptv with a range from 34 to 248 pptv. As atmospheric measurements indicate only a few pptv of CS_2 in the marine boundary layer over the open ocean and ~10 pptv over coastal waters [see Chapter 1, section 1.4], all the sampled waters were highly supersaturated with CS_2 . The supersaturation is found to be ~41% greater when the Henry's law constants of De Bruyn et al. [1995] are used.

4.3 The exchange velocity

For unreactive gases, the exchange velocity is predominantly regulated by turbulence at the air-water interface [Liss and Slater, 1974; Jahne et al., 1987a]. As

Table 4.1 Dimensionless Henry's law constant for CS₂ from Elliott [1989]

T(°C)	Distilled water	0.5 M NaCl	Seawater
0.5	0.22	0.28	0.28
8.0	0.33	0.38	0.42
16.0	0.45	0.55	0.52
24.0	0.59	0.64	0.66
32.0	0.88	0.95	0.94

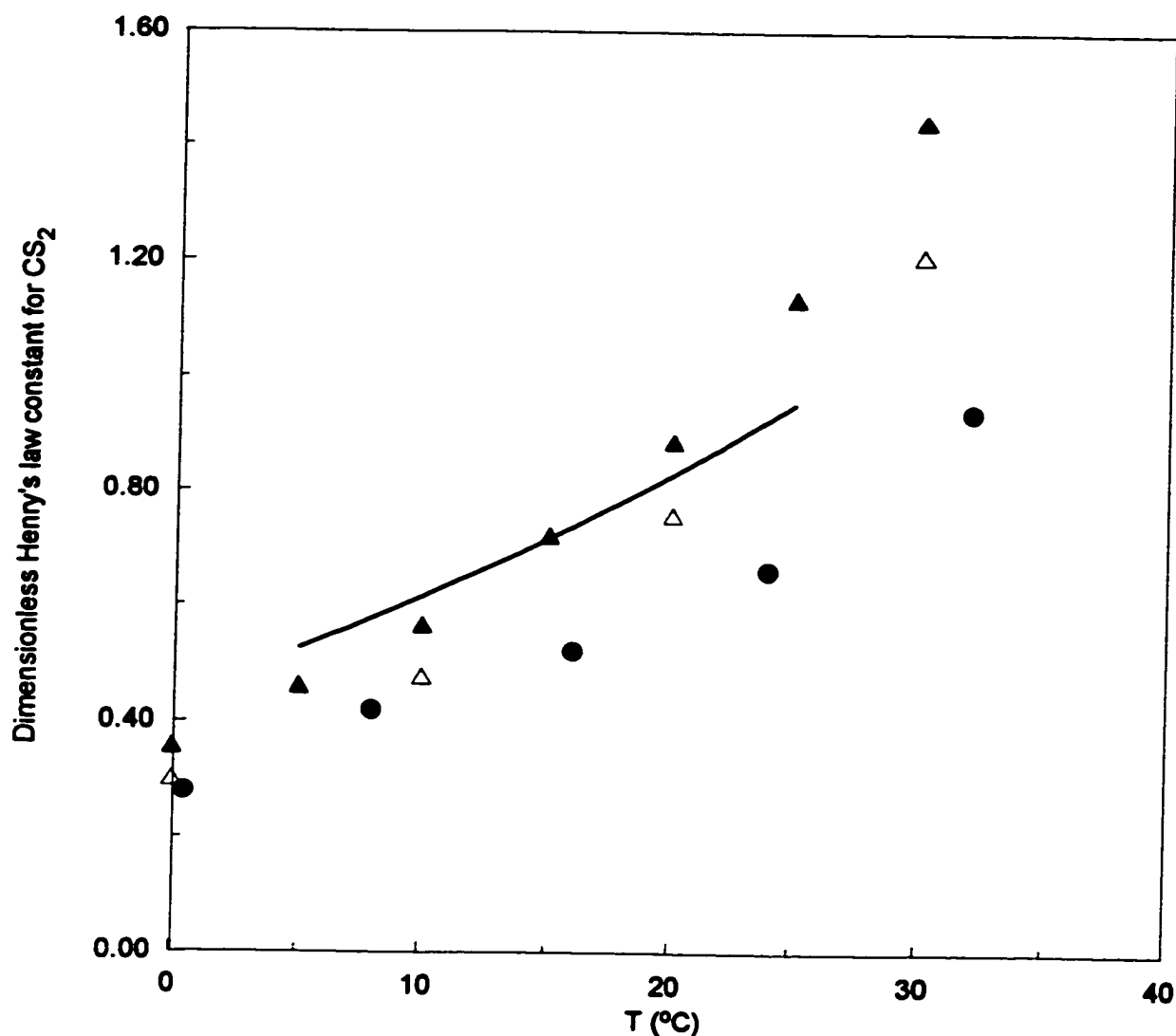


Figure 4.1 Henry's law constant for CS₂ in aqueous solution as a function of temperature. Solid line represents seawater data from De Bruyn et al. [1995]. Solid circles are seawater values from Elliott [1989]. Open triangles denote values derived from the CS₂ vapour pressures and solubilities in Washburn [1928]. Solid triangles signify values derived from the CS₂ vapour pressures in Washburn [1928] and the solubilities in Stephen and Stephen [1963].

wind speed is an important factor influencing surface turbulence and can be easily measured during field surveys, much effort has been made to establish a relationship between gas transfer and wind speed [Deacon, 1980; Liss and Merlivat, 1986; Smethie et al., 1985; Upstill-Goddard et al., 1990, Wanninkhof et al., 1985; Wanninkhof, 1992]. Aside from wind speed, gas exchange also depends on wind duration, fetch, and variability which determines the development of wind field and the distribution of whitecaps [Asher et al., 1992; Wanninkhof, 1992]. Other factors that affect the exchange velocity include boundary layer stability [Erickson III, 1993], injection of bubbles [Memery and Merlivat, 1985] and surfactants [Goldman et al., 1988]. Despite the fact that gas exchange is influenced by many factors, relationships of gas transfer and wind speed are still widely adopted to estimate the exchange velocity.

A number of formulae are available to express the relationship between the exchange velocity and wind speed [Liss and Merlivat, 1986; Wanninkhof, 1992; Erickson, 1993]. Substantial difference exists in the value of K derived from these formulae. Wanninkhof's relationship is normalised to the global measurements of $^{14}\text{CO}_2$ and fitted to wind speed with a quadratic dependence:

$$K = 0.31 u^2 (\text{Sc} / 660)^{-0.5} \quad (4.1)$$

or
$$K = 0.39 u_{av}^2 (\text{Sc} / 660)^{-0.5} \quad (4.2)$$

where u is a spot measurement of wind speed in meters per second, u_{av} is a long-term averaged wind speed, and Sc is the Schmidt number for the gas of interest at the appropriate temperature. The Schmidt number is defined as the ratio of the kinematic viscosity of seawater to the diffusion coefficient of the investigated gas, both of which are functions of temperature.

The Liss and Merlivat [1986] relationship, herein referred as to LM, expresses the exchange velocity as a function of wind speed in three linear segments,

$$K = 0.17 u, \text{ for } u \leq 3.6 \quad (4.3)$$

$$K = 2.85 u - 9.65 \text{ for } 3.6 < u \leq 13 \quad (4.4)$$

$$K = 5.9 u - 49.3, \text{ for } u > 13. \quad (4.5)$$

The three equations are normalised for a gas with $Sc = 600$, and corrections need to be made if $Sc \neq 600$. Specifically, $K \propto Sc^{-2/3}$ for $u \leq 3.6 \text{ m s}^{-1}$, and $K \propto Sc^{-1/2}$ for higher wind speeds [Liss and Merlivat, 1986]. It is suggested that short-term wind speeds are more appropriate than long-term averaged wind speeds for equations 4.3-4.5 [Wanninkhof, 1992]. The LM approach is based on the results from tracer experiments that were conducted on small lakes [Wanninkhof et al. 1985] and from the wind-wave tank work of Broecker and Siems [1984] and Broecker et al. [1978]. Recent dual tracer experiments done at sea [Watson et al., 1991; Liss et al., 1993] provide support for the LM predictions, although the double tracer technique is suspected of yielding low exchange velocities at high wind speeds [Asher et al., 1991; Wanninkhof, 1992]. In Figure 4.2, a comparison is made between the LM relationship and Wanninkhof's. Except for extremely low wind speeds ($\leq 0.5 \text{ m s}^{-1}$), the LM relationship gives significantly lower exchange velocities than Wanninkhof's relationship. For a wind speed range of 1-15 m s^{-1} , the average exchange velocity derived from the LM relationship is 46% lower.

Both Wanninkhof's and the LM relationships contain the Schmidt number. As stated previously, the Schmidt number is a ratio of the kinematic viscosity of seawater to the diffusion coefficient of the gas of interest. Wanninkhof [1992] derived equations for the dependence of Schmidt number on temperature for several gases including CO_2 , CFC-11 and CFC-12. A similar approach was used to obtain the equation for CS_2 . The kinematic viscosity of distilled water was obtained using its dynamic viscosity [Sengers and Waston, 1986] and density [Lide, 1996]; the diffusion coefficient of CS_2 in distilled water was derived from the relationship of Wilke and Chang [1955],

$$D = 7.4 \times 10^{-8} (xM_w)^{0.5} T / (\eta V^{0.6}) \quad \text{where}$$

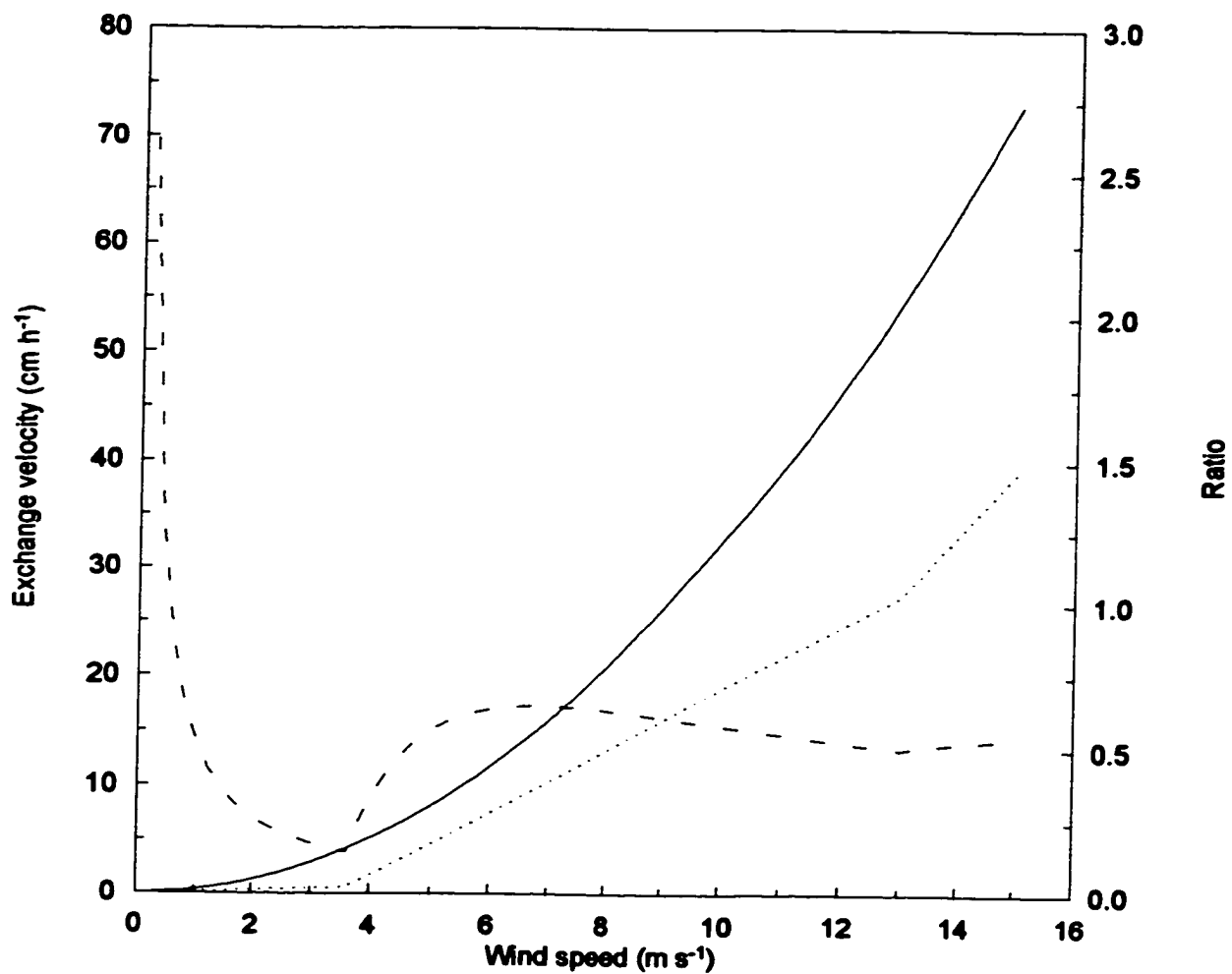


Figure 4.2 Exchange velocity as a function of wind speed. Solid line is from Wanninkhof's relationship (equation (4.1) in text), dotted line from Liss and Merlivat's relationship, and dashed line is the ratio of the dotted line to the solid line.

D = the diffusion coefficient of CS_2 in $\text{cm}^2 \text{s}^{-1}$,

x = the revised association factor of water (2.26) [Hayduk and Laudie, 1974],

M_w = the molar weight of water in g mole^{-1} (18),

T = temperature in Kelvin,

η = the dynamic viscosity of water in centipoise (1 centipoise = $0.01 \text{ g cm}^{-1} \text{ s}^{-1}$),
and

V = the molal volume of CS_2 at normal boiling point in mL mole^{-1} (66) [Wilke and Chang, 1955].

In order to derive the Schmidt number for seawater, the suggestions given by Wanninkhof [1992] are used to convert the freshwater data of kinematic viscosity and diffusion coefficient to seawater values. The kinematic viscosities of distilled water are multiplied by $1.052 + 1.300 \times 10^{-3} t + 5.000 \times 10^{-6} t^2 - 5.000 \times 10^{-7} t^3$ (t in degrees Celsius) to obtain seawater (35 salinity) viscosities. The diffusion coefficients of CS_2 for distilled water are decreased by 6% to account for the difference of diffusion of helium in distilled water and seawater as determined by Jahne et al. [1987b]. The calculated Schmidt number of CS_2 is fitted to a temperature relationship in the range from 0° to 30°C ,

$$Sc = 3377.8 - 221.71 t + 6.9370 t^2 - 0.08751 t^3 \quad (r^2 = 0.9999, n = 301)$$

where t is temperature in degrees Celsius. Figure 4.3 shows that the fitted line is almost indistinguishable from the line established from the calculated data. The mean absolute relative deviation of the fitted values from the calculated ones is 0.6%. Assuming a $Sc^{-0.5}$ dependence and a given wind speed, the exchange velocity, K , varies by a factor of 2.3 over the temperature range encountered during the three ocean cruises for this study (0.6 - 28.8°C).

4.4 Flux calculation

According to section 4.1, CS_2 flux across the air-sea interface can be calculated

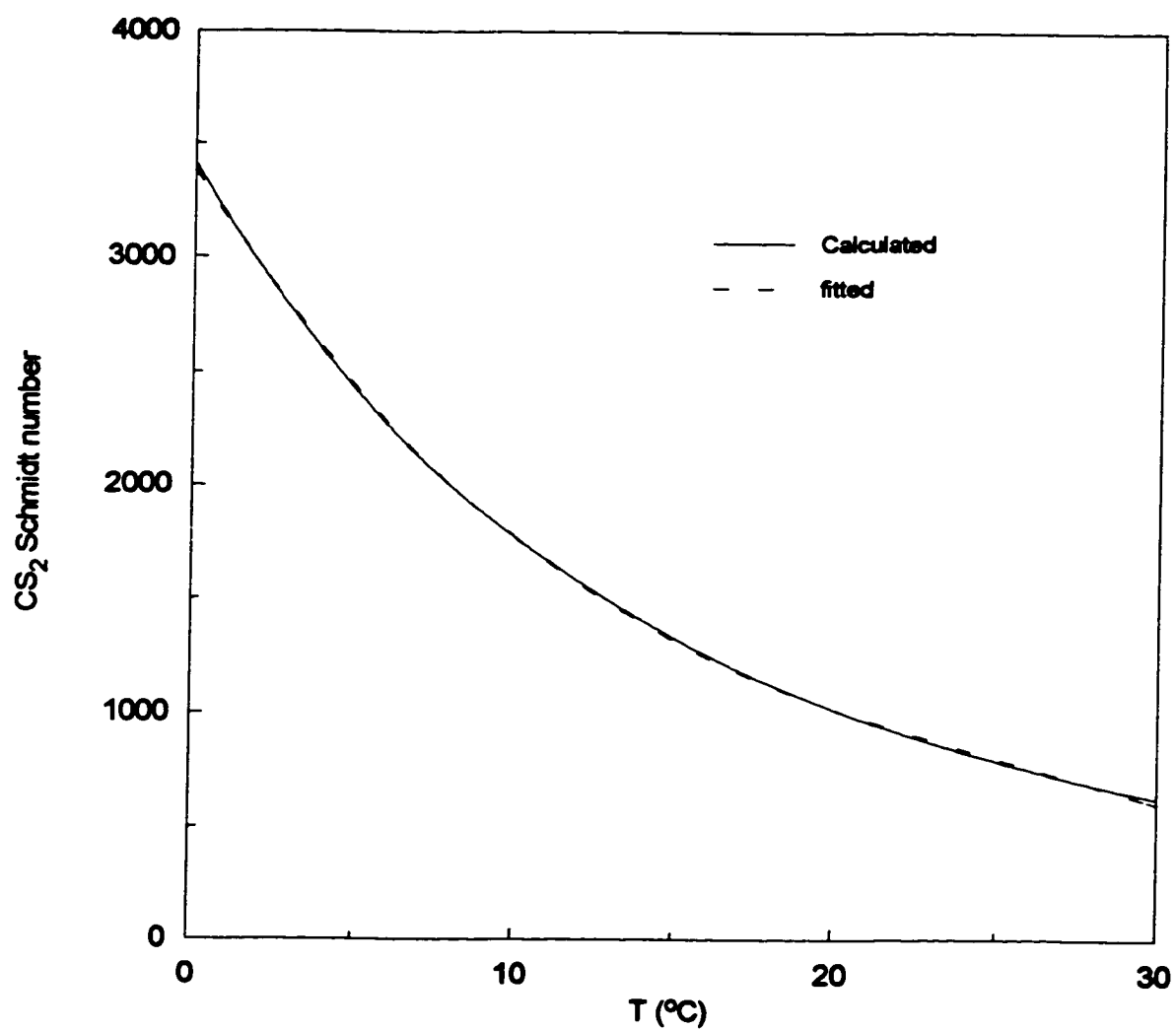


Figure 4.3 Schmidt number for CS₂ as a function of temperature.

from

$$F = K (C_w - C_a / H)$$

Carbon disulphide concentrations in surface water were obtained from the three field campaigns conducted for this study in the North Atlantic and the Pacific Ocean. Mixing ratios in the boundary layer were assumed to be 10 pptv over the coastal waters and 2 pptv over the open ocean [Johnson and Bates, 1993]. Henry's law constant for CS₂ were chosen from Elliott [1989]. Calculation using the Henry's law constants from both Elliott [1989] and De Bruyn [1995] indicated that the atmospheric concentration of CS₂ is negligible compared with the concentration expected from equilibrium with seawater. Thus, choice of either of the data sets will not make any significant difference to flux calculations. Exchange velocities were estimated from equations 4.1, 4.2, or 4.3-4.5. Spot wind speeds, recorded concurrently with sampling of water samples, were employed in equations 4.1 and 4.3-4.5, and long term averaged climatological wind speeds were used for equation 4.2. The climatological wind speeds that are representative of our sampling locations and time were extracted from the Comprehensive Ocean-Atmosphere Data Set (COADS) (1946-1989) which are monthly averages on a 2° × 2° latitude-longitude grid. Moore and Webb [1996] and Moore et al. [1996] pointed out that the influence of wind speed on the column concentration of the gas is realised over a period approximately equivalent to the mixed layer depth divided by the exchange velocity. Assuming the typical values of wind speed, seawater temperature and mixed layer depth to be 6.5 m s⁻¹, 20°C and 50 m, respectively, this period is on the time scale of ~15 days over which the spot wind speeds measured at times of water sampling are not necessarily representative of the distributions of the wind speeds at the sampling locations. In this regard, the climatological wind speed is more appropriate than the spot wind speed. However, the climatological wind speed suffers from its own limitation since the actual wind

speed over the critical period of ~15 days is not necessarily commensurate with the climatological value. Figures 4.4a-c show the wind speed data for the three ocean cruises. As stated in Chapter 2, section 2.5, the spot wind speeds for the *Hudson* cruise are not reliable, and thus are not presented. The mean spot wind speed for the *Discoverer* (7.2 m s^{-1}) cruise was slightly higher than the mean climatological value (6.6 m s^{-1}), while for the *Challenger* expedition the former (6.1 m s^{-1}) was lower than the latter (7.2 m s^{-1}).

The exchange velocities and fluxes derived from equations 4.1 or 4.2 are plotted along the cruise tracks in Figures 4.5-4.7. As would be expected, the exchange velocity and flux calculated from climatological wind speeds are less variable than those from spot wind speeds (Figures 4.6-4.7). Table 4.2 summarises flux estimates for the three cruises. In the coastal region of the Northeast Atlantic, the mean flux obtained from the spot wind speeds is much smaller than that from the climatological wind speeds, indicating that the observed spot wind speeds in this region were greatly biased towards low values. To a lesser extent, this also happens in the open Northeast Atlantic. By contrast, in the Pacific Ocean, the mean flux derived from the spot wind speeds is slightly greater than that from the climatological wind speeds. These observations are in accordance with the discrepancies found between the spot wind speeds and the climatological wind speeds for the *Discoverer* and *Challenger* cruises. Consistent with Figure 4.2, the LM relationship yields significantly lower fluxes than Wanninkhof's formulation. The mean flux derived from the former is only 33% of that from the latter for the coastal water and 57% for the open ocean. The lower percentage for the coastal water is mainly a result of the lower wind speeds encountered during the field investigations. The spot wind speed measured for coastal water of the Northeast Atlantic averaged 4.0 m s^{-1} and ranged from 1.8 to 5.9 m s^{-1} , while the mean spot wind speed for the open ocean was 6.7 m s^{-1} with 70% of the individual wind

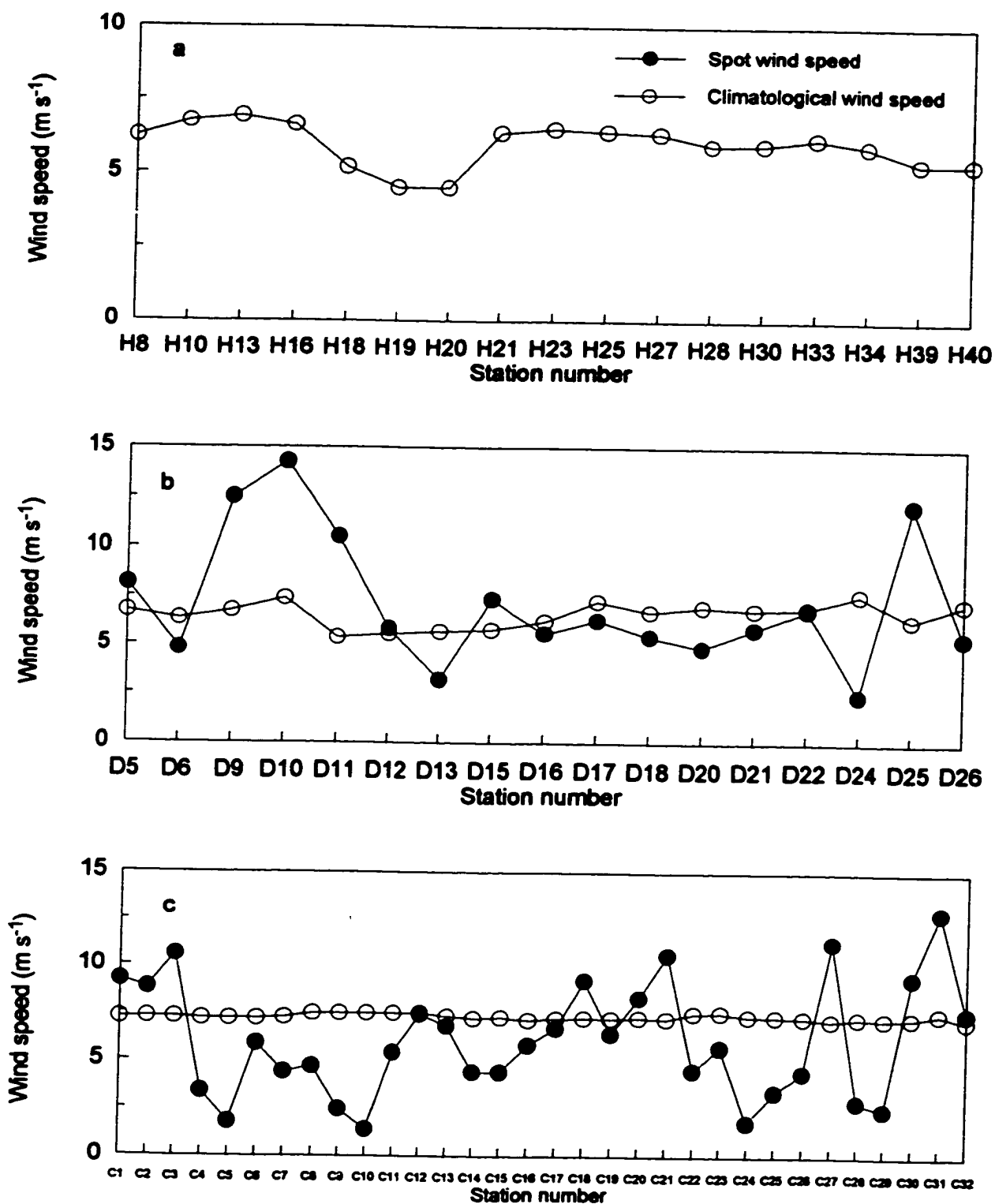


Figure 4.4 Wind speed data for (a) *Hudson* cruise, (b) *Discoverer* cruise, and (c) *Challenger* cruise.

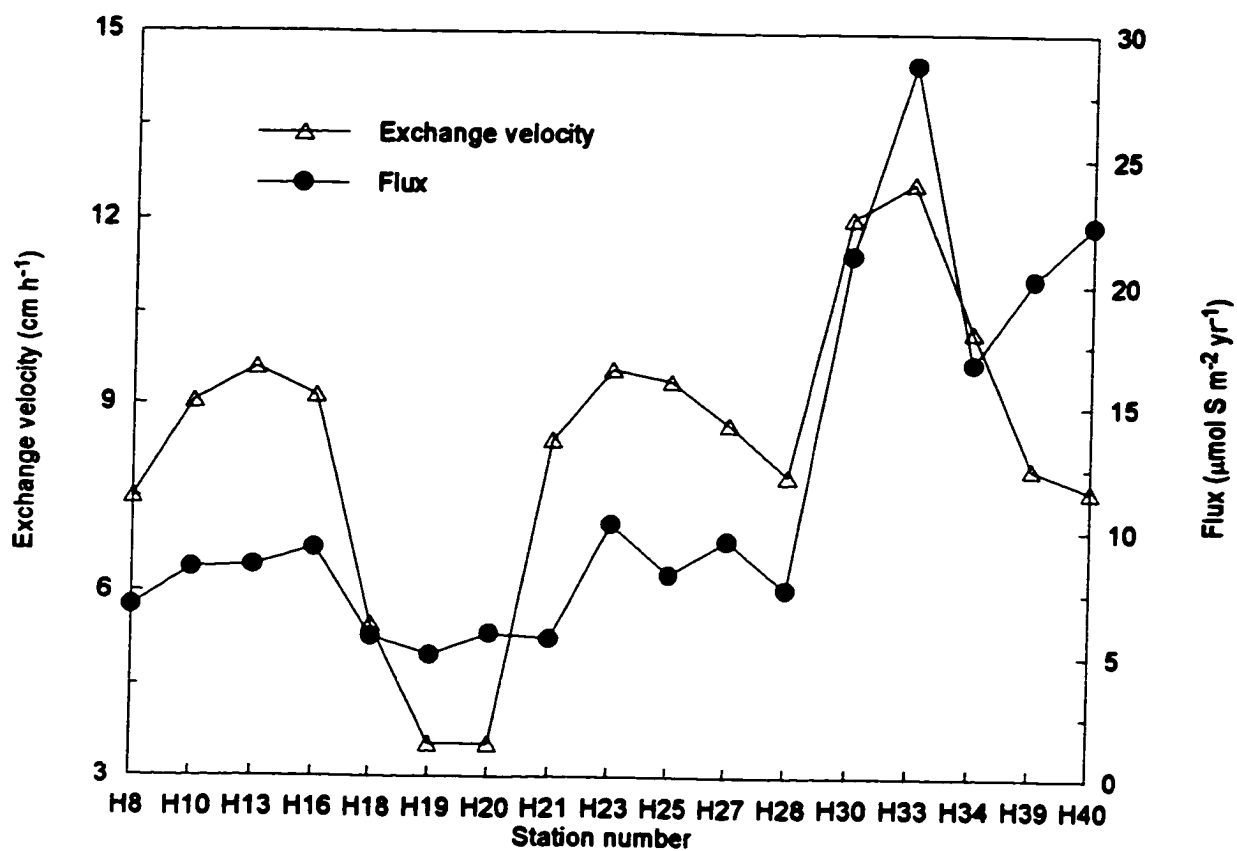


Figure 4.5 Exchange velocity and sea-to-air flux of CS₂ for the *Hudson* cruise. Both variables were calculated from climatological wind speeds.

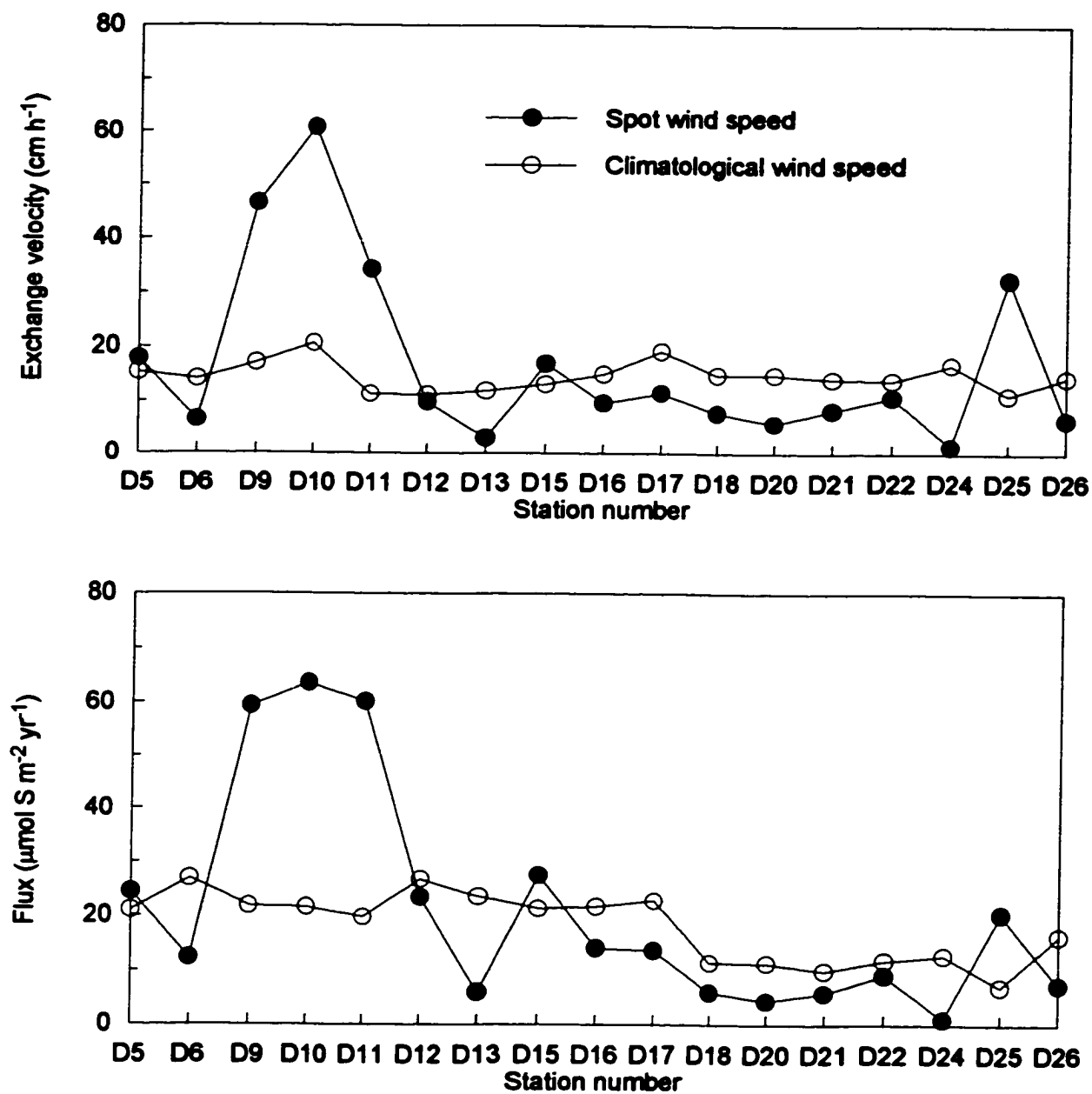


Figure 4.6 Exchange velocity (upper panel) and sea-to-air flux (lower panel) of CS₂ for the *Discoverer* cruise.

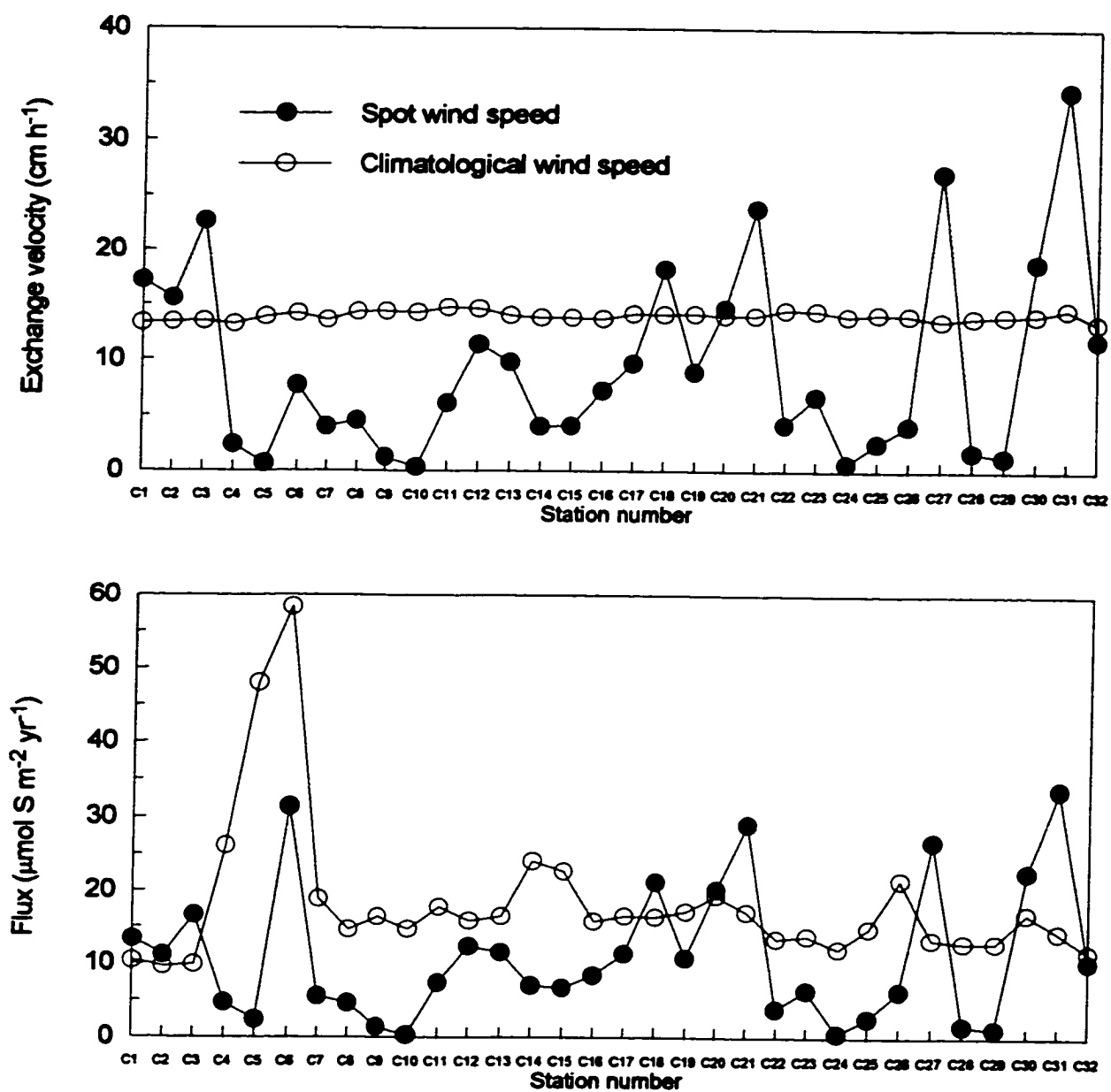


Figure 4.7 Exchange velocity (upper panel) and sea-to-air flux (lower panel) of CS₂ for the *Challenger* cruise.

Table 4.2 Flux estimates of CS₂ ($\mu\text{mol S m}^{-2} \text{ yr}^{-1}$) in the investigated regions.

Surveyed area	Flux (Wanninkhof)		Flux (LM)
	SWS	CWS	SWS
	<i>Coastal waters</i>		
NW Atlantic		13.4 (5.0-22.4)	
NE Atlantic	7.2 (6.7-8.0)	30.8 (22.7-45.6)	2.4 (1.0-3.1)
	<i>Open ocean waters</i>		
NW Atlantic		11.3 (5.6-28.7)	
Pacific Ocean	21.0 (1.0-63.6)	18.0 (6.9-26.9)	11.8 (0.2-34.0)
NE Atlantic	11.2 (0.4-33.8)	15.0 (9.6-21.5)	6.4 (0.1-16.9)

Flux data are mean values with ranges in parentheses. SWS is spot wind speed and CWS is climatological wind speed.

speeds above 5.0 m s^{-1} . As shown in Figure 4.2, the ratio of the exchange velocity from the LM relationship to that from Wanninkhof's equation is much lower at a wind speed of $\sim 4 \text{ m s}^{-1}$ than at $\sim 7 \text{ m s}^{-1}$, which obviously exerts similar effects on the flux ratios derived from these two relationships.

4.5 Extrapolation to the global oceans

Two methods are employed to extrapolate the flux estimates from this study to the global oceans. Following the procedures of Bates et al. [1987] and Mihalopoulos et al. [1992], the first method separates the ocean into coastal and open sea areas, and it further divides the open sea into five latitudinal regions. Each region is assigned a unit area flux obtained from the measurements located in the corresponding region and calculated using exchange velocities from equation 4.2. The calculated regional fluxes and other related data are shown in Table 4.3. The unit area flux gradually decreases poleward except in the subtropical regions where it is smaller than in the temperate waters. This may reflect the seasonal variations in the CS_2 flux, since most of the measurements in the subtropical areas were made in the austral spring while all the field surveys in the temperate latitudes took place in the boreal summer. The contribution of CS_2 evasion from each region to the atmosphere results from a combination of the unit area flux and the area for that region, ranking the tropical oceans as a main contributor and the subarctic areas as a minor one. CS_2 flux from coastal regions is comparable with that from the subtropical or temperate waters. The annual oceanic flux is, thus, estimated to be 0.25 Tg CS_2 .

The second method for estimating global ocean-to-atmosphere flux of CS_2 is based on the observation that CS_2 flux was strongly related to sea surface temperature (Figure 4.8). Figure 4.8 includes all the open ocean flux data from the three cruises, using equation 4.2 to calculate the exchange velocities. The increase

Table 4.3 Flux estimates of CS₂ in the global oceans using method one.

Region	Latitude degree	Area 10¹² m²	Unit area flux μmol S m⁻² yr⁻¹	Flux Tg CS₂ yr⁻¹
Equatorial	0-5	32	25.1	0.030
Tropical	5-20	92	21.4	0.075
Subtropical	20-35	77	14.2	0.042
Temperate	35-50	67	16.8	0.043
Subarctic	50-65	48	13.5	0.025
Coastal	0-50	49	20.8	0.039
Total		365		0.25

All the data of ocean area are from Bates et al. [1987] except the value for the coastal region which is from Kim and Andreae [1987a].

in flux with water temperature is a coupled consequence of the positive correlation found between CS_2 concentration and water temperature (see Chapter 4, section 4.1.2) and the inverse relationship between the Schmidt number and water temperature. The open ocean is divided into three types of waters by temperature, specifically, waters below 10°C , between 10°C and 20°C , and above 20°C . Areas of these waters are estimated from the COADS monthly mean sea-surface temperature data. In a fashion analogous to that of the first method, a unit area flux is assigned to each type of water. Table 4.4 indicates that about 58% of the ocean-to-atmosphere flux of CS_2 is from warm waters (above 20°C). The flux from the waters with temperature between 10 and 20°C is similar to that from the coastal regions, each accounting for about 17% of the total. Waters below 10°C contribute less than 10% of the total. The estimated total global flux using this method is $0.24 \text{ Tg CS}_2 \text{ yr}^{-1}$, in good agreement with the result of the first method. This agreement is not surprising since the regional subdivisions of the world ocean in the first method basically reflect the general patterns of the surface ocean temperature.

The flux estimate will decrease to $0.13 \text{ Tg CS}_2 \text{ yr}^{-1}$ if the LM relationship is used to calculate exchange velocities. Because no consensus exists on which one is more accurate, the best estimate from this study is defined as the average of the fluxes derived from the two relationships, this value being $0.18 \text{ Tg CS}_2 \text{ yr}^{-1}$ with a range from 0.13 and $0.24 \text{ Tg CS}_2 \text{ yr}^{-1}$. The flux estimated by Kim and Andreae [1987a] is $0.26 (0.13\text{-}0.52) \text{ Tg CS}_2 \text{ yr}^{-1}$, based on the measurements in the mid-latitudes of the Northwest Atlantic. Kim and Andreae [1987a] calculated the flux using their mean concentration of CS_2 and a single value of the exchange velocity (11.7 cm h^{-1}), equivalent to the global average exchange velocity for radon [Peng et al., 1979]. In addition, Kim and Andreae's data do not cover the subarctic region where the flux is estimated to be the smallest (Table 4.3). These factors may contribute to the difference in the flux estimate between the two studies.

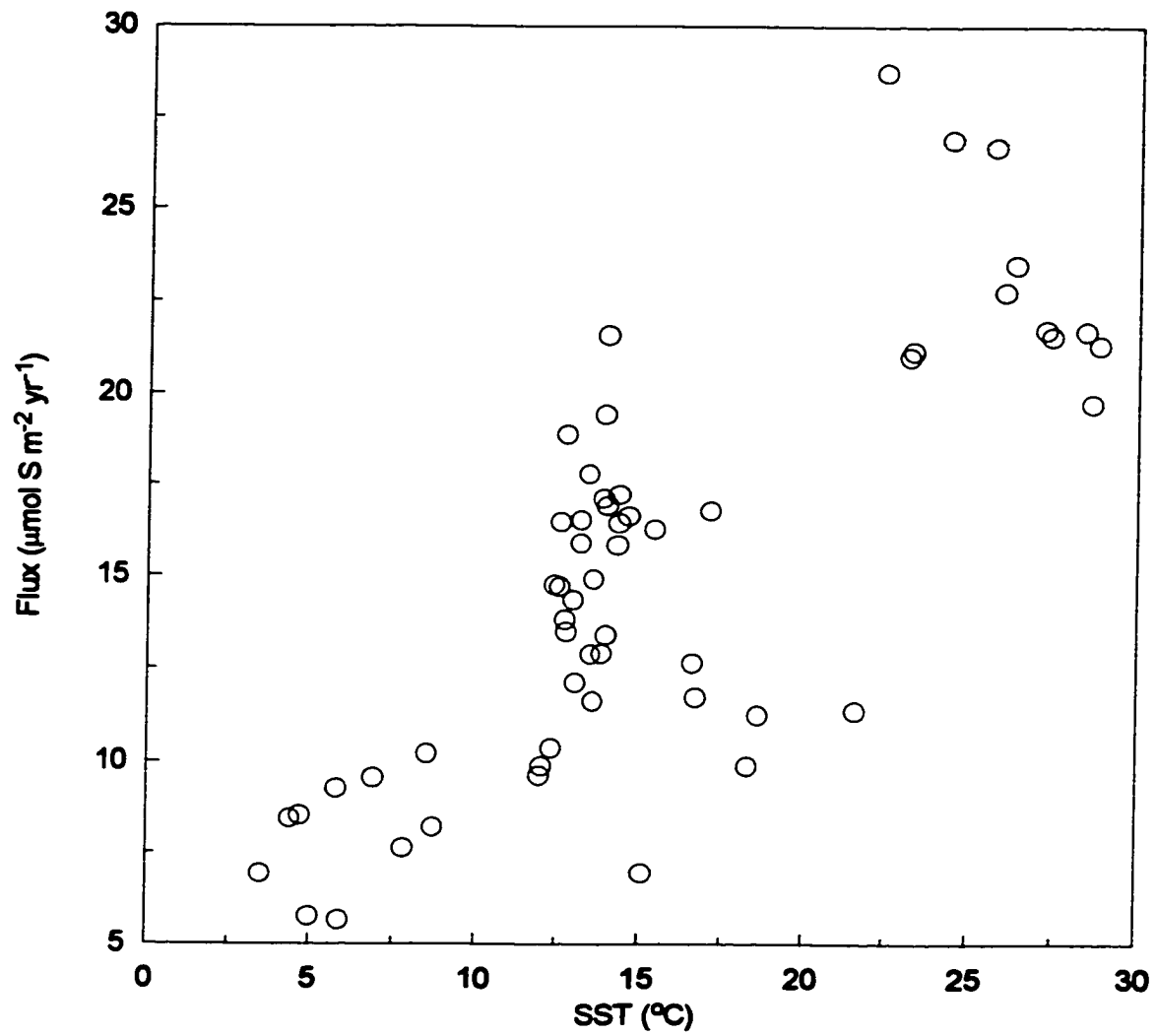


Figure 4.8 Sea-to-air flux of CS₂ vs. sea surface temperature for the open ocean data.

Table 4.4 Flux estimates of CS₂ in the global oceans using method two.

Temperature °C	Area 10 ¹² m ²	Unit area flux μmol S m ⁻² yr ⁻¹	Flux Tg CS ₂ yr ⁻¹
≤10	77	8.0	0.023
10-20	75	14.4	0.041
>20	164	22.1	0.138
Coastal	49	20.8	0.039
Total	365		0.24

References for both the total and coastal areas are the same as in Table 4.3.

Chin and Davis [1993] tried to refine Kim and Andreae's estimate by taking into account potential seasonal and diurnal variations in the flux, and they arrived at a value (mean: 0.18 Tg CS₂ yr⁻¹, range: 0.09-0.36 Tg CS₂ yr⁻¹) similar to that from this work. The result from this study supports the argument that the ocean is the second largest source for atmospheric CS₂, if the global budget for this compound derived by Chin and Davis [1993] is correct (see Chapter 1, section 1.5.1). As CS₂ in the atmosphere is oxidised to OCS with a molar conversion factor of 0.81 [Chin, 1992], an efflux of 0.18 Tg CS₂ yr⁻¹ from the ocean is equivalent to addition of 0.12 Tg OCS yr⁻¹ to the atmosphere. This value is equivalent to 41% of the direct sea-to-air flux of OCS estimated by Weiss et al. [1995].

A number of sources for uncertainty in the flux estimates exist. Seasonal variations in CS₂ flux are not taken into account, owing to lack of data with complete seasonal coverage in the visited ocean areas. In particular, no seawater measurements of CS₂ have ever been made in winter months, making it hard to further refine the flux estimates. The flux estimates in the coastal waters are based on only a few data points that may not be representative of global coastal areas. Moreover, in the flux calculation, the concentration of CS₂ is implicitly assumed not to be affected by wind speed. As pointed out by Moore et al. [1996] in the case of methyl chloride, this is not true if a high wind speed persists for such a time that the resulting elevated flux cannot be sustained simply because the loss terms overtake the production processes in a water column, inevitably leading to a decrease in CS₂ concentration. However, quantification of the uncertainty of this effect in the estimates of CS₂ flux is difficult as I do not know quantitatively the *in situ* loss and production processes for this compound.

None of the present flux estimates is large enough to match the predictions from atmospheric models which suggest an oceanic source on the order of ~10 Tg CS₂ yr⁻¹ [Rodhe and Isaksen, 1980; Wine et al., 1981; Chatfield and Crutzen, 1984;

Toon et al., 1987]. These models utilised ~30 pptv of atmospheric CS₂ at ground level [Sandalls and Penkett, 1977; Maroulis and Bandy, 1980; Bandy et al., 1981; Bandy et al., 1986], which is inappropriately high for unpolluted marine air. A more recent and generally accepted mixing ratio of CS₂ in remote marine boundary layer is a few pptv [Kim and Andreae, 1987a; Bandy et al., 1993; Johnson and Bates, 1993; Thornton and Bandy, 1993], which would lead to much lower predicted fluxes.

4.6 Summary

Saturation ratios for CS₂ were calculated using the surface water concentrations measured in the North Atlantic and the Pacific Ocean and the literature values of atmospheric concentrations and Henry's law constants for this compound. All the measured waters were greatly supersaturated in CS₂ relative to the atmosphere, and thus acted as a source for atmospheric CS₂. Ocean-to-atmosphere fluxes of CS₂ were computed as a product of the air-water concentration difference and the exchange velocity. The exchange velocity was derived from both Wanninkhof's and the LM relationships, using both spot wind speeds and climatological wind speeds. Geographically, tropical waters were estimated to contribute 30% of the total sea-to-air flux of CS₂. Contributions from the subtropical, temperate and coastal waters are comparable to each other and between 16 and 17% of the total flux. Equatorial and subarctic zones release the smallest amount of CS₂, each of them accounting for less than 12%. Classified by temperature, waters above 20°C are the largest oceanic source for CS₂ to the atmosphere, followed by waters between 10 and 20°C, and waters below 10°C. The best flux estimate from this study is 0.18 Tg CS₂ yr⁻¹ in the range 0.13 to 0.24 Tg CS₂ yr⁻¹. The estimated flux accounts for 32% (23- 42%) of the annual input of CS₂ into the atmosphere (0.57 Tg yr⁻¹) reported by Chin and Davis [1993]. Major uncertainties in the flux

estimate arise from the choice of the formula for calculating exchange velocity, and the restricted spatial and temporal coverage of the data. As different approaches were employed in estimating the exchange velocity and flux, a direct comparison is not possible between the results from this study with those from previous investigations [Kim and Andreae, 1987a, 1992].

Chapter 5 Carbon Disulphide Production in Phytoplankton Cultures

5.1 Introduction

Several species of land plants have been reported to be emitters of CS₂ [Aneja and Cooper, 1989 and references therein]. Phytoplankton are the most abundant plants in the ocean and are known to produce a variety of atmospherically reactive gases, such as DMS [Keller et al., 1989], isoprene [Moore et al., 1994; Milne et al., 1995], and methyl halides [Tait and Moore, 1995; Scarratt and Moore, 1996]. Moreover, CS₂ production have been observed in freshwater algal cultures [Caron and Kramer, 1994]. Therefore, marine phytoplankton are obvious candidates as sources of oceanic CS₂. Lovelock [1974] first explored the possibility of CS₂ production from marine algae and reported no release of this compound from the algal species that he examined. Unfortunately, no details about the species tested and the experimental conditions employed were revealed in that paper. Since then no further studies of this potential source have been reported. However, the vertical profiles obtained in the North Pacific central gyre (see Chapter 3, section 3.2.2) showed the coexistence of subsurface maxima in CS₂ and Chl-*a*, suggesting the possibility of an algal source for CS₂. In collaboration with Dr. Michael G. Scarratt who was examining the significance of the production of halocarbons in laboratory phytoplankton cultures, I collected CS₂ data from several of these culture experiments. The experimental materials and procedure are detailed in Chapter 2, section 2.4.

5.2 Results

5.2.1 Growth of the cultures

Axenic conditions were maintained for the duration of the experiments for all the cultures with the exception of the control (12Con) for *Phaeodactylum tricorutum*

and *Phaeocystis* sp.. This control vessel was accidentally contaminated with bacteria at the beginning of the experiment and contained a bacterial population of less than 1.85×10^4 cells mL⁻¹. Carbon-limitation may have occurred in culture 01Ccal as the pH increased to 9.2 during its exponential growth phase, while pH remained below 8.6 for the other cultures, and carbon-limitation was unlikely [Riebesell et al., 1993; Shiraiwa et al., 1993]. All the cultures, however, became nitrate-depleted before or by the end of the log growth phase.

Of the six phytoplankton species tested, three of them, namely, *C. calcitrans*, *P. tricorutum* and *Phaeocystis* sp. were found to produce significant CS₂. Production of CS₂ by the other three species was either undetectable or insignificant when compared with that in the corresponding controls. CS₂ concentrations in the control vessels for 04Con and 07Con remained essentially constant, while appreciable amount of CS₂ accumulated in the 12Con vessel.

Figures 5.1-5.3 show time series of cell population, Chl-*a* and total CS₂ in the cultures of *C. calcitrans*, *Phaeocystis* sp. and *P. tricorutum*. As indicated by cell population growth, culture 01Ccal started with exponential growth and evolved through a phase of declining relative growth, a stationary phase and finally a death phase. Chl-*a* in culture 01Ccal increased rapidly during log growth, but dropped abruptly upon entering the phase of declining relative growth and the stationary phase. Similar phenomena were observed in the other cultures, except culture 09Phcys in which Chl-*a* levelled off before the onset of the stationary phase. Cultures 08Phcys and 09Phcys showed a substantial initial decline of cell population over a fairly long period of time (at least 6 days), thus leading to an extended initial lag phase. Chl-*a* levels during the lag phase in these two cultures remained very low. The initial decrease in the cell population and the extended lag phase might stem from the possibility that a large portion of the inoculated cells was not viable and that the viable parent cells needed a prolonged period for

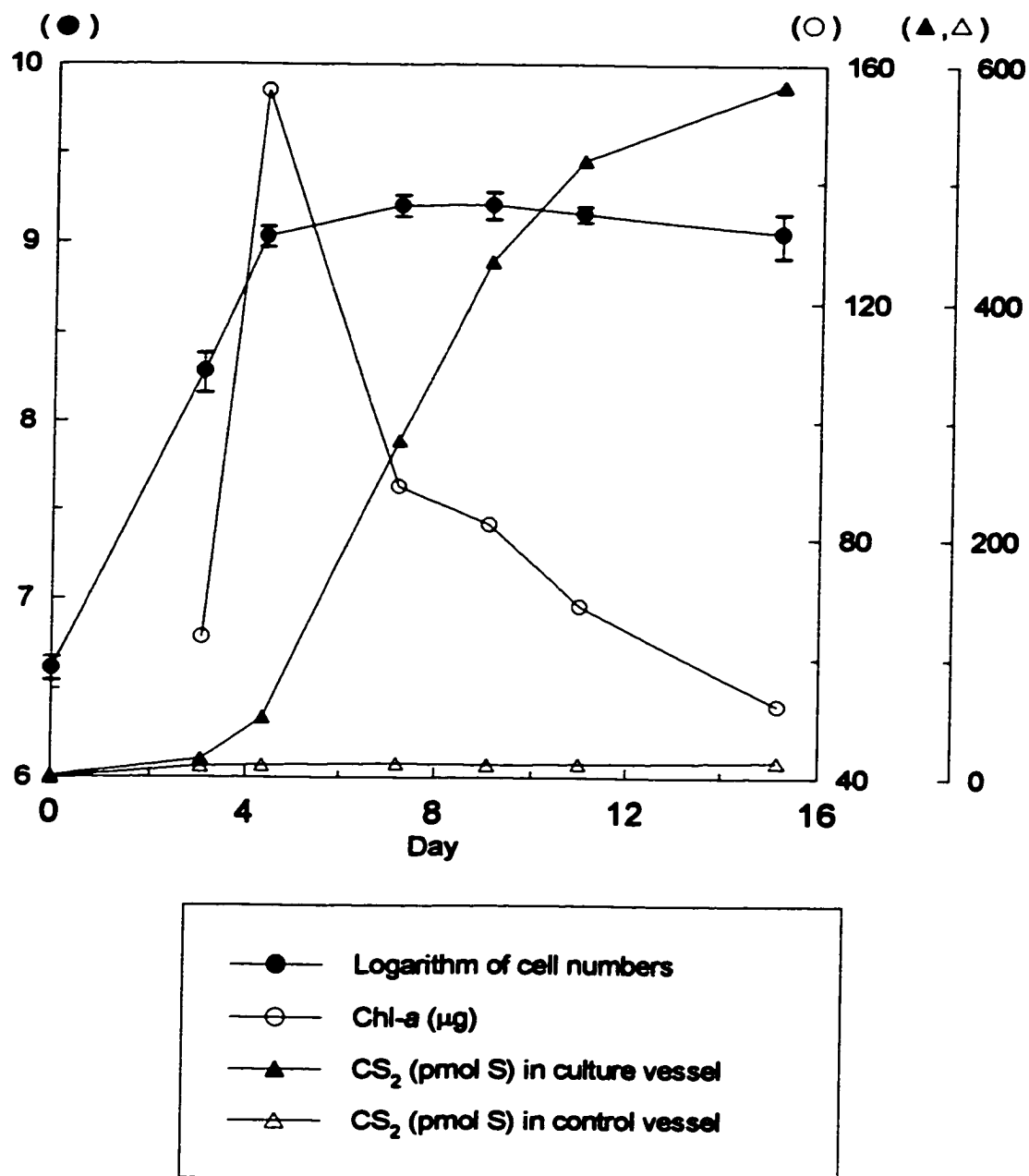


Figure 5.1 Total CS₂, cell number and Chl-*a* as a function of time for the culture of *Chaetoceros calcitrans* (culture 01Ccal and control 04Con). Error bars for cell population are defined as: upper side = $\log_{10}(\text{mean} + 1 \text{ SD})$ and lower side = $\log_{10}(\text{mean} - 1 \text{ SD})$.

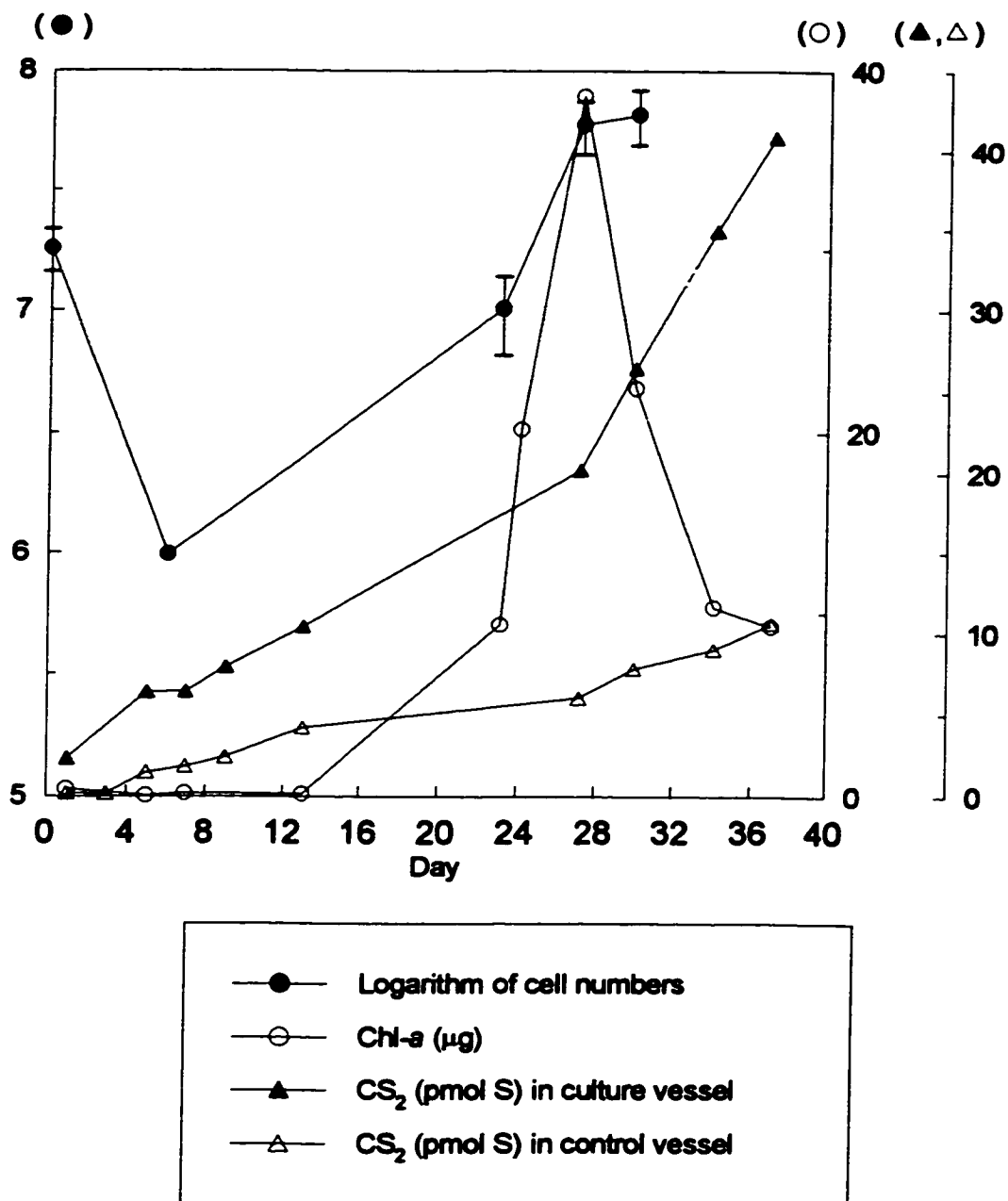


Figure 5.2a Same as Figure 5.1, but for the culture of *Phaeocystis* sp. (culture 08Phcys and control 12Con).

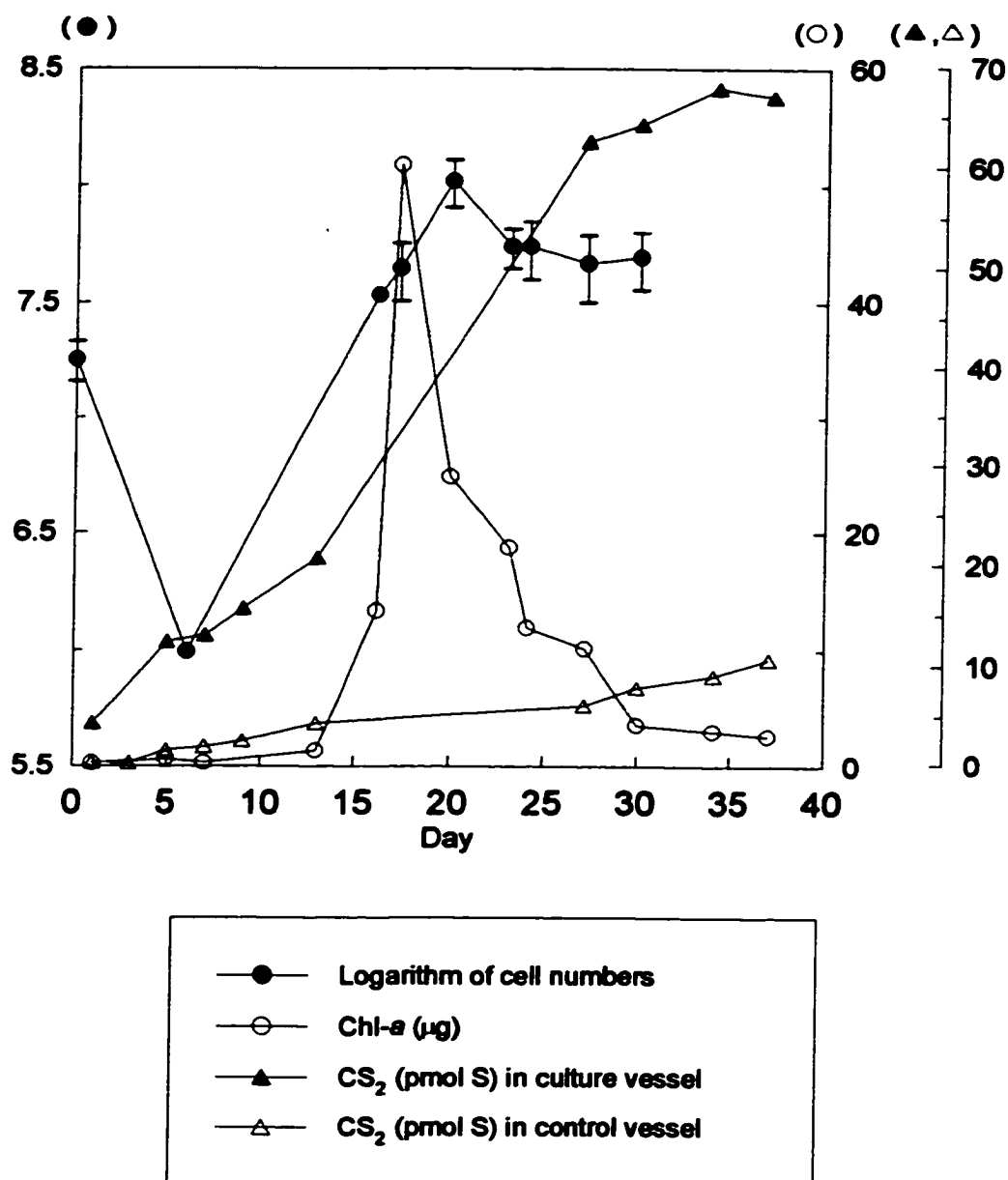


Figure 5.2b Same as Figure 5.1, but for the culture of *Phaeocystis* sp. (culture 09Phcys and control 12Con).

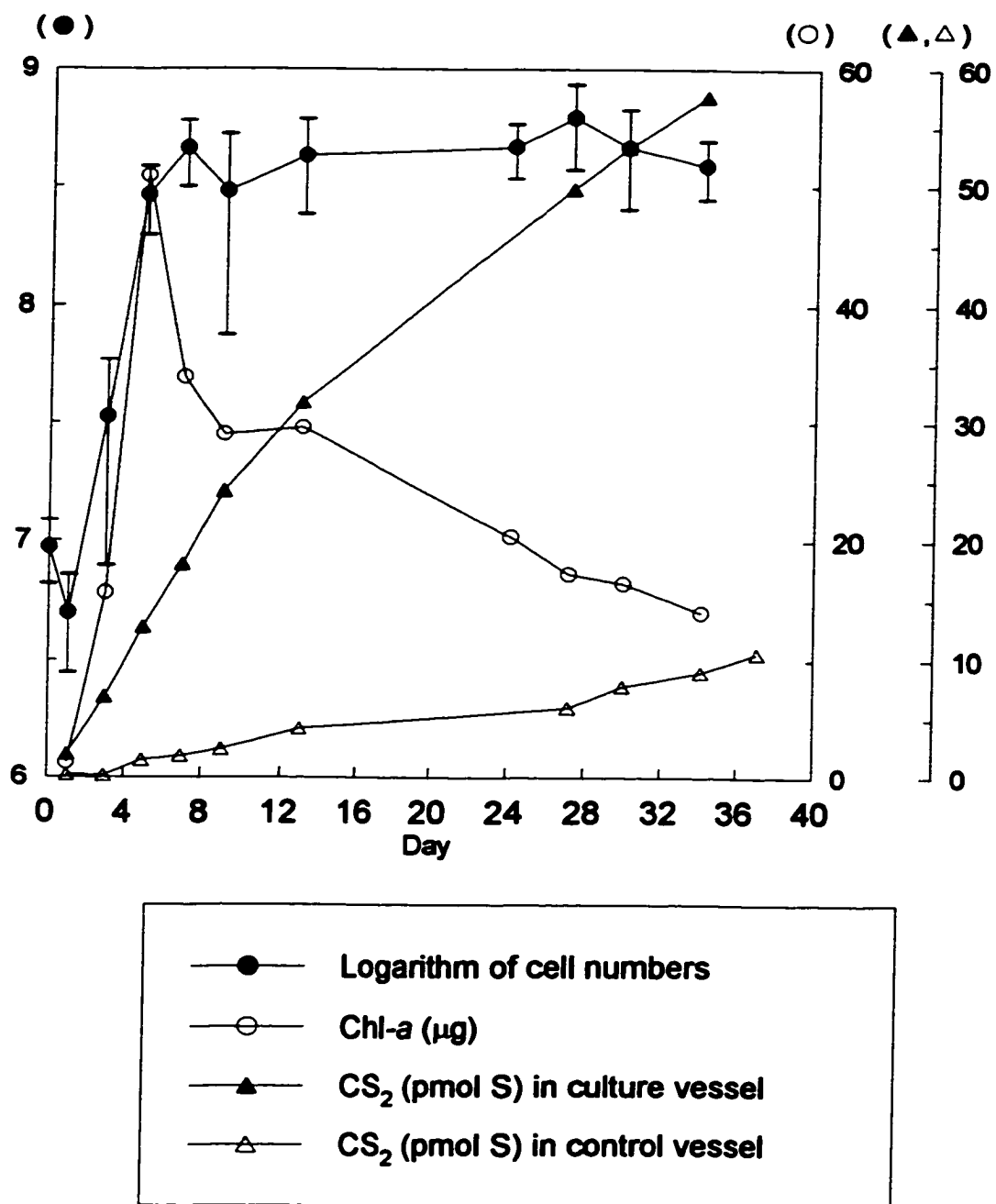


Figure 5.3a Same as Figure 5.1, but for the culture of *Phaeodactylum tricornutum* (Culture 10Ptri. and control 12Con)

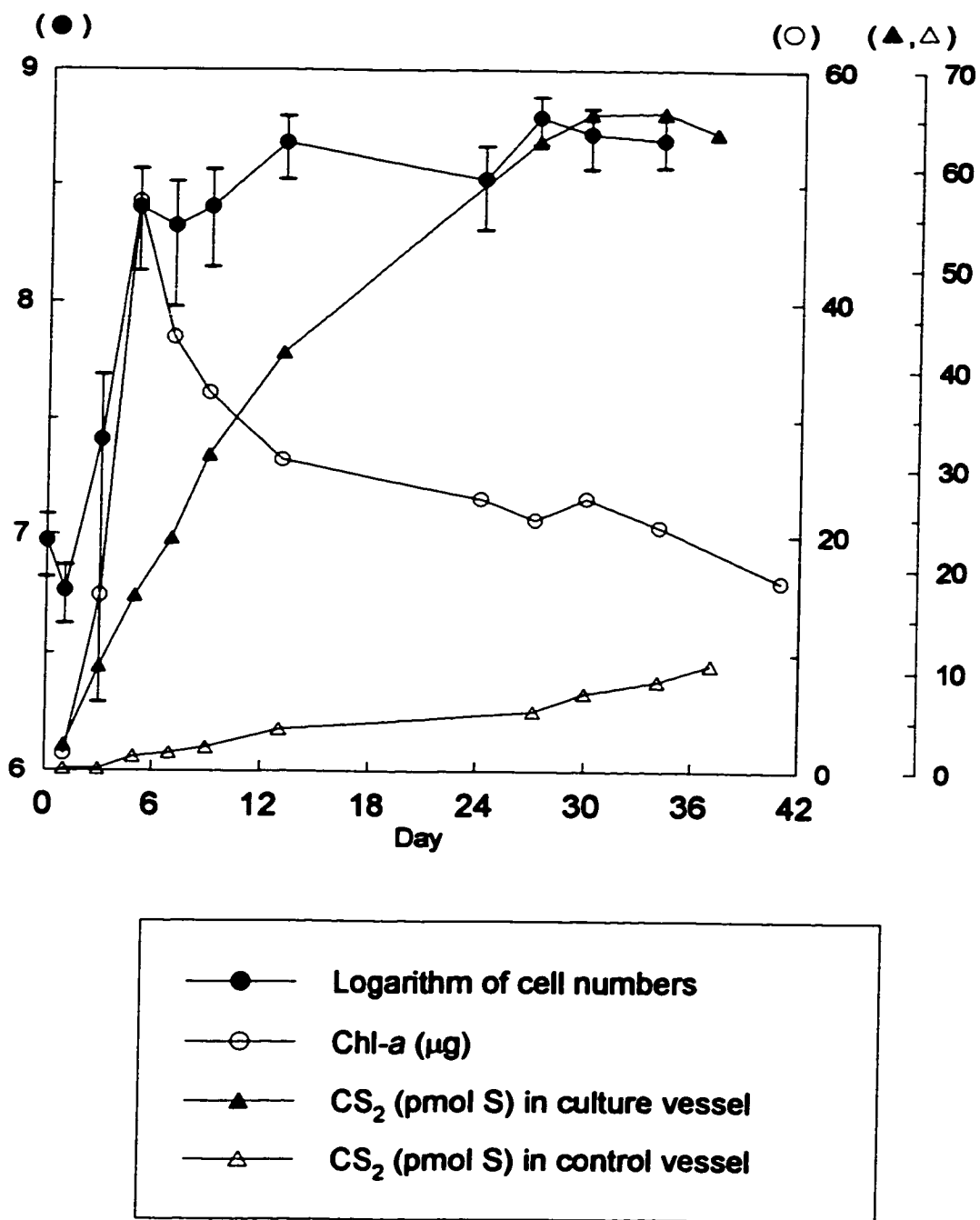


Figure 5.3b Same as Figure 2, but for the cultures of *Phaeodactylum tricornutum* (Culture 11Ptri and control 12Con)

conditioning before active growth could begin. In addition, the small size of the inoculum (5 mL into 1 L) could also delay the growth of the organism. An initial decline of cell numbers also occurred in cultures 10Ptri and 11Ptri, but to a lesser extent and over a shorter duration.

5.2.2 CS₂ production in the cultures

A number of features regarding CS₂ production in the cultures can be discerned from Figures 5.1-5.3. CS₂ in culture 01Ccal (Figure 5.1) was most efficiently produced in the phase of declining relative growth and in the stationary phase with little formation of the compound found in log phase. Continued production of CS₂ occurred during culture senescence, but the production rate decreased significantly. As in the case of culture 01Ccal, the highest CS₂ production rate in culture 08Phcys (Figure 5.2a) was also observed after the onset of the phase of declining growth. It is, however, difficult to ascertain for culture 09Phcys (Figure 5.2b) whether log-phase or stationary-phase production was more important due to the interruption of CS₂ measurement over the time period which straddled the log phase and stationary phase. Significant CS₂ generation was observed in the initial lag phase of cultures 08Phcys and 09Phcys. The duplicate cultures 10Ptri (Figure 5.3a) and 11Ptri (Figure 5.3b) showed largest CS₂ production rates during log growth and part of the stationary phase. With continued decay of cells, more CS₂ was produced at a reduced rate in culture 10Ptri, a feature similar to that in culture 01Ccal, while the total amount of the compound decreased slightly in cultures 11Ptri and 09Phcys.

Table 5.1 shows the maximum production rates that were calculated from the slopes of the total CS₂ curves and normalised to Chl-*a*. This calculation was not available for culture 09Phcys, as it is difficult to decide from the observed curve the time interval over which the maximum production rate occurred. The highest

Table 5.1 Maximum carbon disulphide production rates normalised to Chl-*a* and other related information.

Culture	Day range	Change of CS₂ pmol S d⁻¹	Average Chl-<i>a</i> µg	Production rate nmol S gchl⁻¹ d⁻¹
01Ccal	4.31-8.96	82	108.9	752
08Phcys	27.17-37.08	2.0	22.6	88
10Ptri	2.98-9.00	2.8	33.7	82
11Ptri	2.98-9.00	3.4	34.6	98

biomass-based production rate was observed in *C. calcitrans*, which was about an order of magnitude larger than the rates found in *Phaeocystis* sp. and *P. tricorutum*. *Phaeocystis* sp. and *P. tricorutum* had comparable production rates. Biomass-based production rates in the duplicate cultures of *P. tricorutum* (10Ptri and 11Ptri) were in good agreement with each other. Chl-*a*, instead of cell numbers, is the basis for production rates because (1) biomass in the ocean is rarely determined in terms of cell population, while oceanic Chl-*a* concentrations are relatively well-documented and are recognised as a reasonably good indicator of biomass, and (2) as indicated by the error bars (note the log scale) in the cell density curves in Figures 5.1-5.3, the uncertainty in the measurement of cell population was fairly high as a result of small sample volume (a few μL on a microscope slide) used for cell counting.

5.3 Discussion

5.3.1 Possible pathways for CS₂ production in the cultures

The results from this study indicate that production of CS₂ by marine phytoplankton is undoubtedly occurring, but it is not a universal phenomenon among marine algae. Even among those species which are able to produce CS₂, the biomass-based production rate can vary by a factor of ~ 9 (Table 5.1). The highly species-specific nature of the production implies that no simple correlation between CS₂ concentration and phytoplankton biomass (e.g. Chl-*a*) can be expected in the ocean. This is consistent with the field observations by Kim and Andreae [1992] (also see Chapter 3, section 3.1.4).

Bacterial interference with the formation of CS₂ by the phytoplankton species tested can be excluded, since the cell-containing cultures remained axenic throughout the duration of the experiments. However, the discernible increase of CS₂ in the bacteria-contaminated control vessel (12Con) does raise the possibility

that bacterial activity might produce CS_2 not only in anoxic aquatic environments [Lovelock, 1974; Andreae, 1986], but also in oxic surroundings.

As will be shown in Chapter 6, CS_2 is produced photochemically in seawater. Thus, the question arises of whether formation of the compound in the cultures was a result of photochemical reactions or non-photochemical processes. Figure 5.4 shows the CS_2 quantum-yield spectrum obtained during the *Challenger* cruise and the spectral irradiance of the fluorescent tubes used for incubating the cultures. Evidently, photo-production of CS_2 occurs dominantly in the UV region below 340 nm, while the fluorescent tubes emit mainly visible light, suggesting that photochemical processes should be very inefficient in forming CS_2 in the cultures. This was confirmed by experimental evidence showing that cool-white fluorescent light was incapable of inducing CS_2 photo-production. Specifically, the senescent *P. purpureum* cultures were passed through pre-combusted GF/C glass fibre filters and the resulting cell-free filtrate was irradiated in a solar simulator as described in Chapter 2. CS_2 concentration in the filtrate increased from less than 4 pM S to ~100 pM S after a 20-min exposure, and to ~360 pM S after a 125-min exposure (Figure 5.5). In marked contrast, no significant formation of the sulphur compound occurred in the *P. purpureum* cultures incubated with the fluorescent light. These observations indicate that although highly reactive precursors for CS_2 photo-production were present in the *P. purpureum* cultures, they were photochemically inert to the cool-white fluorescent light.

A photochemical mechanism was also inconsistent with the negative production rates during the stationary phase of cultures 09Phcys (Figure 5.2b) and 11Ptri (Figure 5.3b). Under the illumination of the fluorescent tubes, it was highly unlikely that CDOM could be completely photobleached or that sulphur substrates could be totally depleted photochemically in the stationary phase. As a matter of fact, the dominant formation of CDOM from phytoplankton in the ocean is

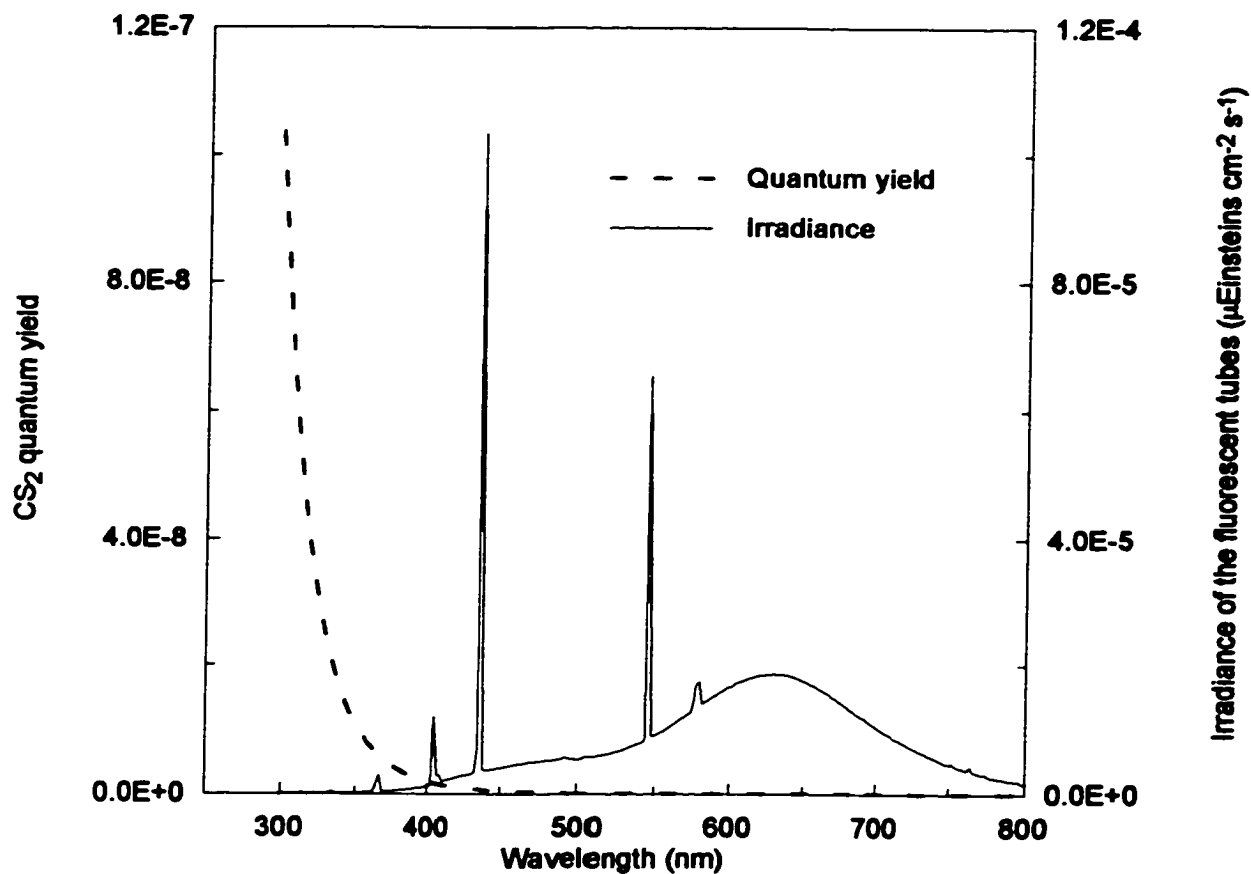


Figure 5.4 Quantum-yield spectrum of CS₂ photo-production and irradiance spectrum of the fluorescent tubes after correction for filtration by the glass wall of a water bath containing the culture vessels. The spectral irradiance of the light source was measured with a UV-visible spectroradiometer (OL 754-O-PMT).

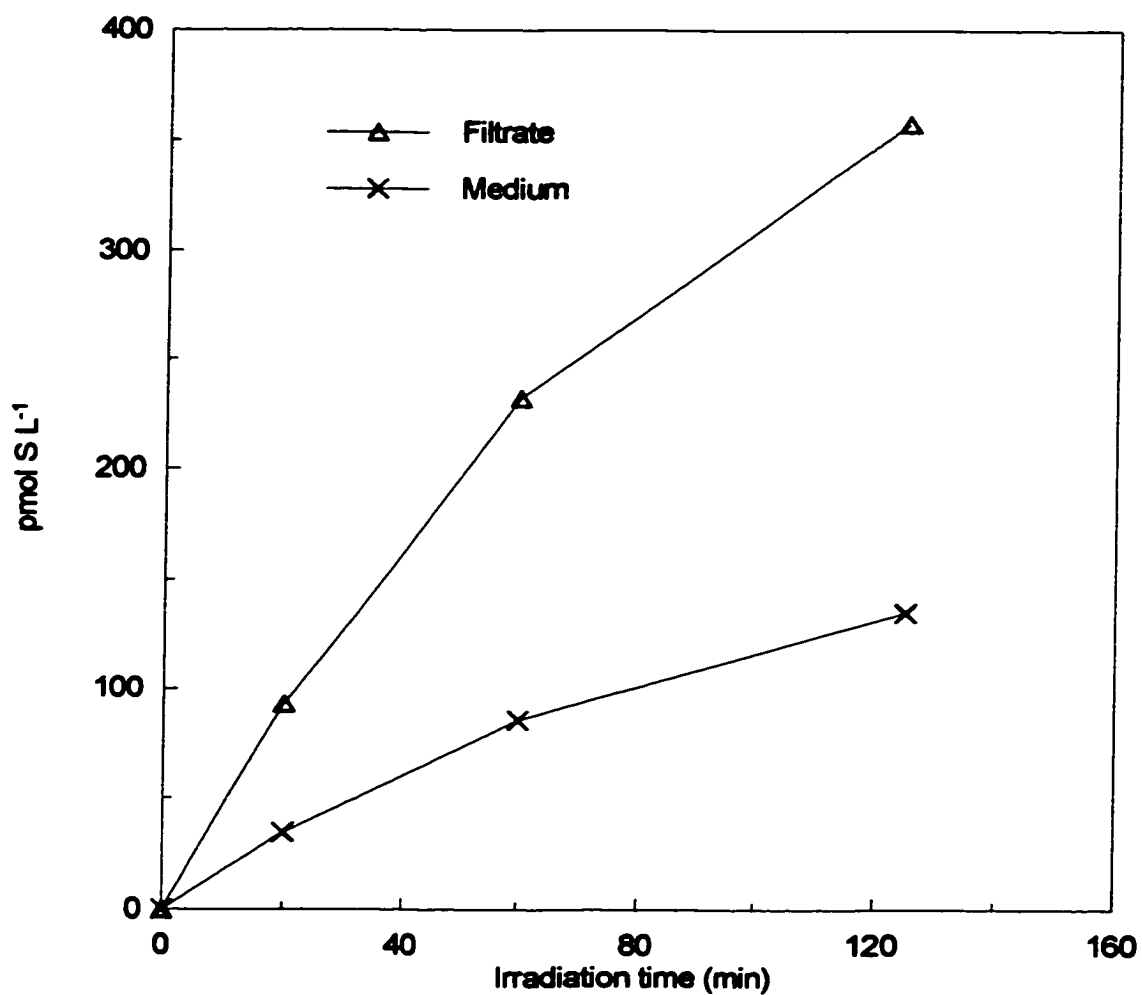


Figure 5.5 Photochemical CS₂ formation in the filtrate of *P. purpureum* and the culture medium (from the control vessel) that were irradiated with simulated solar radiation. Initial concentrations were deducted.

reported to lag behind primary production by 1-2 months [Carder et al., 1989].

The magnitude of CS₂ photo-production occurring in the cultures can be assessed using the following expressions,

$$P_{CS_2} = 2.2A \sum_{\lambda} \sum_t \Phi_{CS_2}(\lambda) I_{CDOM}(\lambda, t), \text{ and}$$

$$I_{CDOM}(\lambda, t) = \frac{a_{CDOM}(\lambda, t)}{a_{CDOM}(\lambda, t) + a_w(\lambda) + 0.5b_{msw}(\lambda) + a_{ph}(\lambda, t)} I(\lambda, t),$$

$$I(\lambda, t) = I_0(\lambda)(1 - e^{-(a_{CDOM}(\lambda, t) + a_w(\lambda) + 0.5b_{msw}(\lambda) + a_{ph}(\lambda, t))L})$$

where

P_{CS_2} = wavelength- and time-integrated photo-production of CS₂ in the culture vessel (μmol),

2.2 = correction coefficient for the curvature of cylindrical vessels [Leifer, 1988],

A = exposure area of the culture vessel (136 cm^2),

$\Phi_{CS_2}(\lambda)$ = quantum yield of CS₂ (Figure 5.4),

$I_{CDOM}(\lambda, t)$ = rate of light absorption by CDOM ($\mu\text{Einsteins cm}^{-2} \text{ s}^{-1}$),

$a_{CDOM}(\lambda, t)$ = absorption coefficient of CDOM (cm^{-1}),

$a_w(\lambda)$ = absorption coefficient of pure water provided by Smith and Baker [1981] (cm^{-1}),

$b_{msw}(\lambda)$ = molecular backscattering coefficient of seawater provided by Smith and Baker [1981] (cm^{-1}),

$a_{ph}(\lambda, t)$ = absorption coefficient of phytoplankton (normalised to Chl-*a*) (cm^{-1}),

$I(\lambda, t)$ = rate of light absorption by CDOM, water, and Chl-*a* ($\mu\text{Einsteins cm}^{-2} \text{ s}^{-1}$),

$I_0(\lambda)$ = irradiance of the fluorescent tubes (Figure 5.4) ($\mu\text{Einsteins cm}^{-2} \text{ s}^{-1}$), and

L = mean pathlength of the culture vessel (7.2 cm).

Variables containing λ and t are wavelength and time-dependent, respectively.

Here $a_{ph}(\lambda)$ is obtained by multiplying the specific phytoplankton absorption

coefficient (as normalised to Chl-*a* concentration) [Vodacek et al., 1994] by the observed Chl-*a* concentration in the cultures. Unfortunately, $a_{\text{CDOM}}(\lambda, t)$ was not measured. To compensate for this, absorption was subsequently measured using filtrates (GF/F filtered) of another two laboratory cultures (unialgal and axenic): *Nitzschia frustula* (diatom) and *Chlamydomonas plethora* (chlorophyte). The filtrates were collected during stationary growth of the cultures which had been incubated under cool-white fluorescent light for 42 days. The Chl-*a* concentration at the time of filtrate collection was $129 \mu\text{g L}^{-1}$ for *N. frustula*, and $97 \mu\text{g L}^{-1}$ for *C. plethora*. These values are much higher than the Chl-*a* concentrations observed for the stationary phase of the cultures shown in Figures 5.1-5.3. It is, therefore, postulated that the concentrations of CDOM (and hence $a_{\text{CDOM}}(\lambda)$) in *N. frustula* and *C. plethora* were greater than those in the cultures for which CS₂ production was studied. Figure 5.6 shows the CDOM absorption spectra, which are assumed to be the final $a_{\text{CDOM}}(\lambda)$ in the cultures of 01Ccal, 08Phcys, 09Phcys, 10Ptri, and 11Ptri. It is further assumed that the initial $a_{\text{CDOM}}(\lambda)$ for each of these cultures is comparable to that for the open ocean waters, and that $a_{\text{CDOM}}(\lambda)$ increased linearly with the age of the cultures. The $a_{\text{CDOM}}(\lambda)$ for the open ocean waters is taken from the average absorption spectrum measured during the *Challenger* cruise.

The estimated mean photo-production rates are shown in Table 5.2. These numbers can account for only 0.5% of the average production rate observed in culture 01Ccal and between 11% and 18% of those in the remaining four cultures. Thus, both the quantitative assessment and experimental observations excluded photochemical processes as a primary mechanism for CS₂ formation in the cultures. However, this conclusion should be viewed with caution since we do not know whether or not the quantum-yield spectrum from natural seawater is applicable to our cultures, or based on the evidence from the *P. purpureum* cultures, whether or not CS₂ precursors and CDOM in other cultures were similar

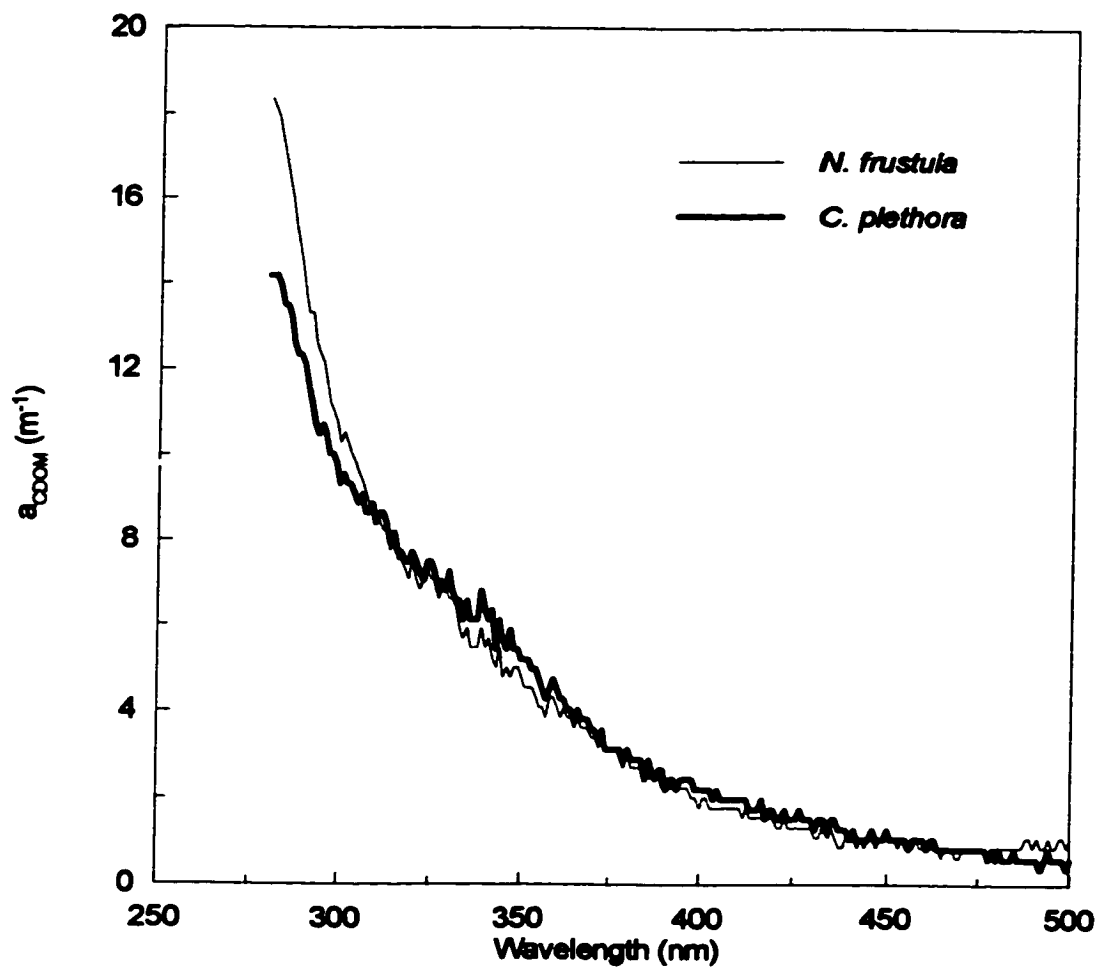


Figure 5.6 Absorption spectra of the filtrates from the cultures of *Nitzschia frustula* and *Chlamydomonas plethora*. Absorbance was measured using a Cary 3 double-beam spectrophotometer (Varian) fitted with a 1-cm quartz cell.

Table 5.2 Net production, potential photo-production and chemical destruction of CS₂. Also shown are the highest pH values and CS₂ concentrations in the liquid phase, which were used for calculating the chemical destruction rates.

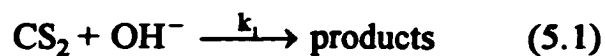
Culture	pH	[CS ₂] pM S	Net production fmol S d ⁻¹	Photo- production fmol S d ⁻¹	Loss fmol S d ⁻¹
01Ccal	9.2	480	38476	188	1194
08Phcys	7.7	28	1102	194	2
09Phcys	8	45	1807	194	6
10Ptri	8.6	39	1689	192	24
11Ptri	8.65	47	1715	192	34

in photochemical reactivities to those in *P. purpureum*.

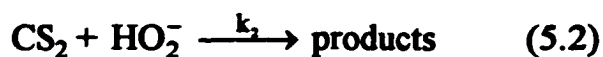
The high production rates of CS₂ observed during exponential growth of *P. tricornutum* suggest that metabolism associated with active cell growth might play a role in producing CS₂. Cell autolysis is another potential mechanism as rapid generation of CS₂ occurred during the stationary phase of *C. calcitrans* and *Phaeocystis* sp.. *Phaeocystis* is a prolific producer of DMSP [Liss et al. 1994] and is able to convert DMSP enzymatically to DMS [Stefels and van Boekel, 1993; Stefels and Dijkhuizen, 1996]. One potential pathway for CS₂ production in *Phaeocystis* sp. is through conversion of DMS and/or DMSP. However, this should not be the case with *C. calcitrans* and *P. tricornutum* since the two species yield little DMS and DMSP [Keller et al., 1989]. Other potential precursors are isothiocyanates. Hydrolysis of isothiocyanates produces OCS, while reaction of these compounds with H₂S forms CS₂ [Challenger, 1959]. Isothiocyanates are synthesized by many terrestrial plants and freshwater algae [Ina et al., 1991; Tsuchiya et al., 1992; Stratmann et al., 1994; Newman, et al., 1996], and a variety of marine sponges [Konig et al., 1996; Dumdei et al., 1997]. It is, however, unknown if marine algae are able to produce isothiocyanates. Clarification of this question in the future may be important to further our understanding of the mechanism responsible for CS₂ and OCS production in the ocean.

5.3.2 Loss of CS₂ in the cultures

Carbon disulphide is destroyed by its basic hydrolysis and reaction with the hydrogen peroxide conjugate base HO₂⁻ [Elliott 1990]:

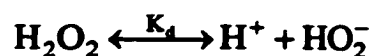


($k_1 = 1.0 \times 10^{-3} \text{ M}^{-1} \text{ s}^{-1}$, room temperature)



($k_2 = 20.4 \text{ M}^{-1} \text{ s}^{-1}$, room temperature)

The rate constants, k_1 and k_2 are from Elliott [1990], and the concentration of OH^- is calculated from the pH measurement. The concentration of HO_2^- can be derived from the acid-dissociation [Evans and Uri, 1949],



($K_d = 2 \times 10^{-12}$)

Hydrogen peroxide in the ocean is formed largely through photochemical reactions induced mainly by solar UV radiation [Cooper et al., 1988; Sikorski and Zika, 1993]. Photo-production of H_2O_2 in our culture vessels was probably not important due to lack of UV from the artificial light source. Using an upper limit estimate (200 nM) for H_2O_2 in coastal waters [Miller and Kester, 1994] and the observed highest concentrations of CS_2 and pH values in our cultures, reactions 5.1 and 5.2 give insignificant loss of CS_2 relative to the net production rates (Table 5.2). These loss rates are also negligible compared with the negative production rates found in the stationary phase of cultures 09Phcys (289 fmol S d^{-1}) and 11Ptri (698 fmol S d^{-1}). However, some phytoplankton species can produce H_2O_2 [Palenik et al., 1987]. Because of the high cell densities in our cultures, reaction 5.2 could be an important sink for CS_2 if the cultured species are efficient producers of H_2O_2 . In that case, the production rates in the cultures might be underestimated and the chemical destruction could then be an important factor, resulting in the level-off of CS_2 production during stationary growth of cultures 09Phcys and 11Ptri.

5.3.3 Extrapolation to the real oceans

Under the assumption that oceanic phytoplankton will produce CS_2 at similar rates to those observed in the cultures, estimates of the global potential for CS_2

production by phytoplankton can be made using the Chl-*a*-normalised production rates (Table 5.1), an average oceanic Chl-*a* concentration of 30 mg m⁻² [Morel and Berthon, 1989], and a total ocean area of 3.6×10^{14} m². The scaled estimates in Gg CS₂ per year are 14 for both *P. tricornutum* and *Phaeocystis* sp. and 112 for *C. calcitrans*, which account for, respectively, 8%, and 62% of the sea-to-air flux of the compound (0.18 Tg CS₂ yr⁻¹) estimated in Chapter 4. Thus, if we assume that the CS₂ production rate measured for *C. calcitrans* is representative of the ocean as a whole, the potential oceanic CS₂ production by phytoplankton can constitute an important fraction of the CS₂ needed to sustain loss to the atmosphere. On the other hand, if such supposition is applied to *P. tricornutum* or *Phaeocystis* sp., this production is insignificant compared with gas exchange. Furthermore, the other three species, *Synechococcus* sp., *Isochrysis* sp. and *Porphyridium purpureum* are non-producers of CS₂. Extrapolation from these three species yields zero production of CS₂. In addition to the species-specific nature, CS₂ formation also depends on the physiological states of the algae. Moreover, only a very limited number of species were examined under controlled conditions which also did not duplicate the condition of the real ocean. Therefore, based on the results from this study, the contribution of phytoplankton to oceanic CS₂ production cannot be clearly demonstrated. The extrapolation made here is intended only to indicate the potential for CS₂ production in phytoplankton, and is not a rigorous estimate of the global processes.

5.4 Summary

Carbon disulphide data were collected from axenic monocultures of six species of marine phytoplankton: *Chaetoceros calcitrans*, *Phaeodactylum tricornutum*, *Phaeocystis* sp., *Porphyridium purpureum*, *Synechococcus* sp. and *Isochrysis* sp.. For a period of between fourteen and forty days, substantial accumulation of CS₂

was found in the cultures of *C. calcitrans*, *P. tricorutum* and *Phaeocystis sp.*, whereas the change of CS₂ concentration in the remaining cultures was insignificant. *C. calcitrans* has a potential for CS₂ production about 10 times higher than *P. tricorutum* or *Phaeocystis sp.*. The formation of the compound was strongly dependent on the physiological state of the cultured species. More investigation is needed to elucidate the mechanisms responsible for CS₂ production by marine phytoplankton.

Chapter 6 Photochemical Production of CS₂ in Marine Waters

6.1 Introduction

Sunlight-initiated chemical production of CS₂ was suggested in the results of the present study from the construction of calibration curves for the GC/MS system using a standard addition method. This method used a secondary liquid standard of CS₂ and seawater to make working standards (see Chapter 2, sections 2.2.3 and 2.2.5). Prior to the calibration, ~2.5 L of seawater (taken from the Northwest Arm of Halifax, Nova Scotia, Canada) was passed through a 0.45- μ m filter and divided into two portions. One portion was then stored in a stoppered flask and left indoors while another portion was placed in an open glass vessel and left outdoors for ~16 hours to reduce the background level of CS₂. Surprisingly, the concentration of CS₂ in the outdoor sample (38 pM S) was found to be ~40% higher than that in the indoor sample (27 pM S). One possibility was photochemical CS₂ formation in the outdoor sample since this sample was directly exposed to sunlight for ~4 hours. Incubations of unfiltered seawater under solar radiation showed substantial production of CS₂ (Figure 6.1a). However, the effects of biological activity could not be eliminated using unfiltered seawater. More rigorous confirmation of photo-production of CS₂ formation was made by irradiating 0.2- μ m filtered (cellulose acetate membrane, Nalgene) seawater with sunlight. The 0.2- μ m filters should remove all algal cells and most bacteria, thus minimising the biotic influence. The results (Figures 6.1b,c) indicate that CS₂ concentration in the irradiated samples increased steadily with time, while no significant concentration change was observed in the dark controls.

In order to assess the significance of photochemical CS₂ formation in the ocean, wavelength-dependent studies, as well as full-spectrum irradiations, were conducted during the *Challenger* cruise in the Northeast Atlantic. Detailed

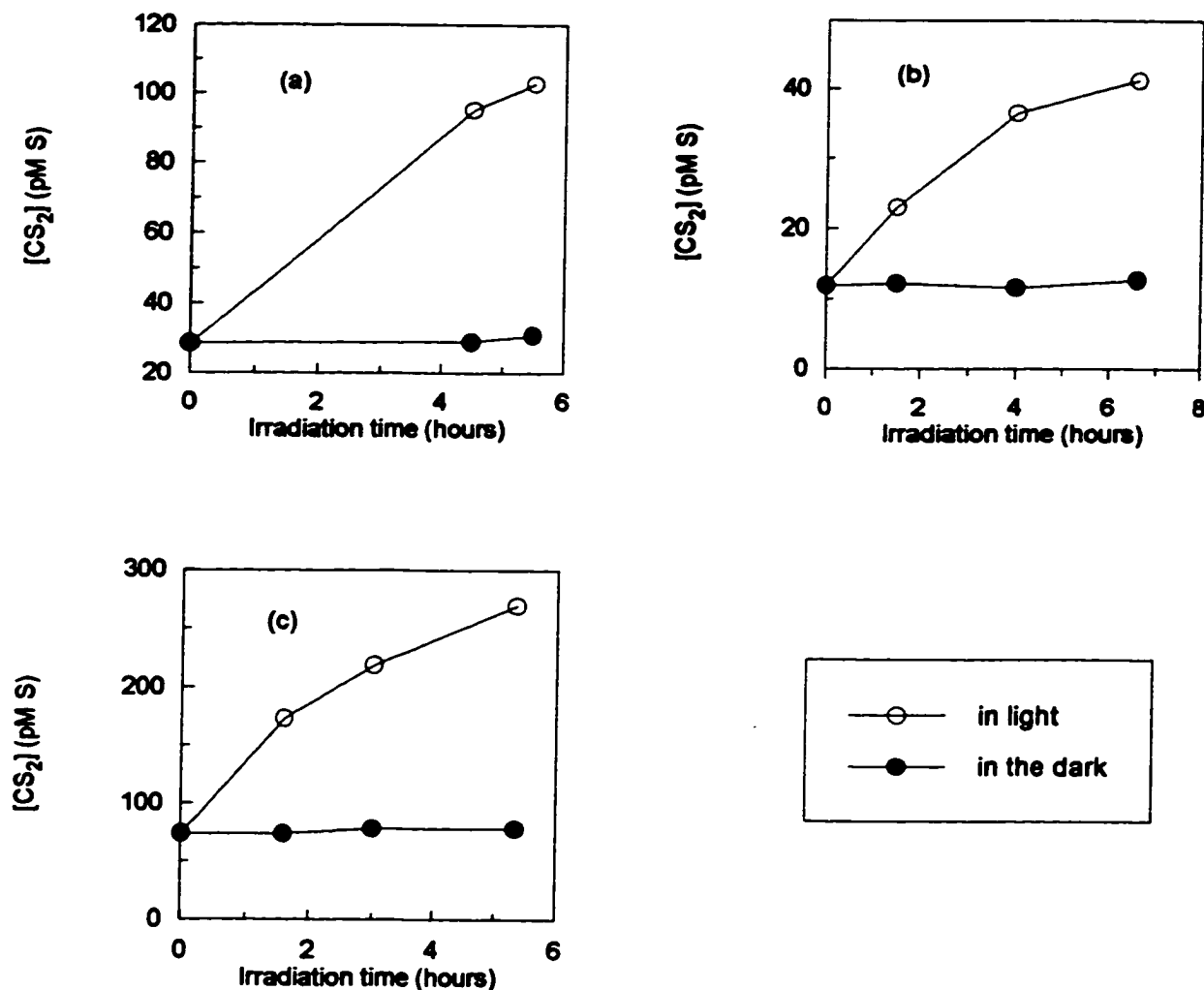


Figure 6.1 Preliminary tests on photochemical formation of CS_2 in seawater. (a) Unfiltered surface seawater collected at station H33 during the *Hudson* cruise. Irradiation was done immediately after sample collection. (b) 0.2- μm filtered surface seawater collected at station H39 during the *Hudson* cruise. Seawater was stored in a 20-L polyethylene bottle for ~14 months. (c) 0.2- μm filtered seawater taken at 10 m from the Northwest Arm of Halifax, Nova Scotia, Canada. Irradiation was done immediately after sample collection. Samples for all the tests were contained in 100-mL ground glass (Pyrex) syringes and irradiated under natural sunlight.

description of the sampling locations and methods, and the irradiation experiments are given in Chapter 2. Laboratory studies provided a brief exploration into possible mechanisms responsible for CS₂ photo-production. These included identification of potential CS₂ precursors and evaluation of the effect of OH radicals on this production.

6.2 CDOM absorptivity

Sixteen CDOM absorption spectra were measured using surface water samples obtained from the *Challenger* expedition in the Northeast Atlantic. Shown in Figure 6-2 are plots of the absorptivity at 350 nm against salinity. The absorptivity at 350 nm averaged 0.318 m⁻¹ and ranged from 0.229 to 0.484 m⁻¹. The brown and less saline water (34.2 salinity) in Galway Bay (station C5) had the highest value, indicating high abundance of CDOM in the bay. While most of the samples for absorption measurements came from in waters of a limited salinity range (35.2-35.5), the absorptivity at 350 nm is fairly variable (2.29-3.91 m⁻¹).

The absorptivity for all the samples decreased approximately exponentially with increasing wavelength. Figure 6.3a displays the average absorption spectrum from this study in both the linear-linear and log-linear fashions. The spectral slope, which is the slope (absolute value) of the fitted line for the log-linear curve, is an important optical parameter that indicates how fast the absorptivity decreases with increasing wavelength. It has been frequently shown that waters dominated by terrestrial CDOM (low salinity) have lower values of the spectral slope than waters dominated by marine CDOM [Blough et al., 1993; Green and Blough, 1994; Nelson and Guarda, 1995; Vodacek et al., 1997]. Figure 6.3b shows plots of the spectral slope against salinity for the data from this work. The spectral slope was determined in the wavelength range 290-500 nm. The mean value of the spectral slope is 0.019, and its range is from 0.017 to 0.024. Unexpectedly, the water

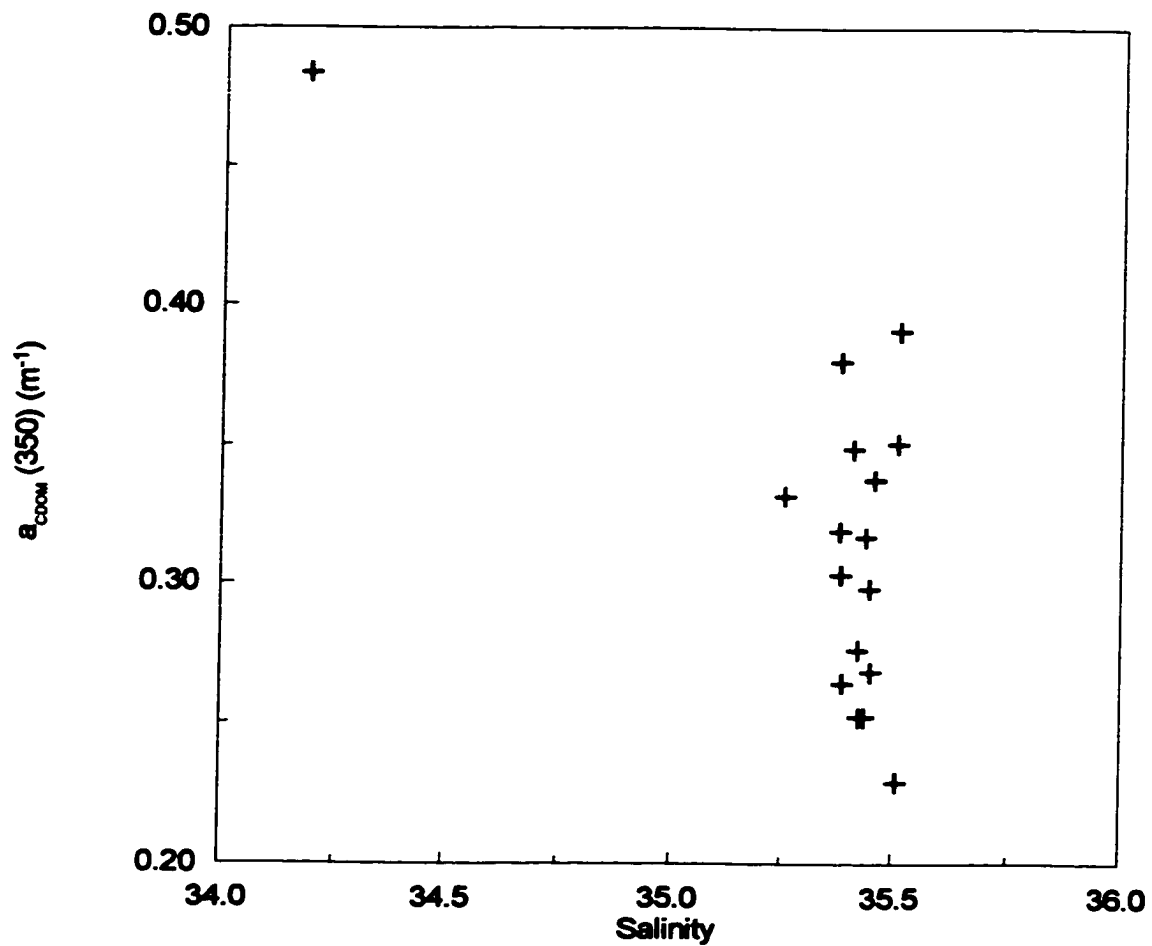


Figure 6.2 Absorptivity at 350 nm as a function of salinity for surface water samples collected during the *Challenger* cruise.

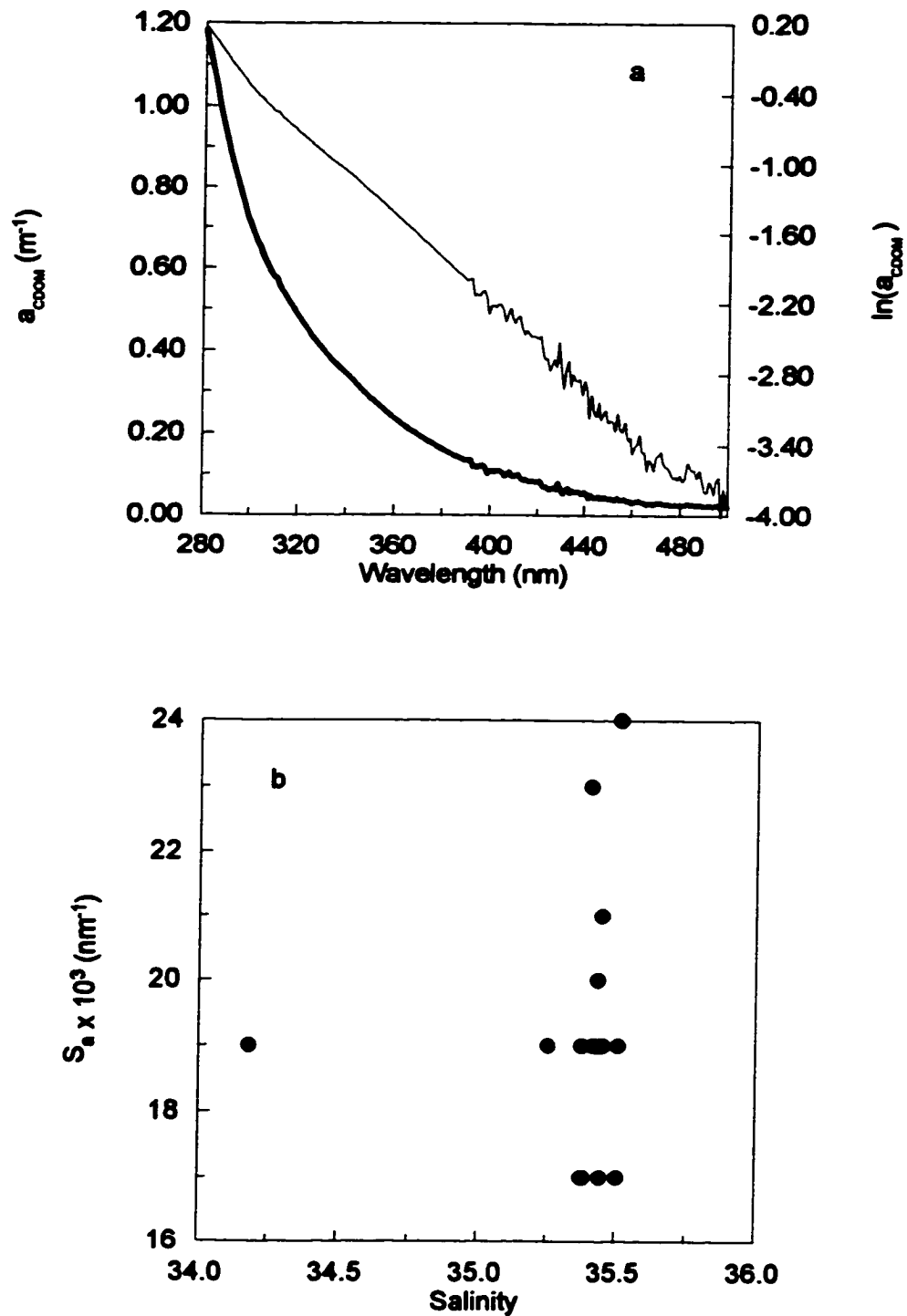


Figure 6.3 (a) Average absorption spectrum for surface water samples. Dark line is the linear-linear relationship and light line is the log-linear relationship. (b) Spectral slope for surface water samples as a function of salinity.

sample with the lowest salinity (station C5) does not possess the lowest spectral slope. In addition, variability in the spectral slope is evident for samples which had salinity around 35.5. The lack of inverse relationship between the spectral slope and salinity is mostly because the variability of salinity is too small to be reflected in the variation of the spectral slope.

Five absorption vertical profiles were obtained from the investigation in the Northeast Atlantic; they are shown in Figure 6.4 along with the temperature and Chl-*a* data. Clearly, no correspondence exists between the absorption and Chl-*a* distributions, suggesting that the abundance of CDOM does not covary with phytoplankton biomass as indexed by Chl-*a* concentration. Vodacek et al. [1997] reported that significant loss of CDOM absorption (photo-bleaching) may occur in the surface mixed layer in summer (August) and that photobleaching is not evident in other seasons and in subsurface water. The absorption profiles obtained from this study do not show lower absorption for samples taken from the mixed layer compared with those from the subsurface. Therefore, photo-bleaching was probably not important to optical properties in this region during the time of our investigation (June).

6. 3 Irradiation time

Preliminary tests (Figure 6.1) showed that CS₂ photo-production rates decreased substantially after a certain period of irradiation. This could result from the consumption of CS₂ precursors and/or the photodegradation of the CDOM which sensitizes reactions responsible for formation of the compound. It was, therefore, necessary to choose an irradiation time which generates a reasonable amount of CS₂ with no significant decrease in the photo-production rate. Figure 6.5 illustrates a time series for irradiation of a surface water sample (station C27) during the *Challenger* cruise with the solar simulator in the wavelength-dependent

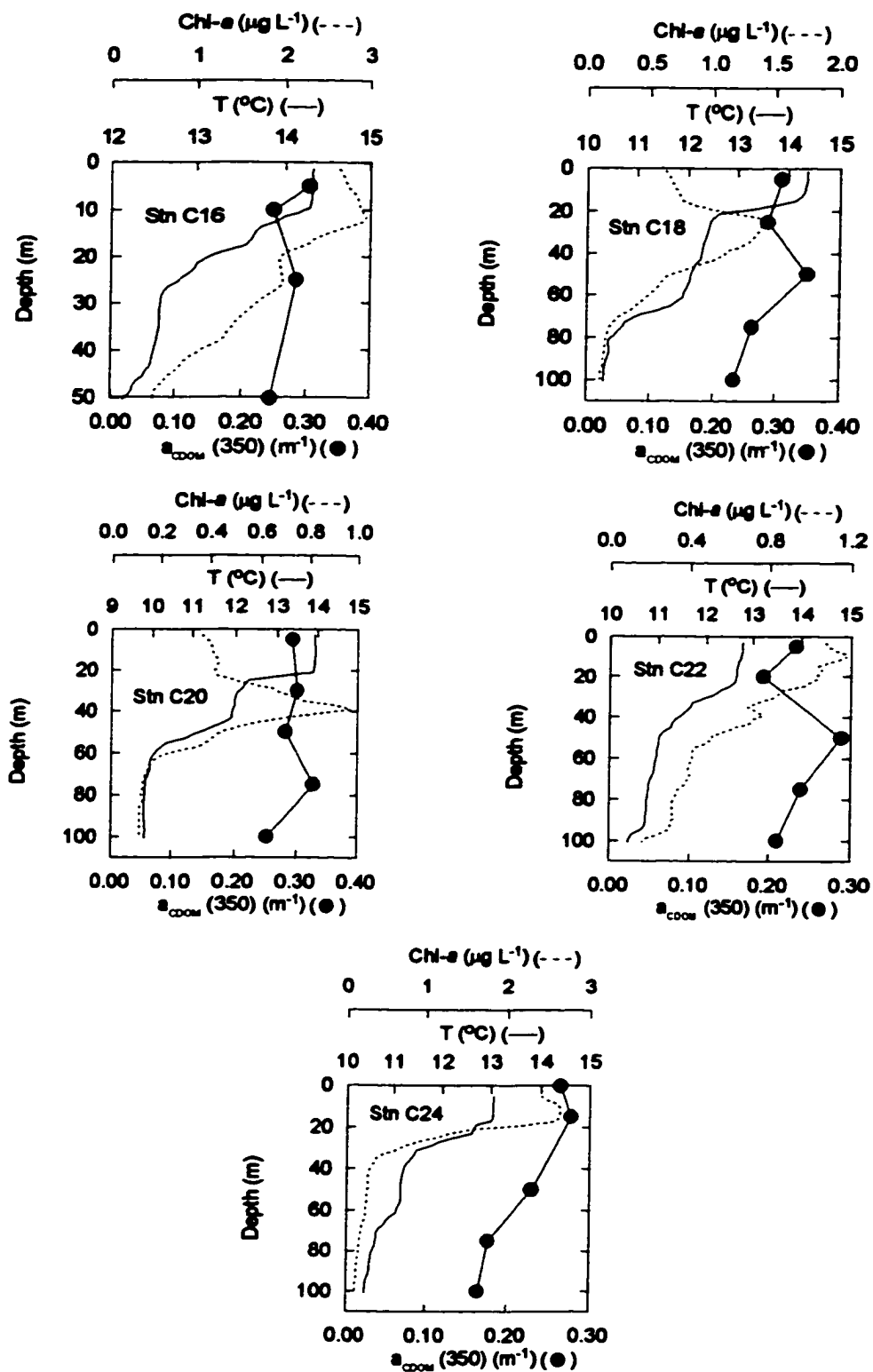
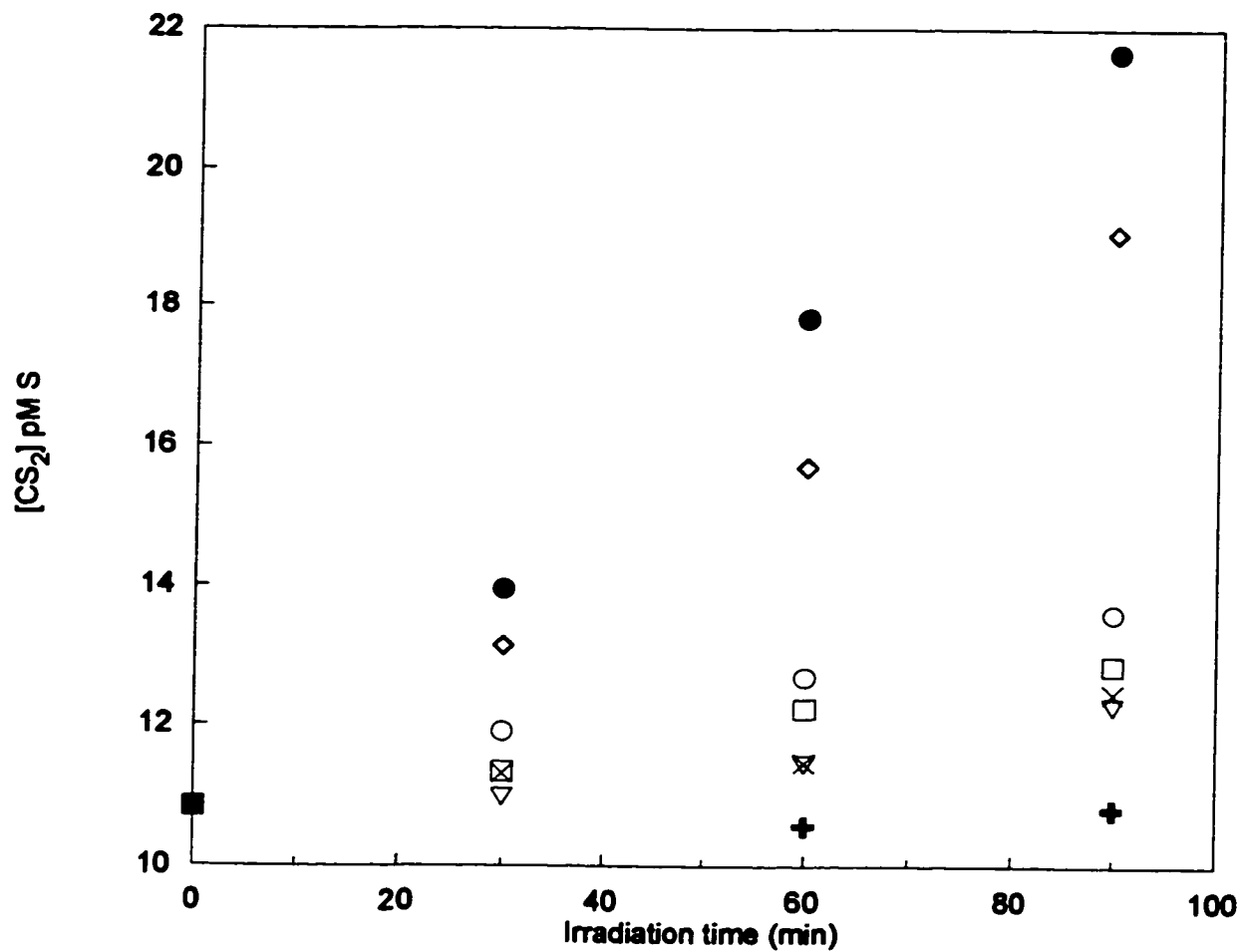


Figure 6.4 Vertical profiles of absorption, temperature and Chl- a .



	Filter No.	cutoff wavelength		Filter No.	cutoff wavelength
●	WG305	286 nm	○	WG345	337 nm
◇	WG320	302 nm	□	GG385	362 nm
×	GG420	407 nm	▽	GG475	468 nm
+	Control				

Figure 6.5 Time series of CS₂ photo-production in a surface sample at station C27 with the solar simulator in the wavelength-dependent irradiation mode.

irradiation mode. Obviously, photo-production dominated in samples irradiated under filters with cutoff wavelengths ≤ 362 nm, and a reasonably linear correlation between CS₂ concentration and irradiation time is seen for these samples during 90-min exposures. In marked contrast, change of CS₂ concentration in samples irradiated under filters with cutoff wavelengths ≥ 407 nm was very small, mostly within 3σ of the blank for the analytical method. Processes other than photochemical reactions might be making an important contribution to variations of CS₂ concentration in these two samples. Perhaps because of this, the irradiation experiments using filters GG420 and GG475 do not show linear relationship between CS₂ concentration and irradiation time. The irradiation time used for the *Challenger* cruise was mostly one hour with the exception of several cases in which samples were exposed for 30 or 45 min. The results from the above tests indicate that such time periods should produce appreciable accumulation of CS₂ with a relatively constant photo-production rate. In the following discussion, unless otherwise stated, the irradiation time was one hour.

6.4 Full-spectrum irradiation

Samples from seven hydrographic casts were irradiated using simulated solar radiation. Examples of profiles established from the original and irradiated samples are shown in the first five panels of Figure 6.6. Increases in CS₂ were observed for all the irradiated samples and were depth-dependent. Analysis of the irradiated 100-m sample for station C7 and 75-m sample for station C16 failed due to technical problems. Change of CS₂ concentration in the dark controls was usually close to the analytical uncertainty or insignificant compared with that in the irradiated samples. Discrete depth samples from station C18 were also illuminated in the wavelength-dependent irradiation mode with the GG420 filter (cutoff at 407 nm) in place (last panel in Figure 6.6). Clearly, the filtered

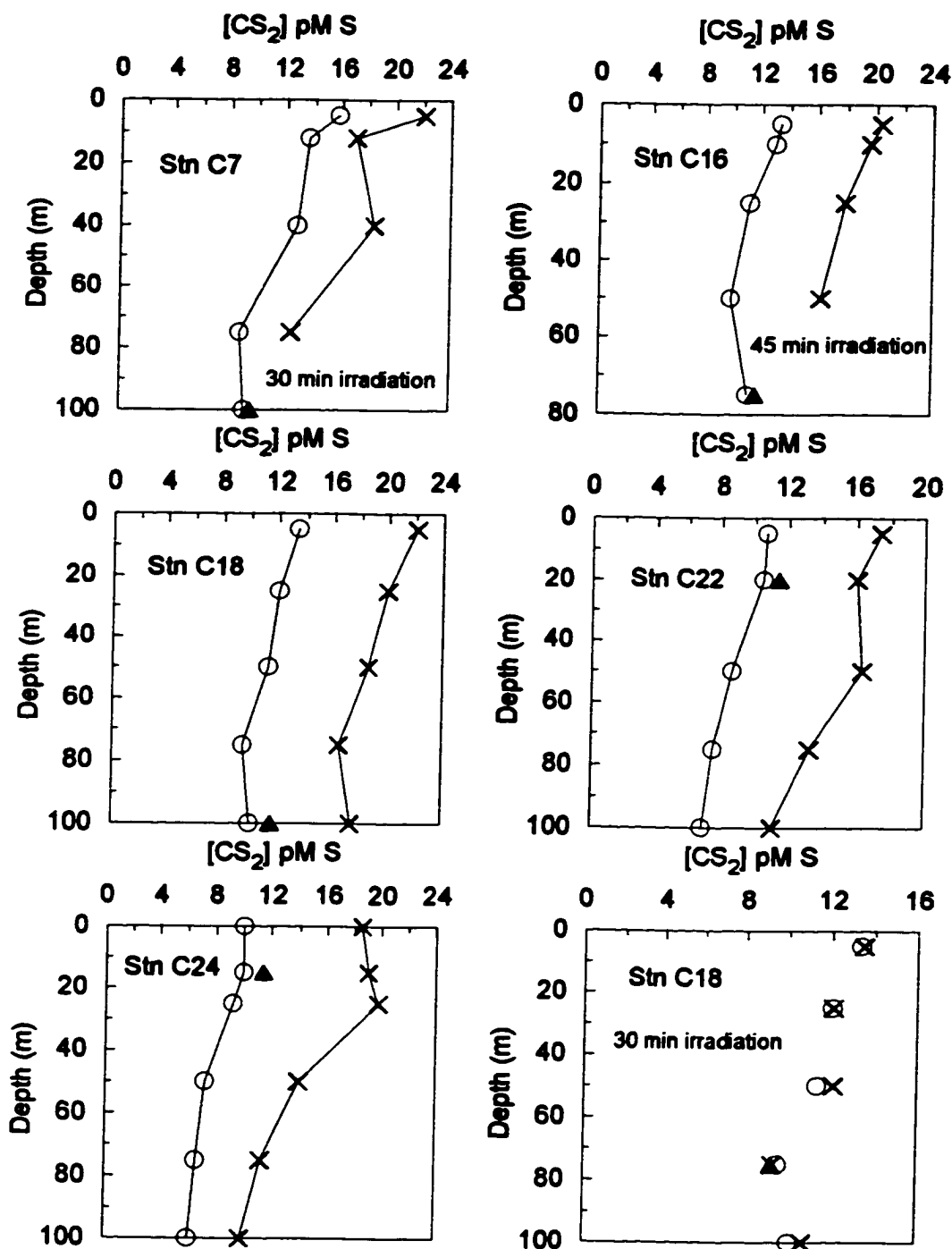


Figure 6.6 Vertical profiles of CS_2 before (circles) and after irradiation (crosses). Triangles are dark controls. The solar simulator was run in the full-spectrum irradiation mode for the first five panels and in the wavelength-dependent irradiation mode with the GG420 filter (cutoff at 407 nm) in place for the last panel.

radiation caused little change in CS₂ concentration, once again indicating that visible light essentially cannot induce photochemical formation of the compound.

Absorbance was measured for five of the seven profiles. Figure 6.7 shows a comparison of the distributions of photo-production rate and absorptivity at 350 nm, a proxy for CDOM concentration. Except for one case (station C18), the vertical distribution of the photo-production rate correlated well with that of the absorptivity. The data from all depths of the five profiles showed a positive linear correlation between the two terms (Figure 6.8), which suggests involvement of CDOM in the photochemical processes responsible for CS₂ generation.

In addition to profile samples, two bucket samples collected in Galway Bay (stations C4 and C5) were also irradiated with simulated solar radiation. CS₂ concentration in the dark controls for these two samples decreased during a 30-min run. The concentration in the control decreased by 1 pM S for the sample from station C4 and 3 pM S for the sample from station C5. Corrected for the dark consumption, the photochemical formation rate was 6 pM S hr⁻¹ at station C4 and 10 pM S hr⁻¹ at station C5. The value at C5 was one of the highest photo-production rates from all the full-spectrum irradiation tests for surface samples, which was consistent with the high absorption observed at this location (see section 6.2). The samples for photochemical studies were passed through 0.7- μ m filters which removes all algal species, but not all bacteria. The conspicuous destruction of CS₂ in the dark might be due to bacterial activity [Smith and Kelly, 1988] that was probably prevalent in the brown waters in Galway Bay.

6.5 Wavelength-dependent irradiation

6.5.1 Photo-production rate vs. wavelength

Bucket samples collected at ten stations were used to investigate the dependence of CS₂ photo-production on wavelength. A Knudsen bottle sample (50 m deep)

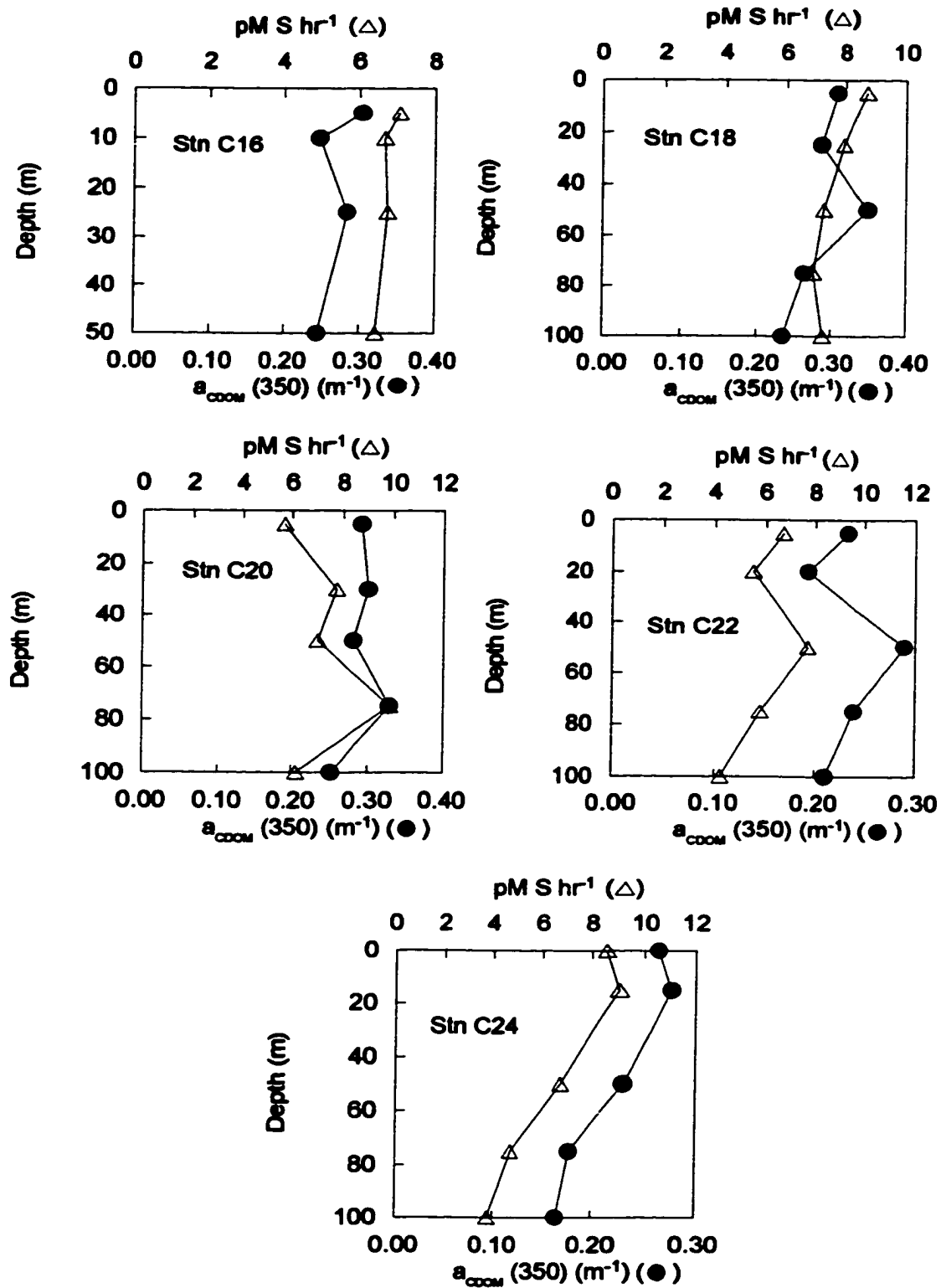


Figure 6.7 Comparison between vertical distributions of CS₂ photo-production rate and absorptivity at 350 nm.

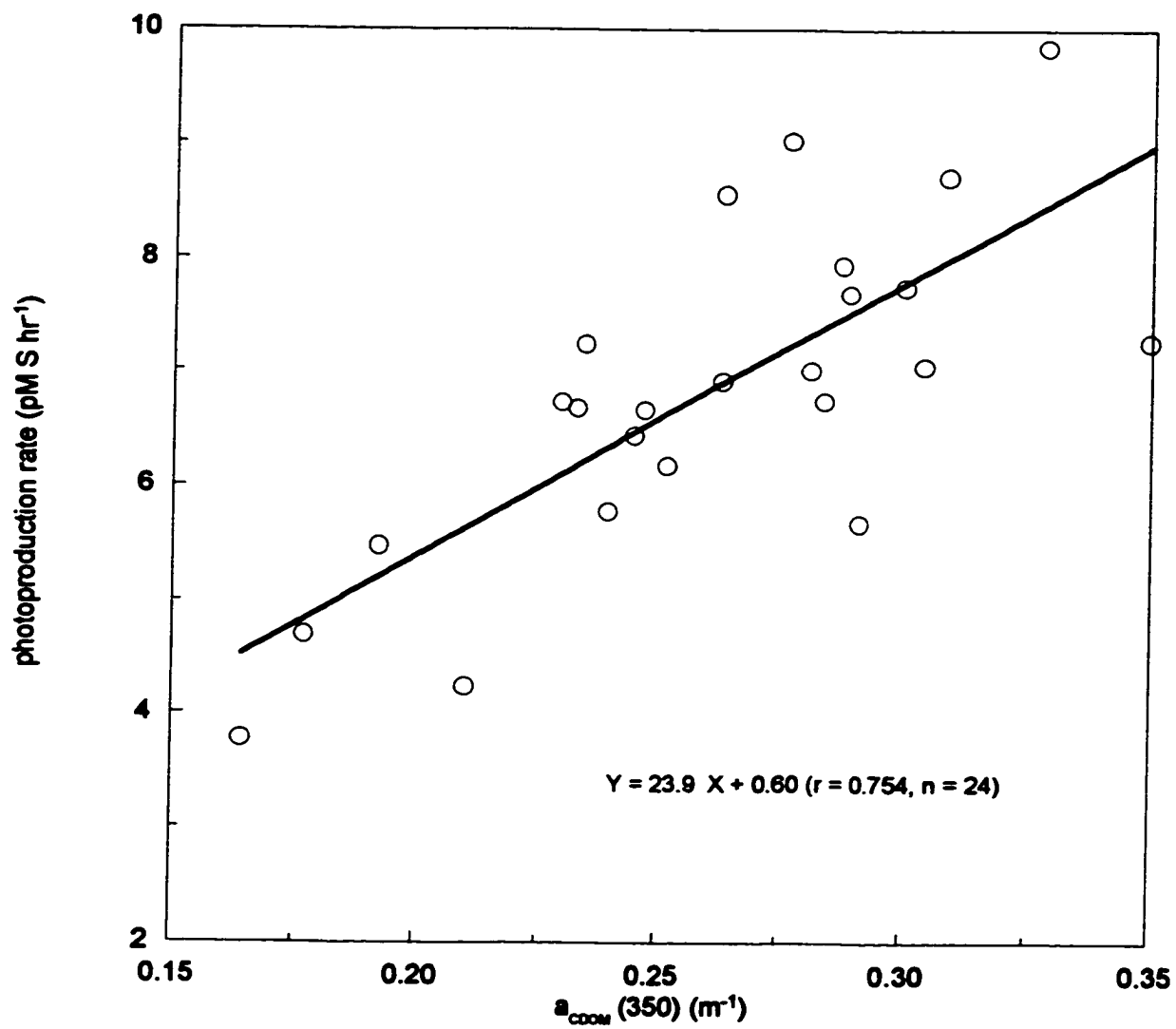


Figure 6.8 Photo-production rate of CS₂ vs. absorptivity at 350 nm.

taken at station C32 was also subjected to wavelength-dependent irradiation. Table 6.1 shows the results from these experiments for each station and Figure 6.9 presents the average photo-production rate as a function of cutoff wavelength. In accordance with the observation in the time-dependent tests (see section 6.3), the photo-production rate was largest when the shorter wavelengths were present and decreased almost exponentially with increase in cutoff wavelength. At 407 and 468 nm cutoffs, the irradiated samples for some stations showed lower concentrations than did the dark controls, thus leading to negative formation rates. The mean photo-production rates at these two wavelengths were comparable to the analytical uncertainty (0.6 pM S hr^{-1}). Notably, the production rates at each wavelength were widely scattered, possibly because various chromophores and precursors were involved in CS_2 photo-production, or alternatively because of the spatial inhomogeneity of these substances. Variations in CS_2 concentration in the control vessels were mostly within or near to the analytical uncertainty. However, the control for station C14 which was quite close to Galway Bay once again showed significant decrease in CS_2 concentration, while discernible accumulation of the compound occurred in the control for station C32 that was relatively far from the bay.

6.5.2 Quantum-yield spectra

6.5.2.1 Introduction

Quantum yield is defined as the ratio of the number of molecules formed to the number of photons absorbed at a given wavelength. As such, to obtain the quantum yield of a compound experimentally, we need to measure the amount of the compound produced and the corresponding quantity of photons absorbed at a specific wavelength. In this regard, monochromators are ideal equipment to determine the quantum yield. The shortcoming of an ordinary monochromator is

Table 6.1 Photo-production rate of CS₂ (pM S hr⁻¹) vs. cutoff wavelength.

Cutoff nm	Station number															Mean	SD
	C10	C13	C14	C17	C19	C21	C23	C25	C27	C29	C32						
286	10.2	6.1	5.9	6.0	6.0	7.1	4.2	10.2	7.0	6.0	8.5	7.0	1.8				
302	5.7	1.4	4.3	3.4	3.7	3.5	2.3	5.2	4.9	2.5	3.5	3.7	1.2				
337	2.8	0.6	2.9	1.7	1.0	2.0	0.4	1.8	1.8	1.4	0.9	1.6	0.8				
362	2.1	-0.2	2.3	0.1	0.7	0.8	0.0	1.1	1.4	1.2	0.1	0.9	0.8				
407	1.0	0.0	0.4	0.4	0.8	0.9	-0.1	0.2	0.6	1.0	-0.7	0.4	0.5				
468	1.1		0.5	0.7	0.5	0.9	0.2	0.2	0.6	0.1	-0.1	0.5	0.4				
Control	-0.3	0.5	-1.4	0.4	-0.7	-0.8	-0.6	0.3	-0.2	-0.1	1.0	-0.2	0.7				

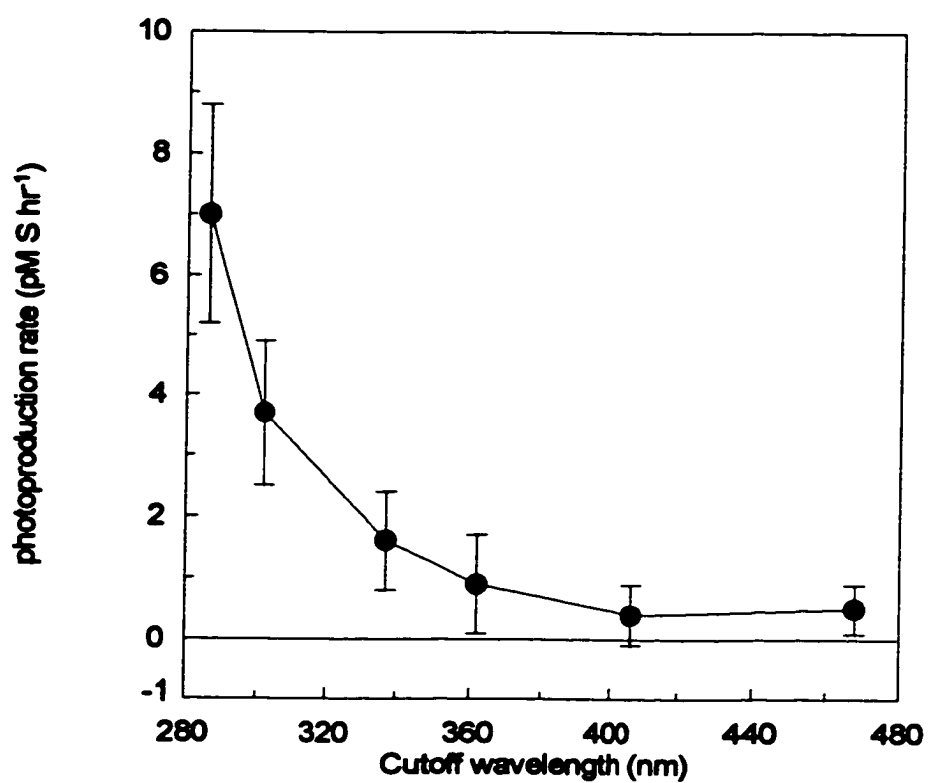


Figure 6.9 Photo-production rate of CS₂ as a function of cutoff wavelength.

its low energy output, which leads to a time-consuming measurement, particularly for those compounds with extremely low quantum yields over the solar spectrum (e.g. OCS and CS₂). The experimental set-up in this study, which combines a powerful xenon lamp with a series of long band-pass cutoff filters, overcome the disadvantage of the monochromator and provides an opportunity to acquire more quantum-yield data in a relatively short period of field investigation. However, as this method does not directly employ monochromatic radiation, derivation of the quantum yield is not as simple as in the case of the monochromator technique.

Two approaches are available to extract quantum yields from the data obtained using the experimental design for this study. The first approach is designated as the differential irradiance method which calculates the quantum yield using the following expression:

$$\bar{\Phi}_{i-(i+1)} = \frac{P_i - P_{i+1}}{I_{i,\text{CDOM}} - I_{i+1,\text{CDOM}}}, \text{ or theoretically,}$$

$$\bar{\Phi}_{i-(i+1)} = \frac{\int \Phi(\lambda) \Delta I_{\text{CDOM}}(\lambda) d\lambda}{\int \Delta I_{\text{CDOM}}(\lambda) d\lambda}$$

where P is the quantity of the compound produced, I_{CDOM} is the irradiance absorbed by CDOM, Φ(λ) is the spectral quantum yield, and ΔI_{CDOM}(λ) is the differential spectral irradiance absorbed by CDOM. Here i and (i+1) denote the ith and (i+1)th cutoff filters, respectively. The calculated $\bar{\Phi}_{i-(i+1)}$ is an average quantity for Φ(λ) over the wavelength band resulting from the transmittance difference between the ith and (i+1)th filters. There are two limitations inherent in this approach. First, the dependence of Φ(λ) on wavelength cannot be adequately demonstrated by $\bar{\Phi}_{i-(i+1)}$ unless the wavelength band is sufficiently narrow that this average value does not change much over that band. If the bandwidth is defined as the width at half-peak height, the bandwidths shown in Figure 2.12

(Chapter 2) range from 17 to 55 nm. Previously determined quantum-yield spectra for OCS [Weiss et al., 1995b], CO [Valentine and Zepp, 1993] and H₂O₂ [Cooper et al., 1988] indicate that the quantum yields for these species decrease rather rapidly and approximately exponentially with increasing wavelength, particularly at short wavelengths. Figure 6.9 seems to suggest similar patterns for the CS₂ quantum-yield spectrum. Thus, because of the relatively broad bandwidths used in this study, the differential irradiance method may introduce significant uncertainties in the resulting quantum-yield data. Second, the differential irradiance method makes it difficult to decide the wavelength at which $\bar{\Phi}_{i-(i+1)}$ is plotted. The appropriate wavelength should be the weighted wavelength,

$$\bar{\lambda}_w = \frac{\int \lambda \Phi(\lambda) \Delta I(\lambda) d\lambda}{\int \Phi(\lambda) \Delta I(\lambda) d\lambda}$$

where $\Delta I(\lambda)$ is the spectral differential irradiance between two successive cutoff filters. This cannot, however, be calculated without knowing the quantum-yield spectrum first. The unweighted average wavelength,

$$\bar{\lambda}_u = \frac{\int \lambda \Delta I(\lambda) d\lambda}{\int \Delta I(\lambda) d\lambda}$$

will be quite different if $\Phi(\lambda)$ varies rapidly over the corresponding wavelength band.

To resolve these problems, a modified approach originally proposed by Rundel [1983] is adopted. The fundamental procedure is to assume an appropriate functional form for the quantum-yield spectrum and then to vary the parameters in that functional form to achieve the best agreement with the measured data. As quantum yield is always positive and tends to fall exponentially with increasing wavelength, one possible functional form for $\Phi(\lambda)$ is

$$\langle \Phi(\lambda) \rangle = \sum_{i=1}^n [a_i \exp(b_i \lambda)]$$

where $\langle \Phi(\lambda) \rangle$ designates the assumed function form of $\Phi(\lambda)$, and a_i and b_i are the parameters to be determined. Using $\langle \Phi(\lambda) \rangle$, we will be able to derive a predicted photo-production rate, $\langle P_i \rangle$, in the vessel under the i^{th} cutoff filter,

$$\langle P_i \rangle = \int \langle \Phi(\lambda) \rangle I_{i,\text{CDOM}}(\lambda) d\lambda$$

The parameters in $\langle \Phi(\lambda) \rangle$ are then varied to minimise the chi-squared error, χ^2 , defined as

$$\chi^2 = \sum_{i=1}^k (P_i - \langle P_i \rangle)^2 / \sigma_i^2$$

where σ_i is the standard deviation of the i^{th} data point and $k = 6$ for this study. As no replicate samples were measured, σ_i is assumed to be the same for every P_i . The number of the parameters that can be adjusted depends on the number of data points available. The maximum adjustable parameters for m data points is $m-2$ since $\Phi(\lambda)$ is a measure of relative effect, and thus, one parameter is for normalization.

6.5.2.2 Results

Table 6.2 shows the quantum-yield data of CS_2 obtained using the differential irradiance method. The unweighted wavelengths and the bandwidths for plotting the quantum yield are also included in Table 6.2. In the calculation, negative photo-production rates shown in Table 6.1 are assumed to be zero, and in the cases in which the photo-production rate at one cutoff wavelength was higher than that at the adjacent shorter cutoff wavelength, the quantum yield was designated as zero. Despite the disadvantages associated with the differential irradiance method, the resulting spectrum (Figure 6.10) is still informative, showing roughly exponential decrease in the quantum yield of CS_2 with the increase in wavelength.

Table 6.2 Carbon disulphide quantum-yield data derived from the differential irradiance method.

Wavelength Bandwidth		Station number													Mean	SD
nm	nm	C10	C13	C14	C17	C19	C21	C23	C25	C27	C29	C32				
308	17	15.0	20.4	5.9	10.9	10.2	14.0	8.3	21.7	6.9	12.0	18.5	13.1	5.1		
340	39	1.9	0.7	1.0	1.2	3.0	1.2	1.9	3.4	2.0	0.8	2.6	1.8	0.9		
370	39	0.3	0.4	0.2	0.8	0.2	0.5	0.2	0.5	0.2	0.1	0.6	0.4	0.2		
402	37	0.3	0.0	0.2	0.0	0.0	0.0	0.0	0.5	0.2	0.1	0.4	0.2	0.2		
456	55	0.0	0.0	0.0	0.0	0.0	0.0	0.0	0.0	0.0	0.3	0.0	0.0	0.1		

Quantum-yield data is quantum yield $\times 10^8$

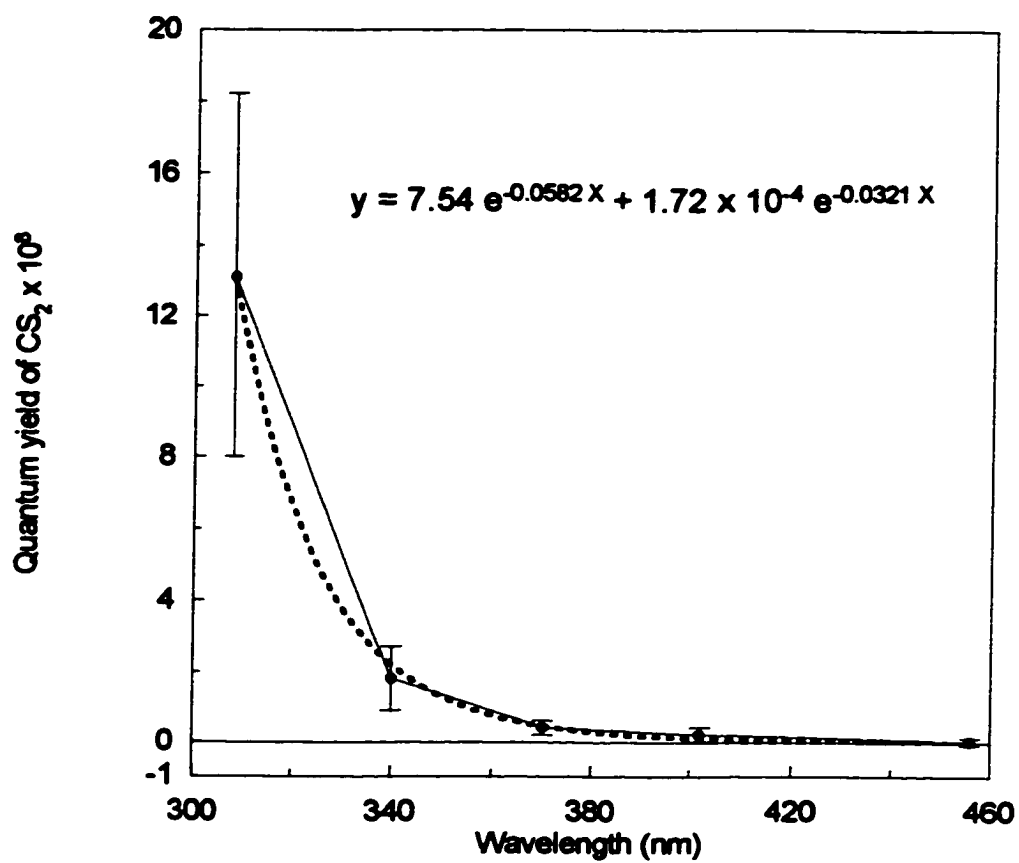


Figure 6.10 Average quantum-yield spectrum of carbon disulphide derived from the differential irradiance data. Error bars are one standard deviation. Dashed line is a double exponential fit to the data points (circle).

The spectrum indicates that solar radiation in the UV region from 290 to 340 nm is most effective at inducing CS₂ photo-production with visible light having little effect. Similar to the observation for the photo-production curve (Figure 6.9), the quantum-yield data are relatively broadly scattered at each plotted wavelength. No distinct difference was found between the surface spectra and the subsurface spectrum (station C32).

To evaluate the accuracy of the differential irradiance method, the resulting quantum-yield spectra, combined with the irradiance data of the solar simulator, can be used to predict the photo-production rates in the samples that had been irradiated to determine the quantum yields. The predicted photo-production rates are then compared with the measured ones. In this evaluation, the data shown in Table 6.2 are linearly extrapolated or interpolated to the wavelengths where the quantum yields are not available. Table 6.3 shows the measured and predicted production rates and their ratios. At 286 and 302 nm cutoffs, the measured values are always smaller than the predictions, and the ratios do not change very much for different stations. At other wavelengths, most of the measured production rates are far greater than the predicted ones and the ratios are quite variable. However, as the determined production rates at 407 and 468 nm cutoffs are mainly within the analytical uncertainty, the comparison between the two data sets at these wavelengths is not meaningful. In fact, the analytical uncertainty can account on average for 70% of the measured production rates even at the 362 nm cutoff. As the natural solar irradiance spectrum is much more similar to the artificial irradiance spectra cut off at 286 or 302 nm than to those cut off at longer wavelengths, this comparison clearly indicates that the quantum-yield spectrum derived from the differential irradiance method will overestimate the photo-production rate if it is applied to the ocean.

Table 6.3 Comparison of measured and predicted CS₂ photo-production rates. The predicted rates were calculated using the quantum-yield data derived from the differential irradiance method.

λ nm	Station number											Mean	SD
	C10	C13	C14	C17	C19	C21	C23	C25	C27	C29	C32		
Measured photo-production rate													
286	10.2	6.1	5.9	6.0	6.0	7.1	4.2	10.2	7.0	6.0	8.5	7.0	1.8
302	5.7	1.4	4.3	3.4	3.7	3.5	2.3	5.2	4.9	2.5	3.5	3.7	1.2
337	2.8	0.6	2.9	1.7	1.0	2.0	0.4	1.8	1.8	1.4	0.9	1.6	0.8
362	2.1	0.0	2.3	0.1	0.7	0.8	0.0	1.1	1.4	1.2	0.1	0.9	0.8
407	1.0	0.0	0.4	0.4	0.8	0.9	0.0	0.2	0.6	1.0	0.0	0.4	0.5
468	1.1		0.5	0.7	0.5	0.9	0.2	0.2	0.6	0.1	0.0	0.5	0.4
Predicted photo-production rate													
286	16.4	13.4	6.6	10.6	9.6	11.8	7.8	18.1	10.2	10.5	15.7	11.9	3.5
302	12.6	9.3	5.2	8.0	7.7	8.6	6.2	13.9	8.5	7.6	11.6	9.0	2.5
337	1.3	0.4	0.7	0.9	0.6	0.6	0.6	1.4	1.1	0.6	1.1	0.9	0.3
362	0.5	0.1	0.3	0.2	0.1	0.1	0.1	0.5	0.4	0.3	0.3	0.3	0.2
407	0.1	0.0	0.1	0.0	0.0	0.0	0.0	0.1	0.1	0.2	0.1	0.1	0.1
468	0.0	0.0	0.0	0.0	0.0	0.0	0.0	0.0	0.0	0.0	0.0	0.0	0.0
Ratio of the measured to the predicted													
286	0.6	0.5	0.9	0.6	0.6	0.6	0.5	0.6	0.7	0.6	0.5	0.6	0.1
302	0.5	0.1	0.8	0.4	0.5	0.4	0.4	0.4	0.6	0.3	0.3	0.4	0.2
337	2.2	1.3	3.9	1.8	1.6	3.0	0.6	1.2	1.6	2.3	0.9	1.8	0.9
362	4.2	0.0	7.7	0.4	10.6	5.9	0.0	2.1	3.5	3.6	0.2	3.1	3.3
407	6.9	0.0	4.8	13.4	24.0	26.0	0.0	1.2	5.4	5.3	0.0	4.7	8.9
468	34.0		31.0	43.3	31.0	56.5	12.9	5.5	37.8	3.9	0.0	22.5	18.0

Photo-production rate is in $\mu\text{M S hr}^{-1}$. Both the measured and predicted photo-production rates are rounded at the third decimal point in the calculation of the ratios.

In the Rundel method, the choice of the presumed functional form for the quantum-yield spectrum is critical. As suggested by the shape of the average quantum-yield curve from the differential irradiance method, several exponential functions were tested:

$$\Phi(\lambda) = a \exp(b\lambda) \quad (6.1)$$

$$\Phi(\lambda) = a \exp(b\lambda) + c \quad (6.2)$$

$$\Phi(\lambda) = a_1 \exp(b_1\lambda) + a_2 \exp(b_2\lambda) \quad (6.3)$$

where a , b , c , a_1 , b_1 , a_2 , and b_2 are parameters determined by the Rundel approach as described in section 3.6.2.1. The best-fit equations and the corresponding quantum-yield spectra are shown in Figure 6.11. Compared with the spectrum from the differential irradiance method (solid line), equation 6.1 (dashed line) produces significantly lower quantum yield throughout the wavelength range of interest, while equations 6.2 (dotted line) and 6.3 (dashed-dotted line) give lower values at short wavelengths, but higher values at long wavelengths. In Figure 6.12 a comparison is made of the mean photo-production rates calculated using the above fitted equations with those calculated from the measured data as given in Table 6.1 and Figure 6.9. Evidently, equation 6.2 (smallest χ^2) agrees best with the measured data, while equation 6.1 (largest χ^2) deviates farthest. However, as shown in Figure 6.11, because of the presence of the constant c , equation 6.2 gives a nearly constant quantum yield (3×10^{-9}) at any wavelength above 360 nm. This is obviously not true, since the irradiation experiments demonstrated that the quantum yield falls rapidly with increasing wavelength and visible light essentially cannot induce photochemical CS_2 formation. This example indicates that the best-fit functional form is not necessarily the right choice. The physical meaning of the assumed function must conform to the experimental results. The fitted curves of equation 6.3, which are in reasonable agreement with the measured data in both magnitude and physical meaning, are thus chosen as the best quantum-yield

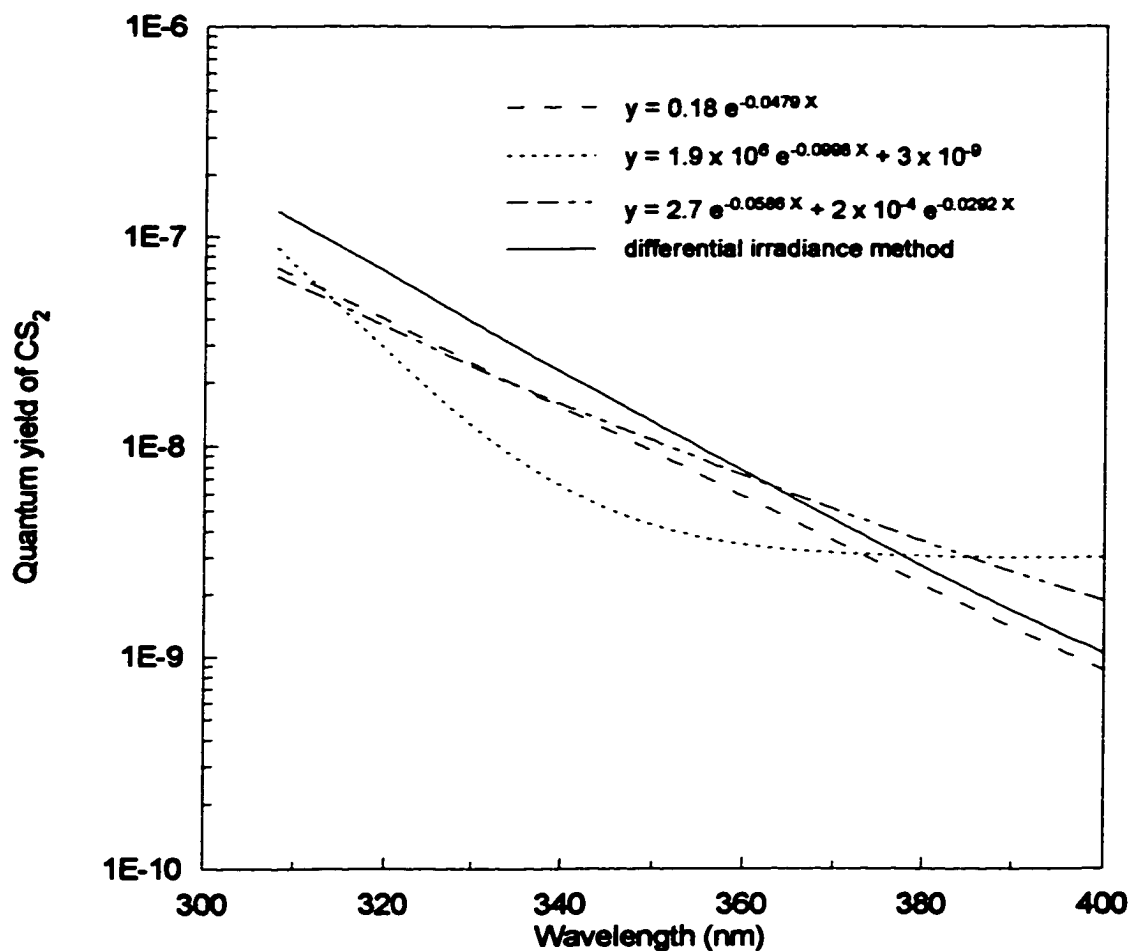


Figure 6.11 Comparison between the average quantum-yield spectra of CS₂ derived from the Rundel method and that from the differential irradiance method. Dashed, dotted, and solid lines are the best fit of equations 6.1, 6.2, and 6.3, respectively. Dashed/dotted line is the fit of the quantum-yield data derived from the differential irradiance method (see Figure 6.10).

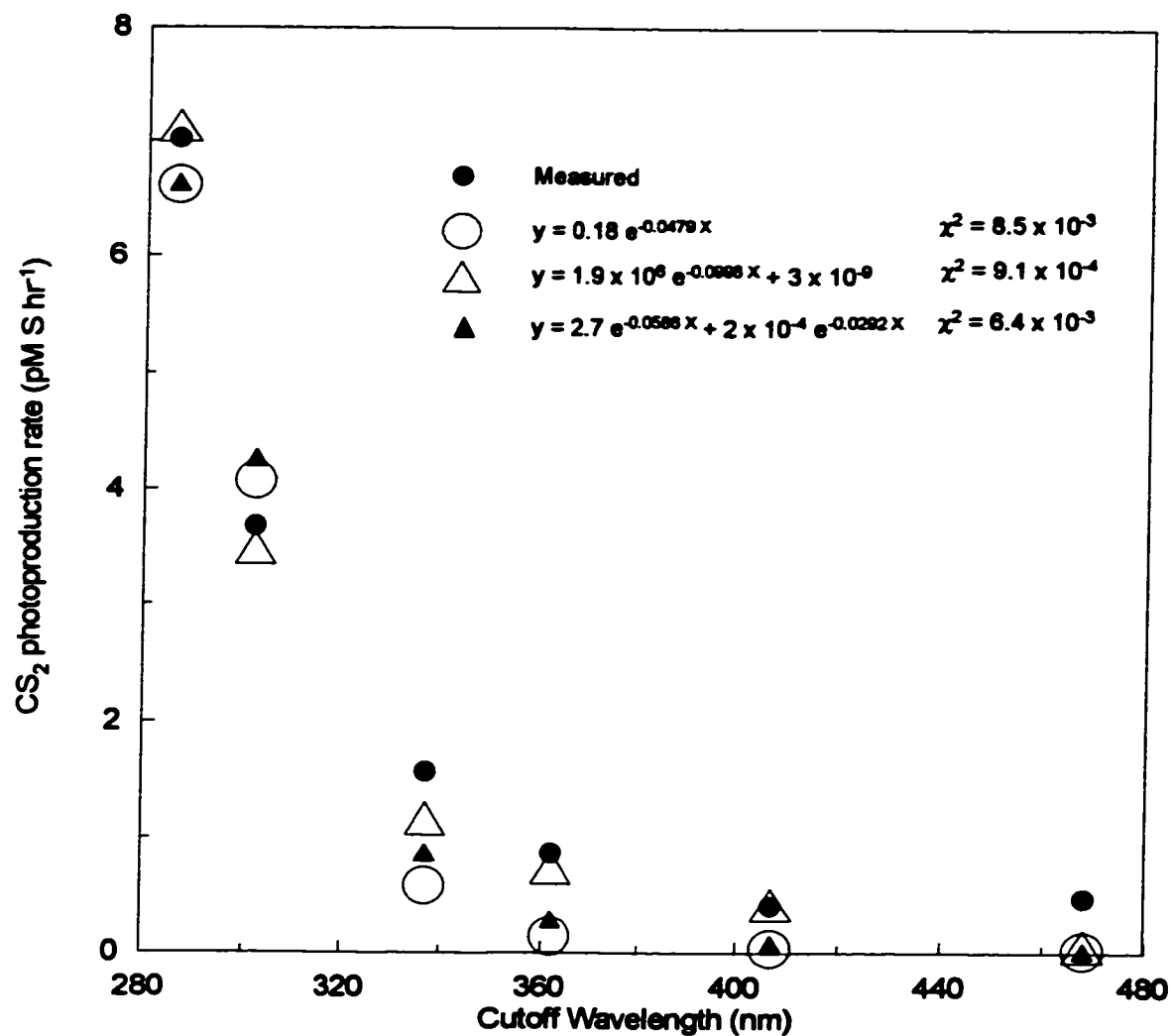


Figure 6.12 Comparison between the mean photo-production rates calculated from the measured values and those calculated using the quantum-yield data derived from the Rundel method.

Table 6.4 Parameters for the least-squares fit of equation 6.3 in the text.

Parameter	Station number											
	C10	C13	C14	C17	C19	C21	C23	C25	C27	C29	C32	Mean
a_1	2.80	3.26	2.62	2.48	2.49	2.48	3.25	3.88	2.48	2.85	2.95	2.70
$b_1 \times 10^2$	-5.86	-5.81	-6.70	-6.87	-5.97	-5.97	-5.80	-5.75	-6.46	-6.20	-5.77	-5.86
$a_2 \times 10^4$	2.2	2.2	2.8	2.8	2.6	2.58	0	2.5	2.37	1.6	1.6	2
$b_2 \times 10^2$	-2.85	-3.2	-2.89	-2.89	-2.9	-2.9		-2.89	-2.86	-2.8	-2.8	-2.92
$\chi^2 \times 10^3$	20.8	16	25	6.3	3.7	8.6	0.078	8.1	6.1	13.3	8.6	5.6

Mean values in this table are not the averages of the individual stations. They were obtained by fitting equation 6.3 to the measured mean photo-production rates using the average absorption spectrum shown in Figure 6.3a. The parameters in equations 6.1 and 6.2 shown in Figure 6.11 were derived in the same manner.

spectra obtained from the Rundel method. The parameters in these curves for different stations are shown in Table 6.4.

6.6 Estimation of CS₂ photo-production in the world oceans

Because of the very limited spatial and temporal coverage, any extrapolation of the results from this study to the global oceans must be done with caution. Many assumptions need to be made for such extrapolations, the major ones being: (1) the average quantum-yield spectrum of CS₂ and CDOM absorption data obtained during the *Challenger* cruise are applicable to the rest of the world oceans and other seasons, (2) CDOM absorption, water absorption and molecular scattering by seawater are the dominant contributors to the attenuation of solar irradiance in the spectral range of interest, (3) all the incident solar irradiance in the UV range is absorbed during its transmission in the water column, and (4) the solar irradiance data provided by Leifer [1988] and the data of the absorption and scattering coefficients of clearest natural seawater supplied by Smith and Baker [1981] are representative of the global oceans.

The photo-production rate of CS₂ can be estimated by the expression,

$$P_{\text{CS}_2} = \sum_{\lambda} \Phi_{\text{CS}_2}(\lambda) I_{\text{CDOM}}(\lambda)$$

where P_{CS_2} is the total column photo-production rate in $\mu\text{mol cm}^{-2} \text{d}^{-1}$, $\Phi_{\text{CS}_2}(\lambda)$ is the spectral quantum yield of CS₂, and $I_{\text{CDOM}}(\lambda)$ is the irradiance absorbed by CDOM in $\mu\text{Einsteins cm}^{-2} \text{d}^{-1} \text{nm}^{-1}$. As no significant photo-production was observed at wavelength longer than 400 nm, the integrated wavelength range is between 298 and 400 nm with 1 nm interval. Using assumption 2 and the formula given by Kettle [1994], the irradiance absorbed by CDOM can be expressed as

$$I_{\text{CDOM}}(\lambda) = I(\lambda) a_{\text{CDOM}}(\lambda) / (a_{\text{CDOM}}(\lambda) + a_w(\lambda) + 0.5b_{\text{msw}}(\lambda))$$

Here $a_{\text{CDOM}}(\lambda)$, $a_w(\lambda)$ and $b_{\text{msw}}(\lambda)$ are the absorption coefficient of CDOM, absorption coefficient of pure water and molecular scattering coefficient of seawater, respectively. The units for these three parameters are all in m^{-1} . $I(\lambda)$ is the solar irradiance just below the sea surface in $\mu\text{Einsteins cm}^{-2} \text{d}^{-1} \text{nm}^{-1}$. $\Phi_{\text{CS}_2}(\lambda)$ is calculated using the average quantum-yield spectrum derived from Rundel's method (equation 6.3). The value of $a_{\text{CDOM}}(\lambda)$ is from the measured mean absorption spectrum of CDOM (Figure 6.3a). $I(\lambda)$ is obtained by interpolating the data furnished by Leifer [1988]. The values of $a_w(\lambda)$ and $b_{\text{msw}}(\lambda)$ are from Smith and Baker [1981]. It should be noted that absorption and backscattering by phytoplankton, detritus and suspended mineral also result in light attenuation in the water column. These effects are, however, not included in this work.

Figure 6.13 shows a comparison of the various absorption terms. The absorption coefficients for phytoplankton (normalized to Chl-*a*) were calculated using the specific absorption coefficients of phytoplankton from Vodacek et al. [1994] and an average oceanic Chl-*a* concentration of 0.6 mg m^{-3} [Morel and Berthon, 1989]. The absorption coefficients for suspended mineral (including detritus) are from Vodacek et al. [1994]. Calculation indicates that phytoplankton and suspended mineral contribute on average less than 10% of the total absorption over the wavelength range from 300 to 400 nm. The backscattering coefficients for phytoplankton and suspended mineral are about an order of magnitude lower than their absorption coefficients [Vodacek et al., 1994]. Therefore, light attenuation due to phytoplankton and suspended mineral may be neglected for this study.

Figure 6.14 shows the CS_2 photo-production spectra at 50°N . The spectra are characterised by sharp peaks, a combined effect of the quantum yield and solar irradiance spectra. The wavelength giving maximal production rate shows a slight seasonal dependence, shifting from 325 nm in summer to 333 nm in winter. This

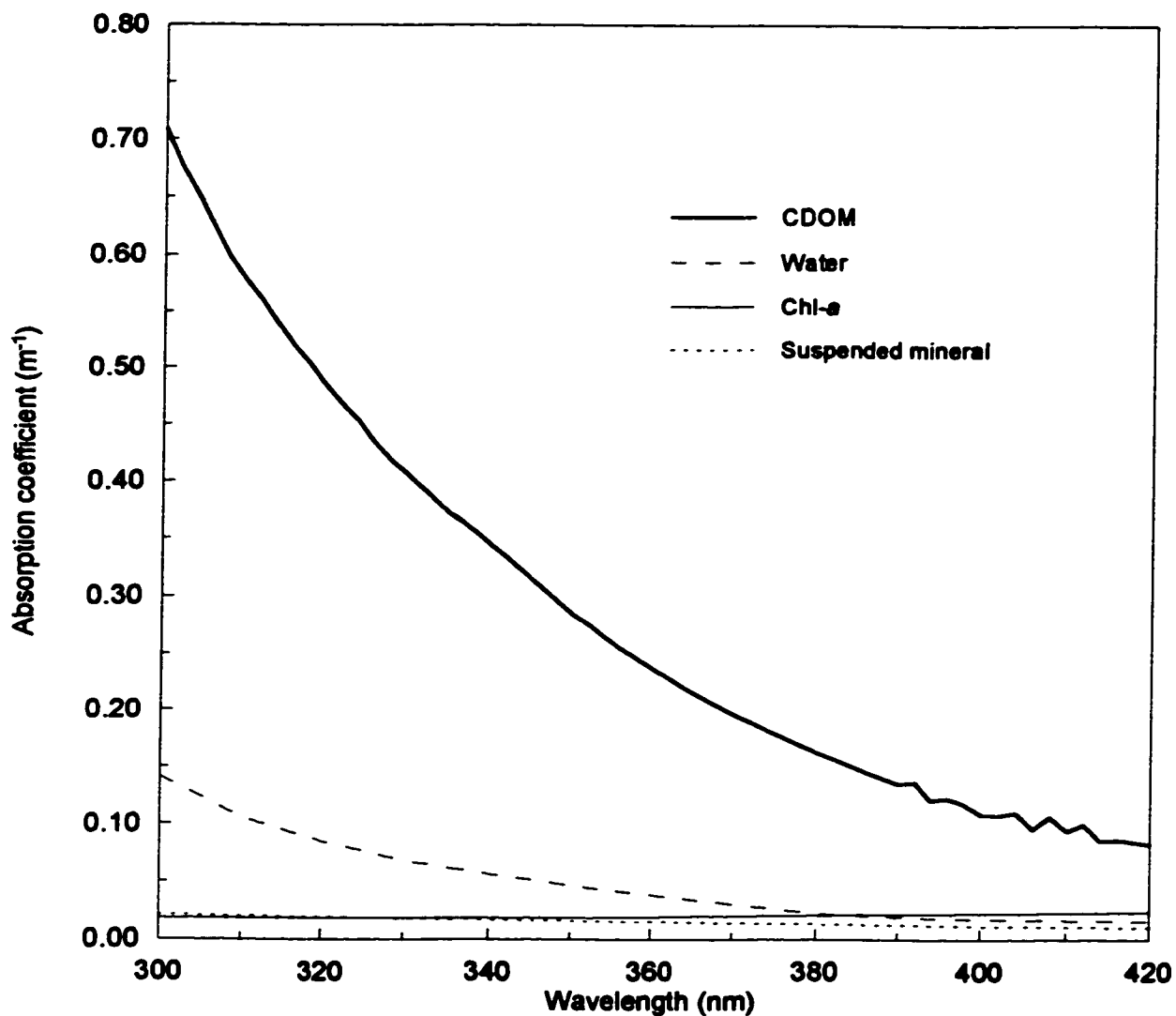


Figure 6.13 Spectral absorption coefficients for CDOM, seawater, phytoplankton (as normalized to Chl-*a*) and suspended mineral (including detritus). The CDOM curve is the mean absorption spectrum obtained during the *Challenger* cruise.

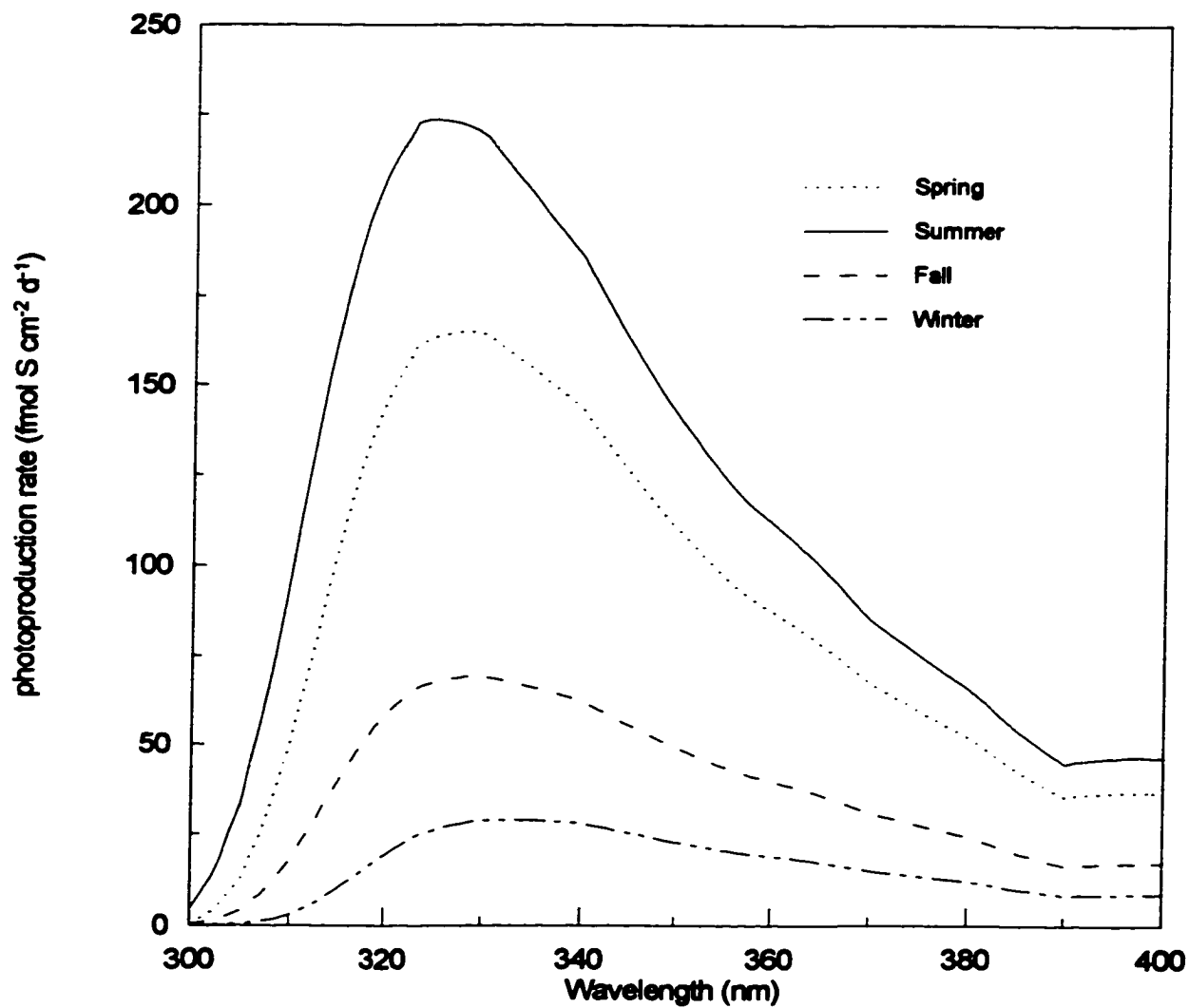


Figure 6.14 Modelled photo-production spectra of CS₂ at 50°N under cloud-free condition.

reflects the seasonal variation in the spectral solar irradiance at 50°N. The area under each of the curves is the total wavelength-integrated production rate for the entire water column. As expected from the geographic distribution of solar irradiance, the total column photo-production rate decreases with increasing latitude, while its seasonal variability grows from low to high latitudes (Figure 6.15). The production rate is in the descending order of summer, spring, fall and winter except at the equator where it is slightly higher in spring and fall than in summer or winter. In order to take into account the spatial variability in estimating the magnitude of CS₂ photo-production on a global scale, the ocean is divided by latitude into eight zones (Table 6.5). Every zone spans 10° except for the last one which spans 20°. Each zone is assigned a unit area photo-production rate that is calculated from the data shown in Figure 6.14. For each zone between 0° and 70°, the mean of two seasonally averaged values within the corresponding zone is taken as the unit area photo-production rate. For the zone above 70°, the seasonally averaged value at 70°N is assumed.

Table 6.5 shows that photochemical CS₂ formation is estimated to be 11.5 Gmol S yr⁻¹ in the world ocean under clear sky condition. If a one-third reduction is made to account for cloud cover [Frederick and Snell, 1990], the value will be 7.7 Gmol S yr⁻¹, equivalent to 0.29 Tg CS₂ yr⁻¹. If the average quantum-yield spectrum obtained from the differential irradiance method (the fitted curve in Figure 6.10) is utilised, the photochemically produced CS₂ is expected to be 0.41 Tg CS₂ yr⁻¹, or 41% higher than the value obtained from the Rundel method. As shown in Chapter 4, section 4.4, the current estimates of the CS₂ emission rate from the ocean to the atmosphere in Tg CS₂ yr⁻¹ are 0.26 (0.13-0.52) [Kim and Andreae, 1987a], 0.18 (0.09-0.36) [Chin and Davis, 1993] and 0.18 (0.13-0.24) from this study. Thus, the magnitude of CS₂ photo-production alone could be comparable to the estimated sea-air flux of this compound. It must, however, be noted that the estimate of the

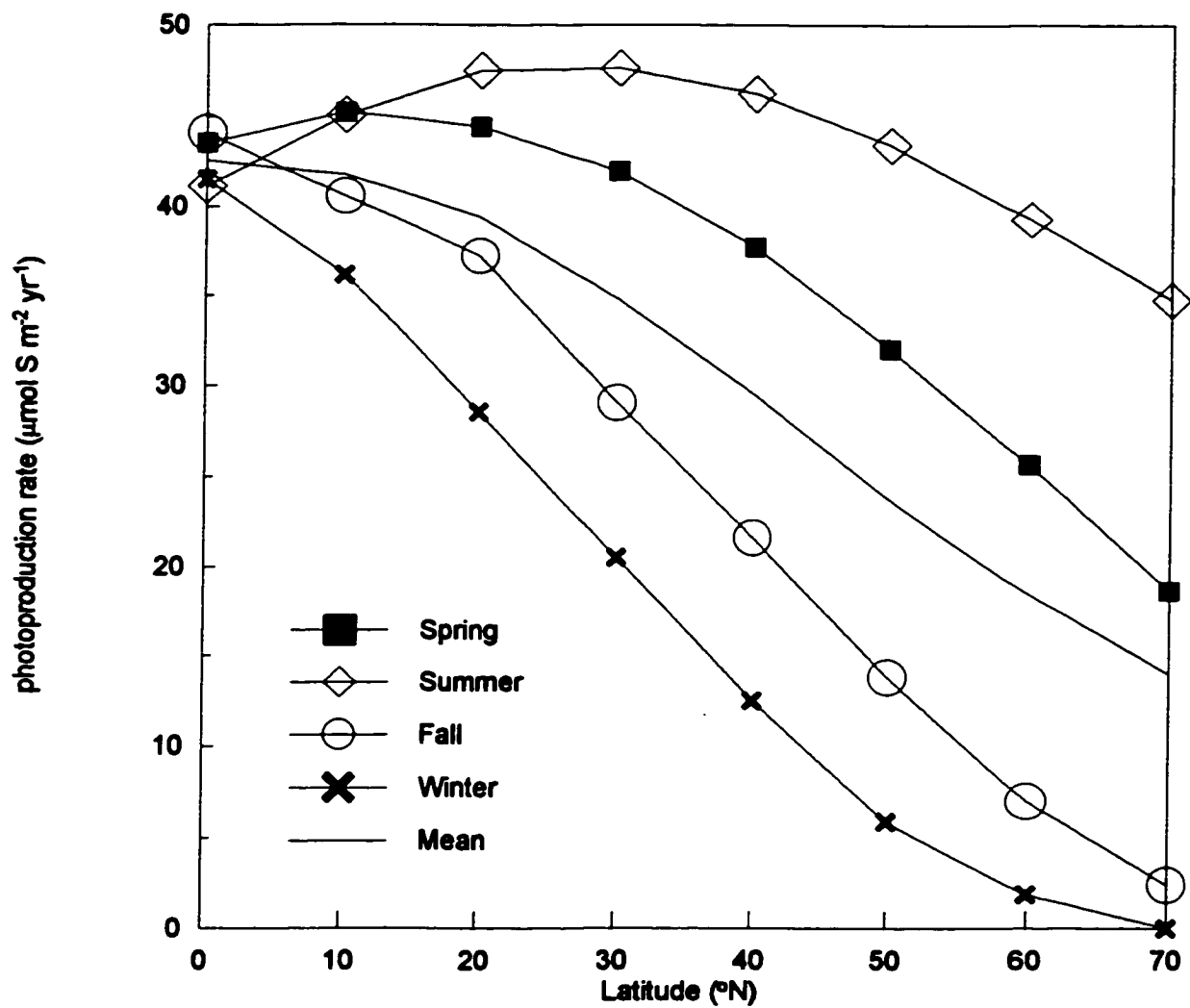


Figure 6.15 Modelled wavelength-integrated photo-production of CS₂ as a function of latitude and its seasonal variability. Cloud-free condition is assumed.

Table 6.5 Estimates of CS₂ photo-production in the world ocean under cloud-free condition.

Latitude range degree	Area 10 ¹⁰ m ²	Unit area production rate μmol S m ⁻² yr ⁻¹	Area-weighted production rate Gmol S yr ⁻¹
0-10	6645	42.2	2.8
10-20	6346	40.6	2.6
20-30	5455	37.1	2.0
30-40	5159	32.2	1.7
40-50	4374	26.6	1.2
50-60	3505	21.1	0.7
60-70	2115	16.2	0.3
70-90	1413	14.0	0.2
Total	35012		11.5

Areas are from Levitus [1982].

photo-production is based on only one quantum-yield data set, covering small time and space scales. The effect of cloud cover on the light field at the earth's surface is poorly understood. The photon flux of UV radiation is strongly influenced by the stratospheric ozone column that varies spatially and temporally. The effect of variability in the ozone column has not been adequately taken into account in estimating the photo-production. As the production rates measured using radiation with wavelengths above 360 nm are close to or within the analytical uncertainty, the quantum yields at these wavelengths are ill-defined. In addition, the initial temperature of our water samples was between 9-15°C, and the temperature rose to ~26°C during irradiation. It is not clear whether temperature would exert any effect on the photochemical CS₂ formation. All these factors may contribute to uncertainties in the estimates of CS₂ photo-production in this study.

6.7 Identification of CS₂ precursors

During incubation of soils treated with sulphur-containing amino acids, Banwart and Bremner [1975] found that CS₂ is produced from microbial decomposition of cysteine and cystine. Zepp and Andreae [1994] reported enhanced photochemical formation of OCS in aqueous solutions spiked with cysteine and methionine. Following the work of Zepp and Andreae [1994], I have tested the photo-reactivities of cysteine, cystine and methionine for CS₂ production. The three amino acids are the purest grades obtainable commercially from Sigma-Aldrich Co. The screening procedure involved irradiating seawater samples with and without addition of the amino acids. Seawater was collected from the Dalhousie University's Aquatron facility which has an intake at about 10 m below the surface of the Northwest Arm, Halifax, Nova Scotia. The bulk sample was 0.2-µm filtered and purged prior to irradiation for at least 18 hours with zero air to decrease the background level of CS₂ in the medium. The purge stream contained 350 ppmv of

CO_2 to prevent significant change in the pH of the medium. The exposure set-up and vessels were identical to those described for the *Challenger* cruise. The solar simulator was operated in the full-spectrum irradiation mode and set to its maximum output. The quartz ampoules were placed horizontally on a specimen tray.

Figure 6.16 shows the effects of cysteine and cystine on the photo-production of CS_2 and OCS. Obviously, both CS_2 and OCS (recorded in peak area) were produced photochemically in considerable amount from cysteine and its dimer, cystine. For methionine, the results are quite different. Instead of enhancing photochemical formation of CS_2 and OCS, samples spiked with methionine showed slight decrease in the production of the two compounds compared with the pure seawater samples (Figure 6.17). The results from these tests seem to imply that thiol group-bearing amino acids and their dimers could be important precursors of CS_2 and OCS.

Flock et al. [1997] assessed the OCS-producing capabilities of a variety of environmentally relevant organosulphur compounds. These compounds are glutathione (GSH), the sodium salt of its oxidised dimeric disulphide (Na-GSSG), cysteine, methionine, methane sulphonic acid, dimethylsulphonium propionate, 3-mercaptopropionic acid, and methyl mercaptan. They found that OCS is efficiently produced from glutathione and cysteine, while other compounds yield little or no OCS. Therefore, their results regarding the photoreactivities of cysteine and methionine are in agreement with those from this study. However, Flock et al. [1997] did not observe any significant production of OCS from the glutathione dimer, Na-GSSG, which is in contrast to the finding from this study that cystine, the dimer of cysteine, is a good precursor of OCS. Zepp and Andreae [1994] reported photochemical formation of OCS from methionine, though it was produced less efficiently than from cysteine. Their results are obviously

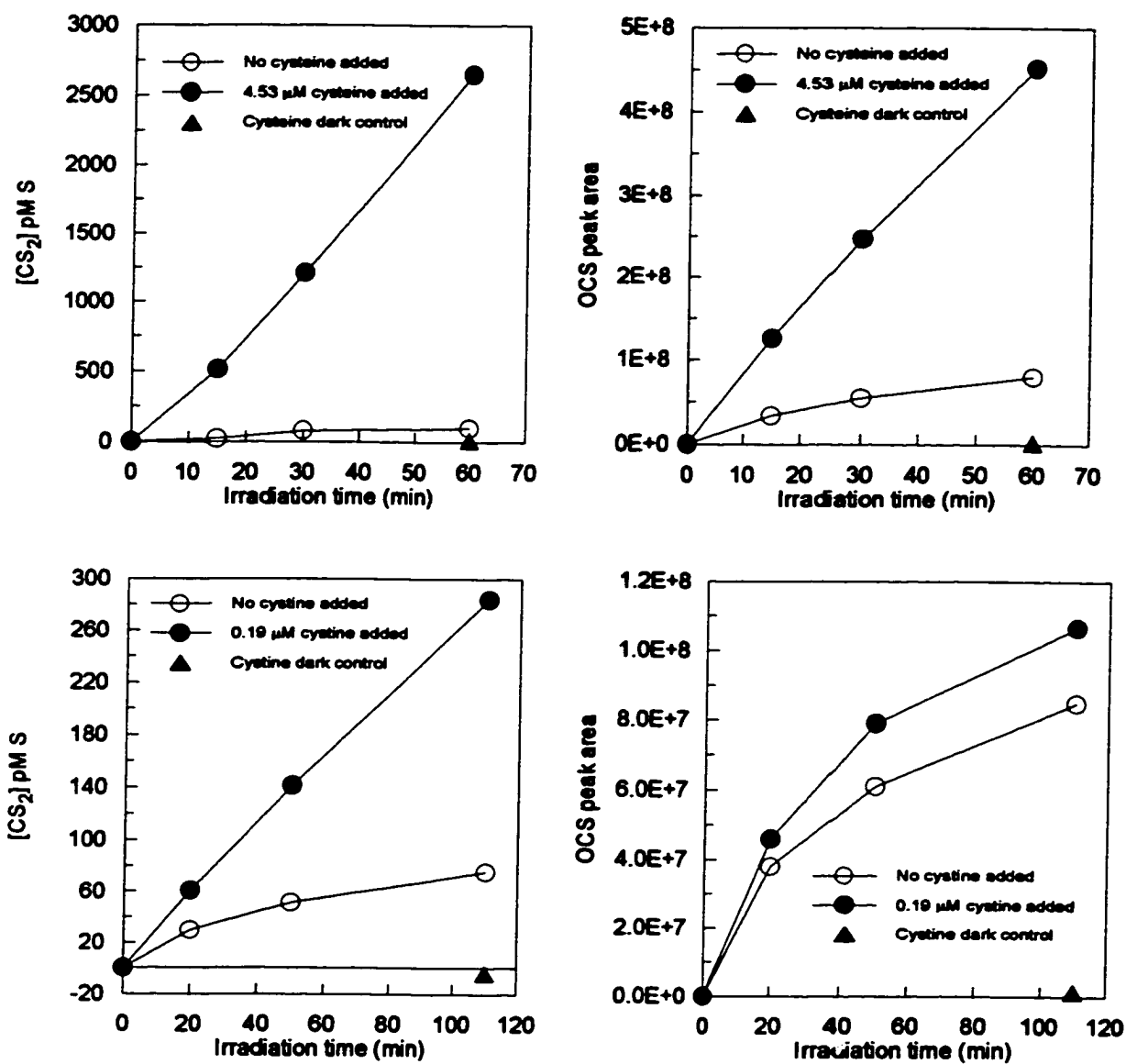


Figure 6.16 Enhancement of CS₂ and OCS photo-production caused by addition of cysteine or cystine to water samples.

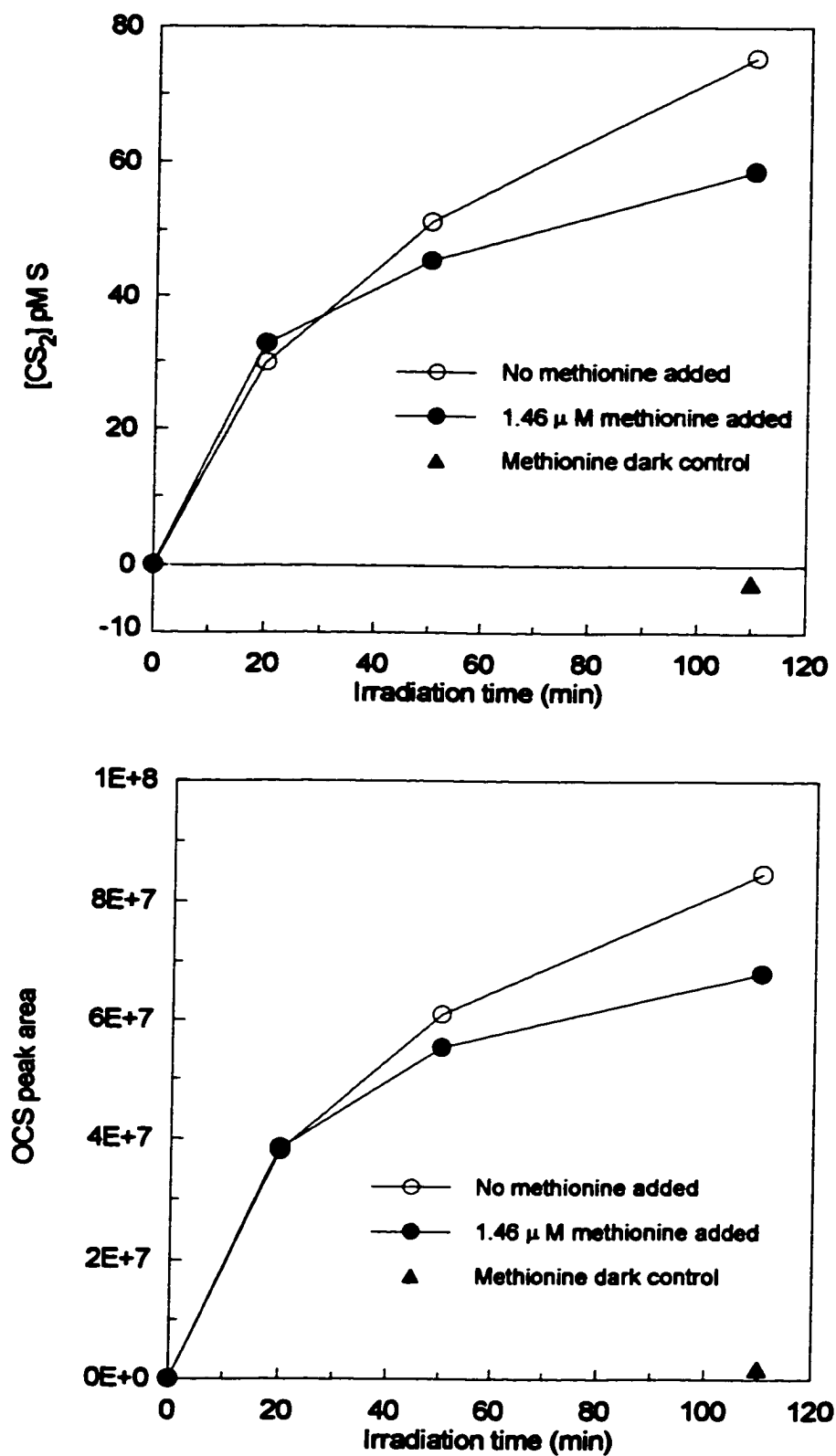


Figure 6.17 Effects of methionine on photo-production of CS₂ and OCS.

inconsistent with those from Flock et al. [1997] and this work. The reason for this difference is unclear.

Sulphur-containing amino acids are present both in humic substances [Malcolm, 1990] and in the low-molecular-weight fraction of dissolved organic matter (DOM) [Romankevich, 1984]. Tada and Maita [1993] reported a high abundance of free sulphur-containing amino acids (including cystine) in surface seawater, and suggested that the observation was related to a spring bloom of diatoms. It seems likely that part of the photochemically produced CS_2 in the ocean is from these biogenic amino acids. To further illustrate the involvement of biological activities in CS_2 photo-production, irradiations were conducted using samples of filtrate from an axenic culture of the red alga, *Porphyridium purpureum*. The photo-production rate in the filtrate was consistently higher than that in the medium which was used for incubating the alga (Chapter 5, Figure 5.5). Short-chain thiols are transparent to light with wavelengths longer than 280 nm [Caspari and Granzow, 1970], which leads to a couple of implications concerning the photochemical decomposition of free sulphur-containing amino acids in seawater. First, photo-degradation of these amino acids must be realised via photosensitization in the ocean where solar radiation below 280 nm is absent. Second, although the free sulphur-containing amino acids do not absorb solar radiation in the ocean, they can greatly affect the photo-production rates of CS_2 and OCS. Thus, variations in the concentration and distribution of these amino acids may significantly alter the quantum-yield spectra of the two compounds.

Irradiations were also conducted using a series of seawater solutions containing varying concentration of cysteine. The photo-production rate of CS_2 increased exponentially with increasing cysteine concentration (Figure 6.18). The exponential factor is 1.37 under the experimental conditions employed. Because little is known about the mechanisms responsible for CS_2 photo-production, it is

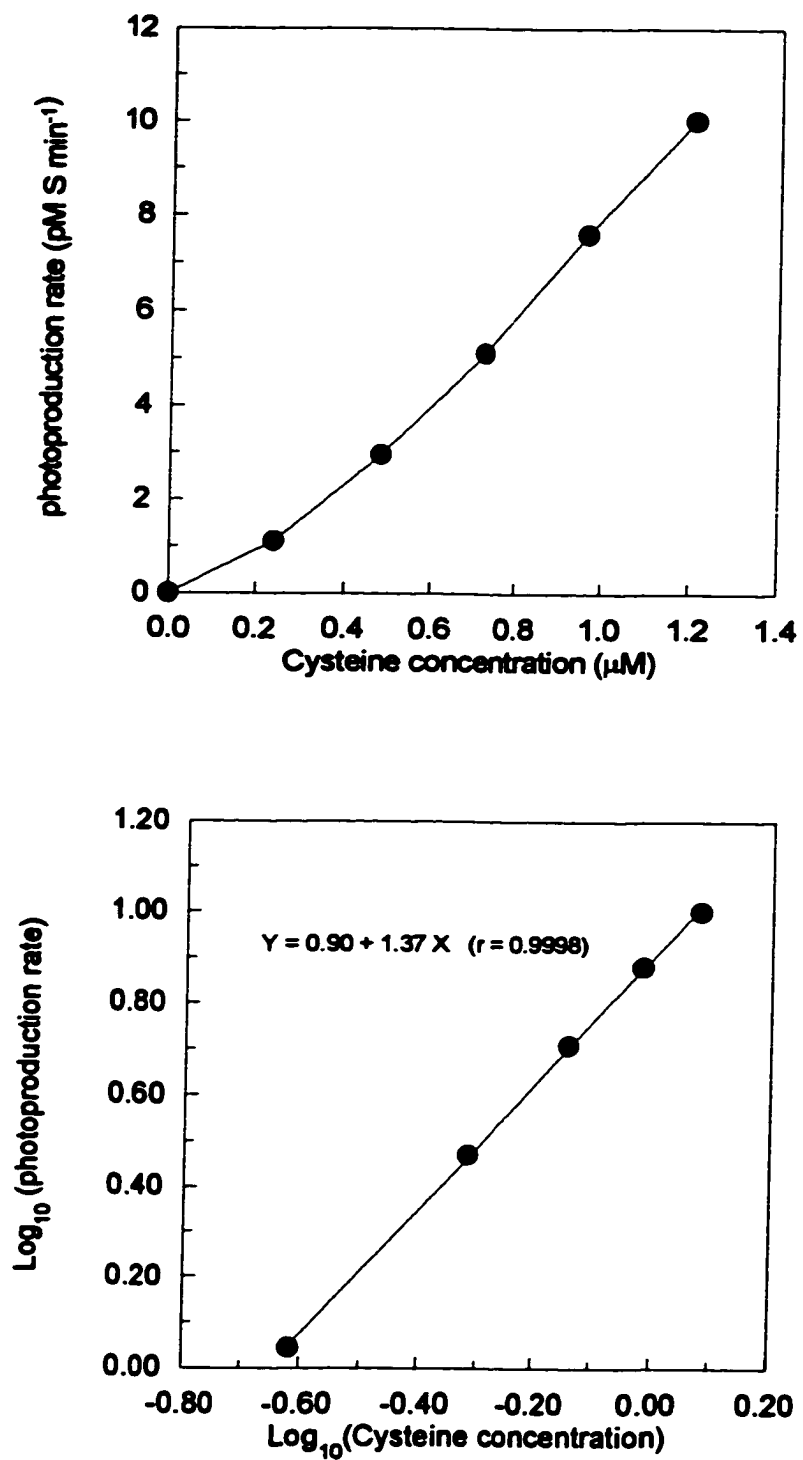
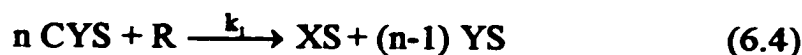


Figure 6.18 Effect of changing cysteine concentration on photo-production of CS_2 . Photo-production in pure seawater has been deducted. The irradiation time was 45 min.

impossible to interpret these data theoretically. A simplified scheme is proposed here to give a tentative explanation. In this scheme, it is assumed that cysteine reacts with an excited photosensitiser or an inorganic/organic radical (R) to produce a sulphur-containing radical (XS) which subsequently reacts with a carbon-donating compound (ZC) to produce CS₂. It is further assumed that, in addition to XS, other sulphur-containing radicals or compounds (signified as a single symbol, YS) are also formed. The overall reactions are given by



where CYS designates cysteine, and k_1 and k_2 are the rate constants for reactions 6.4 and 6.5, respectively. From the two reactions, it is easy to show that the production of XS is $k_1 [\text{R}] [\text{CYS}]^n$ and destruction of XS is $2 \frac{d[\text{CS}_2]}{dt}$. If reaction 6.4 is the rate-limiting step and a steady state in the production of XS is reached, production of XS will be equal to destruction of XS, i.e.

$$\frac{d[\text{CS}_2]}{dt} = \frac{k_1}{2} [\text{R}] [\text{CYS}]^n \quad (6.6)$$

The experimental results (Figure 6.18) suggest that $k_1[\text{R}]$ should be a constant and the value of n should be 1.37 under my experimental conditions. Therefore, this scheme implies that nearly 73% of the radicals formed from photo-degradation of cysteine results in CS₂ production.

6.8 Effect of OH radicals on CS₂ photo-production

Zepp and Andreae [1994] suggested that hydroxyl radical (OH) may be indirectly involved in the photo-production of OCS by reacting with bromide and carbonate to form dibromine and carbonate radicals which in turn rapidly react with organic sulphur compounds, including sulphur-containing amino acids

[Adams et al., 1972; Chen and Hoffman, 1973]. To assess the role that the OH radical may have in the production of CS₂ and OCS, a series of seawater solutions containing varying concentrations of nitrite were irradiated. Nitrite is an efficient producer of OH when radiated with sunlight [Zafiriou and True, 1979b,c; Mopper and Zhou, 1990]. Two sets of water samples (taken from the Aquatron facility and treated in the way described as in section 6.7) were irradiated, one with no cysteine added and another with addition of 0.63 μM of cysteine. Addition of nitrite to water samples without added cysteine had almost no effect on CS₂ or OCS production (Figure 6.19a). The production rates of these two compounds were, however, greatly elevated by addition of nitrite to the water samples containing added cysteine (Figure 6.19b). The reason for this may be that the background level of organic sulphur substrates was so low that the concentration of the OH radical generated by CDOM in the pure seawater alone was sufficiently high to make the reactions proceed at their maximal rates. Another interesting phenomenon is that the photo-production of both the compounds in the cysteine-added samples was saturated when the concentration of nitrite exceeded 1.54 μM. This observation suggests that, with the increase in the concentration of nitrite, the reaction system switched from being limited by the OH radical to being limited by the substrate concentration. However, based on these results alone, the exclusive role of the OH radical in CS₂ and OCS production cannot be proven since photolysis of nitrite produces other radicals (e.g. NO) in addition to OH.

6.9 Comparison between photo-production of CS₂ and OCS

Several lines of evidence suggest that the mechanisms for photo-production of CS₂ and OCS are probably similar to each other. As described in section 6.6, CS₂ and OCS may have common precursors in the ocean, and amino acids containing the thiol group possibly are the most efficient. The results of the nitrite test

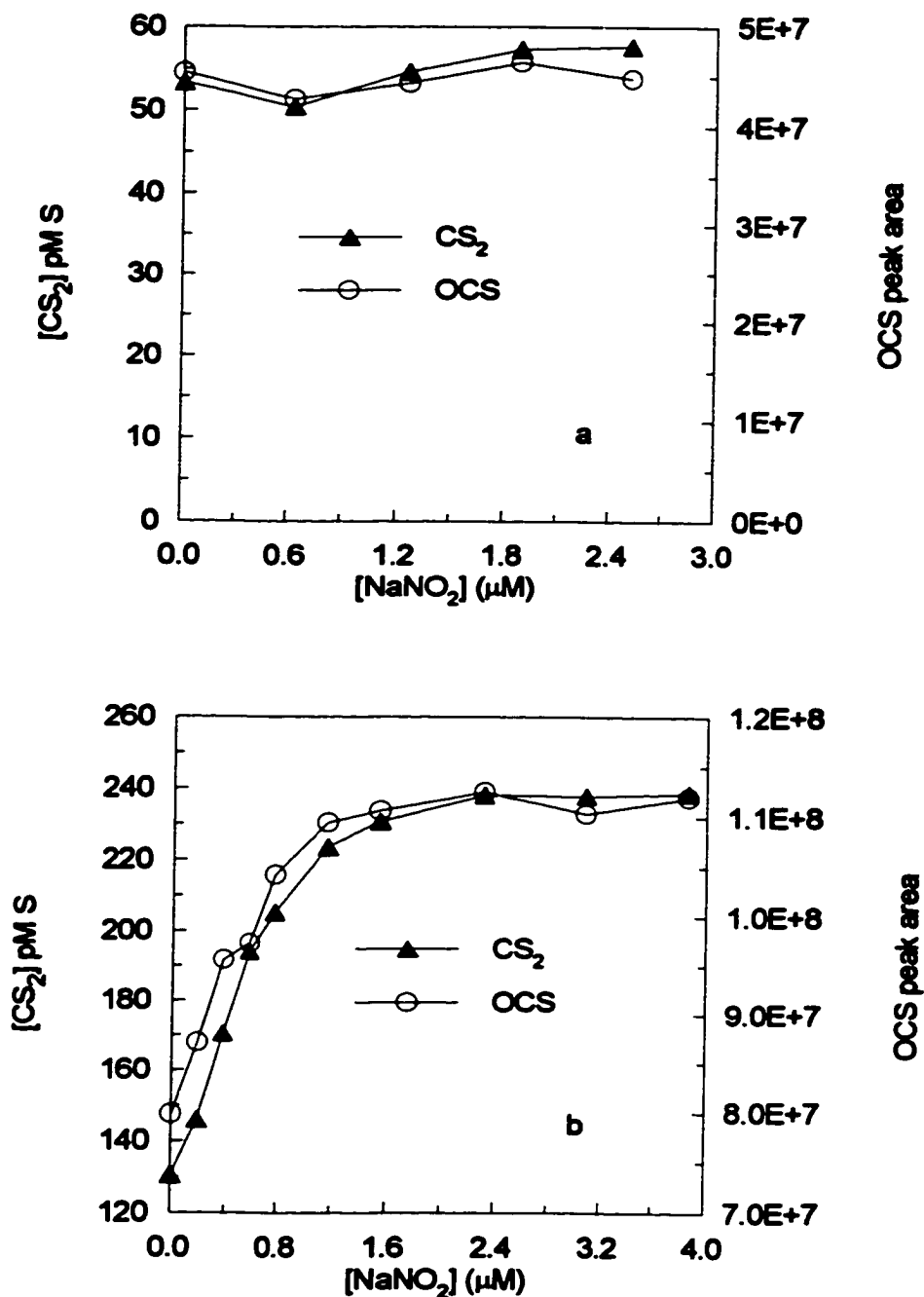


Figure 6.19 Effect of nitrite on the photo-production of CS₂ and OCS, (a) water samples without addition of cysteine (20 min exposure) and (b) water samples with 0.63 μM cysteine added (30 min exposure). OCS was recorded in peak area. Initial concentrations of CS₂ and OCS before irradiation were deducted.

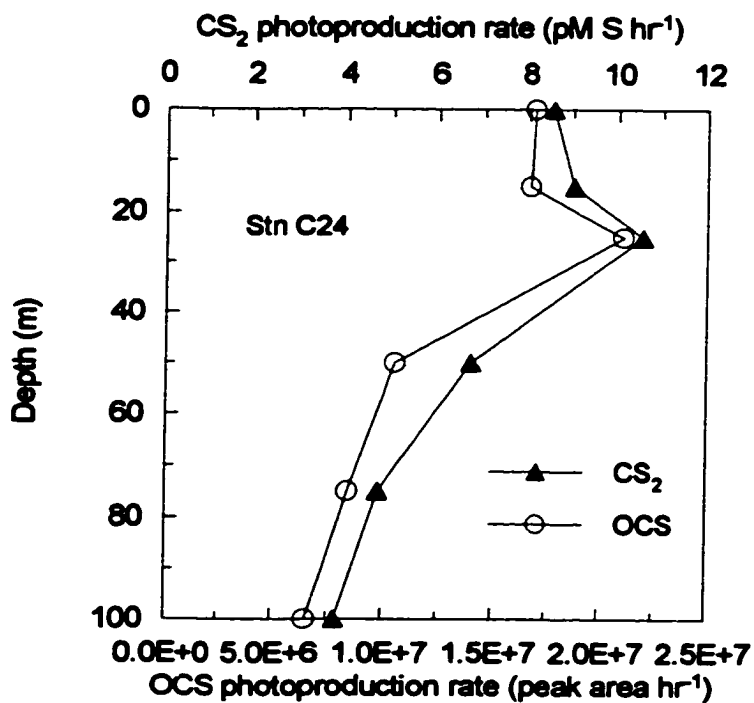
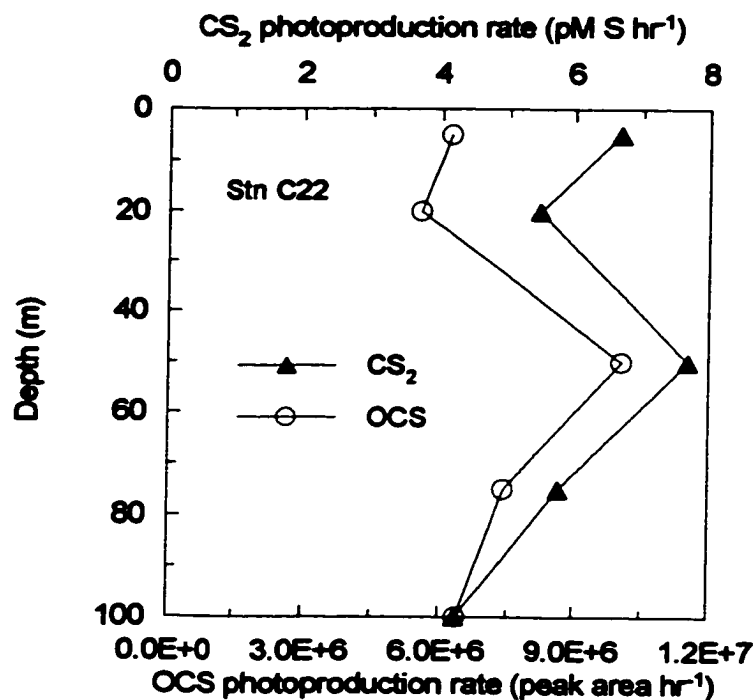


Figure 6.20 Examples showing similarity in the vertical distributions of CS₂ and OCS photo-production rates obtained during the *Challenger* cruise. OCS was recorded in peak area.

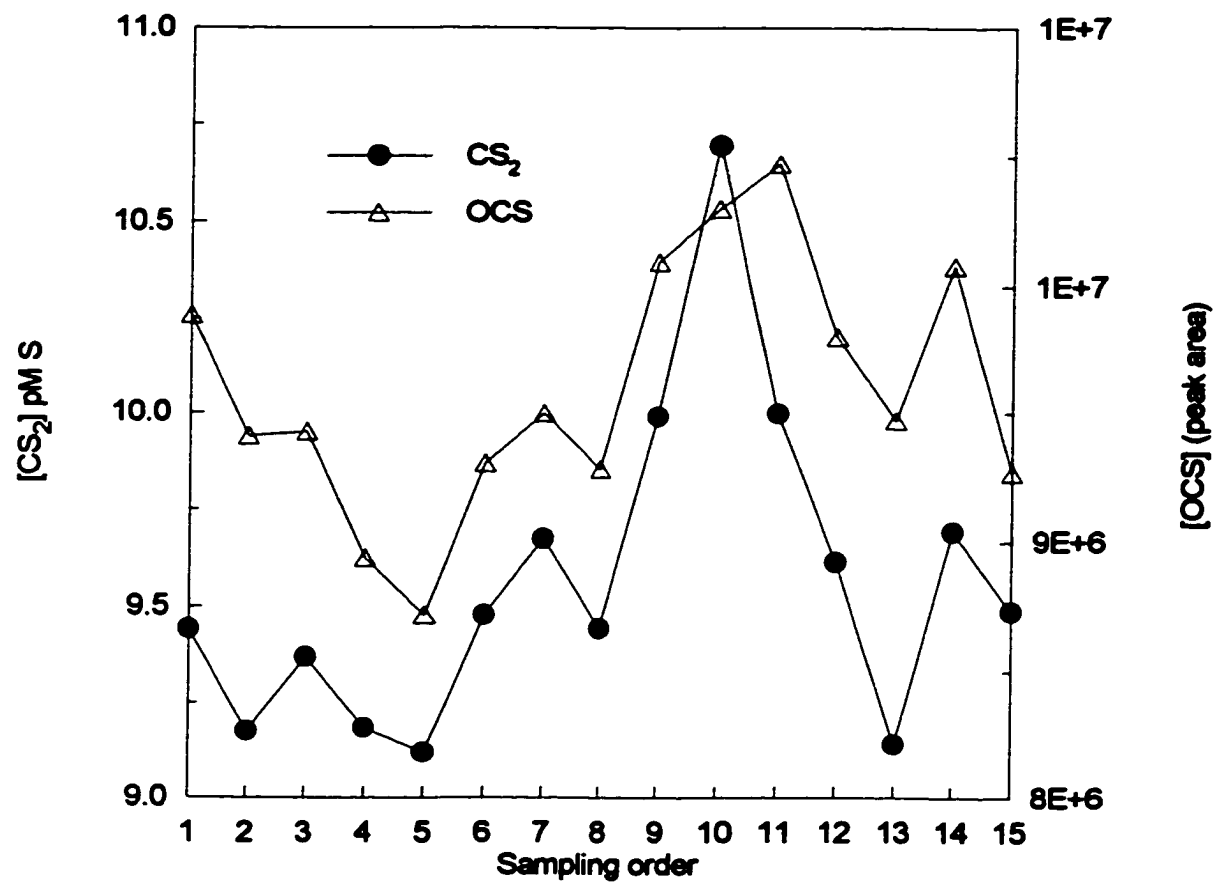


Figure 6.21 CS_2 and OCS distributions in surface water along a transect during the *Challenger* cruise.

(Figure 6.19) demonstrate that photo-production of the two species are affected by the OH radical in a similar way. Irradiation of water samples collected at discrete depths from two stations during the *Challenger* cruise showed similar depth profiles of photo-production rate for CS₂ and OCS (Figure 6.20). Additionally, the distribution of surface water concentration of CS₂ along a transect during the *Challenger* expedition strongly resembled that of OCS (Figure 6.21).

A comparison can also be made between the average quantum-yield spectrum of CS₂ from this study and that of OCS obtained by Weiss et al. [1995b] in south Pacific Ocean waters (Figure 6.22). The similarity of the shapes of the two spectra, especially in the UV-B region (280-320 nm), is impressive despite the obvious difference between the two locations. However, the quantum yield of OCS is on average 12 times higher than that of CS₂ in the range 297-400 nm. Employing the same approach as described in section 6.5, I estimated the oceanic photo-production of OCS to be 83.9 Gmol yr⁻¹. As the photochemical source for CS₂ is approximately 7.7 Gmol S yr⁻¹, the ratio of photo-production of OCS to that of CS₂ is 11.

Loss processes for CS₂ and OCS in the surface ocean include ventilation to the atmosphere, chemical destruction and downward mixing. A preliminary assessment indicates that evasion to the atmosphere accounts for the major loss of oceanic CS₂ and that the dominant loss term for oceanic OCS is its hydrolytic degradation. The lifetimes of CS₂ and OCS in the surface ocean are, therefore, controlled by ventilation to the atmosphere and chemical destruction, respectively. In that case, the lifetime of CS₂ is equal to the mixed layer depth divided by its exchange velocity. If the mixed layer depth is taken to be 50 m and the mean exchange velocity (3.1 m d⁻¹) obtained from this study is used, the lifetime of CS₂ is 16 days. The lifetime of OCS with respect to its hydrolysis is ~1 day at 20°C [Radford-Knoery and Cutter, 1994]. Therefore, if the mixed layer depth is 50 m

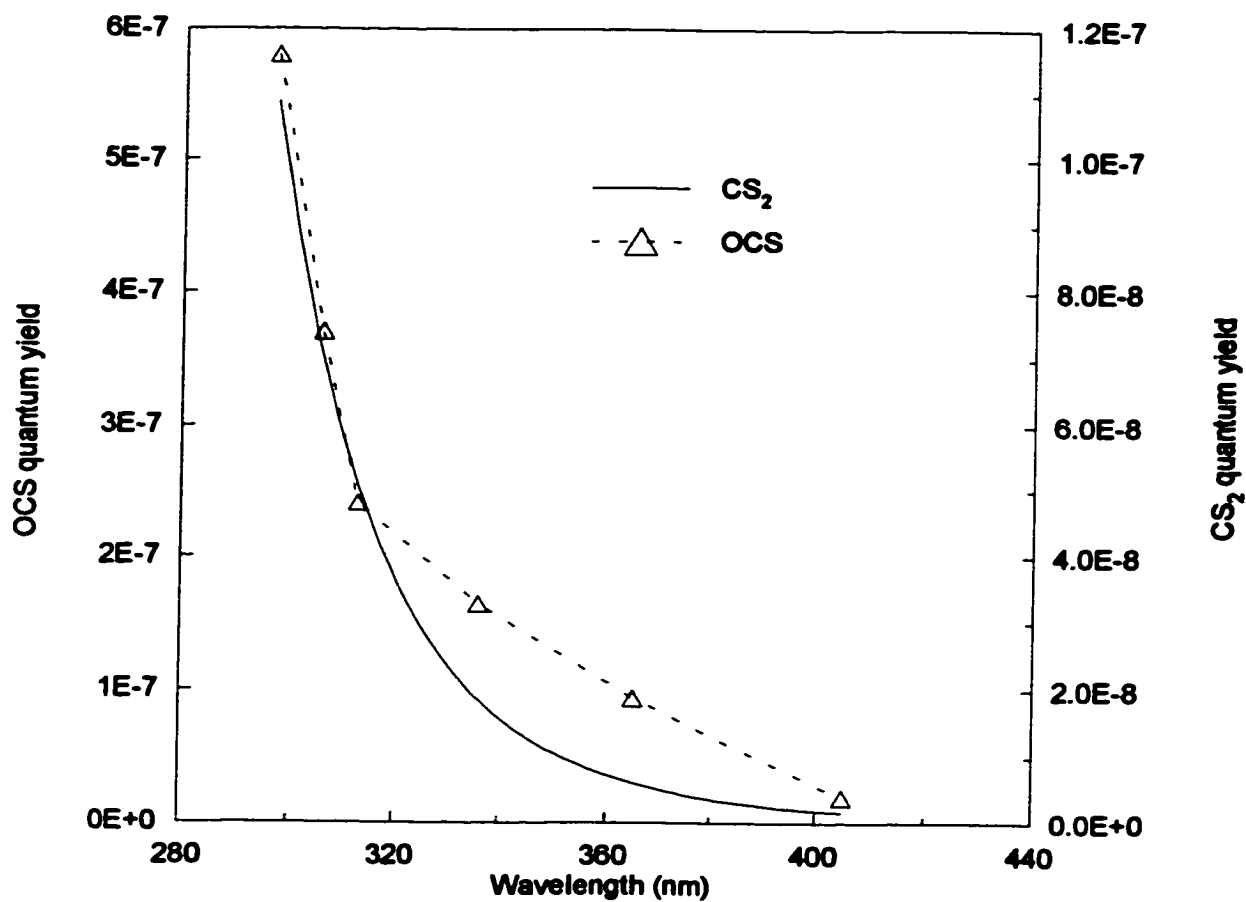


Figure 6.22 comparison between the average apparent quantum-yield spectrum of CS₂ derived from the Rundel method and that of OCS from Weiss et al. [1995b].

and the surface ocean temperature is 20°C, the lifetime of CS₂ will be ~16 times longer than that of OCS. As the mean concentration of CS₂ in surface waters is similar to that of OCS (~15 pM) [Ulshofer et al., 1995; Ulshofer et al., 1996; Ulshofer and Andreae, 1997], the total loss of OCS (and hence its total production) in the surface ocean could also be ~16 times higher than that of CS₂, which is in reasonable agreement with the factor of 11 resulting from the difference in the photo-production rates for these two compounds.

6.10 Summary

Irradiation of seawater samples using natural and simulated sunlight confirms that CS₂ is produced photochemically in the ocean. Solar UV radiation in the wavelength range 290-340 nm is most important for this production with visible light having negligible effect. The apparent quantum-yield spectrum of the compound was derived by both the differential irradiance method and the Rundel method. The differential irradiance method overestimates the quantum yield by a mean value of 53% in the range 308-362 nm as compared with the Rundel method. Under appropriate assumptions, the magnitude of CS₂ photo-production in the global ocean is estimated to be 0.29 Tg CS₂ yr⁻¹. This is comparable to the sea-to-air flux estimates of this compound (see Chapter 4, section 4.4). Photo-production of CS₂ is probably mediated by CDOM, and OH radicals are likely to be an important transient intermediates. Thiol group-bearing amino acids and their dimers are suggested to be efficient precursors of CS₂. The processes responsible for photo-production of CS₂ are probably similar to those for OCS.

Chapter 7 Conclusions and Directions for Future Studies

7.1 Conclusions

This thesis attempts to re-investigate the ocean-to-atmosphere flux of CS₂, and to identify and quantify potential CS₂ sources within the ocean. Surface and subsurface water concentrations of CS₂ were measured during three ocean cruises: two in the North Atlantic and one in the Pacific Ocean. Spatial distribution of CS₂, its relationship with hydrographic parameters, and its implication for oceanic production of this compound are discussed. The emission rates of CS₂ from the ocean to the atmosphere are calculated and extrapolated to the global scale. Photochemical processes and phytoplankton activity are identified as potential sources for oceanic CS₂. The sizes of these two sources are evaluated and compared with the estimates of CS₂ efflux from the ocean. The main conclusions can be summarised as follows:

- (1) Two analytical methods were developed for measuring CS₂ in marine waters: oxygen-doped GC/ECD and GC/MS. Both methods employed a purge-and-trap system for preconcentration of CS₂. The detection limits of the two methods are comparable to each other (1.5 pM S in a 40 mL sample), and their linear response is up to at least 600 pM S, covering the CS₂ concentrations occurring in most marine waters. The oxygen-doped GC/ECD system is highly sensitive to CS₂ and provides an alternative to the GC/FPD method [Kim and Andreae, 1987b] for analyzing CS₂ in aquatic environments. Oxygen doping is critical in enhancing the sensitivity and lowering the detection limit of the ECD.
- (2) An irradiation system was developed for studies on photochemical production of CS₂ in the ocean. The system combines a powerful xenon lamp with a series of successive long band-pass cutoff light filters. Compared with an ordinary monochromator, this experimental set-up provides high energy output and thus

makes it possible to acquire more quantum-yield data in a relatively short period of investigation. However, the wavelength bandwidths produced by the successive cutoff filters are usually too wide to allow a straightforward calculation of the quantum yield. It is recommended that the approach proposed by Rundel [1983] be used to extract the quantum yield from the data obtained using the irradiation system devised for this study.

- (3) Carbon disulphide is more abundant in coastal waters than in open ocean waters. In the areas that have been investigated for this study, the mean surface water concentrations are 30 and 13 pM S for coastal and oceanic waters, respectively. This is generally consistent with the concentrations reported by other workers [Lovell, 1974; Kim and Andreae, 1987a; Kim and Andreae, 1992]. The higher abundance of CS₂ in coastal waters possibly originates from greater sedimentary input and higher photo-production rates of the compound in coastal environments. Warm waters usually contain higher levels of CS₂ than cool waters, which could result from enhanced photo-production in intensely irradiated (and hence warm) waters. No clear relationship was observed between phytoplankton biomass (Chl-*a*) and CS₂ concentration in surface waters.
- (4) Vertical profiles observed in temperate waters typically show decreasing CS₂ concentration with increasing depth, indicative of production of CS₂ in the surface. Profiles obtained from warm waters of tropical and subtropical gyres are characterised by the co-occurrence of deep CS₂ and Chl-*a* maxima, suggesting the possibility of biological CS₂ production. Some profiles show a distinct increase in CS₂ concentration near the seafloor, indicating an input of the compound from the underlying sediments. Probably as a result of downward and upward transportation and its slow chemical destruction, CS₂ is not totally depleted in mid or deep waters.

- (5) The mean saturation ratio for CS₂ in seawater is 41. The ocean is thus highly supersaturated in CS₂ and acts as a source for atmospheric CS₂. The oceanic source strength is estimated to be 0.18 Tg CS₂ yr⁻¹ with a range from 0.13 to 0.24 Tg CS₂ yr⁻¹, confirming that the ocean is the second largest source for atmospheric CS₂. As CS₂ in the troposphere is oxidised to OCS with a molar conversion efficiency of 0.81, the ocean indirectly delivers 0.12 (0.09-0.16) Tg OCS yr⁻¹ to the atmosphere in the form of CS₂. This indirect OCS source is equivalent to 41% of the direct emission of OCS from sea to air.
- (6) Laboratory culture experiments demonstrate that production of CS₂ by marine phytoplankton is undoubtedly occurring, but is not a universal phenomenon among marine algae. The capability of producing CS₂ varies widely for different phytoplankton species and in different physiological states. Cell autolysis and metabolism are possible mechanisms responsible for formation of CS₂ by phytoplankton. Extrapolation from bottle cultures to the real ocean is fraught with uncertainty since only a very limited number of species were examined under conditions that were much different from the real ocean. The strong dependence of CS₂ formation on phytoplankton species and physiological states will add more uncertainty to such extrapolation. The maximum potential for CS₂ production by phytoplankton in the ocean is estimated to be 0.11 Tg CS₂ yr⁻¹, or 62% of the ocean-to-atmosphere flux estimate of this compound. However, it must be noted that three of six phytoplankton species tested are non-producers of CS₂. Production of CS₂ by phytoplankton in the real ocean may be far below the maximum potential value.
- (7) Carbon disulphide is photochemically produced in the ocean. Solar UV below 340 nm is mainly responsible for inducing CS₂ photo-production with visible light having little effect. The quantum yield of CS₂ decreases with increasing

wavelength approximately in a double exponential manner. The potential photo-production of CS₂ in the ocean is evaluated to be 0.29 Tg CS₂ yr⁻¹, which is comparable to the sea-to-air flux estimates of this compound. Major factors contributing to uncertainties in this estimate include limited spatial and temporal coverage of the quantum-yield data, the effect of clouds on the flux of solar UV reaching the sea surface, ill-defined quantum yields in wavelengths above 360 nm, and the effects of water temperature on photochemical CS₂ formation.

- (8) Photochemical production of CS₂ shows significantly positive correlation with the absorption coefficient at 350 nm, suggesting that this production is mediated by CDOM. Hydroxyl radicals are probably important transient intermediates. Thiol group-containing amino acids and their dimers are likely efficient precursors to CS₂. Evidence from field survey and laboratory experiments suggests that CS₂ and OCS are photochemically produced through similar mechanisms.

7.2 Future studies

As photochemical processes, and possibly phytoplankton activity, are important sources for CS₂, it is expected that CS₂ concentration and its flux to the atmosphere would exhibit seasonal and diurnal variations. So far no CS₂ data have been collected in winter. Time-series measurements are required to address the diurnal variation. More field investigations are needed to further demonstrate the concentration differences between coastal and open ocean waters, and between cold and warm waters. Simultaneous measurement of CS₂ concentration in both the water and air phases will be useful to further refine the flux estimates

The lifetime of CS₂ in the ocean, which is an essential parameter in estimating its loss rate, has not been adequately determined. Without giving details, Lovelock

[1974] stated that CS_2 is stable at least for 10 days in oxic seawater. Elliott [1990] determined the reaction constants in distilled water for CS_2 hydrolysis and its reaction with the hydrogen peroxide conjugate base HO_2^- (see Chapter 5, section 5.3.2). With $\text{pH} = 8$ and $[\text{H}_2\text{O}_2] = 1 \mu\text{M}$, the lifetime (e-folding time) of CS_2 with respect to its hydrolysis and reaction with HO_2^- is 6.4 years. As the concentration of H_2O_2 is mostly far below $1 \mu\text{M}$ in the open ocean, the corresponding lifetime will be even longer. However, the dark controls conducted during the irradiation experiments for water samples collected in Galway Bay suggest that the lifetime of CS_2 in the bay water could be as short as 10 hours. As water samples for the irradiation tests were passed through GF/F filters (pore size $0.7 \mu\text{m}$), the filtered seawater will contain bacteria. The consumption of CS_2 in the dark controls may, therefore, be associated with microbial processes that can be prevalent in the brown waters in the bay. Nevertheless, the microbial consumption of CS_2 must be highly space- and time-dependent since the dark controls for stations far away from the bay did not show any significant decrease in CS_2 concentration.

More investigations are needed to quantify the role of phytoplankton in the formation of oceanic CS_2 . Algal species representative of various water masses in the ocean should be studied to improve the estimate of potential CS_2 production by phytoplankton. As all the phytoplankton cultures conducted in this study are axenic, the effect of bacteria on CS_2 production is unknown. New approaches are needed to further reveal the mechanisms responsible for biogenic production of CS_2 in marine waters.

The CS_2 quantum-yield data obtained during this study cover only one season (June) and a rather restricted region in the Northeast Atlantic. It is unknown if these data can be applied to other ocean areas and seasons. Terrestrial CDOM is thought to be more photochemically reactive than marine CDOM [Kieber et al., 1990; Dister and Zafiriou, 1993]. However, this difference is not apparent from the

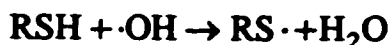
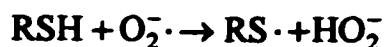
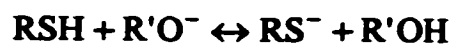
quantum-yield spectra obtained in this study since none of the water samples for determining the quantum yield were collected in areas that are strongly influenced by terrestrial run-off. The properties of CDOM also change with its irradiation history and are affected by hydrographic structure of the water column. CDOM in a shallow surface mixed layer that receives strong and prolonged solar radiation could be significantly photobleached [Siegel and Michaels, 1996; Vodacek et al., 1997], thus reducing its photochemical reactivity. Furthermore, the CS₂ quantum yield is also likely affected by the properties and the concentrations of the sulphur substrates which obviously have seasonal and spatial variations due to their close linkage to the biotic and physical processes in the ocean. Therefore, in order to improve the estimate of the magnitude of CS₂ photo-production in the ocean, more field surveys are needed to demonstrate the temporal and spatial variations in the quantum-yield spectrum of CS₂ photo-production.

One question arising from this study is why the concentration of CS₂ in warm, saline and oligotrophic waters (tropical and subtropical ocean gyres) is much higher than that in cool and biologically productive waters (temperate areas). There are several directions that can be followed to address this issue. First, warm waters usually receive more solar radiation than cool waters. It is, therefore, possible that more CS₂ is photochemically produced in warm waters than in cool waters. However, the magnitude of photo-production is dependent not only on the amount of incident light, but also on the photochemical quantum yield and the concentrations and properties of the sulphur substrates and CDOM. In order to quantify the difference in CS₂ photo-production between warm and cool waters, we must clarify the difference in the quantum-yield and CDOM absorption spectra between the two water bodies. Second, the effect of temperature on CS₂ photo-production should be tested. Since photochemical production of CS₂ is most likely a secondary process, it is possible that this process is temperature-dependent. Last,

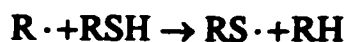
oligotrophic waters are enriched with DMSP and DMS [Andreae, 1990]. It is unclear so far if DMSP and DMS are precursors to CS₂.

Elucidation of the mechanisms for photochemical CS₂ and OCS formation in seawater is another important area for future studies. Photochemical processes usually involve formation and reactions of radicals. Since short-chain thiols do not absorb the solar radiation reaching the Earth's surface, the processes responsible for CS₂ and OCS production must be photosensitised. Flock et al. [1997] hypothesised that free thiyl radicals (RS·) play a critical role in the production of OCS and that the following two schemes account for formation of thiyl radicals in seawater:

Scheme 1: Formation of thiyl radicals from thiols and thiolates by interaction with reactive oxygen species.



Scheme 2: Formation of thiyl radicals by metal catalysis.



Since scheme 1 is oxygen-dependent while scheme 2 is oxygen-independent, this proposition can explain why photo-production of OCS can occur in both oxygen-enriched and -depleted environments [Ferek and Andreae, 1984; Zepp and Andreae, 1994]. As reactive oxygen species in aquatic environments are dominantly created through photochemical transformations of CDOM [Blough and Zepp, 1995], scheme 1 also agrees with the observation that OCS formation is enhanced by addition of extracted natural DOM or artificial humic acid [Flock et al., 1997]. Thiols with higher S-H acidity form thiolates more easily than those with lower S-H acidity. Thus, scheme 1 explains why glutathione and cysteine are much more efficient precursors to OCS than methyl mercaptan and 3-mercaptopropionic acid. Formation of thiyl radicals according to the above schemes is not possible with disulphides, thio ethers, sulphonic acids and tertiary sulphonium salts, which is consistent with the results reported by Flock et al. [1997]. However, the work conducted for this thesis has shown that cystine, a dimeric disulphide of cysteine, is a good precursor to both CS₂ and OCS. If the thiyl radical is the sole sulphur-containing radical that leads to the formation of CS₂ and OCS, then cystine must be able to produce thiyl radicals. In fact, the dissociation energy of the S-S bond (~73 kcal mol⁻¹) is lower than that of the S-H bond (~89 kcal mol⁻¹) [Oae and Doi, 1991], and thiyl radicals can be formed from disulphides by homolytic cleavage [Still, 1985]. Therefore, the significance of this pathway in the photo-production of CS₂ and OCS should be investigated.

Flock et al. [1997] proposed further that carbon monoxide (CO), which is also photochemically produced in the ocean, could be a carbonyl donor to OCS. Pos et al. [1998] reported indirect evidence that photo-production of CO and OCS shares a common pathway, and that production of OCS results from the addition of sulphur-centred radicals, such as thiyl radicals (RS·) and sulphhydryl radicals (HS·), to carbonyl groups (RCO). The mechanism for OCS production proposed by Pos

et al. [1998] involves the formation of thioacids (RCOSH) or thioesters (RCOSR') as intermediates. This mechanistic scheme also suggests the possibility of the formation of dithioacids (HOCSSH) or dithioesters (RCSSR'), which can easily decompose to CS₂. Isotopic studies, using ¹³C-labelled carbonyl groups and ³³S-labelled-sulphur donors, can verify if these proposed mechanisms for photochemical formation of CO, OCS and CS₂ are valid.

Finally, the sedimentary source for oceanic CS₂ needs to be quantified and the mechanisms for CS₂ production in sediments need to be elucidated. Production of CS₂ in marine sediments is inferred from elevated CS₂ concentrations in sediment porewaters relative to the overlying water column [Lovelock, 1974] or from vertical profiles showing increases in CS₂ concentrations towards the sea floor [Kim and Andreae, 1992]. Results from laboratory incubations of anoxic sediments suggest that microbial processes are responsible for generating a variety of volatile sulphur species, such as DMS, MeSH, H₂S [Kiene, 1988; Kiene and Capone, 1988], and OCS [Zhang et al., 1998]. Evidence of a direct involvement of microbial activity in CS₂ formation has yet to be investigated. Zhang et al. [1998] demonstrated that OCS production in sediments is coupled to microbial sulphate reduction. It will be interesting to know if sulphate-reducing bacteria play a similar role in CS₂ production. Banwart and Bremner [1975] identified sulphur-containing amino acids as the substrates for microbial CS₂ formation in soils and suggested similar possibilities in marine sediments. Nevertheless, the mechanisms responsible for this pathway essentially remain unknown. In order to calculate a budget for oceanic CS₂, it is necessary to have a quantitative knowledge of CS₂ input from sediments to the water column. Zhang et al. [1998] have shown that diffusion of OCS from sediments could contribute 2-75% of the total sources of OCS in the Chesapeake Bay, depending on the season and location investigated.

Any attempt to estimate the sediment-water flux of CS₂ should also take into account the spatial and temporal variations in the flux.

Bibliography

- Adams, D. F., S. O. Farwell, E. Robinson, M. R. Pack, and W. L. Barnesberger, Biogenic sulfur source strength, *Environ. Sci. Technol.*, **15**, 1493-1498, 1981.
- Adams, G. E., J. E. Aldrich, R. H. Bisby, R. B. Cundall, J. L. Redpath, and R. L. Willson, Selective free radical reactions with proteins and enzymes: Reactions of inorganic radical anions with amino acids, *Radiation Research*, **49**, 278-280, 1972.
- Andreae, M. O., Climatic effects of changing atmospheric aerosol levels, in *Future Climates of the World: A Modelling Perspective*, *World Survey of Climatology*, edited by A. Henderson-Sellers, pp. 347-398, Elsevier, Amsterdam, 1995.
- Andreae, M. O., Ocean-Atmosphere Interactions in the Global Biogeochemical Sulfur Cycle, *Mar. Chem.*, **30**, 1-29, 1990.
- Andreae, M. O., The ocean as a source of atmospheric sulfur compounds. in *The role of Air-Sea Exchange in Geochemical Cycling*, edited by P. Buat-Menard, pp. 331-362, D. Reidel, Hingham, Mass., 1986.
- Andreae, T. W., G. A. Cutter, N. Hussain, J. Radford-Knoery, and M. O. Andreae, Hydrogen sulfide and radon in and over the Western North Atlantic Ocean, *J. Geophys. Res.*, **96**, 18,753-18,760, 1991.
- Aneja, V. P., and W. J. Cooper, Biogenic sulfur emissions: A review, in *Biogenic sulfur in the Environment*, edited by E. S. Saltzman and W. J. Cooper, pp. 2-13, Am. Chem. Soc., Washington, D.C., 1989.
- Asher, W. E., P. J. Farley, R. Wanninkhof, E. C. Monahan, and T. S. Bates, Laboratory and field experiments on the correlations of fractional area whitecap coverage with air-sea gas transport, in *Precipitation Scavenging and Atmosphere-Surface Exchange, Vol. 2, The Semonin Volume*, pp. 815-828, edited by S. E. Schwartz and W. G. N. Slinn, Hemisphere, Washington, 1992.
- Asher, W. E., E. C. Monahan, R. Wanninkhof, and T. S. Bates, Correlation of fractional foam coverage with gas transport rates, in *Proceedings of the Second International Symposium on Gas Transfer at water Surfaces*, edited

by S. C. Wilhelms and J. S. Gulliver, pp. 536-545, American Society of Civil Engineers, New York, 1991.

- Avilova, G., A. Cavalleri, D. Djuric, S. Hernberg, E. Lukas, A. A. E. Massoud, W. O. Phoon, V. Rose, S. Tarkowski, J. Teisinger, H. Thiele, S. Yamaguchi, and S. H. Zaidi, *Environment Health Criteria 10: Carbon Disulphide*, World Health Organization, Geneva, 1979.
- Bandy, A. R., D. C. Thornton, and J. E. Johnson, Carbon disulfide measurements in the atmosphere of the Western North Atlantic and the Northwestern South Atlantic Oceans, *J. Geophys. Res.*, **98**, 23449-23457, 1993.
- Bandy, A. R., T. L. Bandy, O. Youngbluth, and T. L. Owens, Trace gas measurements from tethered balloon platforms, *J. Atmos. Ocean. Technol.*, **3**, 581-584, 1986.
- Bandy, A. R., P. J. Maroullis, B. Bonsang, and C. A. Brown, Emissions of sulfur gases to the atmosphere from estuaries and coastal areas, in *Estuarine Comparisons*, edited by V. S. Kennedy, pp. 303-312, Academic, Orlando, Fla., 1982.
- Bandy, A. R., P. J. Maroulis, L. Shalaby, and L. A. Wilner, Evidence for a short tropospheric residence time for carbon disulfide, *Geophys. Res. Lett.*, **8**, 1180-1183, 1981.
- Banwart, W. L., and J. M. Bremner, Volatilization of sulfur from unamended and sulfate-treated soils, *Soil Biol. Biochem.*, **8**, 19-22, 1975a.
- Banwart, W. L., and J. M. Bremner, Formation of volatile sulfur compounds by microbial decomposition of sulfur-containing amino acids in soils, *Soil Biol. Biochem.*, **7**, 359-364, 1975b.
- Barnes, I., K. H. Becker, and I. Patroescu, The tropospheric oxidation of dimethyl sulfide: A new source of carbonyl sulfide, *Geophys. Res. Lett.*, **21**, 2389-2392, 1994.
- Barns, I., K. H. Becker, E. H. Fink, A. Reimer, F. Zabel, and H. Niki, Rate constant and products of the reaction $\text{CS}_2 + \text{OH}$ in the presence of O_2 , *Int. J. Chem. Kinet.*, **15**, 631-645, 1983.

- Bates, T. M., J. D. Cline, R. H. Gammon, and S. R. Kelly-Hansen, Regional and seasonal variations in the flux of oceanic dimethylsulfide to the atmosphere, *J. Geophys. Res.*, *92*, 2930-2938, 1987.
- Blough, N. V., and R. G. Zepp, Reactive oxygen species in natural waters, in *Active Oxygen in Chemistry*, edited by C. S. Foote, J. S. Valentine, A. Greenberg, and J. F. Liebman, pp. 280-333, Chapman and Harc, 1995.
- Blough, N. V., O. C. Zafiriou, and J. Bonilla, Optical absorption spectra of waters from the Orinoco River outflow: Terrestrial input of colored organic matter to the Caribbean, *J. Geophys. Res.*, *98*, 2271-2278, 1993.
- Bonsang, B., C. Polle, and G. Lambert, Evidence for marine production of isoprene, *Geophys. Res. Letts.*, *19*, 1129-1132, 1992.
- Bremner, J. L., and W. L. Banwart, Identifying volatile S compounds by gas chromatography, *Sulfur Inst. J.*, *10*, 6-9, 1974.
- Brimblecombe, P., and D. Shooter, Photo-oxidation of dimethylsulphide in aqueous solution, *Mar. Chem.*, *19*, 343-353, 1986.
- Broecker, H. C., and W. Siems, The role of bubbles for gas transfer from water to air at higher windspeeds: Experiments in the wind-wave facility in Hamburg, in *Gas Transfer at Water Surfaces*, edited by W. Brutsaert and G. H. Jirka, pp. 229-238, D. Reidel, Hingham, Mass., 1984.
- Broecker, H. C., J. Peterman, and W. Siems, The influence of wind on CO₂ exchange in a wind-wave tunnel, including the effects of mono layers, *J. Mar. Res.*, *36*, 595-610, 1978.
- Brune, W. H., J. G. Anderson, D. W. Toohey, D. W. Fahey, S. R. Kawa, R. L. Jones, D. S. Mckenna, and L. R. Poole, The potential for ozone depletion in the Arctic polar stratosphere, *Science*, *252*, 1260-1266, 1991.
- Bushaw, K. L., R. G. Zepp, M. A. Tarr, D. Schulz-Jander, R. A. Bourbonniere, R. E. Hodson, W. L. Miller, D. A. Bronk, and M. A. Moran, Photochemical release of biologically available nitrogen from aquatic dissolved organic matter, *Nature (London)*, *381*, 404-407, 1996.
- Carder, K. L., R. G. Steward, G. R. Harvey, and P. B. Ortner, Marine humic and fulvic acids: Their effects on remote sensing of ocean chlorophyll., *Limnol. Oceanogr.*, *34*, 68-81, 1989.

- Caron, F., and J. R. Kramer, Formation of volatile sulfides in freshwater environments, *the Science of the Total Environment*, 153, 177-194.
- Carroll, M. A., Measurements of OCS and CS₂ in the free troposphere, *J. Geophys. Res.*, 90, 10483-10486, 1985.
- Caspari, G., and A. Granzow, The flash photolysis of mercaptans in aqueous solutions, *J. Phys. Soc.*, 74, 836-839, 1970.
- Challenger, F., Aspects of the Organic Chemistry of Sulfur, pp. 253, Academic Press, New York, 1959.
- Charlson, R. J., J. E. Lovelock, M. O. Andreae, and S. G. Warren, Oceanic phytoplankton, atmospheric sulphur, cloud albedo and climate, *Nature*, 326, 655-661, 1987.
- Charlson, R. J., T. L. Anderson, and R. E. McDuff, Chapter 13: The sulfur Cycle, in *Global Biogeochemical Cycles*, edited by S S. Butcher, R. J. Charlson, G. H. Orians, and G. V. Wolfe, pp. 285-300, Academic Press Limited, 1992.
- Chatfield, R. B., and P. J. Crutzen, Sulfur dioxide in remote oceanic air: cloud transport of reactive precursors, *J. Geophys. Res.*, 89, 7111-7132, 1984.
- Chen, S.-N., and M. Z. Hoffman, Rate constants for the reaction of the carbonate radical with compounds of biochemical interest in neutral aqueous solution, *Radiation Research*, 56, 20-47, 1973.
- Chin, Mian, An atmospheric study of carbonyl sulfide and carbon disulphide and their relationship to stratospheric background sulfur aerosol, Ph. D. thesis, Ga. Inst. of Technol., Atlanta, 1992.
- Chin, M., and D. D. Davis, Global sources and sinks of OCS and CS₂ and their distribution, *Global Biogeochemical Cycles*, 7, 321-337, 1993.
- Clegg, S. L., and M. Whitfield, Activity coefficients in natural waters, in *Activity coefficients in electrolyte solutions*, 2nd ed., edited by K. S. Pitzer, pp. 279-434, CRC press, Boca Raton, Fla., 1991.
- Conrad, R., W. Seiler, G. Bunse, and H. Giehl, Carbon monoxide in seawater (Atlantic Ocean), *J. Geophys. Res.*, 87, 8839-8852, 1982.

- Cooper, W. J., R. G. Zika, R. G. Petasne, and J. M. C. Plane, Photochemical formation of H_2O_2 in natural waters exposed to sunlight, *Environ. Sci. Tech.* **22**, 1156-1160, 1988.
- Crutzen, P. J., The possible importance of COS for the sulfate layer of the stratosphere, *Geophys. Res. Lett.*, **3**, 73-76, 1976.
- Cutter, G. A., and J. Radford-Knoery, Carbonyl sulfide in two estuaries and shelf waters of the western North Atlantic Ocean, *Mar. Chem.*, **43**, 225-233, 1993.
- Cutter, G. A., and C. F. Krahforst, Sulfide in surface water of the Western Atlantic Ocean, *Geophys. Res. Lett.*, **15**, 1393-1396, 1988.
- De Bruyn, W. L., E. Swartz, J. H. Hu, J. A. Shorter, P. Davidovits, D. R. Worsnop, M. S. Zahniser, and C. E. Kolb, Henry's law solubilities and Setchenow coefficients for biogenic reduced sulfur species obtained from gas-liquid uptake measurements, *J. Geophys. Res.*, **100**, 7245-7251, 1995.
- Deacon, E. L., Sea-air gas transfer: The wind speed dependence, *Boundary layer meteorol.*, **21**, 31-37, 1980.
- Dister, B., and O. C. Zafiriou, Photochemical free radical production rates in the Eastern Caribbean, *J. Geophys. Res.*, **98**, 2341-2352, 1993.
- Dumdei, E. J, A. E. Flowers, M. J. Garson, and C. J. Moore, The biosynthesis of sesquiterpene isocyanides and isothiocyanates in the marine sponge *Acanthella cavernosa* (Dendy); evidence for dietary transfer to the dolid nudibranch *Phyllidiella pustulosa*, *Compar. Biochem. Physiol., Ser. A, Molecular and Integrative Physiology*, **118**, 1385-1392, 1997.
- Elliott, S., Effect of hydrogen peroxide on the alkaline hydrolysis of carbon disulfide, *Environ. Sci. Technol.*, **24**, 264-267, 1990.
- Elliott, S., E. Lu, and S. Rowland, Carbonyl sulfide hydrolysis as a source of hydrogen sulfide in open ocean seawater, *Geophys. Res. Lett.*, **14**, 131-134, 1987.
- Engel, A., and U. Schmidt, Vertical profile measurements of carbonylsulphide in the stratosphere, *Geophys. Res. Lett.*, **21**, 2219-2222, 1994.

- Erickson, D. J., III, A stability dependent theory for air-sea gas exchange, *J. Geophys. Res.*, **98**, 8471-8488, 1993.
- Evans, M. G., and N. Uri., The dissociation constant of hydrogen peroxide and the electron affinity of the HO₂ radical, *Trans. Faraday Soc.*, **45**, 224-230, 1949.
- Flock, O. R., M. O. Andreae, and M. Drager, Environmentally relevant precursors of carbonyl sulfide in aquatic systems, *Mar. Chem.*, **59**, 71-85, 1997.
- Flock, O. R., and M. O. Andreae, Photochemical and non-photochemical formation and destruction of carbonyl sulfide and methyl mercaptan in ocean waters, *Mar. Chem.*, **54**, 11-26, 1996.
- Frederick, J. E., and H. E. Snell, Tropospheric influence on solar ultraviolet radiation: The role of clouds, *Journal of Climate*, **3**, 373-381, 1990.
- Goldman, J. C., M. R. Dennet, and N. M. Frew, Surfactant effects on air-sea gas exchange under turbulent conditions, *Deep Sea Res.*, **35**, 1953-1970, 1988.
- Grasshoff, K., and T. Almgren, *Methods of Seawater Analysis*, Verlag Chemie, New York, NY, 317 pp., 1976.
- Green, S. A., and N. V. Blough, Optical absorption and fluorescence properties of chromophoric dissolved organic matter in natural waters, *Limnol. Oceanogr.*, **39**, 1903-1916, 1994.
- Gregg, M. C., C. S. Cox, and P. W. Hacker, Vertical microstructure measurements in the central North Pacific, *J. Phys. Oceanogr.*, **3**, 458-469, 1973.
- Grimsrud, E. P., and D. A. Miller, Oxygen doping of carrier gas in measurement of halogenated methanes by gas chromatography with electron capture detection, *Anal. Chem.*, **50**, 1141-1145, 1978.
- Guillard R. R. L., and J. H. Ryther, Studies of marine planktonic diatoms I: *Cyclotella nana* Hustedt and *Detonula confervacea* (Cleve) Gran.. *Can. J. Microbiol.*, **8**, 229-239, 1962.
- Hatchard, G. G., and C. A. Parker, A new sensitive chemical actinometer. II. Potassium ferrioxalate as a standard chemical actinometer, *Proc. Roy. Soc. (London), Ser. A*, **235**, 518-536, 1956.

- Hayduk, W., and H. Laudie, Prediction of diffusion coefficients for nonelectrolytes in dilute aqueous solutions, *AIChE J.*, **20**, 611-615, 1974.
- Head, E. J. H., and E. P. W. Horne, Pigment transformation and vertical flux in an area of convergence in the North Atlantic, *Deep Sea Res.*, **40**, 329-346, 1993.
- Hofmann, D. J., Increase in the stratospheric background sulfuric acid aerosol mass in the past 10 years, *Science*, **248**, 996-1000, 1990.
- Holm-Hansen, O., C. J. Lorenzen, R. W. Holmes, and J. D. H. Strickland, Fluorometric determination of chlorophyll, *J. Cons. Int. Explor. Mer.*, **30**, 3-15, 1965.
- Ina, K., H. Etoh, and K. Sakata, Safe antifouling technology utilizing the functions of marine organisms, *Abstracts of the second international marine biotechnology conference*, Baltimore, MD, 1991.
- Iverson, R. L., F. L. Nearhoof, and M. O. Andreae, Production of dimethylsulfonium propionate and dimethylsulfide by phytoplankton in estuarine and coastal waters, *Limnol. and Oceanogr.*, **34**, 53-67, 1989.
- Jahne, B., K. O. Munnich, R. Bosinger, A. Dutzi, W. Huber, and P. Libner, On parameters influencing air-water gas exchange, *J. Geophys. Res.*, **92**, 1937-1949, 1987a.
- Jahne, B., G. Heinz, and W. Dietrich, Measurement of the diffusion coefficients of sparingly soluble gases in water with a modified Barrer method, *J. Geophys. Res.*, **92**, 10,767-10,776, 1987b.
- Jørgensen, B. B., and B. Okholm-Hansen, Emission of biogenic sulfur gases from a Danish estuary, *Atmos. Environ.*, **19**, 1737-1749, 1985.
- Johnson, J. E., and T. S. Bates, Sources and sinks of carbon monoxide in the mixed layer of the tropical South Pacific Ocean, *Global Biogeochem. cycles*, **10**, 347-359, 1996.
- Johnson, J. E., and T. S. Bates, Atmospheric measurements of carbonyl sulfide, dimethyl sulfide, and carbon disulphide using the electron capture sulfur detector, *J. Geophys. Res.*, **98**, 23,411-23421, 1993

- Johnson, J. E., and J. E. Lovelock, Electron capture sulfur detector: Reduced sulfur species detection at the femtomole level, *Anal. Chem.*, *60*, 812-816, 1988.
- Johnson, J. E., and H. Harrison, Carbonyl sulfide concentrations in the surface waters and above the Pacific Ocean, *J. Geophys. Res.*, *91*, 7883-7888, 1986.
- Jones, B. R., R. A. Cox, and S. A. Penkett, Atmospheric chemistry of carbon disulphide, *J. Atmos. Chem.*, *1*, 65-86, 1983.
- Keller, M. D., W. K. Bellows, and R. R. L. Guillard, Dimethyl sulfide production in marine phytoplankton, in *Biogenic Sulfur in the Environment*, edited by E. S. Saltzman and W. J. Cooper, pp. 167-182, Am. Chem. Soc., Washington, D.C., 1989.
- Kettle, A. J., A model of the temporal and spatial distribution of carbon monoxide in the mixed layer, M. Sc. thesis, Woods Hole Oceanographic Institution and Massachusetts Institute of Technology, Woods Hole, MA, 1994.
- Khalil, M. A. K., and R. A. Rasmussen, Global sources, lifetimes and mass balances of carbonyl sulfide (OCS) and carbon disulfide (CS₂) in the Earth's atmosphere, *Atmos. Environ.*, *18*, 1805-1813, 1984.
- Kieber, R. J., X. Zhou, and K. Mopper, Formation of carbonyl compounds from UV-induced photodegradation of humic substances in natural waters: Fate of riverine carbon in the sea. *Limnol. Oceanogr.*, *35*, 1503-1515, 1990.
- Kieber, D. J., J. Jiao, R. P. Kiene, and T. S. Bates, Impact of dimethylsulfide photochemistry on methyl sulfur cycling in the equatorial Pacific Ocean, *J. Geophys. Res.*, *101*, 3715-3722, 1996.
- Kieber, D. J., J. A. McDaniel, and K. Mopper, Photochemical source of biological substrates in seawater: Implications for geochemical carbon cycling, *Nature (London)*, *341*, 637-639, 1989.
- Kiene, R. P., Production of methanethiol from dimethylsulfoniopropionate in marine surface waters, *Mar. Chem.*, *54*, 69-83, 1996.
- Kiene, R. P., and T. S. Bates, Biological removal of dimethyl sulphide from seawater, *Nature*, *345*, 702-705, 1990.

- Kiene, R. P., Dimethyl sulfide metabolism in salt marsh sediments, *FEMS Microbiol. Ecol.*, *53*, 71-78, 1988.
- Kiene, R. P., and D. G. Capone, Microbial transformations of methylated sulfur compounds in anoxic salt marsh sediments, *Microb. Ecol.*, *15*, 275-291, 1988.
- Kim, K.-H., and M. O. Andreae, Carbon disulfide in the estuarine, coastal and oceanic environments, *Mar. Chem.*, *40*, 179-197, 1992.
- Kim, K.-H., and M. O. Andreae, Carbon disulphide in seawater and the marine atmosphere over the North Atlantic, *J. Geophys. Res.*, *92*, 14733-14738, 1987a.
- Kim, K.-H., and M. O. Andreae, Determination of carbon disulphide in natural waters by adsorbent preconcentration and gas chromatography with flame photometric detection, *Anal. Chem.*, *59*, 2670-2673, 1987b.
- Konig, G. M., A. D. Wright, and C. K. Angerhofer, Novel Potent Antimalarial Diterpene Isocyanates, Isothiocyanates, and Isonitriles from the Tropical Marine Sponge *Cymbastela hooperi*, *J. Organ. Chem.*, *61*, 3259-3267, 1996.
- Oae, S., and J. T. Doi, Organic Sulfur Chemistry: Structure and Mechanism, pp. 1-8, 1992.
- Large, W. G., and S. Pond, Open ocean momentum flux measurements in moderate to strong winds, *J. Phys. Oceanogr.*, *11*, 324-336, 1981.
- Lay, M. D. S., M. W. Sauerhoff, and D. R. Saunders, Carbon disulfide, in *Alumna's Encyclopedia of Industrial Chemistry*, *A5*, pp. 185-195, VCH Verlagsgesellschaft mbH, Weiheim, Ger., 1986.
- Ledwell, J. R., A. J. Watson, and C. S. Law, Evidence for slow mixing across the pycnocline from an open-ocean tracer-release experiment, *Nature*, *364*, 701-703, 1993.
- Leifer, A., *The Kinetics of Environmental Aquatic Photochemistry: Theory and Practice*, pp. 255-264, Am. Chem. Soc., Washington, D.C., 1988.
- Levitus, S., Climatological atlas of the world ocean, *NOAA Prof. Pap.*, *13*, 173pp., 1982.

- Li, Y. H., T. H. Peng, W. S. Broecker, and H. G. Ostlund, The average vertical mixing coefficient for the oceanic thermocline, *Tellus, Ser. B*, 36, 212-217, 1984.
- Lide, D. R., *Handbook of Chemistry and Physics*, 77th edition CRC Press Ann Arbor, 1996/1997.
- Liss, P. S., G. Malin, S. M Turner, and P. M. Holligan, Dimethyl sulphide and Phaeocystis: A review. *J. Mar. Syst.*, 5, 41-53, 1994.
- Liss, P. S., A. J. Watson, M. I. Liddicoat, G. Malin, P. D. Nightingale, S. M. Turner, and R. C. Upstill-Goddard, Trace gases and air-sea exchange, *Phil. Trans. R. Soc. Lond., Ser. A*, 343, 531-541, 1993.
- Liss, P. S., and L. Merlivat, Air-sea gas exchange rates: Introduction and synthesis, in *The Role of Air-Sea Exchange in Geochemical Cycling*, edited by P. Buat-Menard, pp. 113-129, D. Reidel, Hingham, Mass., 1986.
- Liss, P. S., and P. G. Slater, Flux of gases across the air-sea interface, *Nature*, 247, 181-184, 1974.
- Logan, J. A., M. B. McElroy, S. C. Wofsy, and M. J. Prather, Oxidation of CS₂ and OCS: sources for atmospheric SO₂, *Nature*, 281, 185-188, 1979.
- Lovelock, J. E., CS₂ and the natural sulfur cycle, *Nature*, 248, 625-626, 1974.
- Lueck, R., and T. Osborn, The dissipation of kinetic energy in a warm-core ring, *J. Geophys. Res.*, 91, 803-818, 1986.
- Luther, G. W., and E. Tsamakis, Concentration and form of dissolved sulfide in the oxic water column of the ocean, *Mar. Chem.*, 27, 165-177, 1989.
- Malcolm, R. L., The uniqueness of humic substances in each of soil, stream and marine environments, *Anal. Chim. Acta*, 232, 19-30, 1990.
- Manley, S. L., and J. L. de la Cuesta, Methyl iodide production from marine phytoplankton cultures, *Limnol. Oceanogr.*, 42, 142-147, 1997.
- Maroulis, P. J. and A. R. Bandy, Measurements of atmospheric concentrations of CS₂ in the eastern United States, *Geophys. Res. Lett.*, 7, 681-684, 1980.

- McCormick, M. P., P.-H. Wang, and L. R. Poole, Chapter 8: Stratospheric aerosols and clouds, In *Aerosol-Cloud-Climate*, edited by P. V. Hobbs, pp. 205-223, Academic press, Inc., Harcourt Brace and Company, 1993.
- McKay, W. A., M. F. Turner, B. M. R. Jones, and C. M. Halliwell, Emissions of hydrocarbons from marine phytoplankton—Some results from controlled laboratory experiments, *Atmos. Environ.*, *30*, 2583-2593, 1996.
- Memery, L., and L. Merlivat, Modelling of gas flux through bubbles at the air-water interface, *Tellus, Ser. B*, *37*, 272-285, 1985.
- Mihalopoulos, N., B. C. Nguyen, J. P. Putaud, and S. Belviso, The oceanic source of carbonyl sulfide, *Atmos. Environ.*, *26A*, 1383-1394, 1992.
- Miller, G. C., R. G. Zepp, Extrapolating photolysis rates from the laboratory to the environment, *Residue Reviews*, *85*, 89-110, 1983.
- Miller, W. L., and D. R. Kester, Peroxide variations in the Sargasso Sea. *Mar. Chem.*, *48*, 12-29, 1994.
- Miller, W. L., An investigation of peroxide, iron and iron bioavailability in irradiated marine waters, Ph. D. thesis, University of Rhode Island, Rhode Island, 1990.
- Miller, W. L., and R. G. Zepp, Photochemical production of dissolved inorganic carbon from terrestrial organic matter: Significance to the oceanic organic carbon cycle, *Geophys. Res. Letts.*, *22*, 417-420, 1995.
- Milne, P. J., D. D. Riemer, R. G. Zika, and L. E. Brand, Measurement of vertical distribution of isoprene in surface seawater, its chemical fate, and its emission from several phytoplankton monocultures, *Mar. Chem.*, *48*, 237-244, 1995.
- Moffett, J. W., and R. G. Zika, Reaction kinetics of hydrogen peroxide with copper and iron in seawater, *Environ. Sci. Technol.*, *21*, 804-810, 1987.
- Mohnen, V. A., Stratospheric ion and aerosol chemistry and possible links with cirrus cloud microphysics—a critical assessment, *J. Atmos. Sci.*, *47*, 1933-1948, 1990.
- Moore, L. R., R. Goericke, and S. W. Chisholm, Comparative physiology of *Synechococcus* and *Prochlorococcus*: influence of light and temperature on

- growth, pigments, fluorescence and absorptive properties, *Marine Ecology Progress Series*, 116, 259-275, 1995.
- Moore, R. M., W. Groszko, and S. Niven, Ocean-atmosphere exchange of methyl chloride: Results from NW Atlantic and Pacific Ocean studies, *J. Geophys. Res.*, 101, 28529-28538, 1996.
- Moore, R. M., and M. Webb, The relationship between methyl bromide and chlorophyll *a* in high latitude ocean waters, *Geophys. Res. Lett.*, 23, 2951-2954, 1996.
- Moore, R. M., D. E. Oram, and S. A. Penkett, Production of isoprene by marine phytoplankton cultures, *Geophys. Res. Lett.*, 21, 2507-2510, 1994.
- Mopper, K., and X. Zhou, Hydroxyl radical photoproduction in the sea and its potential impact on marine processes, *Science*, 250, 661-664, 1990.
- Morel, A., and J.-F. Berthon, Surface pigments, algal biomass profiles and potential production of the euphotic layer: Relationships reinvestigated in view of remote sensing application, *Limnol. Oceanogr.*, 34, 1545-1562, 1989.
- Murov, S. L., I. Carmichael, and G. L. Hug, Handbook of Photochemistry, pp. 299-305, Marcel Dekker, New York, 1993.
- Nelson, J. R., and S. Guarda, Particulate and dissolved spectral absorption on the continental shelf of the southeastern United States, *J. Geophys. Res.*, 100, 8715-8732, 1995.
- Newman, R. M., W. C. Kerfoot, and Z. Hanscom III, Watercress allelochemical defends high-nitrogen foliage against consumption: Effects on freshwater invertebrate herbivores, *Ecology*, 77, 2312-2323, 1996.
- Palinek, B., O. C. Zafiriou, and F. M. M. Morel, Hydrogen peroxide production by marine phytoplankter, *Limnol. Oceanogr.*, 32, 1365-1369, 1987.
- Parsons, T. R., Y. Maita, and C. M. Lalli, in *A Manual of Chemical and Biological Methods for Seawater Analysis*, 173 pp., Pergamon, Oxford, 1984.
- Peng, T. H., W. S. Broecker, G. G. Mathieu, Y. H. Li, and A. E. Bainbridge, Radon evasion rates in the Atlantic Pacific Oceans as determined during the GEOSECS Program, 1979, *J. Geophys. Res.*, 84, 2471-2486.

- Peyton, T. O., R. V. Steele, and W. R. Mabey, , Carbon disulphide and carbonyl sulfide: Literature review and environmental assessment, Stanford Res. Inst., Menlo Park, Calif., 1976
- Poole, L. R., and M. P. McCormick, Polar stratospheric clouds and the Antarctic ozone hole, *J. Geophys. Res.*, *93*, 8423-8430, 1988.
- Pos, W. H., P. J. Milne, D. D. Riemer, and R. G. Zika, Photoinduced oxidation of H₂S species: A sink for sulfide in seawater, *J. Geophys. Res.*, *102*, 12831-12837, 1997.
- Pos, W. H., D. D. Riemer, and R. G. Zika, Carbonyl sulfide (OCS) and carbon monoxide (CO) in natural waters: evidence of a coupled production pathway, *Mar. Chem.*, *62*, 89-101, 1998.
- Qian, J., and K. Mopper, Impact of marsh DOM run-off on the photochemical reactivity of coastal waters, *Abstracts of The Oceanography Society Scientific Meeting*, Seattle, Washington, 1997.
- Radford-Knoery, J. R., and G. A. Cutter, Biogeochemistry of dissolved hydrogen sulfide species and carbonyl sulfide in the western North Atlantic Ocean, *Geochim. Cosmochim. Acta*, *58*, 5421-5431, 1994.
- Rasmussen, R. A., and M. A. K. Khalil, Isoprene over the Amazon Basin, *J. Geophys. Res.*, *93*, 1417-1421, 1988.
- Reibesell, U., D. A. Wolf-Gladrof, and V. Smetacek, Carbon dioxide limitation of marine phytoplankton growth rates, *Nature*, *361*, 249-251, 1993.
- Reid, E. E., *Organic Chemistry of Bivalent Sulfur*, vol. 4, pp. 131-179, Chem. Publ., New York, 1962.
- Rinsland, C. P., R. Zander, E. Mahieu, P. Demoulin, A. Goldman, D. H. Ehhalt, and J. Rudolph, Ground-based infrared measurements of carbonyl sulfide total column abundances: Long-term trends and variability, *J. Geophys. Res.*, *97*, 5995-6002, 1992.
- Rodhe, H., and I. Isaksen, Global distribution of sulfur compounds in the troposphere estimated in a height/latitude transport model, *J. Geophys. Res.*, *85*, 7401-7409, 1980.

- Romankevich, E. A., *Geochemistry of organic matter in the ocean*, Springer, 1984.
- Rundel, D. R., Action spectra and estimation of biologically effective UV radiation, *Physiol. Plant.*, *58*, 360-366, 1983.
- Sandalls, F. J., and S. A. Penkett., Measurements of carbonyl sulphide and carbon disulphide in the atmosphere, *Atmos. Environ.*, *11*, 197-199, 1977.
- Scarratt, M. G., and R. M. Moore, Production of methyl bromide and methyl chloride in laboratory cultures of marine phytoplankton II, *Mar. Chem.*, *59*, 311-320, 1997.
- Scarratt, M. G., and R. M. Moore, Production of methyl chloride and methyl bromide in laboratory cultures of marine phytoplankton, *Mar. Chem.*, *54*, 263-272, 1996.
- Sengers, J. V., and J. T. Watson, Improved international formulations for the viscosity and thermal conductivity of water substances, *J. Phys. Chem. Ref. Data*, *15:4*, 1291-1300, 1986
- Shooter, D., and P. Brimblecombe, Dimethylsulphide oxidation in the ocean, *Deep Sea Res., Part A*, *36*, 577-585, 1989.
- Siegel, D. A., and A. F. Michaels, Quantification of non-algal light attenuation in the Sargasso Sea: Implication for biogeochemistry and remote sensing, *Deep Sea Res. II*, *43*, 321-345, 1996.
- Sikorski, R. J., and R. G. Zika, Modeling mixed-layer photochemistry of H₂O₂: Physical and chemical modeling of distribution, *J. Geophys. Res.*, *98*, 2329-2340, 1993.
- Skipper, H. D., and D. T. Westermann, Comparing effects of propylene oxide, sodium azide, and autoclaving on selected soil properties, *Soil Biol. Biochem.*, *5*, 409-414, 1973.
- Smethie, W. M., T. T. Takahashi, D. W. Chipman, and J. R. Ledwell, Gas exchange and CO₂ flux in the tropical Atlantic Ocean determined from ²²²Rn and pCO₂ measurements, *J. Geophys. Res.*, *90*, 7005-7022, 1985.
- Smith, N. A., and D. P. Kelly, Oxidation of carbon disulphide as the sole source of energy for the autotrophic growth of *Thiobacillus thioparus* strain TK-m, *J. Gen. Microbiol.*, *134*, 3041-3048, 1988.

- Smith, R. C., and K. S. Baker, Optical properties of the clearest natural waters (200-800 nm), *Appl. Opt.*, 20, 177-184, 1981.
- Staubes, R., and H.-W. Georgii, Biogenic sulfur compounds in seawater and the atmosphere of the Antarctic region, *Tellus, Ser. B*, 45, 127-137, 1993.
- Staubes R., H.-W. Georgii, and G. Ockelmann, Flux of COS, DMS and CS₂ from various soils in Germany, *Tellus, Ser. B*, 41, 305-313, 1989.
- Stedman, D. H., M. Z. Creech, P. L. Cloke, S. E. Kesker, and M. Gardner, Formation of CS₂ and OCS from decomposition of metal sulfides, *Geophys. Res. Lett.*, 1, 858-860, 1984.
- Stefels, J., and L. Dijkhuizen, Characteristics of DMSP-lyase in *Phaeocystis* sp. (Prymnesiophyceae), *Mar. Ecol. Prog. Ser.*, 131, 307-313, 1996.
- Stefels, J., and W. H. M. van Boekel, Production of DMS from dissolved DMSP in axenic cultures of the marine phytoplankton species *Phaeocystis* sp., *Mar. Ecol. Prog. Ser.*, 97, 11-18, 1993.
- Stephen, H., and T. Stephen, *Solubilities of inorganic and organic compounds*, Pergamon, New York, 1963.
- Stuedler, P. A., and B. J. Peterson, Contribution of the gaseous sulfur from salt marshes to the global sulfur cycle, *Nature*, 311, 455-457, 1984.
- Still, I. W. J., Photochemistry of organic sulfur compounds, in *Organic Sulfur Chemistry: Theoretical and Experimental Advances*, edited by F. Bernardi, I. G. Csizmadia and A. Mangini, pp. 596-659, Elsevier, Amsterdam, 1985.
- Stookey, L. L., A new spectrophotometric reagent for iron, *Anal. Chem.*, 42, 779-781, 1970.
- Stratmann, K., R. E. Moore, R. Bonjouklian, J. B. Deeter, G. M. L. Patterson, S. Shaffer, C. D. Smith, and T. A. Smitka, Welwitindolinones, Unusual Alkaloids from the Blue-Green Algae *Hapalosiphon welwitschii* and *Westiella intricata*. Relationship to Fischerindoles and Hapalindoles, *J. Am. Chem. Soc.*, 116, 9935-9942, 1994.

- Sunda, W. G., S. A. Huntsman, and G. R. Harvey, Photoreduction of manganese oxides in seawater and its geochemical and biological implications, *Nature (London)*, *301*, 234-236, 1983.
- Sze, N. D., and M. K. W. Ko, CS₂ and OCS in the stratospheric sulfate budget, *Nature*, *280*, 308-310, 1979.
- Sze, N. D., and M. K. W. Ko, Photochemistry of OCS, CS₂, CH₃SCH₃, and H₂S: Implication for the atmospheric sulfur cycle, *Atmos. Environ.*, *14*, 1223-1239, 1980.
- Tada, K., and Y. Maita, High abundance of sulfur containing amino acids in low molecular weight proteinaceous fraction isolated from coastal surface seawater, *Geochem. J.*, *27*, 1-5, 1993.
- Taguchi, S., G. R. Ditullio, and E. A. Laws, Physiological characteristics and production of mixed layer and chlorophyll maximum phytoplankton populations in the Caribbean Sea and western Atlantic Ocean, *Deep-Sea Res.*, *35*, 1363-1377, 1988.
- Tait, V. K., and R. M. Moore, Methyl chloride (CH₃Cl) production in phytoplankton cultures, *Limnol. Oceanogr.*, *40*, 189-195; 1995.
- Taylor, C. H., E. K. Stephen, and P. L. Cloke, Sulfur gases produced by the decomposition of sulfide minerals: application to geochemical exploration. *J. Geochem. Expl.*, *17*, 165-185, 1982.
- Thompson, A. M., and R. J. Cicerone, Possible perturbations to atmospheric CO, CH₄, and OH, *J. Geophys. Res.*, *91*, 10,853-10,864, 1986.
- Thornton, D. C., and A. R. Bandy, Sulfur dioxide and dimethyl sulfide in the central Pacific troposphere, *J. Atmos. Chem.*, *17*, 1-13, 1993.
- Thornton, F. C., and A. R. Bandy, Distribution of CS₂ over the equatorial southern Atlantic Ocean (abstract), *EOS Trans., AGU*, *72(17)*, Spring Meet. Suppl., 64, 1991.
- Toon, O. B., J. F. Kasting, R. P. Turco, and M. S. Liu, The sulfur cycle in the marine atmosphere, *J. Geophys. Res.*, *92*, 943-963, 1987.

- Tsuchiya, Y., M. F. Watanabe, and M. Watanabe, Volatile organic sulfur compounds associated with blue-green algae from inland waters of Japan, *Wat. Sic. Tech.*, 25, 123-130, 1992.
- Tucker, B. J., P. J. Maroulis, and A. R. Bandy, Free tropospheric measurements of CS₂ over a 45°N to 45°S latitude range, *Geophys. Res. Lett.*, 12, 9-11, 1985.
- Turner, S. M., and P. S. Liss, Measurements of various sulphur gases in a coastal marine environment, *J. Atmos. Chem.*, 2, 223-232, 1985.
- Uher, G., and M. O. Andreae, Photochemical production of carbonyl sulfide in North Sea water: A process study, *Limnol. and Oceanogr.*, 42, 432-442, 1997.
- Ulshöfer, V. S., and M. O. Andreae, Carbonyl sulfide (COS) in the surface ocean and the atmospheric COS budget, *Aquatic Geochem.*, in press.
- Ulshöfer, V. S., O. R. Flöck, G. Uher, and M. O. Andreae, Photochemical production and air-sea exchange of carbonyl sulfide in the eastern Mediterranean Sea, *Mar. Chem.*, 53, 25-39, 1996.
- Ulshöfer, V. S., G. Uher, and M. O. Andreae, Evidence for a winter sink of atmospheric carbonyl sulfide in the northeast Atlantic Ocean, *Geophys. Res. Lett.*, 22, 2601-2604, 1995.
- Upstill-Goddard, R. C., A. J. Watson, P. S. Liss, and M. I. Liddicoat, Gas transfer in lakes measured with FS₆, *Tellus, Ser. B*, 42, 364-377, 1990.
- Valentine, R. L., and R. G. Zepp, Formation of carbon monoxide from the photodegradation of terrestrial dissolved organic carbon in natural waters, *Environ. Sci. Technol.*, 27, 409-412, 1993.
- Vodacek, A., N. V. Blough, M. D. DeGrandpre, E. T. Peltzer, and R. K. Nelson, Seasonal variation of CDOM and DOC in the Middle Atlantic Bight: Terrestrial inputs and photooxidation, *Limnol. Oceanogr.*, 42, 674-686, 1997.
- Vodacek, A., S. A. Green, and N. V. Blough, An experimental model of the solar-stimulated fluorescence of chromophoric dissolved organic matter, *Limnol. and Oceanogr.*, 39, 1-11, 1994.

- Wakeham, S. G., B. L. Howes, J. W. H. Dacey, R. P. Schwarzenbach, and J. Zeyer, Biogeochemistry of dimethylsulfide in a seasonally stratified coastal salt pond, *Geochim. Cosmochim. Acta*, 51, 1675-1684, 1987.
- Walsh, R. S., G. A. Cutter, W. M. Dunstan, J. Radford-Knoery, and J. Elder, The biogeochemistry of H₂S: phytoplankton production in the surface ocean, *Limnol., Oceanogr.*, 39, 941-948, 1994.
- Wanninkhof, R., Relationship between windspeed and gas exchange over the ocean, *J. Geophys. Res.*, 97, 7373-7382, 1992.
- Wanninkhof, R., J. R. Ledwell, and W. S. Broecker, Gas exchange-wind speed relationship measured with sulfur hexafluoride on a lake, *Science*, 227, 1224-1226, 1985.
- Washburn, E. W. (Ed.), *International critical tables*, published for the national research council, McGraw Hill, New York, 1928.
- Watson, A. J., R. C. Upstill-Goddard, and P. S. Liss, Air-sea gas exchange in rough and stormy seas measured by a dual tracer technique, *Nature*, 349, 145-147, 1991.
- Weiss, P. S., J. E. Johnson, R. H. Gammon, and T. S. Bates, Reevaluation of the open ocean source of carbonyl sulfide to the atmosphere, *J. Geophys. Res.*, 100, 23,083-23,092, 1995a.
- Weiss, P. S., S. S. Andrews, J. E. Johnson, and O. C. Zafiriou, Photoproduction of carbonyl sulfide in south Pacific Ocean waters as a function of irradiation wavelength, *Geophys. Res. Lett.*, 22, 215-218, 1995b.
- Wennberg, P. O., R. C. Cohen, R. M. Stimpfle, J. P. Koplou, J. G. Anderson, R. J. Salawitch, D. W. Fahey, E. L. Woodbridge, E. R. Keim, R. S. Gao, C. R. Webster, R. D. May, D. W. Toohey, L. M. Avallone, M. H. Proffitt, M. Loewenstein, J. R. Podolske, K. R. Chan, S. C. Wofsy, Removal of stratospheric O₃ by radicals: In situ measurements of OH, HO₂, NO, NO₂, ClO, and BrO, *Science*, 266, 398-404, 1994.
- White, W., and R. Bernstein, Large-scale vertical eddy diffusion in the main pycnocline of the central North Pacific, *J. Phys. Oceanogr.*, 11, 434-441, 1981.

- Wilke, C. R., and P. Chang, Correlation of diffusion coefficients in dilute solutions, *AIChE J.*, *1*, 264-270, 1955.
- Wine, P., and A. R. Ravishankara, Kinetics of OH reaction with troposphere sulfur compounds, in *Proc. 2nd Symp. on the Composition of the Nonurban Troposphere*, Am. Meteorol. Soc., Boston, Mass. 1982.
- Wine, P. H., W. L. Chameides, and A. R. Ravishankara, Potential role of CS₂ photooxidation in tropospheric sulfur chemistry, *Geophys. Res. Lett.*, *8*, 543-546, 1981.
- Zafiriou, O. C., and M. B. True, Nitrate photolysis in seawater by sunlight, *Mar. Chem.*, *8*, 33-42, 1979a.
- Zafiriou, O. C., and M. B. True, Nitrite photolysis in seawater by sunlight, *Mar. Chem.*, *8*, 9-32, 1979b.
- Zafiriou, O. C., and M. B. True, Nitrite photolysis as a source of free radicals in productive surface waters, *Geophys. Res. Lett.*, *6*, 81-84, 1979c.
- Zepp, R. G., and D. M. Cline, Rates of direct photolysis in aquatic environment, *Environ. Sci. Technol.*, *11*, 359-366, 1977.
- Zepp, R. G., and M. O. Andreae, Factors affecting the photochemical production of carbonyl sulfide in seawater, *Geophys. Res. Lett.*, *21*, 2813-2816, 1994.
- Zepp, R. G., B. C. Faust, and J. Hoigne, Hydroxyl radical formation in aqueous reactions (pH 3-8) of iron (II) with hydrogen peroxide: The Photo-Fenton reaction, *Environ. Sci. Technol.*, *26*, 313-319, 1992.
- Zhang, L., R. S. Walsh, and G. A. Cutter, Estuarine cycling of carbonyl sulfide: production and sea-air flux, *Mar. Chem.*, *61*, 127-142, 1998.